

Design, synthesis and self-assembly of β -cyclodextrin based donor-acceptor systems for charge transfer and photoinduced electron transfer applications

THESIS SUBMITTED TO ACADEMY OF SCIENTIFIC AND INNOVATIVE
RESEARCH (AcSIR) FOR THE AWARD OF THE DEGREE OF
DOCTOR OF PHILOSOPHY IN CHEMISTRY
UNDER THE FACULTY OF SCIENCE



By
ATHIRA K. J.
Enrollment No: 10CC14J39019

Under the Supervision of
Dr. K. R. Gopidas



PHOTOSCIENCES AND PHOTONICS SECTION
CHEMICAL SCIENCES AND TECHNOLOGY DIVISION
CSIR-NATIONAL INSTITUTE FOR INTERDISCIPLINARY
SCIENCE AND TECHNOLOGY (CSIR-NIIST)
THIRUVANANTHAPURAM - 695019, KERALA

AUGUST 2020

Dedicated to My Parents, My Teachers and The Almighty

DECLARATION

I hereby declare that the matter embodied in the Ph. D. thesis entitled: “**Design, synthesis and self-assembly of β -cyclodextrin based donor-acceptor systems for charge transfer and photoinduced electron transfer applications**” is the result of an independent work carried out by me at the Photosciences and Photonics Section, Chemical Sciences and Technology Division of the CSIR-National Institute for Interdisciplinary Science and Technology (CSIR-NIIST), Trivandrum, under the supervision of Dr. K. R. Gopidas and the same has not been submitted elsewhere for other degree or diploma.

In keeping with the general practice of reporting scientific observations, research material obtained from other investigations has been duly cited and acknowledged in the thesis.


ATHIRA K. J.

Thiruvananthapuram

August 2020



सीएसआईआर- राष्ट्रीय अंतर्विषयी विज्ञान तथा प्रौद्योगिकी संस्थान
CSIR- NATIONAL INSTITUTE FOR INTERDISCIPLINARY SCIENCE & TECHNOLOGY

इन्डस्ट्रियल एस्टेट पी.ओ., तिरुवनंतपुरम- 695 019, केरल, भारत
Industrial Estate P.O., Thiruvananthapuram- 695 019, Kerala, INDIA

के. आर. गोपिदास, एफ.ए.एससी

K.R. Gopidas, F.A.Sc.

सर्वोच्च प्रतिष्ठित वैज्ञानिक

H-Emeritus Scientist

रसायन विज्ञान तथा प्रौद्योगिकी प्रभाग

Chemical Sciences and Technology Division

August 6, 2020

CERTIFICATE

This is to certify that the work incorporated in this Ph.D. thesis entitled: "**Design, synthesis and self-assembly of β -cyclodextrin based donor-acceptor systems for charge transfer and photoinduced electron transfer applications**" has been carried out by Ms. Athira K. J. under my supervision at the Photosciences and Photonics, Chemical Sciences and Technology Division of the CSIR-National Institute for Interdisciplinary Science and Technology (CSIR-NIIST), Trivandrum and the same has not been submitted elsewhere for a degree.

Athira

Athira K. J.

(Student)

Gopidas

Dr. K. R. Gopidas

(Thesis Supervisor)

ACKNOWLEDGEMENTS

I have great pleasure in placing on record my deep sense of gratitude to Dr. K. R. Gopidas, my thesis supervisor, for suggesting the research problem and for his valuable guidance, constant support, help, encouragement, and profound scientific knowledge he has shared with, throughout my research career, leading to the successful completion of this work.

I wish to express my sincere gratitude to Late Professor M. V. George for being a real motivation during the tenure of this work.

I wish to thank Dr. A. Ajayaghosh, Dr. Suresh Das and Dr. Gangan Pratap, present and former Directors of the CSIR-National Institute for Interdisciplinary Science and Technology, Thiruvananthapuram, for providing me the necessary facilities for carrying out this work.

Dr. Sujatha Devi, Dr. K. N. Narayanan Unni, Dr. Joshy Joseph, Dr. K. Yoosaf, Dr. Karunakaran Venugopal, Dr. Biswapriya Deb, Dr. C. Vijayakumar, Dr. V. K. Praveen, Dr. Suraj Soman, Scientists of the Photosciences and Photonics section, Chemical Sciences and Technology Division, are greatly acknowledged for their help and support.

I sincerely acknowledge Dr. C. H. Suresh, Dr. R. Luxmi Varma, and Dr. Mangalam S. Nair, present and former AcSIR coordinators, for their help in the successful completion of the course work.

I extend my sincere thanks to my Doctoral Advisory Committee members Dr. Joshy Joseph, Dr. K. Yoosaf and Dr. K. N. Narayanan Unni, for their valuable comments and suggestions to improve the quality of my work.

I wish to thank all my group members, Dr. K. Retheesh, Dr. A. M. Rakhi, Dr. Vinayak M. V., Dr. Tony George Thomas, Dr. K. Sreedevi, Mr. T. M. Lakshmykanth, Dr. Prakash S. P., Dr. Sumesh Babu Krishnan, Dr. Nagaraj Nayak, Mr. Muhammed Yoosuf, and Mrs. Daisymol K. B. for their advice, cordial support and care. I am extremely indebted and grateful to Dr. Sumesh Babu Krishnan for his valuable advice, help and support from the beginning of my research work. I am also thankful to M. Sc. Project students Ms. Asawthy, Ms. Chithrambari, Mr. S. Chinraj, Ms. Jasmine, for helping me in carrying out the experiments.

I sincerely thank Mr. Rajeev for the device fabrications, Mr. Robert Philip for the general and technical help, Mr. Kiran Mohan for the TEM analysis, Mrs. Saumini Mathew, Mr. Saran and Mr. Gokul for NMR analysis, Mrs. Viji for the HRMS analysis, Mr. Ashwin, Mr. Vishnu and Mr. Vibhu Darshan for AFM analysis, Mr. Harish Raj and Mr. Chandrakanth for SEM analysis. I also thank Ms. Chinju Govind for helping with the Femtosecond analysis.

I am very much cherished with the friendship by Ms. Anila, Ms. Sajitha, Ms. Ranjana, Ms. Parvathy, Hostel mates and all present and former members of Photosciences and Photonics Section.

I would also like to extend my wholehearted thanks and appreciation to all my teachers for their help and blessings.

I sincerely thank the University Grants Commission (UGC), Government of India, for financial support.

I am deeply indebted to my parents, sister and grandmother for their endless love, care and support, especially to my mother for being my real source of inspiration to overcome all difficulties faced in my life. I am deeply grateful to my loving husband, Mr. Praveen, for being my backbone, for his patience, understanding, help, care and support helped me a lot for the successful completion of my thesis work.

Finally, I thank The Almighty for everything.


ATHIRA K. J.

CONTENTS

	Page
Dedication	i
Declaration	ii
Certificate	iii
Acknowledgements	iv
Contents	vi
Preface	ix
List of Abbreviations	xii
Chapter 1	Cyclodextrin Mediated Donor-Acceptor Self-Assembly for Charge Transfer and Photoinduced Electron Transfer Applications
1.1	Introduction 1
1.2	Structure and Properties of Cyclodextrins 2
1.3	Charge Transfer Complexes 6
1.3.1	Mulliken's theory 7
1.3.2	CT interaction assisted by encapsulation 8
1.3.3	Charge transfer complexes in organic electronics 16
1.4	Natural and Artificial Photosynthesis 19
1.4.1	PET in CD based supramolecular systems 27
1.5	Origin of the Thesis 29
1.6	References 31
Chapter 2	Hierarchically Self-Assembled Nanofiber Networks of Mixed Stack Charge Transfer Complex for Organic Electronic Applications
2.1	Abstract 41
2.2	Introduction 42
2.3	Results and Discussions 44
2.3.1	Synthesis and characterisation of molecules 44
2.3.2	Charge transfer complexation in PYCD-NDIAD 45
2.3.2.1	HRMS studies 45

2.3.2.2	UV-Visible absorption spectroscopy studies	46
2.3.2.3	Isothermal titration calorimetric studies	48
2.3.2.4	¹ H NMR titration studies	51
2.3.2.5	Circular dichroism studies	58
2.3.2.6	DLS and Tyndall effect studies	61
2.3.2.7	Morphological analysis	62
2.3.2.8	Mechanism of self-assembly	63
2.3.2.9	Femtosecond transient absorption studies	66
2.3.2.10	Conductivity measurements	69
2.4	Conclusions	71
2.5	Experimental Sections	72
2.5.1	Instrumentation and methods	72
2.5.2	Materials	74
2.6	References	76
Chapter 3	Self-Assembly and Photoinduced Electron Transfer in a Bis(β-Cyclodextrin)-Linked Pyrene/ Bis(Adamantane)-Linked Methyl Viologen Donor-Acceptor System in Aqueous Solution	
3.1	Abstract	82
3.2	Introduction	83
3.3	Results and Discussions	89
3.3.1	Synthesis and characterization of molecules	89
3.3.2	¹ H NMR titration studies	92
3.3.3	Photophysical properties of CD-PY-CD/AD-MV ²⁺ -AD	95
3.3.4	DLS and Tyndall effect studies	98
3.3.5	Morphological analysis	99
3.3.6	Mechanism for self-assembly in CD-PY-CD/AD-MV ²⁺ -AD	101
3.3.7	Photoinduced electron transfer in CD-PY-CD/AD-MV ²⁺ -AD	104
3.3.7.1	Steady-state fluorescence quenching	104
3.3.7.2	Time resolved fluorescence quenching studies	106
3.3.7.3	Nanosecond laser flash photolysis studies	110
3.4	Conclusions	113
3.5	Experimental Sections	114
3.5.1	Instrumentation and methods	114

3.5.2	Materials	115
3.6	References	119
Chapter 4	Generation of Long-Lived Charge Separated State in a Supramolecular Donor-Acceptor System Self-Assembled into Vesicles and Fibers	
4.1	Abstract	125
4.2	Introduction	126
4.3	Results and Discussions	128
4.3.1	Synthesis and characterization of molecules	128
4.3.2	¹ H NMR titration studies	129
4.3.3	Photophysical properties of CD-PY-CD/Ms-(AD-MV ²⁺) ₃	132
4.3.4	DLS and Tyndall effect studies	135
4.3.5	Morphological analysis	135
4.3.6	Mechanism of self-assembly in CD-PY-CD/Ms-(AD-MV ²⁺) ₃	137
4.3.7	Photoinduced electron transfer in CD-PY-CD/Ms-(AD-MV ²⁺) ₃	139
4.3.7.1	Steady-state fluorescence quenching	139
4.3.7.2	Time resolved fluorescence quenching studies	140
4.3.7.3	Nanosecond laser flash photolysis studies	143
4.4	Conclusions	147
4.5	Experimental Sections	148
4.5.1	Instrumentation and methods	148
4.5.2	Materials	149
4.6	References	150
	List of Publications and Posters Presented at Conferences	154
	Attachment of the Photocopy of Publications	

PREFACE

This thesis is mainly focused on the design and study of β -Cyclodextrin (β -CD) mediated Donor-Acceptor (D-A) systems for charge transfer and electron transfer applications. CDs are a class of water-soluble macrocyclic oligosaccharides made up of various numbers of D-glucopyranose units linked through α -1, 4-glycosidic linkages and classified into three major CDs namely α , β and γ with 6, 7, and 8 glucopyranose units, respectively. CDs have a hydrophobic cavity that can encapsulate hydrophobic guest molecule of suitable size from aqueous medium. The cavity size of β -CD matches well with the molecular dimensions of adamantane (AD) and hence the β -CD/AD complexation exhibits very high association constant. For the past few years, our research group was involved in the study of charge transfer (CT) and photoinduced electron transfer (PET) in native as well as functionalized β -Cyclodextrin (β -CD) based D-A systems. A general strategy we employed is to covalently link the donor to the CD and assemble the acceptor by inclusion binding with the CD. Since adamantane (AD) derivatives exhibit a very high affinity for inclusion binding in β -CD cavity, we have linked the acceptors to AD for assembling the D-A systems.

We have combined our observations and findings into four chapters. Chapter 1 of the thesis provide an overview of two important aspects of D-A systems such as charge-transfer and photoinduced electron transfer. An elaborate literature review of the CT interaction assisted by encapsulation and applications of CT complexes in organic electronics are provided in this chapter. In addition, a detailed literature review on PET in β -CD based supramolecular D-A systems is also presented in this chapter.

One important drawback of CT complexes is their low association constants, which limit their potential to form organized structures with long range order. Researchers have

solved this issue and confirmed the enhancement of association constant by reinforcing the CT interaction with other non-covalent forces such as hydrogen bonding, π -stacking and hydrophobic interactions. Chapter 2 explores the effective utilization of the β -CD/AD host-guest interaction to enhance the stability of the CT complex. In this chapter, we studied mixed stack charge transfer complex formation from pyrene-linked to β -CD as a donor (PYCD), and naphthalene diimide, linked to AD on one side and a pyridinium group on the other, as an acceptor (NDIAD). The pyridinium group is used to impart water solubility to the molecule. When dissolved in water, the molecules formed a CT complex where the pyrene-naphthalene diimide CT interaction is reinforced several fold by the strong β -CD/AD inclusion binding interaction. We were successful in constructing a CT complex that exhibited one of the highest association constants ($K_a = 3.6 \times 10^7 \text{ M}^{-1}$) reported so far in the literature. We observed that the CT complex underwent hierarchical self-assembly to give twisted nanofibers. The nanofibers exhibited horizontal conductivity of $1.2 \times 10^{-3} \text{ S/cm}$, suggesting that the CT complex may have potential applications in organic electronics. We have also studied the excited state relaxation process in the charge transfer complex by femtosecond time-resolved pump-probe spectroscopy.

Mimicking the natural photosynthetic process of converting sunlight into useful energy has always attracted the researchers to tackle the energy crisis. PET leading to long-lived charge separated (CS) states is inevitable for solar energy harvesting. Exquisite organization of the electron donor-acceptor moiety is an essential factor in achieving long-lived CS states. For important applications such as solar water splitting, the generation of long-lived CS states in aqueous solution is crucial. In the third and fourth chapters we have

attempted to attain long lived CS states by careful design of D-A systems, which utilized the propensity of AD group to undergo inclusion complexation in β -CD cavity.

In the third chapter, we employed pyrene (PY) linked to two β -CD molecules (CD-PY-CD) as donor and methyl viologen (MV^{2+}) linked to two AD groups (AD- MV^{2+} -AD) as acceptor and studied D-A interaction in great detail. The CD-PY-CD/AD- MV^{2+} -AD interaction was studied by 1H NMR, 2D ROESY NMR and circular dichroism spectroscopies. We observed that the bis-inclusion complex formed undergo hierarchical self-assembly to give closed loop structures, which then stack together to give toroids. The self-assembled system did not exhibit CT absorption in the longer wavelength region. The fluorescence due to the CD-PY-CD was highly quenched in the self-assembled system which was attributed to PET from the PY to MV^{2+} . Nanosecond laser flash photolysis experiments confirmed PET taking place in the system through observation of product radical ions. Although very facile PET occurred in the system, this did not lead to formation of long-lived CS states.

In the fourth chapter, we employed the same donor (CD-PY-CD) but used an acceptor that has AD-linked MV^{2+} moieties on all three arms of a mesitylene core ($Ms-(AD-MV^{2+})_3$). The D-A system self-assembled in aqueous solution into vesicles, which later coalesced to give long fibers. Self-assembly in this case was studied using 1H NMR, 2D NMR, ICD, AFM, SEM and TEM. We observed that fluorescence of the pyrene chromophore was quenched within the self-assembled system due to efficient PET from PY to MV^{2+} . PET was again confirmed through the identification of long lived radical ions in nanosecond flash photolysis experiments. Steady-state irradiation of the self-assembled system in an optical bench imparted blue colour to the solution, which is indicative of the formation of long-lived methyl viologen radical cation ($MV^{\bullet+}$).

LIST OF ABBREVIATIONS

A: Acceptor

AD: Adamantane

Å: Angstrom

AdNH₂: Amantadine

AN: Anthracene

AFM: Atomic force microscopy

AD-MV²⁺-AD: Methylviologen linked to two adamantane groups

AD-AN-AD: Bis-adamantane linked anthracene

ACN: Acetonitrile

BET: Back electron transfer

CT: Charge transfer

CD: Cyclodextrin

CDs: Cyclodextrins

α-CD: Alpha cyclodextrin

β-CD: Beta cyclodextrin

γ-CD: Gama cyclodextrin

CS: Charge separated state

CB[n]: Cucurbit[n]urils

cm: Centimetre

CR: Charge recombination

C₆₀: Fullerene

C-AFM: Conductive atomic force microscopy

°C: Degree Celsius

CaF₂: Calcium fluoride

CD-PY-CD: Pyrene linked to two β -cyclodextrin

CDCl_3 : Deuterated chloroform

DHNp: 2,6-Dihydroxynaphthalene

D: Donor

DBTTF: Dibenzotetrathiafulvalene

DMF: Dimethyl formamide

DCC: N,N'-Dicyclohexylcarbodiimide

DMSO- d_6 : Deuterated dimethyl sulphoxide

D_2O : Deuterated water

DLS: Dynamic light scattering

d_{cc} : Center to center distance between donor and acceptor

2D: Two dimensional

δ : Chemical shift

EDA: Electron donor- acceptor

Equiv.: Equivalent

eV: Electron volt

E_{ox} : Oxidation potential

E_{red} : Reduction potential

$E_{0,0}$: Excitation energy

ϵ : solvent dielectric constant

fs: Femtosecond

FTIR: Fourier transform infrared

ΔG° : Free energy change

HOMO: Highest occupied molecular orbital

HSCT: Host stabilized charge transfer

HRTEM: High resolution transmission electron microscopy

1-HOBt: 1-Hydroxybenzotriazole

HRMS: High resolution mass spectroscopy

ΔH : Change in enthalpy

h: Hour

H₂SO₄: Sulphuric acid

Hz: Hertz

ITC: Isothermal titration calorimetry

ICD: Induced circular dichroism

I-V: Current- Voltage

I: Fluorescence intensity

J: Electrostatic reorganization energy

K_a: Association constant

kcal: Kilocalorie

k_{CR}: Rate of charge recombination

kV: Kilo volt

KBr: Potassium bromide

K_{et}: Rate of electron transfer

kHz: Kilohertz

k_{BET}: Rate of back electron transfer

LUMO: Lowest unoccupied molecular orbital

LASO: Lock arm supramolecular ordering

M: Molar

MV²⁺: Methyl viologen

mM: Millimolar

MLCT: Metal-ligand charge transfer

MV^{•+}: Methyl viologen radical cation

MHz: Megahertz

mL: Milliliter

mmol: Millimole

mp: Melting point

min: Minute

Ms-(AD-MV²⁺)₃: Three AD-linked MV²⁺ moieties on mesitylene core

v: Frequency

μC: Microcoulomb

μs: Microsecond

μcal: Microcalorie

NDIAD: Naphthalene diimide linked adamantane

NMR: Nuclear magnetic resonance

Np: Naphthalene

NDI^{•-}: Naphthalene diimide radical anion

nm: Nanometer

ns: Nanosecond

NDI: Naphthalene diimide

n: Binding stoichiometry

Nd: Neodymium

OFET: Organic field effect transistor

PYCD: Pyrene linked beta cyclodextrin

PET: Photoinduced electron transfer

PIL: Poly (ionic liquid)

PY: Pyrene

PIAD: Adamantane linked pyromellitic diimide

PS: Photosynthetic unit

ps: Picosecond

PMDI: Pyromellitic diimide

PI-PI: Bis-pyromellitic diimide derivative

PY^{•+}: Pyrene radical cation

PYP: Pyrene linked with pyridinium moiety

ppm: Parts per million

³PY: Triplet pyrene

Q: Quencher

ROESY: Rotating-frame overhauser effect spectroscopy

Ru: Ruthenium

RC: Reaction center

R: Resistance

s: second

SEM: Scanning electron microscopy

S: Siemen

ΔS : Change in entropy

SCE: Saturated Calomel Electrode

σ : Horizontal conductivity

TEOA: Triethanolamine

TCNQ: Tetracyanoquinodimethane

TTF: Tetrathiofulvalene

TW: Terawatt

TPA: Triphenylamine

THF-d₈: Deuterated tetrahydrofuran

τ : Fluorescence lifetime

θ : Dihedral angle

UV: Ultraviolet

λ_{max} : Wavelength at absorption maxima

V: Voltage

Vis: Visible

YAG: Yttrium aluminium garnet

Cyclodextrin Mediated Donor-Acceptor Self-Assembly for Charge Transfer and Photoinduced Electron Transfer Applications

1.1. Introduction

The incredible elegance and precision that exists in biological systems generated by the assembly of small building blocks have encouraged researchers to emulate nature in designing complex molecular systems.^{1,2} This interest has led to the creation of diverse self-organized materials from abiotic units. In 1987 the Nobel Prize in chemistry was awarded to Lehn, Cram and Pedersen for formal developments in this field through their initial discoveries of host-guest systems. Lehn coined the term “supramolecular chemistry” and defined it as ‘chemistry beyond the molecule’, bearing on the organized entities of higher complexity that result from the association of two or more chemical species held together by intermolecular forces.¹ The intermolecular forces include hydrogen bonding, π - π stacking, metal-ligand co-ordination, host-guest interactions, van der Waals forces, electrostatic, hydrophilic and hydrophobic interactions. These non-covalent interactions are weak and dynamic in nature but they enable the construction of complex supramolecular materials from simple molecules. Supramolecular chemistry has now grown in importance because it goes beyond the molecule promising a fresh interface with the biological and material sciences.³

This thesis deals with functional supramolecular systems constructed using host-guest interaction as the non-covalent assembling motif. We have employed β -

cyclodextrin (β -CD) as the host and adamantane (AD) as the guest. We have attached different chromophores to β -CD as well as AD. Depending on the nature of the chromophores attached, host-guest complexation resulted in the formation of hierarchical assemblies with desirable properties. In Chapter 2 of the thesis we report the synthesis and self-assembly of pyrene-linked β -CD (PYCD) and naphthalene diimide-linked AD (NDIAD). Host-guest complexation in this case is assisted by charge transfer (CT) interaction involving pyrene and naphthalene diimide chromophores. The complex formed further self-assembled into twisted nanofibers. In Chapters 3 and 4 of the thesis we employed pyrene linked to two β -CD groups as the host. In the presence of bis- or tris-AD linked methyl viologen (MV^{2+}) derivatives, the host-guest complexes generated hierarchical assemblies which upon irradiation gave long-lived photoinduced charge separation. In order to place our work in the proper context, some fundamental aspects of cyclodextrins, CT complexation and photoinduced electron transfer (PET) are essential. In this chapter brief descriptions of these topics are presented.

1.2. Structure and Properties of Cyclodextrins

Cyclodextrin (CD) was first discovered by the French chemist Antoine Villier in early 1890's during the enzymatic degradation of carbohydrates.⁴ CDs are a class of water-soluble macrocyclic oligosaccharides with hydrophobic cavities made up of α -D-glucopyranoside units linked through α -1,4-glycosidic linkages with a 4C_1 chair conformation. Based on the number of glucopyranoside units present in the macrocycle, CDs are classified as α -, β - and γ -CDs. These have six, seven and eight D-glucopyranose units, respectively.⁵ Internal diameter of α , β and γ -CDs are 5.7, 7.8 and 9.5 Å,

respectively, with same height of 7.8 Å. A schematic representation of the cyclodextrins along with inner and outer dimensions are presented in Figure 1.1.

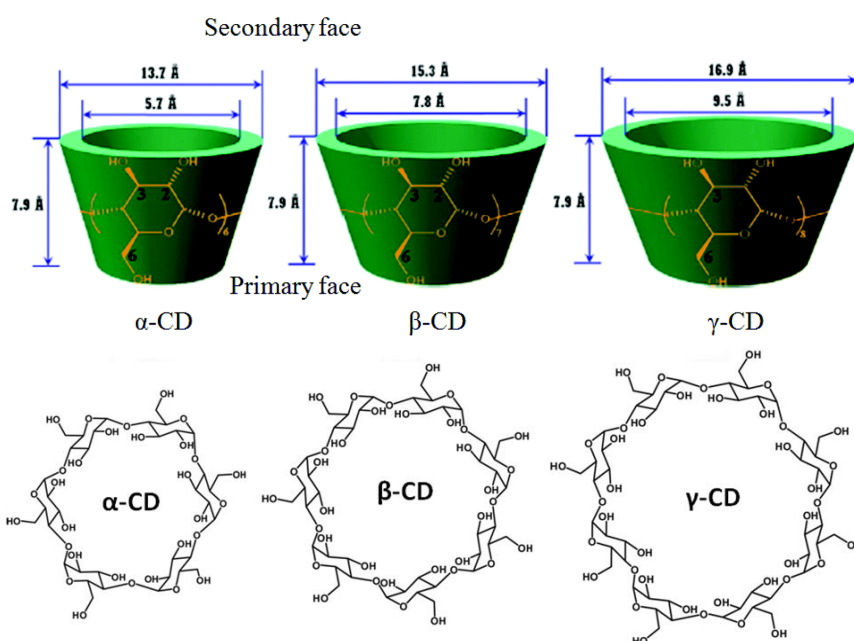


Figure 1.1. Schematic representation of various cyclodextrins with their inner and outer cavity dimensions.

Cyclodextrins have truncated cone structures with a wider rim at one end, narrow rim at the other end and hollow inner cavity of specific volume. The primary hydroxyl groups attached to the C-6 carbon of the glucose monomers are lined along the narrow rim and hence this side is referred to as the primary rim. The secondary hydroxyls attached to the C-2 and C-3 carbons of the glucose monomers are assembled on the wider rim which is referred to as the secondary rim.⁵ The inner CD cavity is lined up with the hydrogen atoms attached to C-3, C-5 and C-6 carbons of glucose units. The OH groups in the wider rim are involved in a H-bonding belt between the C2-OH of one glucopyranose unit with C3-OH of the adjacent unit. Compared to α - and γ -CDs, this H-bonding belt is complete and very rigid in β -CD, which explains its lower solubility in water, compared to the other two. The inner cavity of CDs is lined with the ethereal oxygen with their non-bonding electron pairs directed towards the interior of cavity.⁶

This makes the inner cavity more hydrophobic compared to outside, which is hydrophilic due to the presence of hydroxyl groups. An important property of CDs is their transparency to UV and visible light, which make them very attractive hosts for photochemical reactions.⁵

The CD cavity can encapsulate small molecules as guests. Encapsulation of the guest molecule inside the CD cavity is promoted by the van der Waals forces and hydrophobic interactions.⁷⁻¹¹ Native CDs contain few molecules of water encapsulated within their cavity. Since the interior of the cavity is hydrophobic, the water molecules are considered to be in a 'high energy' state. When a guest is encapsulated within the cavity, the water molecules present in the cavity are released to the outside water pool and this process also constitutes a driving force for guest encapsulation. When a guest is encapsulated in the CD cavity, the process is known as inclusion binding and CD-guest complexes are known as inclusion complexes. Since the CDs are highly water soluble, the inclusion complexes formed from water-insoluble guests are generally water soluble. Most of the industrial applications of CDs, particularly in the drugs and pharmaceutical industry, arise from their ability to solubilize insoluble molecules through inclusion complexation. In general, the guest molecules enter the CD cavity through the wider rim as the free rotation of the primary hydroxyl groups at the narrow rim blocks the guest entrance to the cavity through it.

Stability of inclusion complexes depends on the hydrophobicity and space-filling nature of the guest. A guest which can occupy all the space available within the cavity can displace all the water molecules from the cavity resulting in high stability for the inclusion complex. In this thesis we have used only β -CD for complexation and the best guest molecule for β -CD is adamantane. Several AD derivatives are known to bind to β -

CD with $K_a > 10^4 \text{ M}^{-1}$ and ΔG^0 values close to $-30 \text{ kcal mol}^{-1}$.¹²⁻¹⁴ The adamantane group has a roughly spherical shape with a diameter of $\sim 6.5 \text{ \AA}$ and it perfectly fits the β -CD cavity which has inner diameter of $6.0\text{-}7.8 \text{ \AA}$.^{15, 16} Binding occurs as shown in Figure 1.2.

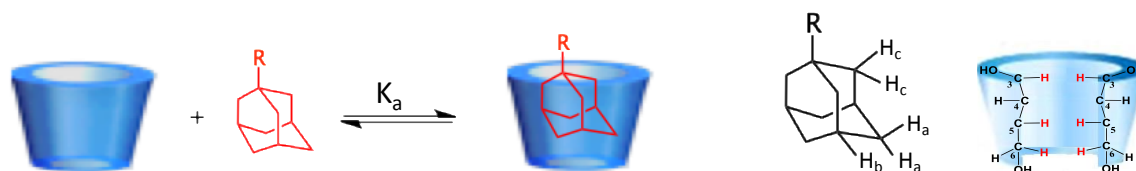


Figure 1.2. Complexation of β -CD with AD derivative.

The complexation can be studied by ^1H NMR and 2D ROESY NMR spectroscopy. Upon inclusion within the CD cavity the AD protons H_a , H_b and H_c undergo significant chemical shift changes along with signal broadening (see Figure 1.2 for labelling of H atoms of AD and β -CD). The β -CD protons, H-3, H-5 and H-6, which are placed inside the cavity, also undergo significant chemical shift changes. In addition, the 2D ROESY NMR will show cross peaks between the CD interior protons and AD protons due to close spatial approach within the cavity. The strong association of AD derivatives with β -CD has been exploited for different purposes by many groups. For example, Harada and co-workers have successfully demonstrated the phenomenon of molecular recognition at macroscopic level using β -CD-AD recognition motif.¹⁷ The β -CD-AD interaction was also effectively utilized to design targeted gene delivery systems for cancer treatment.¹⁸⁻²⁶ Our group has exploited the β -CD-AD interaction to construct supramolecular vesicles capable of drug encapsulation.²⁷ The encapsulated drug could be released using a competitive β -CD binder such as adamantane carboxylate.

1.3. Charge Transfer Complexes

CT complexes, also known as electron donor-acceptor (EDA) complexes arise by the interaction of a donor (D) molecule with an acceptor (A) molecule, resulting in the transfer of a fraction of electronic charge from D to A. The CT interaction can be intermolecular or intramolecular. Generally, the CT interactions are very weak and the enthalpy changes associated with these interactions are only in the range of 0-4 kcal mol⁻¹. A characteristic feature or signature of CT complexes is the presence of CT absorption band that usually appear in the visible region of the electromagnetic spectrum. Since the absorption is in the visible region, CT complexes are generally colored. As the interactions are weak, the color will be observed only at moderately high concentrations of D and/or A. The CT band arises due to the transfer of charge from the highest occupied molecular orbital (HOMO) of D to the lowest unoccupied molecular orbital (LUMO) of A. The degree of charge transfer from D to A can vary from zero to complete electron transfer. Over the last 50 years, large numbers of CT systems were studied. Structures of donor and acceptor molecules commonly employed in these studies are collected in Figure 1.3.^{28, 29}

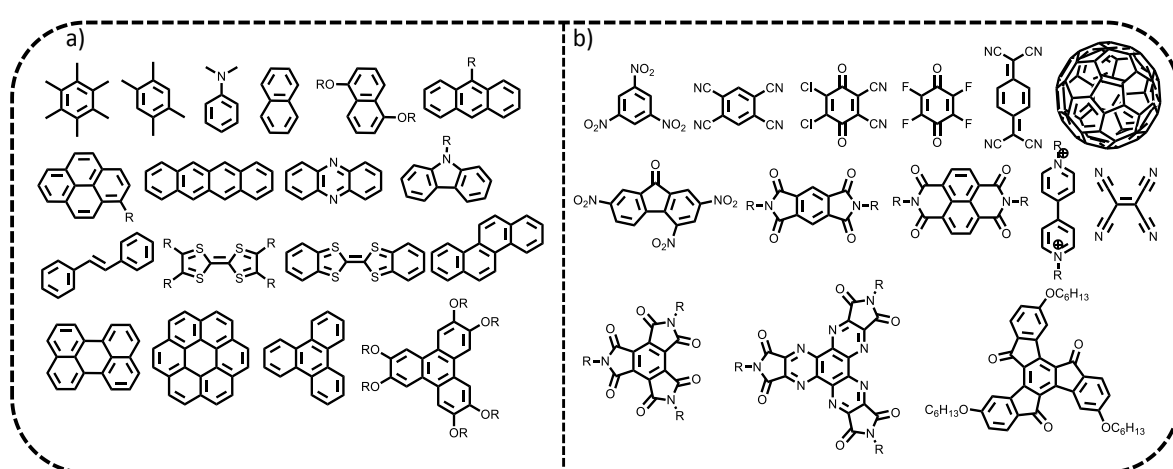
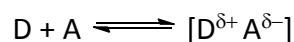


Figure 1.3. Structures of commonly used a) electron donors and b) electron acceptors in CT interaction studies.

1.3.1. Mulliken's theory

Consider the formation of a weak CT complex upon mixing D and A.



Mulliken has proposed that the wave function $\Psi_N(D,A)$ for the ground state of this weak interaction can be approximately represented by the expression.³⁰

$$\Psi_N(D,A) = a\Psi_0(D,A) + b\Psi_1(D^+A^-)$$

where a and b are coefficients, Ψ_0 is the wave function for the non-ionic (or no-bond state) and Ψ_1 is the wave function for the ionic state corresponding to complete transfer of electron from D to A. In complexes, where the interactions are weak, the non-ionic state will be predominant and hence $a \gg b$. Similarly, the wave function for the excited state $\Psi_E(D,A)$ can be represented by the expression

$$\Psi_E(D,A) = a^*\Psi_1(D^+A^-) - b^*\Psi_0(D,A)$$

Where $a \approx a^*$ and $b \approx b^*$. The optical absorption of the D-A complex results from the transition $\Psi_N \rightarrow \Psi_E$. Substantial overlap of the HOMO of D with LUMO of A is necessary to get a significant contribution from the ionic state. In addition, the D and A has to orient in such a way to get maximum orbital overlap. Based on quantum mechanical treatment, it has been argued that the complex exists as a resonance hybrid between the non-ionic state (D,A) and ionic state ($D^{\delta+} \dots A^{\delta-}$). Energy characteristics of the CT state largely depends on the ionization potential of D, electron affinity of A and electrostatic reorganisation energy.

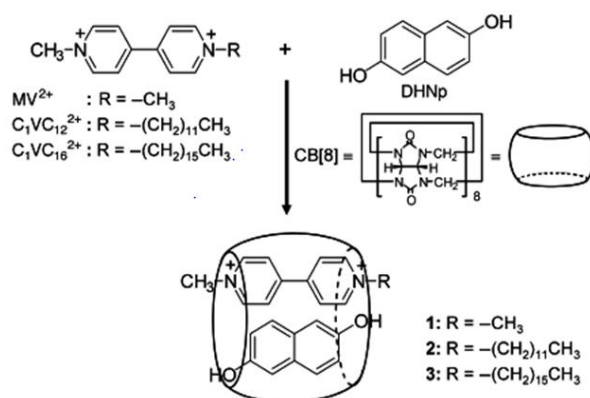
1.3.2. CT interaction assisted by encapsulation

Although CT interactions are very weak in nature, it can be amplified by synergizing it with other weak interaction such as H-bonding, π -stacking, hydrophobic interactions, host-guest interactions etc. Using CT interactions in conjunction with other non-covalent forces, large numbers of supramolecular architectures such as fibers, nanotubes, polymers, foldamers, micelles, vesicles etc. have been constructed.³¹⁻⁴⁰ Since the underlining theme of this thesis is inclusion binding, few examples of CT interactions synergized by inclusion binding are presented in this section.

Cucurbit[n]urils (CB[n]) are widely used macrocyclic host molecules made up of 'n' glycoluril monomers linked by methylene bridges. CB[n]s allow hydrophobic interaction due to the cavity and electrostatic interaction due to the polar carbonyl groups that line the ends of the cavity. CB[n]s act as ideal hosts for a variety of guest molecules and exhibit high selectivity and strong binding affinity towards cationic guest molecules.

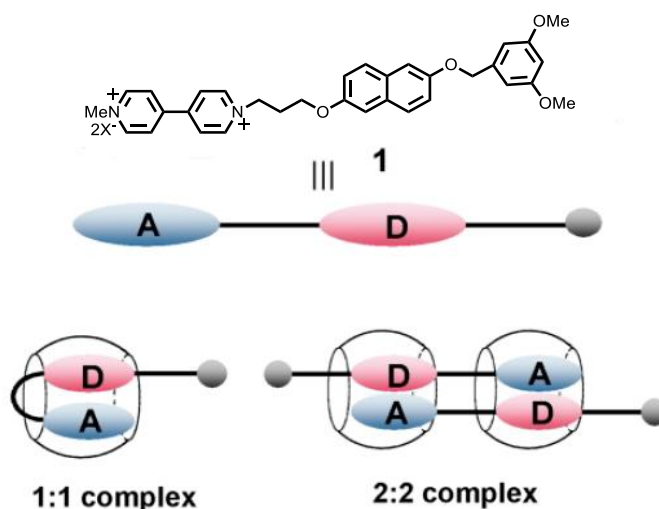
Kim and co-workers have carried out pioneering work in the area of host assisted inter and intramolecular CT interaction to build supramolecular assemblies like molecular necklaces,⁴¹ vesicles,⁴² molecular machines,⁴³ rotaxane dendrimers⁴⁴ etc. using CB[8]. The group has shown that CB[8] has a cavity comparable to that of γ -CD and forms stable 1:1:1 ternary inclusion complexes with methyl viologen (MV^{2+}) and 2,6-dihydroxynaphthalene (DHNp) as shown in Scheme 1.1.⁴⁵ When the viologen molecules are substituted with long alkyl chains the ternary inclusion complexes spontaneously formed giant vesicles that behave like a large supramolecular amphiphile.⁴² Since both DHNp and MV^{2+} are redox active, these vesicles can be easily disrupted by redox

processes. Oxidation of DHNp or reduction of MV^{2+} would disrupt CT complexation and lead to collapse of the vesicle. The authors have used ceric ammonium nitrate to oxidize DHNp to naphthaquinone, which led to disappearance of the CT band and collapse of the vesicles.



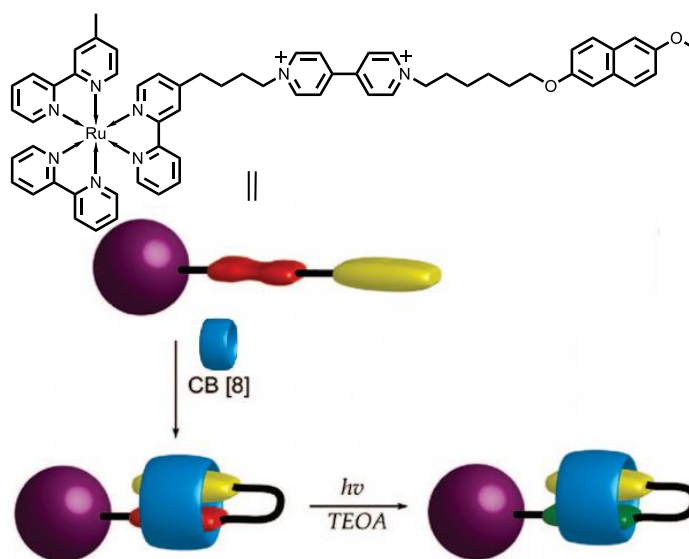
Scheme 1.1. Schematic representation of the formation of the stable ternary complexes.

In a subsequent work, the authors modified the CT system by covalently linking DHNp and MV^{2+} through a three carbon chain and studied the intramolecular CT complex formation induced by inclusion in CB[8].⁴⁶ The linked system could undergo intramolecular or intermolecular complexation as shown in Scheme 1.2. They observed that only the intramolecular 1:1 CT complex is formed which involved backfolding of the linked system as in Scheme 1.2.



Scheme 1.2. Schematic representation of possible CT interaction inside CB[8].

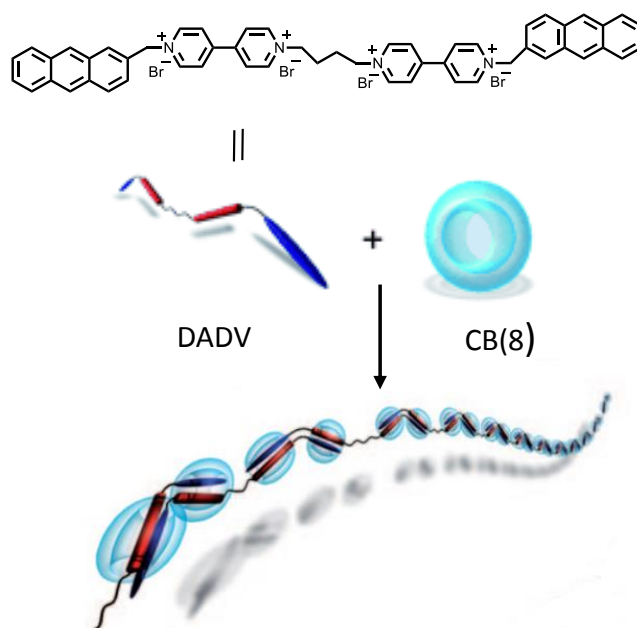
Zou *et al.* have studied the complexation of the molecular triad tris(bipyridyl)ruthenium-viologen-naphthol (Ru-MV²⁺-Np) with CB[8].⁴⁷ Ru-MV²⁺-Np and CB[8] forms a stable 1:1 inclusion complex in which the Np group is back-folded and insert into the cavity together with MV²⁺ (Scheme 1.3). The authors also studied complexation of Ru-MV²⁺-Np with β -CD and found that the molecule binds better with CB[8]. Up on irradiating the Ru(II) chromophore, PET occurs to generate the viologen radical cation and Ru(III). When the irradiation is performed in the presence of the sacrificial electron donor triethanolamine (TEOA), the Ru(III) formed is converted back to Ru(II), which prevents charge recombination and stabilizes the viologen radical cation which remains inside the cavity along with Np.



Scheme 1.3. Inclusion complexation of Ru²⁺-MV²⁺-Np with CB[8].

Zhang and co-workers synthesized a dianthracene-diviologen (DADV) molecule by linking anthracene groups at the ends of a linked bis-viologen molecule.⁴⁸ When dissolved in water in the presence of CB[8], multiple host-stabilized charge transfer (HSCT) interaction between anthracene and viologen take place as shown in Scheme 1.4, leading to formation of a supramolecular polymer. They observed formation of a deep

purple supramolecular polymer gel upon increasing the DADV concentration to 4 mM and CB[8] concentration to 8 mM.



Scheme 1.4. Schematic representation of supramolecular polymer formation from DADV/CB[8] system.

Mulliken's theory suggests a simple dependence of CT absorption maximum on the ionization potential of D, the electron affinity of A, and an electrostatic reorganization energy J . Since the ionization potential is related to $E_{\text{HOMO(D)}}$ and electron affinity is related to $E_{\text{LUMO(A)}}$, the Mulliken's theory can be written as:

$$E_{\text{CT}(\lambda_{\text{max}})} = E_{\text{HOMO(D)}} - E_{\text{LUMO(A)}} + J$$

Where $E_{\text{CT}(\lambda_{\text{max}})}$ is the energy level of the CT absorption maximum (\propto to $1/\lambda_{\text{max}}$). Since J cannot be directly measured or calculated, it is generally assumed that for a series of similar D and similar A molecules, J is constant. Experimental verification of this equation is difficult because of the very low binding strength of the CT complex and the very small specific absorbance of the CT band. In order to observe the CT band clearly, very high concentrations of D and/or A have to be used. At this concentration, D-D and A-A interactions may occur and complicate the analysis of the data. Additionally, different D-

A geometries such as face-to-face or T-shaped stacking can be present which create additional drawbacks for theoretical modelling of the data. Biedermann and Scherman found that use of CB[8] as a host for CT complex formation can eliminate most of the problems.⁴⁹ They found that 2,6-dihydroxynaphthalene as donor and methyl viologen as acceptor (Figure 1.4) form stable CT complexes within CB[8] in aqueous environments. The CT complexes are formed at very low concentrations. D-D or A-A interactions are not significant at the low concentrations and only face-to-face π - π stacking takes place within CB[8]. The authors observed good proportionality between $E_{CT(\lambda_{max})}$ and $E_{HOMO(D)}$ as well as $E_{LUMO(A)}$, in good agreement with the classical CT model of Mulliken. They found that the CT interaction energy did not contribute much to ΔG^0 for ternary complexation. The well defined face-to-face stacking geometry of the D-A pair as well as the high binding affinity to each other in the presence of CB[8] are the major contributing factors.

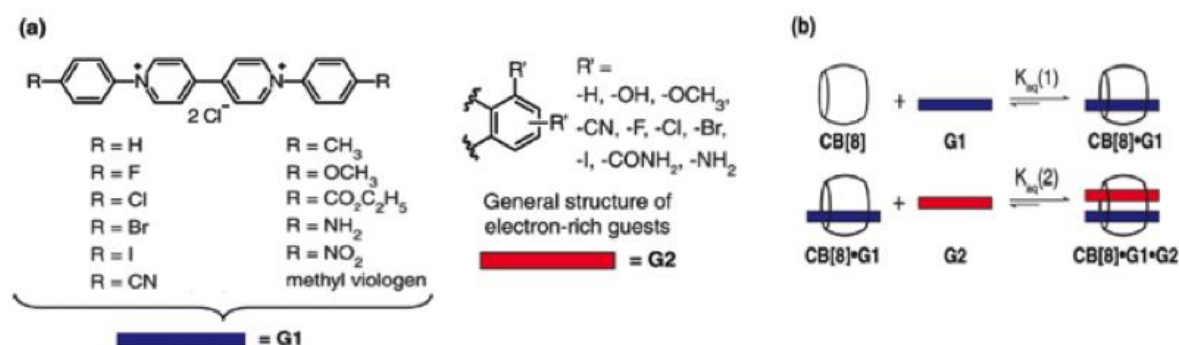


Figure 1.4. a) Chemical structures of several derivatives of D and A used and b) Stepwise formation of ternary complexes.

As is evident from the studies mentioned earlier, HSCT complexation inside CB[8] is widely used to build supramolecular structures. High stability for HSCT interaction is taken for granted in these studies. Recently Ji *et al.* have shown that HSCT interactions can be weakened by external factors.⁵⁰ They have prepared poly(N-isopropylacrylamide) (PNIPAM) having naphthalene (Np) groups at both ends. When the polymer is dissolved

in water in the presence of CB[8] and a dimeric viologen, cyclic polymers are formed by joining the polymer ends through HSCT interactions involving the Np end groups, viologen and CB[8] as shown in Figure 1.5a. The authors found that the cyclic polymer can undergo heat induced self-assembly to form aggregates. When the aggregates are formed, the interior of the polymeric structure became highly hydrophobic, which weakens the HSCT interaction and releases the CB[8] with included dimeric viologen (Figure 1.5b). The HSCT dissociation was driven by the incompatibility of the cationic HSCT complex within the hydrophobic environment of the PNIPAM aggregate. This study showed that the HSCT interaction leading to formation of 1:1:1 ternary complexes, is not stable under all conditions.

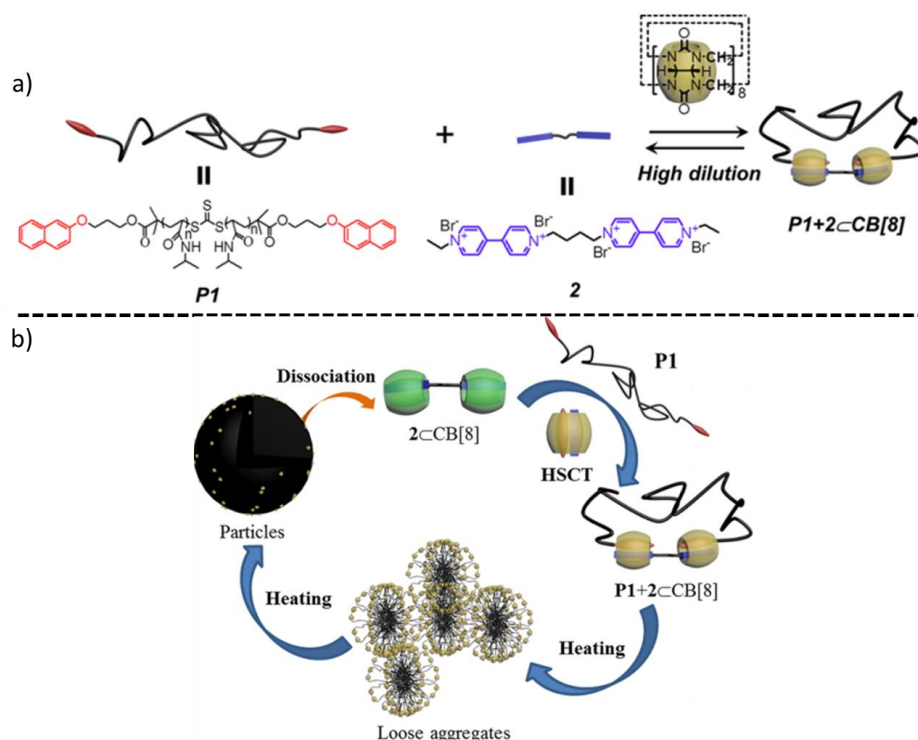
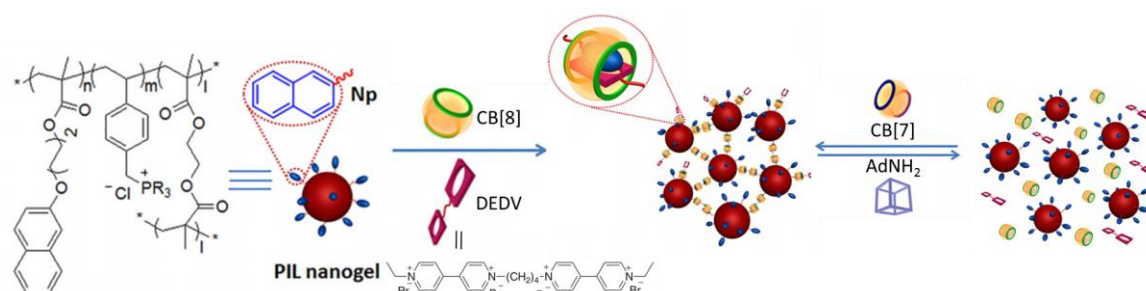


Figure 1.5. Schematic representation of a) cyclic polymer formation and b) formation of aggregates and release of viologen encapsulated CB[8].

Recently Tang *et al.* synthesized and studied supramolecular assembly of naphthyl (Np) functionalized poly(ionic liquid) [PIL] based nanogels through the HSCT interaction.⁵¹ The nanogel particles have Np groups on the outside which can undergo

HSCT with CB[8] and viologen derivatives. The authors employed the bisviologen compound DEDV. Upon addition of DEDV and two equivalents of CB[8], HSCT interactions occur as shown in Scheme 1.5, which brings together the particles to form a supramolecular gel network. They observed that HSCT complex dissociates and gel disintegrates upon addition of the competitive guest amantadine (AdNH_2), which has better affinity toward CB[8] than Np and form the stable CB[8]- AdNH_2 complex. Since AdNH_2 has better affinity for CB[7] than CB[8], addition of CB[7] leads to dissociation of CB[8]- AdNH_2 and formation of CB[7]- AdNH_2 . The CB[8] liberated in this way again undergo HSCT with Np and DEDV and regenerates the supramolecular gel network. (Scheme 1.5).



Scheme 1.5. Schematic representation of HSCT complex formation and dissociation.

For the past few years, our research group was involved in the study of CT interactions in native as well as functionalized β -CD based D-A systems.^{52,53} The donor chromophore employed is pyrene (PY) and the acceptor is pyromellitic diimide (PI) in these studies. The molecules employed are shown in Figure 1.6. The pyridinium groups attached to PI in these cases are to make them water soluble.

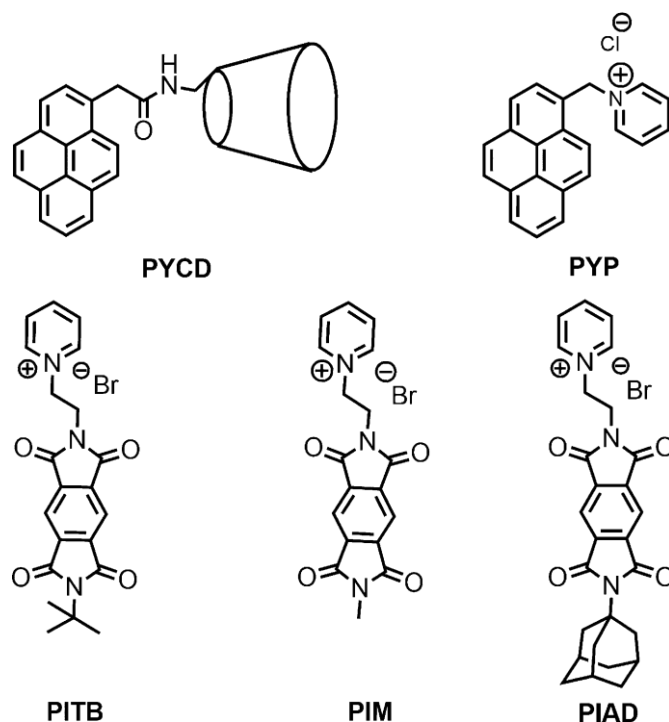


Figure 1.6. Structures of donors (PYCD, PYP) and acceptors (PITB, PIM, PIAD) employed in our previous study.

The CT interaction between PY and PI is augmented by β -CD-PI binding interactions in these cases. When the alkyl group is AD as in PIAD, a 1:1 complex was formed with a very high association constant ($K_a = 1.82 \times 10^6 \text{ M}^{-1}$). In this case the CT interaction is reinforced by inclusion binding of the AD group in the β -CD cavity leading to the formation of 2D sheets, which undergo twisting to give twisted fibres. When the alkyl group is tert-butyl, a 1:2 complex was formed with a high association constant ($K_a = 2.91 \times 10^4 \text{ M}^{-1}$). A detailed analysis showed that the tert-butyl PI undergoes both inclusion and rim-binding interactions with the β -CD. The charge-transfer complex further self-assembled into chiral nanostructures in this case also. In the case of N-methyl PI, the interaction with β -CD-linked PY was only through rim binding, which resulted in the formation of a weak charge-transfer complex with $K_a = 4.2 \times 10^3 \text{ M}^{-1}$. Formation of a hierarchical assembly was not observed in this case. We have also studied the CT complexation of all these PI derivatives with PYP (Figure 1.6) which does

not have β -CD group. Our studies showed that the CT interactions are weak in these cases.

1.3.3. Charge transfer complexes in organic electronics

CT complexes are expected to be good candidates for electronic applications.^{54,55} Studies in this direction were initiated by the discovery of electrical conductivity similar to metallic conductors in the crystals of tetracyanoquinodimethane (TCNQ) - tetrathiofulvalene (TTF) CT complex by Coleman *et al.* in 1973.⁵⁶ Structures of these molecules are given in Figure 1.7. In the TCNQ-TTF CT crystal, TCNQ and TTF molecules are arranged independently in separate parallel stacks. Electron transfer occurs from TTF stack to TCNQ stack. The electrons and holes concentrated in the stacks traverse in a one-dimensional direction along the TCNQ and TTF columns, respectively, when an electrical potential is applied to the ends of the crystal in the stack direction. Recent studies are aimed at developing CT complexes with technologically advanced properties useful for ambipolar transport, ferroelectricity, photoconductivity and organic field effect transistors applications.⁵⁷⁻⁶²

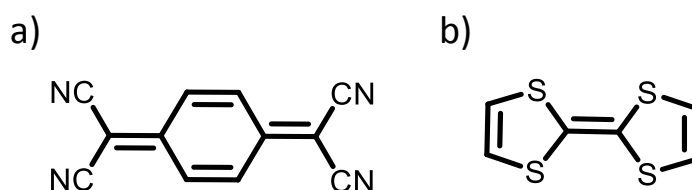


Figure 1.7. Structures of a) TCNQ and b) TTF.

Pan and co-workers reported the CT complex dibenzotetrathiafulvalene - tetracyanoquinodimethane (DBTTF-TCNQ, see Figure 1.7 for structure) as a potential candidate for ambipolar semiconductor applications. The authors prepared co-crystal microrods of DBTTF-TCNQ with mixed stack structure via solution processing. The prepared microrods were directly used to fabricate prototype devices. The device

demonstrated ambipolar charge transporting behavior with electron mobility of $0.13 \text{ cm}^2\text{V}^{-1}\text{s}^{-1}$ and hole mobility of $0.04 \text{ cm}^2\text{V}^{-1}\text{s}^{-1}$.⁶³ Recently Torrent and co-workers developed ambipolar field effect transistor using solution processed thin films of DBTTF-TCNQ CT complex.⁶⁴ They blended the CT complex with polystyrene to improve the film stability, reproducibility and film processability (Figure 1.8). The fabricated thin film device exhibited air stability along with ambipolar OFET behavior with average electron mobility $0.6 \times 10^{-4} \text{ cm}^2\text{V}^{-1}\text{s}^{-1}$ and hole mobility $2.7 \times 10^{-4} \text{ cm}^2\text{V}^{-1}\text{s}^{-1}$. This work has opened a new paradigm for fabrication of high throughput printed OFET devices and work in this direction has already appeared in the literature.^{65,66}

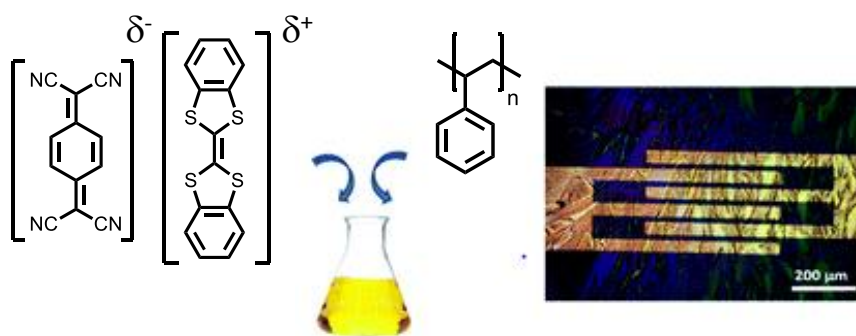


Figure 1.8. Ambipolar field effect transistor device fabricated using DBTTF-TCNQ CT complex blended with polystyrene.

Several CT crystals have a mixed stack arrangement in which the D and A chromophores are arranged in an alternating fashion. In these crystals a collective transfer of electrons from D to A molecules results in the formation of dipoles that can be realigned by the application of an external field. Such materials will have applications as ferroelectric capacitor, ferroelectric random access memory devices, sensors etc.⁶⁷ Tayi and co-workers have developed a supramolecularly self-assembled mixed stack CT system for room temperature ferroelectric applications.⁶⁸ They utilized pyromellitic diimide as acceptor and derivatives of naphthalene, pyrene and tetrathiafulvalene as donors (see Figure 1.9 for structures). The D and A molecules crystallize in a mixed stack

and this arrangement is stabilized by hydrogen bonding, van der Waals forces and π - π stacking in addition to CT interaction. The authors refer to this modular design as lock arm supramolecular ordering (LASO). These self-assembled mixed stack donor-acceptor network exhibit room temperature ferroelectricity with appreciable remnant polarization.

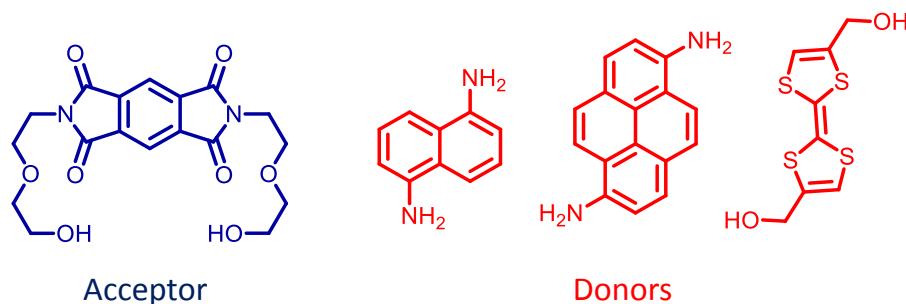


Figure 1.9. Structures of D and A that form LASO stacks.

Govindaraju and co-workers fabricated a solution-processable thin film ferroelectric capacitor using multi stimuli responsive chiral mixed stack CT hydrogels (Figure 1.10).⁶⁹ They employed a dipyrrene tweezer as donor and alanine methyl ester functionalized naphthalenediimide as acceptor. CT complex formed in this case is stabilized further by tweezer inclusion sandwich process and H-bonding interactions. Ferroelectric device fabricated using the CT complex exhibited appreciable room temperature remnant polarization of $4 \mu\text{C}/\text{cm}^2$.

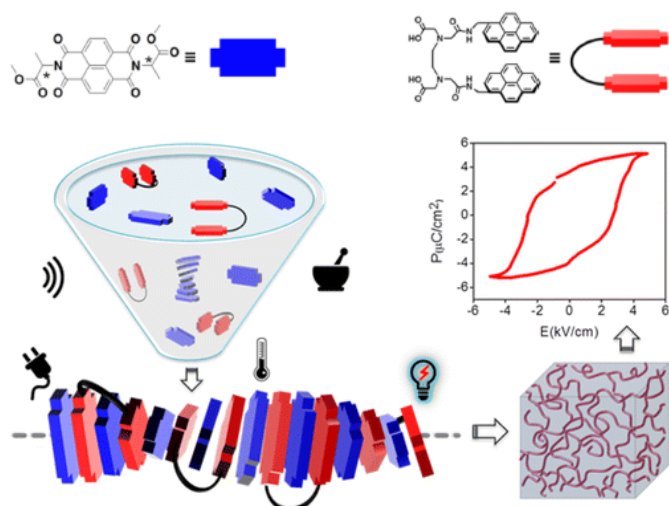


Figure 1.10. Pictorial representation of the CT self-assembly through tweezer inclusion sandwich process supported with hydrogen bonding interactions.

1.4. Natural and Artificial Photosynthesis

Most of the energy that we are using comes from fossil fuels. Combustion of fossil fuels such as coal and petroleum will lead to the formation of carbon dioxide, which is one of the major greenhouse gases causing climate change. Also, the amount of fossil fuels on earth is limited. Hence it is important to have clean and renewable methods for generating and storing energy. Sun, the primary energy source of our planet continuously generates 120,000 TW of electromagnetic energy. Harvesting of 0.1% of this energy would be sufficient to meet our everyday needs, and several ideas have been floated from time to time to achieve this dream. Solar energy driven chemical processes that can lead to the generation of hydrogen is an excellent way of solving the energy and pollution issues.^{70,71}

Natural photosynthesis is an excellent example of harvesting solar energy. Researchers are trying to mimic natural photosynthetic processes through artificial photosynthetic systems. Artificial photosynthesis, broadly defined, is any attempt to mimic aspects of photosynthetic energy conversion by photochemical processes in

laboratory-made systems. The basis of artificial photosynthesis is to learn from the natural photosynthetic process to design systems capable of producing energy or fuels.

In the photosynthetic reaction center, light is absorbed by a chromophore which initiates the series of energy and electron transfer processes between the donor and acceptors that are placed at specific distances and orientations relative to one another by the surrounding protein matrix. In green or purple bacteria, only one photosynthetic unit (PS II) carry out the light-to-chemical products conversion whereas the green plants have two photosynthetic units (PS I and PS II).⁷² The purple bacterial reaction centre (RC) remains as the best 'model system' for mimicking photosynthesis.⁷³ X-ray structures of the purple bacterium *Rhodospseudomonas viridis* shows four bacteriochlorophyll (B_A) molecules (two of which make up a "special pair", D), two bacteriopheophytin ($\phi_{A/B}$) molecules, two quinone ($Q_{A/B}$) molecules, and one non-heme iron atom as shown in Figure 1.11. These are arranged in pairs with approximate C_2 symmetry. Left and right side of the C_2 axis is denoted as A and B side, respectively. The bacterial RC only utilizes the A-side cofactors for electron transfer.⁷⁴ Among the four $B_{A/B}$ molecules two are electronically coupled and held very closely. This is termed as 'special pair' and it act as the donor. Photosynthetic process in purple bacteria is initiated by excitation transfer from antenna to this special pair to get singlet excited special pair. Thereafter a series of electron transfer takes place as shown in Scheme 1.6, which also gives the rates of forward and back electron transfers at every step.

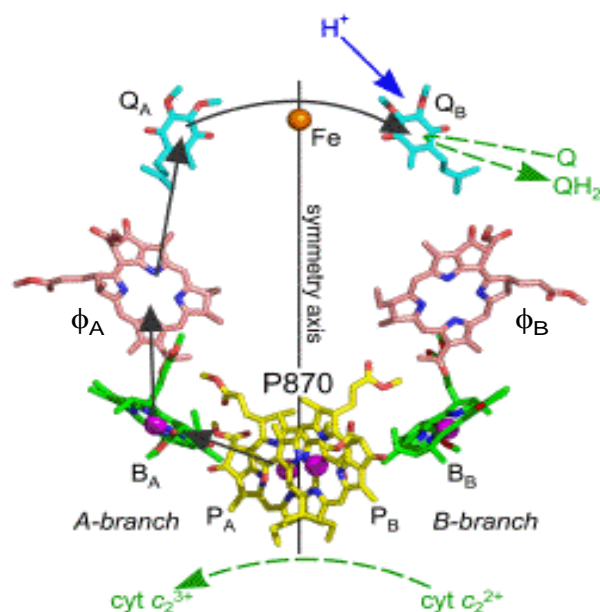
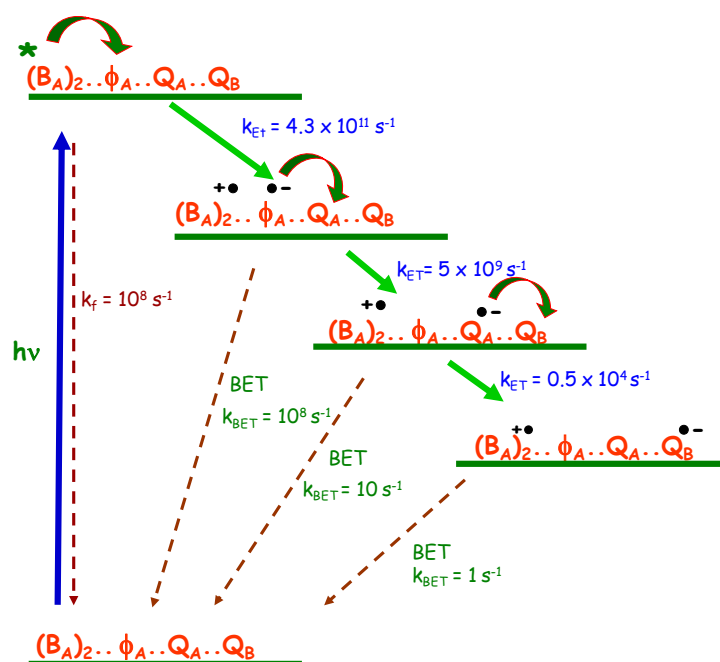


Figure 1.11. Photosynthetic unit of purple bacteria.

Initially electron is transferred from $^*(B_A)_2$ to ϕ_A through B_A forming radical cation of special pair and radical anion of ϕ_A within 3 ps. The electron then moves to ubiquinone Q_A in ~ 200 ps forming $(B_A)_2^{\bullet+}-\phi_A-Q_A^{\bullet-}$. The electron is subsequently transferred to Q_B in ~ 200 μ s. The positive charge remaining on the special pair, is quenched by an electron transfer from the iron porphyrin situated on the outer side of the membrane. After a two-electron, two-proton reduction, Q_BH_2 is released from the RC. The releasing of the quinol protons into the periplasm is followed by the oxidation of the free hydroquinone by cytochrome bc_1 complex. A transmembrane proton gradient is created and that is utilized for ATP synthesis. The net result of the multistep electron transfer in bacterial photosynthetic system is the charge separated (CS) state with quantum yield of near unity. The high degree of organization of the donors and acceptors in the RC leads to the extremely high quantum yield of the PET processes in the natural systems.



Scheme 1.6. Schematic representation of PET in bacterial photosynthetic system.

Several important light-induced processes such as artificial photosynthesis, photovoltaics and photocatalysis rely on the generation of long-lived CS state in D-A systems. The fundamental process in all these cases is a PET reaction that transfers an electron from D to A. In most cases of PET, the transferred electron goes back to D in a process known as charge recombination (CR) or back electron transfer (BET), resulting in very short-lived CS state. Generation of long-lived CS state has thus become an important goal in the study of PET. The reaction center in photosynthetic bacteria provided the best example of long-lived photoinduced CS state. Large numbers of molecular systems were designed drawing inspiration from the structure and properties of the bacterial reaction center. The molecular systems generally featured covalently linked D and A suitably placed for sequential electron transfer, but none of them exhibited the quantum yield and long-lifetime of the CS state in the bacterial reaction center.⁷⁵⁻⁸⁰ A few examples are given in Figure 1.12.

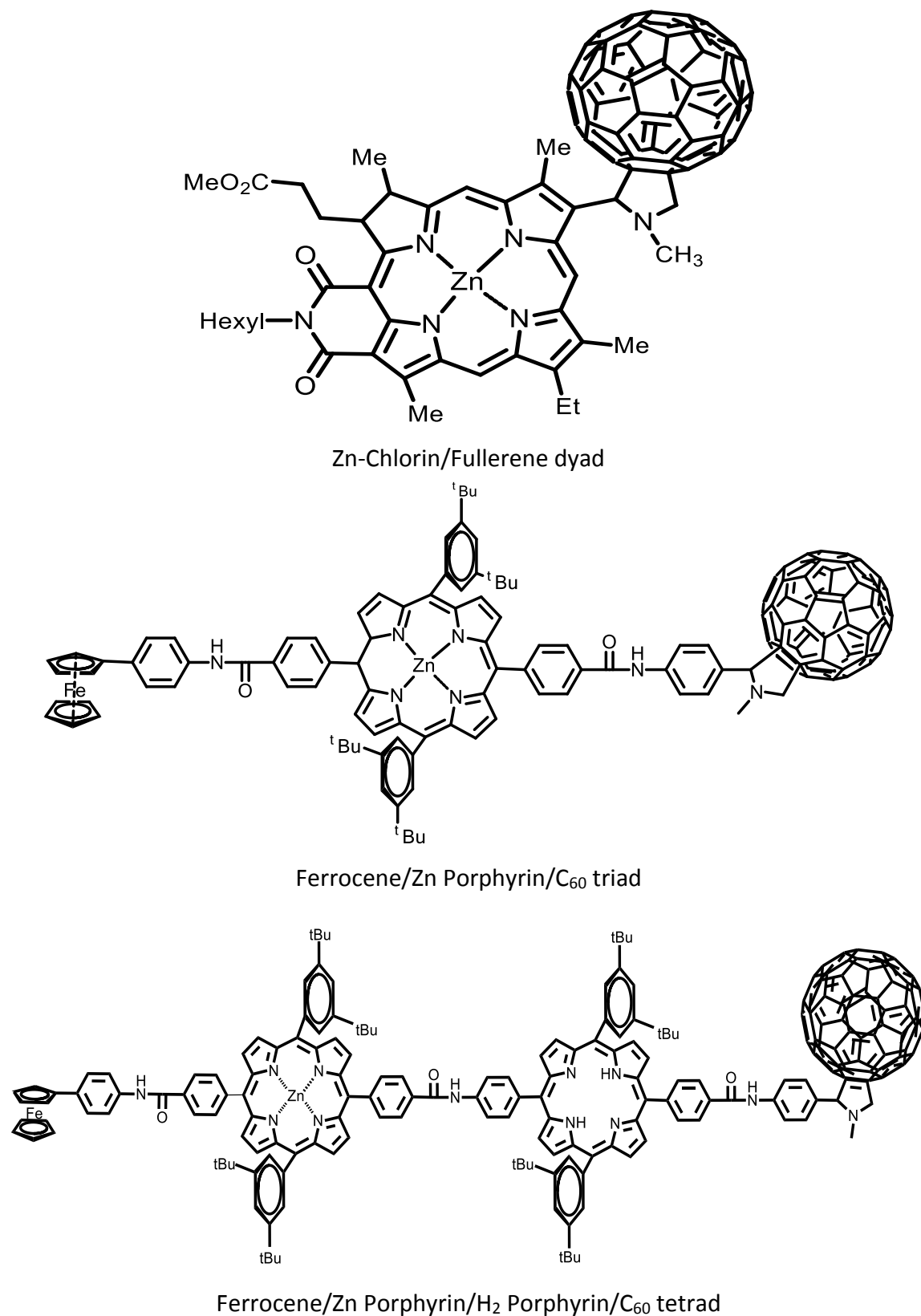


Figure 1.12. Examples of covalently-linked dyad, triad and tetrad.

In the bacterial reaction center the donors and acceptors are not covalently linked, but are disposed non-covalently at specific locations. In an attempt to emulate PET in the bacterial reaction center, large numbers of non-covalently assembled D-A systems were studied. Although the systems assembled include dyads, triads and tetrads, the non-covalent assembly is invoked only in one step and hence the synthetic efforts in preparing these are similar to covalently linked systems. CS state lifetimes measured in most of these systems are less than a few ns. A couple of examples are presented below.

Guildi and co-workers assembled a ZnPc/C₆₀ non-covalent dyad through metal-ligand coordination involving ZnPc and pyridine-linked fulleropyrrolidine as shown in Figure 1.13.⁸¹ Analysis by Jobs plot established formation of a 1:1 complex. Using fluorescence quenching experiments, K_a for complex formation was determined as $1.26 \times 10^6 \text{ M}^{-1}$. Excitation of the complex with 676 nm laser led to formation of the CS state with absorptions corresponding to ZnPc^{•+} at 540, 720 and 850 nm and C₆₀^{•-} at 1024 nm. The CS state lifetime measured was $9 \pm 0.5 \text{ ns}$.

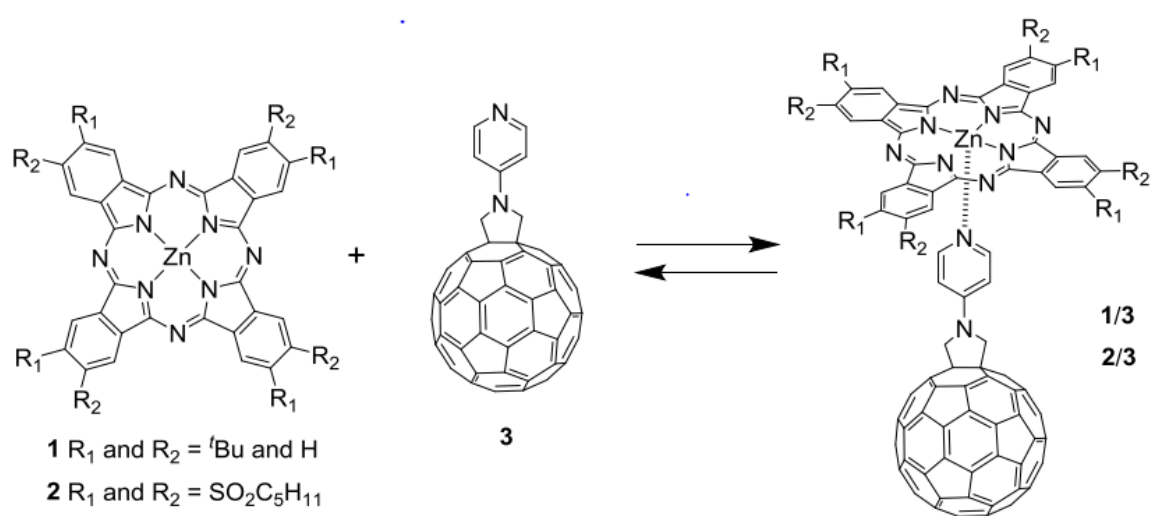


Figure 1.13. Formation of ZnPc/C₆₀ complex through metal-ligand coordination.

D'Souza and co-workers assembled a non-covalent D-A system capable of undergoing ultrafast energy and electron transfer reactions.⁸² In this system a covalently linked triad consisting of triphenylamine (TPA), boron dipyrin (BDP) and zinc porphyrin (ZnP) was linked to imidazole-functionalized C₆₀, which acts as the electron acceptor, through metal-ligand complexation (Figure 1.14). Excitation of TPA leads to ultrafast energy transfer as shown to generate ZnP excited state, which then transfers an electron to C₆₀. k_{CS} and k_{CR} were evaluated in TPA-BDP-ZnP-C₆₀Im by monitoring the rise and decay of the C₆₀Im* at 1000 nm. The calculated values were $k_{CS} = 5 \times 10^9 \text{ s}^{-1}$ and $k_{CR} = 2.10 \times 10^8 \text{ s}^{-1}$. CS state lifetime obtained was 4.1 ns in this case.

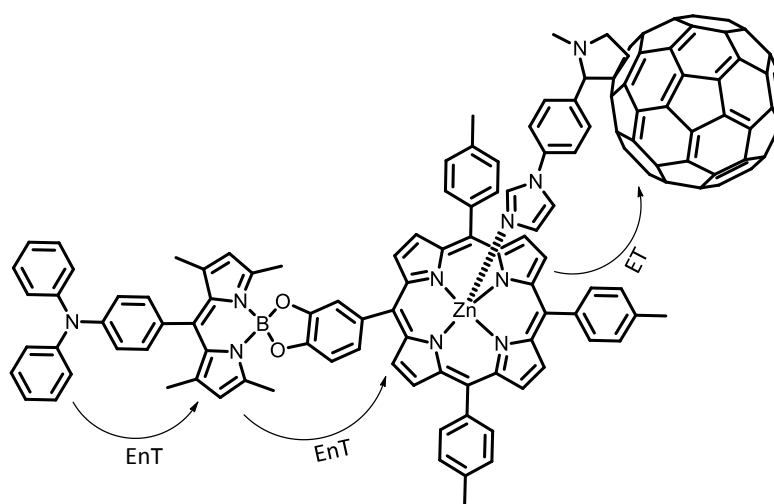


Figure 1.14. Structure of TPA-BDP-ZnP-C₆₀Im.

Guildi and co-workers documented the use of two complementary supramolecular motifs, namely multi-point H-bonding and metal-ligand complexation to assemble the non-covalent system in Figure 1.15.⁸³ Time resolved experiments revealed that excitation of the perylenediimide chromophore results in energy transfer to the metalloporphyrin in $53 \pm 3 \text{ ps}$. An electron transfer then occurred from the excited ZnP to the C₆₀ in $12 \pm 1 \text{ ps}$. The resulting CS state exhibited a lifetime of only $3.8 \pm 0.2 \text{ ns}$. All

these studies suggested that ultra-long lifetime for the CS state as observed in the bacterial RC cannot be achieved in covalently or non-covalently linked polyads.

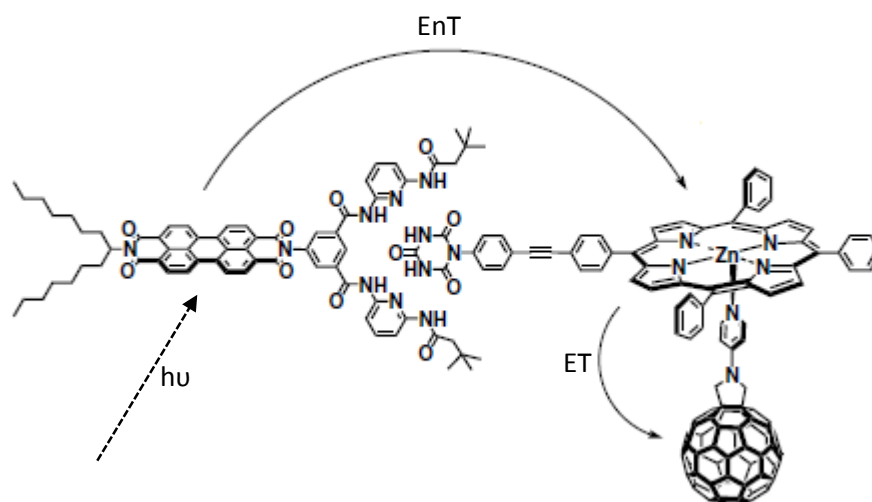


Figure 1.15. Supramolecular triad assembled using two non-covalent motifs.

Few reports have shown that CS state lifetimes of covalently linked D-A systems are enhanced when subjected to spatial confinement. Kimoto *et al.* have shown that the CS state lifetime in triphenylamine-naphthalenediimide dyads having oligo(phenyleneethynylene) linker got enhanced from a few nanoseconds to few milliseconds when dispersed in polymer matrices.⁸⁴ Imahori and co-workers have shown that ferrocene-porphyrin-fullerene triads containing cation moieties undergo aggregation in cell-membrane-like lipid bilayers which result in several fold enhancement in the CS state lifetime and quantum yield.⁸⁵ Jin *et al.* have shown that covalent organic frameworks containing ordered D on D and A on A π -columnar stacks sustained photoinduced CS state for few microseconds.⁸⁶ Hariharan and co-workers have prepared a directly linked naphthalene-naphthalimide dyad wherein the D and A segments are in near orthogonal conformation as shown in Figure 1.16. In acetonitrile the dyad exists as monomer and exhibited CS state lifetime of 110 ps, whereas in

chloroform it existed as aggregates in which the CS state exhibited 10,000-fold enhancement in lifetime.⁸⁷

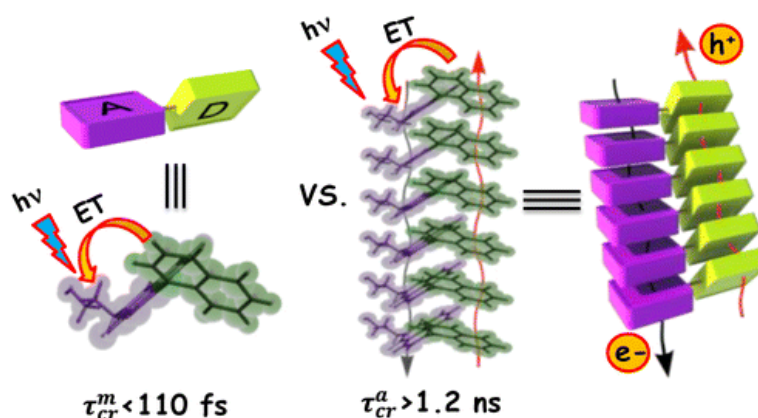


Figure 1.16. Schematic representation showing photoexcitation of non-parallel stacked naphthalene-naphthalimide D-A system.

Subsequently the authors have prepared triphenylamine-naphthalimide dyads which existed as monomeric species in acetonitrile, but formed spherical/vesicular aggregates in THF. The CS state lifetime enhanced from 110 fs in the monomeric state to 2.67 ns in the vesicular aggregate.⁸⁸ All these strategies pertain to specific situations and cannot be employed as general strategies to enhance CS state lifetime.

1.4.1. PET in CD based supramolecular systems

CDs can be used as a vehicle to carry out PET reactions in aqueous media and large number of examples are available in the literature.⁸⁹⁻⁹³ The general strategy employed in all these studies is to link one of the electron transfer partners to the primary or secondary rim of the CD and then assemble the other component through encapsulation in the CD cavity. Steady-state and time-resolved fluorescence measurements were then carried out to obtain the PET rates in these systems. Laser flash photolysis experiments to characterize the radical ions formed in the PET reactions and estimate the CS state lifetimes were carried out only in very few cases.

Our own group has reported the self-assembly of a β -CD-based supramolecular dyad in which the donor anthracene (AN) moiety is covalently linked to the smaller rim of the CD and the acceptor pyromellitic diimide (PMDI) is encapsulated within the CD cavity (Figure 1.17). We observed that at higher concentrations of PMDI, the equilibrium is largely in favour of the supramolecular dyad and intra-ensemble PET occur with $k_{CS} = 2.5 \times 10^8 \text{ s}^{-1}$ and quantum yield (Φ_{PET}) = 0.72. We observed that about 8% of the CS state was long-lived and survived for more than 200 μs .⁹⁴

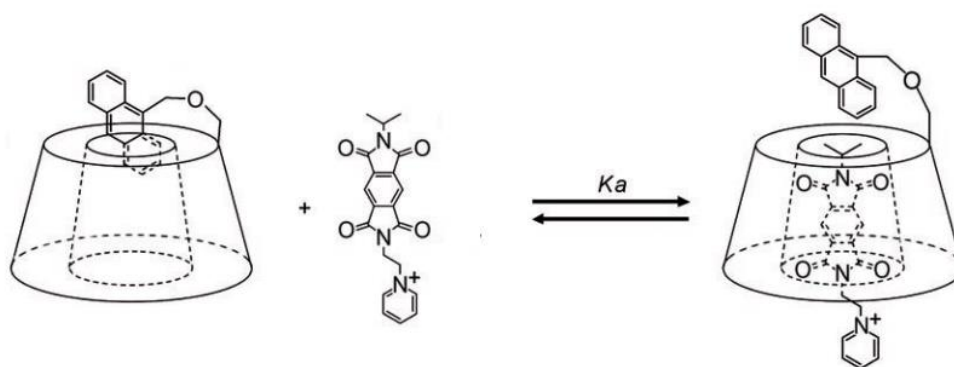


Figure 1.17. Assembly of ANCD/PMDI complex for PET.

We have also assembled a tris(bipyridyl)ruthenium–pyrene–methylviologen (Ru-PY-MV²⁺) supramolecular triad through inclusion complexation of AD-linked Ru-PY dyad in MV²⁺-linked β -CD (Figure 1.18).⁹⁵ Excitation of the tris(bipyridyl)ruthenium chromophore populated its ³MLCT which transfers its triplet energy to PY. The ³PY thus generated donates an electron to MV²⁺ to give Ru(II)-Py^{•+}-MV^{•+}. A second electron transfer then occurs from Ru(II) to Py^{•+} to give the supramolecular Ru(III)-Py-MV^{•+} charge separated state. Laser flash photolysis experiments confirmed formation of MV^{•+} which exhibited 100 μs lifetime. Steady state irradiation of the self-assembled system in the presence of sacrificial donor triethanolamine also led to formation of long-lived MV^{•+}.

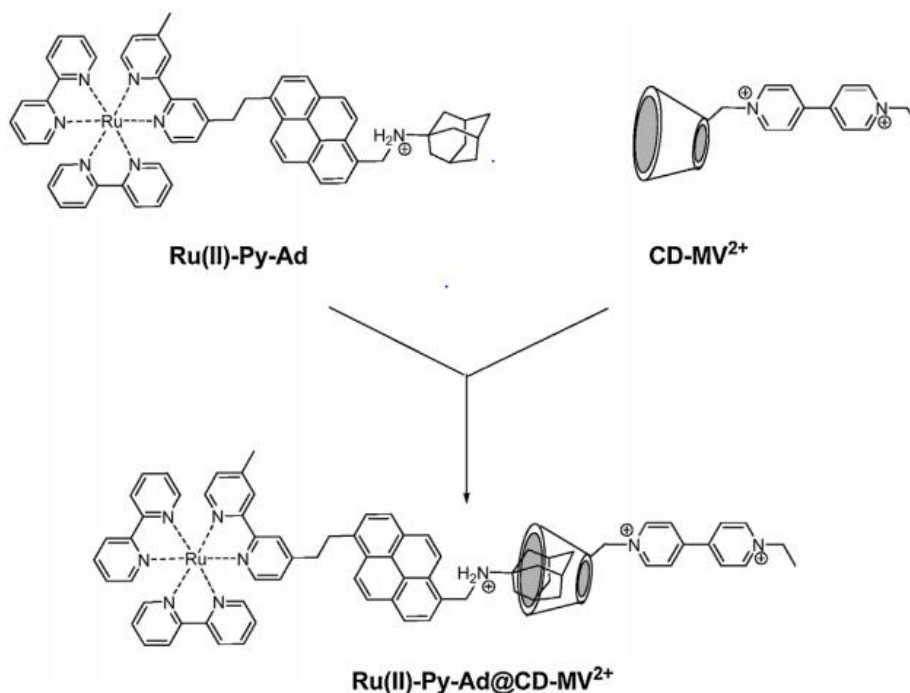


Figure 1.18. Structures of Ru(II)-PY-AD, CD-MV²⁺ and Ru(II)-PY-AD@CD-MV²⁺.

1.5. Origin of the Thesis

Study of supramolecular D-A complexes are very important as these systems found applications as conducting, dielectric, magnetic and optical materials. CT complexes are used in technologically advanced applications such as ambipolar transport, ferroelectricity, photoconductivity and organic field effect transistors. One important drawback of CT complexes is their low association constants, which limit their potential to form organized structures with long range order. The strength of D-A interaction depends on factors such as electron donating ability of D, electron accepting ability of A, steric crowding imparted by substituents, solvent polarity and proper match between the π surfaces of D and A. It has been shown recently that the association constant can be increased by reinforcing the CT interaction with other non-covalent forces such as hydrogen bonding, π -stacking and hydrophobic interactions.

For the last several years our research group was involved in the study of β -CD assisted D-A interactions. A general strategy we employed is to link one of the partners to the CD and assemble the other constituent by inclusion binding or rim-binding with the CD. In order to enhance the strength of inclusion binding we have linked one of the constituents to AD, which exhibit very high affinity for binding to β -CD cavity. We found that this strategy can give CT complexes with very high association constants. Recently we have extended our work to D linked to two β -CD units and A linked to two AD units. In this thesis these studies are extended further using new D-A systems.

In the **second chapter** of this thesis we employed pyrene-linked to β -CD as donor and naphthalene diimide linked to AD on one side and a pyridinium group on the other as acceptor. The pyridinium group is used to impart water solubility to the molecule. When dissolved in water the molecules formed a CT complex where the CT interaction is augmented by inclusion binding of AD in the CD cavity. The CT complexation was studied by ^1H NMR, isothermal titration calorimetry, and circular dichroism techniques. The association constant obtained is among the highest reported ever for CT complexes. We observed that the inclusion complex undergoes hierarchical self-assembly to give twisted nanofibers. Morphology of the nanostructures were investigated using TEM and AFM. We also employed femtosecond pump-probe spectroscopy to study the excited state processes in the CT complex. The horizontal conductivity of the nanofibers was measured using C-AFM.

In the **third chapter** of the thesis we employed pyrene linked to two β -CD molecules as donor and methylviologen linked to two adamantane groups as acceptor. The interaction between these molecules was studied by ^1H NMR, 2D ROESY NMR and circular dichroism spectroscopies. We observed that the bis-inclusion complex formed

undergo hierarchical self-assembly to give closed loop structures, which then stack together to give toroids. And we observed that irradiation of the toroidal system did not lead to formation of long-lived charge separated states.

In the **fourth chapter** of the thesis we employed the same donor but used an acceptor that has AD-linked MV²⁺ moieties on all three arms of a mesitylene core. The D-A system self-assembled in aqueous solution into vesicles which later coalesced to give long fibers. Self-assembly in this case was studied using ¹H NMR, 2D NMR, circular dichroism, AFM, SEM and TEM. We observed that excitation of the D-A system led to very long-lived CS state. Up on Irradiation in an optical bench the colour of the solution changed to blue indicating the formation of long-lived viologen radical cation.

1.6. References

- (1) Lehn, J. -M. Supramolecular chemistry, concepts and perspectives, VCH, Weinheim, **1995**.
- (2) De Greef, T. F. A.; Smulders, M. M. J.; Wolffs, M.; Schenning, A. P. H. J.; Sijbesma, R. P.; Meijer, E. W. Supramolecular polymerization. *Chem. Rev.* **2009**, *109*, 5687–5754.
- (3) Desiraju, G. R. Chemistry beyond the molecule. *Nature* **2001**, *412*, 397–400.
- (4) Crini, G. Review: A history of cyclodextrins. *Chem. Rev.* **2014**, *114*, 10940–10975.
- (5) Szejtli, J. Introduction and general overview of cyclodextrin chemistry. *Chem. Rev.* **1998**, *98*, 1743–1753.
- (6) Harata, K. Structural aspects of stereodifferentiation in the solid state. *Chem. Rev.* **1998**, *98*, 1803–1827.
- (7) Barone, G.; Castronuovo, G.; Del Vecchio, P.; Elia, V.; Muscetta, M. Thermodynamics of formation of inclusion compounds in water. α -Cyclodextrin-alcohol adducts at 298.15 K. *J. Chem. Soc., Faraday Trans 1* **1986**, *82*, 2089–2101.
- (8) Fujiwara, H.; Arakawa, H.; Murata, S.; Sasaki, Y. Entropy changes in the inclusion complex formation of α -cyclodextrin with alcohols as studied by the titration

- calorimetry. *Bull. Chem. Soc. Jpn.* 1987, 3891–3894.
- (9) Saenger, W. Cyclodextrin inclusion compounds in research and industry. *Angew. Chem. Int. Ed. Engl.* **1980**, *19*, 344–362.
- (10) Harrison, J. C.; Eftink, M. R. Cyclodextrin–adamantanecarboxylate inclusion complexes: A model system for the hydrophobic effect. *Biopolymers* **1982**, *21*, 1153–1166.
- (11) Tabushi, I.; Kiyosuke, Y. ichi; Sugimoto, T.; Yamamura, K. Approach to the aspects of driving force of inclusion by α -cyclodextrin. *J. Am. Chem. Soc.* **1978**, *100*, 916–919.
- (12) Gelb, R. I.; Schwartz, L. M.; Laufer, D. A. Adamantan-1-ylamine and Adamantan-1-ylamine hydrochloride complexes with cycloamyloses. *J. Chem. Soc. Perkin Trans. II* **1984**, 15–21.
- (13) Tellini, V. H. S.; Jover, A.; García, J. C.; Galantini, L.; Meijide, F.; Tato, J. V. Thermodynamics of formation of host-guest supramolecular polymers. *J. Am. Chem. Soc.* **2006**, *128*, 5728–5734.
- (14) Sadrerafi, K.; Moore, E. E.; Lee Jr, M. W. Association constant of β -cyclodextrin with carboranes, adamantane, and their derivatives using displacement binding technique. *J. Incl. Phenom. Macrocycl. Chem.* **2015**, *83*, 159–166.
- (15) Chamberlain, R. V.; Slowinska, K.; Majda, M.; Bühlmann, P.; Aoki, H.; Umezawa, Y. Electrostatically-induced inclusion of anions in cyclodextrin monolayers on electrodes. *Langmuir* **2000**, *16*, 1388–1396.
- (16) Zhong, X.; Hu, C.; Yan, X.; Liu, X.; Zhu, D. Aggregate morphology transition of an adamantane-containing surfactant via the host-guest interaction with β -cyclodextrin. *J. Mol. Liq.* **2018**, *272*, 209–217.
- (17) Harada, A.; Kobayashi, R.; Takashima, Y.; Hashidzume, A.; Yamaguchi, H. Macroscopic self-assembly through molecular recognition. *Nat. Chem.* **2011**, *3*, 34–37.
- (18) Sun, Y.; Zhu, J.; Qiu, W. X.; Lei, Q.; Chen, S.; Zhang, X. Z. Versatile supermolecular inclusion complex based on host-guest interaction for targeted gene delivery. *ACS Appl. Mater. Interfaces* **2017**, *9*, 42622–42632.
- (19) Hu, Y.; Zhao, N.; Yu, B.; Liu, F.; Xu, F. J. Versatile types of polysaccharide-based

- supramolecular polycation/PDNA nanoplexes for gene delivery. *Nanoscale* **2014**, *6*, 7560–7569.
- (20) Liu, J.; Hennink, W. E.; Van Steenbergen, M. J.; Zhuo, R.; Jiang, X. Versatile supramolecular gene vector based on host-guest interaction. *Bioconjugate Chem.* **2016**, *27*, 1143–1152.
- (21) Karim, A. A.; Dou, Q.; Li, Z.; Loh, X. J. Emerging supramolecular therapeutic carriers based on host-guest interactions. *Chem. Asian J.* **2016**, *11*, 1300–1321.
- (22) Elamin, K. M.; Yamashita, Y.; Higashi, T.; Motoyama, K.; Arima, H. Supramolecular complex of methyl- β -cyclodextrin with adamantane- grafted hyaluronic acid as a novel antitumor Agent. *Chem. Pharm. Bull.* **2018**, *66*, 277–285.
- (23) Lee, D. W.; Jo, J.; Jo, D.; Kim, J.; Min, J. J.; Yang, D. H.; Hyun, H. Supramolecular assembly based on host-guest interaction between beta-cyclodextrin and adamantane for specifically targeted cancer imaging. *J. Ind. Eng. Chem.* **2018**, *57*, 37–44.
- (24) Zhang, J.; Ma, P. X. Cyclodextrin-based supramolecular systems for drug delivery: Recent progress and future perspective. *Adv. Drug Deliv. Rev.* **2013**, *65*, 1215–1233.
- (25) Isenbügel, K.; Ritter, H.; Branscheid, R.; Kolb, U. Nanoparticle vesicles through self assembly of cyclodextrin- and adamantyl-modified silica. *Macromol. Rapid Commun.* **2010**, *31*, 2121–2126.
- (26) Böhm, I.; Isenbügel, K.; Ritter, H.; Branscheid, R.; Kolb, U. Cyclodextrin and adamantane host-guest interactions of modified hyperbranched poly(ethylene imine) as mimetics for biological membranes. *Angew. Chem. Int. Ed.* **2011**, *50*, 7896–7899.
- (27) Nayak, N.; Gopidas, K. R. Unusual self-assembly of a hydrophilic β -cyclodextrin inclusion complex into vesicles capable of drug encapsulation and release. *J. Mater. Chem. B* **2015**, *3*, 3425–3428.
- (28) Das, A.; Ghosh, S. Supramolecular assemblies by charge-transfer interactions between donor and acceptor chromophores. *Angew. Chem. Int. Ed.* **2014**, *53*, 2038–2054.
- (29) Goetz, K. P.; Vermeulen, D.; Payne, M. E.; Kloc, C.; McNeil, L. E.; Jurchescu, O. D.

- Charge-transfer complexes: New perspectives on an old class of compounds. *J. Mater. Chem. C* **2014**, *2*, 3065–3076.
- (30) Mulliken, R. S.; Person, W. B. Donor-acceptor complexes. *Annu. Rev. Phys. Chem.* **1962**, *13*, 107–126.
- (31) Hill, D. J.; Mio, M. J.; Prince, R. B.; Hughes, T. S.; Moore, J. S. A field guide to foldamers. *Chem. Rev.* **2001**, *101*, 3893–4011.
- (32) Colquhoun, H. M.; Zhu, Z. Recognition of polyimide sequence information by a molecular tweezer. *Angew. Chem.* **2004**, *116*, 5150–5155.
- (33) Ghosh, S.; Ramakrishnan, S. Aromatic donor–acceptor charge-transfer and metal-ion-complexation-assisted folding of a synthetic polymer. *Angew. Chem.* **2004**, *116*, 3326–3330.
- (34) Ghosh, S.; Ramakrishnan, S. Small-molecule-induced folding of a synthetic polymer. *Angew. Chem. Int. Ed.* **2005**, *44*, 5441–5447.
- (35) Colquhoun, H. M.; Zhu, Z.; Williams, D. J. Extreme complementarity in a macrocycle-tweezer complex. *Org. Lett.* **2003**, *5*, 4353–4356.
- (36) Maitra, U.; Kumar, P. V.; Chandra, N.; D’Souza, L. J.; Prasanna, M. D.; Raju, A. R. First donor-acceptor interaction promoted gelation of organic fluids. *Chem. Commun.* **1999**, 595–596.
- (37) Babu, P.; Sangeetha, N. M.; Vijaykumar, P.; Maitra, U.; Rissanen, K.; Raju, A. R. Pyrene-derived novel one- and two-component organogelators. *Chem. Eur. J.* **2003**, *9*, 1922–1932.
- (38) Das, A.; Molla, M. R.; Banerjee, A.; Paul, A.; Ghosh, S. Hydrogen-bonding directed assembly and gelation of donor-acceptor chromophores: Supramolecular reorganization from a charge-transfer state to a self-sorted state. *Chem. Eur. J.* **2011**, *17*, 6061–6066.
- (39) Das, A.; Molla, M. R.; Maity, B.; Koley, D.; Ghosh, S. Hydrogen-bonding induced alternate stacking of donor (D) and acceptor (A) chromophores and their supramolecular switching to segregated states. *Chem. Eur. J.* **2012**, *18*, 9849–9859.
- (40) Liu, Y.; Zheng, N.; Li, H.; Yin, B. Supramolecular gels based on monopyrrolotetrathiafulvalene and its TCNQ charge-transfer complex. *Soft*

- Matter* **2013**, *9*, 5261–5269.
- (41) Ko, Y. H.; Kim, K.; Kang, J. K.; Chun, H.; Lee, J. W.; Sakamoto, S.; Yamaguchi, K.; Fettinger, J. C.; Kim, K. Designed self-assembly of molecular necklaces using host-stabilized charge-transfer interactions. *J. Am. Chem. Soc.* **2004**, *126*, 1932–1933.
- (42) Jeon, Y. J.; Bharadwaj, P. K.; Choi, S. W.; Lee, J. W.; Kim, K. Supramolecular amphiphiles: Spontaneous formation of vesicles triggered by formation of a charge-transfer complex in a host. *Angew. Chem. Int. Ed.* **2002**, *41*, 4474–4476.
- (43) Jeon, W. S.; Kim, E.; Ko, Y. H.; Hwang, I.; Lee, J. W.; Kim, S. Y.; Kim, H. J.; Kim, K. Molecular loop lock: A redox-driven molecular machine based on a host-stabilized charge-transfer complex. *Angew. Chem. Int. Ed.* **2005**, *44*, 87–91.
- (44) Lee, J. W.; Han, S. C.; Kim, J. H.; Ko, Y. H.; Kim, K. Formation of rotaxane dendrimers by supramolecular click chemistry. *Bull. Korean Chem. Soc.* **2007**, *28*, 1837–1840.
- (45) Kim, H. J.; Heo, J.; Jeon, W. S.; Lee, E.; Kim, J.; Sakamoto, S.; Yamaguchi, K.; Kim, K. Selective inclusion of a hetero-guest pair in a molecular host: Formation of stable charge-transfer complexes in Cucurbit[8]uril. *Angew. Chem. Int. Ed.* **2001**, *40*, 1526–1529.
- (46) Lee, J. W.; Kim, K.; Choi, S. W.; Ko, Y. H.; Sakamoto, S.; Yamaguchi, K.; Kim, K. Unprecedented host-induced intramolecular charge-transfer complex formation. *Chem. Commun.* **2002**, 2692–2693.
- (47) Zou, D.; Andersson, S.; Zhang, R.; Sun, S.; Åkermark, B.; Sun, L. A host-induced intramolecular charge-transfer complex and light-driven radical cation formation of a molecular triad with cucurbit[8]uril. *J. Org. Chem.* **2008**, *73*, 3775–3783.
- (48) Liu, Y.; Yu, Y.; Gao, J.; Wang, Z.; Zhang, X. Water-soluble supramolecular polymerization driven by multiple host-stabilized charge-transfer interactions. *Angew. Chem. Int. Ed.* **2010**, *49*, 6576–6579.
- (49) Biedermann, F.; Scherman, O. A. Cucurbit[8]uril mediated donor–acceptor ternary complexes: A model system for studying charge-transfer interactions. *J. Phys. Chem. B* **2012**, *116*, 2842–2849.
- (50) Ji, Z.; Li, J.; Chen, G.; Jiang, M. Fate of host-stabilized charge transfer complexation based on cucurbit[8]uril: Inducing cyclization of PNIPAM and dissociation in self-

- assembly of the cyclic polymer. *ACS Macro Lett.* **2016**, *5*, 588–592.
- (51) Tang, Y.; Wang, K.; Zuo, Y.; Chen, X.; Xiong, Y.; Yuan, Y. Supramolecular assembly of poly (ionic liquid) nanogel driven by host-stabilized charge transfer interaction. *J. Polym. Sci.* **2019**, *57*, 2251–2259.
- (52) Krishnan, S. B.; Gopidas, K. R. Observation of supramolecular chirality in a hierarchically self-assembled mixed-stack charge-transfer complex. *Chem. Eur. J.* **2017**, *23*, 9600–9606.
- (53) Krishnan, S. B.; Krishnan, R.; Gopidas, K. R. Effect of N-alkyl substituents on the hierarchical self-assembly of β -cyclodextrin-linked pyrene-pyromellitic diimide charge-transfer complex. *Chem. Eur. J.* **2018**, *24*, 11451–11460.
- (54) Horiuchi, S.; Hasegawa, T.; Tokura, Y. Molecular donor-acceptor compounds as prospective organic electronics materials. *J. Phys. Soc. Jpn* **2006**, *75*, 051016(1-14).
- (55) Soos, Z. G. Theory of π -molecular charge-transfer crystals. *Annu. Rev. Phys. Chem.* **1974**, *25*, 121–153.
- (56) Coleman, L. B.; Cohen, M. J.; Sandman, D. J.; Yamagishi, F. G.; Garito, A. F.; Heeger, A. J. Superconducting fluctuations and the peierls instability in an organic solid. *Solid State Commun.* **1973**, *12*, 1125–1132.
- (57) Zhu, L.; Yi, Y.; Li, Y.; Kim, E. G.; Coropceanu, V.; Brédas, J. L. Prediction of remarkable ambipolar charge-transport characteristics in organic mixed-stack charge-transfer crystals. *J. Am. Chem. Soc.* **2012**, *134*, 2340–2347.
- (58) Horiuchi, S.; Kobayashi, K.; Kumai, R.; Minami, N.; Kagawa, F.; Tokura, Y. Quantum ferroelectricity in charge-transfer complex crystals. *Nat. Commun.* **2015**, *6*, 7469.
- (59) Sakai, N.; Bhosale, R.; Emery, D.; Mareda, J.; Matile, S. Supramolecular n/p-heterojunction photosystems with antiparallel redox gradients in electron- and hole-transporting pathways. *J. Am. Chem. Soc.* **2010**, *132*, 6923–6925.
- (60) Sung, M. J.; Luzio, A.; Park, W. T.; Kim, R.; Gann, E.; Maddalena, F.; Pace, G.; Xu, Y.; Natali, D.; de Falco, C. High-mobility naphthalene diimide and selenophene-vinylene-selenophene-based conjugated polymer: N-channel organic field-effect transistors and structure–property relationship. *Adv. Funct. Mater.* **2016**, *26*, 4984–4997.
- (61) García-Iglesias, M.; De Waal, B. F. M.; Gorbunov, A. V.; Palmans, A. R. A.;

- Kemerink, M.; Meijer, E. W. A Versatile method for the preparation of ferroelectric supramolecular materials via radical end-functionalization of vinylidene fluoride oligomers. *J. Am. Chem. Soc.* **2016**, *138*, 6217–6223.
- (62) Shivakumar, K. I.; Swathi, K.; Goudappagouda; Das, T. C.; Kumar, A.; Makde, R. D.; Vanka, K.; Narayan, K. S.; Babu, S. S.; Sanjayan, G. J. Mixed-stack charge transfer crystals of pillar[5]quinone and tetrathiafulvalene exhibiting ferroelectric features. *Chem. Eur. J.* **2017**, *23*, 12630–12635.
- (63) Wu, H.-D.; Wang, F.-X.; Xiao, Y.; Pan, G.-B. Preparation and ambipolar transistor characteristics of co-crystal microrods of dibenzotetrathiafulvalene and tetracyanoquinodimethane. *J. Mater. Chem. C* **2013**, *1*, 2286–2289.
- (64) Salzillo, T.; Campos, A.; Mas-Torrent, M. Solution-processed thin films of a charge transfer complex for ambipolar field-effect transistors. *J. Mater. Chem. C* **2019**, *7*, 10257–10263.
- (65) Sagade, A. A.; Rao, K. V.; George, S. J.; Datta, A.; Kulkarni, G. U. A Charge transfer single crystal field effect transistor operating at low voltages. *Chem. Commun.* **2013**, *49*, 5847–5849.
- (66) Sato, R.; Dogishi, M.; Higashino, T.; Kadoya, T.; Kawamoto, T.; Mori, T. Charge-transfer complexes of benzothienobenzothiophene with tetracyanoquinodimethane and the n-channel organic field-effect transistors. *J. Phys. Chem. C* **2017**, *121*, 6561–6568.
- (67) Qin, W.; Xu, B.; Ren, S. An organic approach for nanostructured multiferroics. *Nanoscale* **2015**, *7*, 9122–9132.
- (68) Tayi, A. S.; Shveyd, A. K.; Sue, A. C.-H.; Szarko, J. M.; Rolczynski, B. S.; Cao, D.; Kennedy, T. J.; Sarjeant, A. A.; Stern, C. L.; Paxton, W. F. Room-temperature ferroelectricity in supramolecular networks of charge-transfer complexes. *Nature* **2012**, *488*, 485–489.
- (69) Pandeewar, M.; Senanayak, S. P.; Narayan, K. S.; Govindaraju, T. Multi-stimuli-responsive charge-transfer hydrogel for room-temperature organic ferroelectric thin-film devices. *J. Am. Chem. Soc.* **2016**, *138*, 8259–8268.
- (70) Balzani, V.; Moggi, L.; Manfrin, M. F.; Bolletta, F.; Gleria, M. Solar energy conversion by water photodissociation: Transition metal complexes can provide

- low-energy cyclic systems for catalytic photodissociation of water. *Science* **1975**, *189*, 852–856.
- (71) Amouyal, E. Photochemical production of hydrogen and oxygen from water: A review and state of the art. *Sol. Energy Mater. Sol. Cells* **1995**, *38*, 249–276.
- (72) Kavarnos, G. J. Fundamentals of photoinduced electron transfer, VCH, New York, **1993**.
- (73) Sinnecker, S.; Flores, M.; Lubitz, W. Protein-cofactor interactions in bacterial reaction centers from rhodobacter sphaeroides R-26: Effect of hydrogen bonding on the electronic and geometric structure of the primary quinone. A density functional theory study. *Phys. Chem. Chem. Phys.* **2006**, *8*, 5659–5670.
- (74) Hutter, M. C.; Hughes, J. M.; Reimers, J. R.; Hush, N. S. Modeling the bacterial photosynthetic reaction center. 2. A combined quantum mechanical/molecular mechanical study of the structure of the cofactors in the reaction centers of purple bacteria. *J. Phys. Chem. B* **1999**, *103*, 4906–4915.
- (75) Hou, Y.; Zhang, X.; Chen, K.; Liu, D.; Wang, Z.; Liu, Q.; Zhao, J.; Barbon, A. Charge separation, charge recombination, long-lived charge transfer state and intersystem crossing in organic electron donor/acceptor dyads. *J. Mater. Chem. C* **2019**, *7*, 12048–12074.
- (76) Fukuzumi, S.; Lee, Y.; Nam, W. Mimicry and functions of photosynthetic reaction centers. *Biochem. Soc. Trans.* **2018**, *46*, 1279–1288.
- (77) El-khouly, M. E.; El-mohsnawy, E.; Fukuzumi, S. Solar energy conversion : From natural to artificial photosynthesis. *J. Photochem. Photobiol. C* **2017**, *31*, 36–83.
- (78) Llansola-portoles, M. J.; Gust, D.; Moore, T. A.; Moore, A. L. Artificial photosynthetic antennas and reaction centers. *Comptes Rendus Chim.* **2017**, *20*, 296–313.
- (79) Rudolf, M.; Kirner, S. V; Guldi, D. M. A multicomponent molecular approach to artificial photosynthesis—the role of fullerenes and endohedral metallofullerenes. *Chem. Soc. Rev.* **2016**, *45*, 612–630.
- (80) Sherman, B. D.; Vaughn, M. D.; Bergkamp, J. J.; Gust, D.; Moore, A. L.; Moore, T. A. Evolution of reaction center mimics to systems capable of generating solar fuel. *Photosynth. Res.* **2014**, *120*, 59–70.

- (81) Trukhina, O.; Rudolf, M.; Bottari, G.; Akasaka, T.; Echegoyen, L.; Torres, T.; Guldi, D. M. Bidirectional electron transfer capability in phthalocyanine–Sc₃N@Ih–C₈₀ complexes. *J. Am. Chem. Soc.* **2015**, *137*, 12914–12922.
- (82) El-khouly, M. E.; Wijesinghe, C. A.; Nesterov, V. N.; Zandler, M. E.; Fukuzumi, S.; D'Souza, F. Ultrafast photoinduced energy and electron transfer in multi-modular donor – acceptor conjugates. *Chem. Eur. J.* **2012**, *18*, 13844–13853.
- (83) Grimm, B.; Schornbaum, J.; Jasch, H.; Trukhina, O.; Wessendorf, F.; Hirsch, A.; Torres, T.; Guldi, D. M. Step-by-Step self-assembled hybrids that feature control over energy and charge transfer. *Proc. Natl. Acad. Sci. U.S.A.* **2012**, *109*, 15565–15571.
- (84) Kimoto, K.; Satoh, T.; Iwamura, M.; Nozaki, K.; Horikoshi, T.; Suzuki, S.; Kozaki, M.; Okada, K. Very long-lived photoinduced charge-separated states of triphenylamine – naphthalenediimide dyads in polymer matrices. *J. Phys. Chem. A* **2016**, *120*, 8093–8103.
- (85) Cai, N.; Takano, Y.; Numata, T.; Inoue, R.; Mori, Y.; Murakami, T.; Imahori, H. Strategy to attain remarkably high photoinduced charge-separation yield of donor – acceptor linked molecules in biological environment via modulating their cationic moieties. *J. Phys. Chem. C* **2017**, *121*, 17457–17465.
- (86) Jin, S.; Supur, M.; Addicoat, M.; Furukawa, K.; Chen, L.; Nakamura, T.; Fukuzumi, S.; Irle, S.; Jiang, D. Creation of superheterojunction polymers via direct polycondensation: Segregated and bicontinuous donor-acceptor π -columnar arrays in covalent organic frameworks for long-lived charge separation. *J. Am. Chem. Soc.* **2015**, *137*, 7817–7827.
- (87) Mallia, A. R.; Salini, P. S.; Hariharan, M. Nonparallel stacks of donor and acceptor chromophores evade geminate charge recombination. *J. Am. Chem. Soc.* **2015**, *137*, 15604–15607.
- (88) Mallia, A. R.; Hariharan, M. Self-assembled donor-acceptor trefoils: Long-lived charge separated state through aggregation. *J. Phys. Chem. C* **2017**, *121*, 4778–4788.
- (89) Dryza, V.; Bieske, E. J. Electron injection and energy-transfer properties of spiropyran-cyclodextrin complexes coated onto metal oxide nanoparticles:

- Toward photochromic light harvesting. *J. Phys. Chem. C* **2015**, *119*, 14076–14084.
- (90) Zhang, Y.-M.; Chen, Y.; Zhuang, R.-J.; Liu, Y. Supramolecular architecture of tetrathiafulvalene-bridged bis(β -cyclodextrin) with porphyrin and its electron transfer behaviors. *Photochem. Photobiol. Sci.* **2011**, *10*, 1393–1398.
- (91) Deng, W.; Onji, T.; Yamaguchi, H.; Ikeda, N.; Harada, A. Competitive photoinduced electron transfer by the complex formation of porphyrin with cyclodextrin bearing viologen. *Chem. Commun.* **2006**, 4212–4214.
- (92) Ghosh, S.; Mondal, S. K.; Sahu, K.; Bhattacharyya, K. Ultrafast electron transfer in a nanocavity. Dimethylaniline to coumarin dyes in hydroxypropyl γ -cyclodextrin. *J. Phys. Chem. A* **2006**, *110*, 13139–13144.
- (93) Liang, P.; Zhang, H.-Y.; Yu, Z.-L.; Liu, Y. Solvent-controlled photoinduced electron transfer between porphyrin and carbon nanotubes. *J. Org. Chem.* **2008**, *73*, 2163–2168.
- (94) Balan, B.; Gopidas, K. R. An anthracene-appended β -cyclodextrin-based dyad: Study of self-assembly and photoinduced electron-transfer processes. *Chem. Eur. J.* **2007**, *13*, 5173–5185.
- (95) Rakhi, A. M.; Gopidas, K. R. Generation of long-lived methylviologen radical cation in the triplet-state mediated electron transfer in a β -cyclodextrin based supramolecular triad. *Chem. Phys. Lett.* **2015**, *618*, 192–197.

Hierarchically Self-Assembled Nanofiber Networks of Mixed Stack Charge Transfer Complex for Organic Electronic Applications

2.1. Abstract

In this chapter, we have studied mixed stack charge transfer (CT) complex formation, where the charge transfer interaction was augmented by inclusion binding of adamantane moiety in β -cyclodextrin. Pyrene linked to β -cyclodextrin was the donor and naphthalene diimide linked to adamantane was the acceptor. Association constant for CT complexation was $3.6 \times 10^7 M^{-1}$, which is the highest value reported so far for any CT complex. Complex formation was probed using 1H NMR, isothermal titration calorimetry, and circular dichroism studies. The results suggested that within the CT complex the donor and acceptor exist as alternating units with a dihedral angle $> 50^\circ$ between them with each donor-acceptor pair rotated slightly with respect to the preceding and succeeding pairs. The CT complex underwent hierarchical self-assembly to give twisted nanofibers as confirmed by AFM and TEM studies. The excited state relaxation process in the charge transfer complex was investigated by femtosecond time-resolved pump-probe spectroscopy. The horizontal conductivity of the nanofibers was measured using C-AFM.

2.2. Introduction

Low or moderate association constants (K_a) of Intermolecular CT interactions between aromatic donor (D) and acceptor (A) molecules restrict the formation of organized assemblies with long-range order. Researchers adopted several methods to enhance CT interactions by enforcing it with other non-covalent forces such as hydrogen bonding,¹⁻³ π -stacking,⁴⁻⁶ metal-ligand coordination,^{7,8} and hydrophobic interactions.⁹ Even after reinforcement with additional non-covalent interactions the currently available 'high' K_a values for CT complexation is only in the 10^3 – 10^4 M^{-1} range. Wilson and co-workers performed a systematic study on the co-assembly of homopolymers containing different pendent D and A groups and concluded that pyrene (PY)-naphthalene diimide (NDI) system is the best D-A pair for CT complexation.¹⁰ Several studies determined the association constants for the PY-NDI CT complex by varying conditions and the reported values include 6.0×10^3 M^{-1} in methylcyclohexane,¹¹ 9.0×10^2 M^{-1} in 2:1 water:methanol,¹² and 8.9×10^2 M^{-1} in 99:1 water:DMF.¹³ Various research groups attempted to reinforce the PY-NDI CT interactions with other non-covalent forces.¹⁴⁻¹⁹ For example, Khalily *et al.* constructed supramolecular 1D nanowires of PY-NDI system exhibiting high K_a value of 5.18×10^5 M^{-1} by reinforcing CT with H-bonding and electrostatic interactions,²⁰ which was the highest K_a value reported for the PY-NDI system so far. Thin films obtained by drop-casting this CT complex solution exhibited conductivity of 1.65×10^{-5} S/cm.

Herein we report the construction of a highly stable PY-NDI CT complex where the CT interaction is augmented by adamantane (AD)/ β -cyclodextrin (β -CD) inclusion binding. The β -CD moiety is linked to PY to give the donor system designated here as

PYCD. One of the N atoms of NDI is connected to AD group through a methylene linker, and the other N atom is linked to a pyridinium moiety to increase water solubility. The AD-linked NDI is designated as NDIAD in this study. Structures of PYCD and NDIAD are given in Figure 2.1. We also used a water-soluble pyrene derivative PYP (Figure 2.1) for few control experiments. We observed that PYCD/NDIAD system exhibited $K_a > 10^7 \text{ M}^{-1}$ and underwent hierarchical self-assembly to give long fibers.

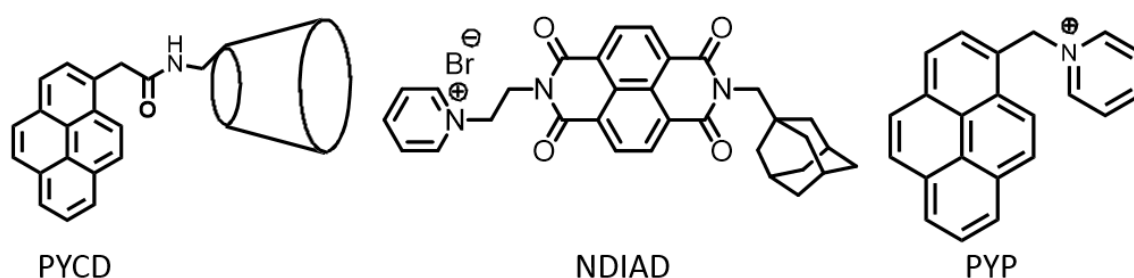


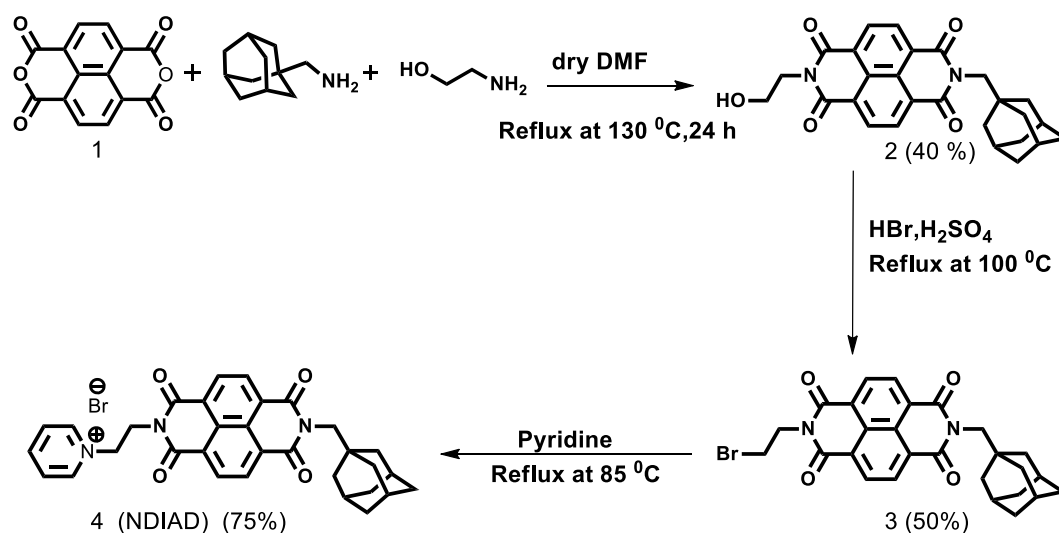
Figure 2.1. Structures of molecules employed in this study.

According to Mulliken's theory, excitation of the CT band should result in the direct formation of radical ion pair ($D^{\bullet+}/A^{\bullet-}$) states.^{21,22} Kochi and co-workers studied the ultrafast formation and decay of radical ion pairs by exciting the CT band in several D/A systems.^{23,24} However, to the best of our knowledge only one study is available which reported formation of ion pairs in self-assembled nanostructures of CT complexes.²⁵ Herein we report the femtosecond pump-probe spectroscopic study of the PYCD/NDIAD CT complex. We observed direct formation of the radical ion pair when the CT band is excited. The charge separated state was extremely short lived (~ 6 ps), thereby confirming the close proximity of the donor and acceptor in the hierarchically self-assembled system. Since CT complexes have electronic applications, we also determined the horizontal conductivity of the CT nanostructure.

2.3. Results and Discussions

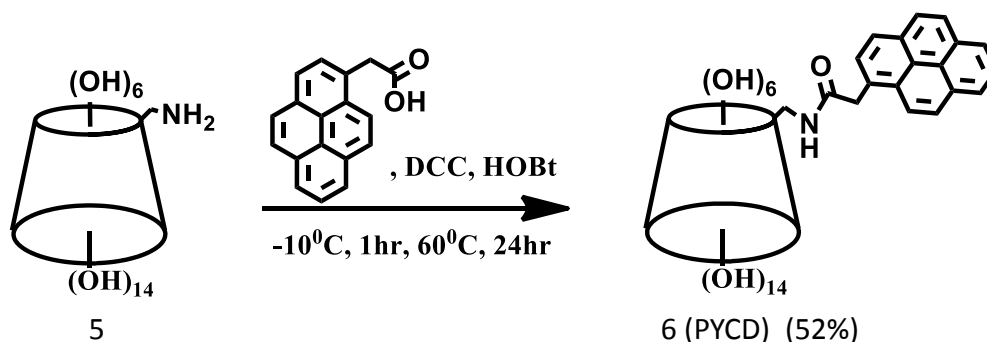
2.3.1. Synthesis and characterisation of molecules

NDIAD was synthesized as shown in Scheme 2.1. 1,4,5,8-naphthalenetetracarboxylic dianhydride **1** was refluxed with 1-adamantylmethylamine and 2-Amino-1-ethanol (1:1 molar ratio) in dry DMF under argon for 24 h at 130 °C to give the corresponding hydroxy derivative **2** in 40% yield. **2** was then converted to the bromo derivative **3** in 50% yield by refluxing with hydrobromic acid and sulphuric acid for 3 h at 100 °C. The water soluble pyridinium derivative **4** (NDIAD) was obtained in 75% yield by refluxing **3** with pyridine for 24 h at 85 °C.



Scheme 2.1. Scheme for the synthesis of NDIAD.

PYCD was synthesized as shown in Scheme 2.2. The synthesis involved the amide coupling reaction of 1-pyrene acetic acid with the β -CD monoamine derivative **5** in the presence of DCC and 1-HOBt. The pure product was obtained in 52% yield by repeated column chromatography using methanol/water mixture (1:1) over reverse phase silica gel. The intermediates and final products are well characterized using state of the art spectroscopic methods.



Scheme 2.2. Scheme for the synthesis of PYCD.

2.3.2. Charge transfer complexation in PYCD-NDIAD

When PYCD and NDIAD (1:1) are dissolved in aqueous solution they form a very stable CT complex, which we designate as NDIAD@PYCD. The CT complexation between these two molecules in aqueous solution was studied by High resolution mass spectroscopy (HRMS), UV-Vis absorption spectroscopy, Isothermal titration calorimetry (ITC), circular dichroism (CD) spectroscopy and ^1H NMR spectroscopy. In some of these studies we have compared the results with corresponding properties of NDIAD/PYP complex, which is designated as NDIAD@PYP. The results of these studies are presented in the following sections.

2.3.2.1. HRMS studies

ESI-HRMS of NDIAD@PYCD is shown in Figure 2.2. The spectrum shows the m/z peak at 1895.66. The calculated molecular weight of 1:1 NDIAD@PYCD complex is 1895.67, if the Br^- counter ion is not considered. In Figure 2.2b the spectral region is expanded and shows peaks at 1895.66 and 1896.66, which correspond to $[\text{NDIAD}+\text{PYCD}]^+$ and $[\text{NDIAD}+\text{PYCD}+\text{H}]^+$, respectively. The results confirmed that the NDIAD@PYCD complex contained the constituents, NDIAD and PYCD, in 1:1 ratio.

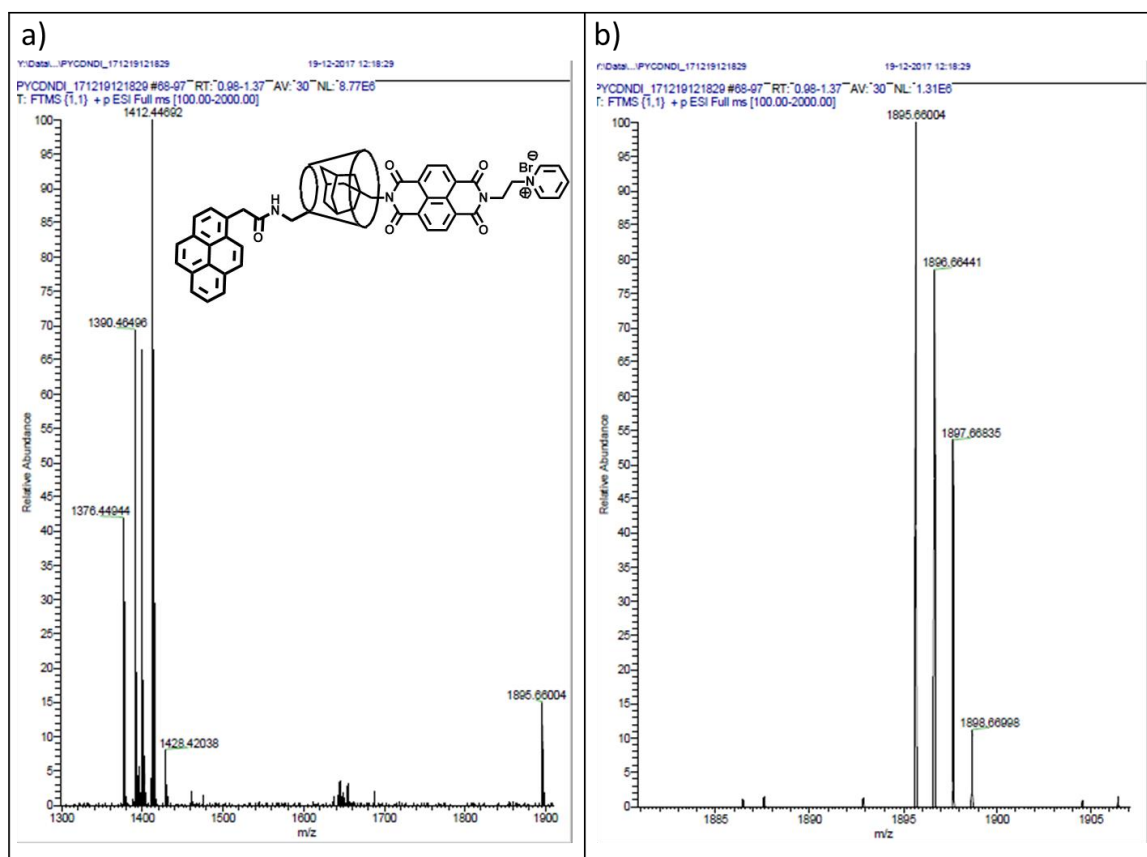


Figure 2.2. a) HRMS (ESI) spectrum of NDIAD@PYCD complex and b) Enlarged portion of 1895.66 peak region.

2.3.2.2. UV-Visible absorption spectroscopy studies

UV-Visible spectroscopy is a powerful tool to characterize CT complexes. CT complexes are characterized by a low energy band in the visible region, known as CT band, which correspond to the transfer of a fraction of charge from the HOMO of donor to the LUMO of the acceptor. Figure 2.3a and b show the absorption spectra of PYCD and NDIAD (each 2.5×10^{-5} M), respectively. Figure 2.3c shows the absorption spectrum of NDIAD@PYCD (2.5×10^{-5} M). The spectrum is different from the sum of the absorptions of the constituents in the 250-400 nm region, suggesting considerable interaction in the ground state. The CT band is seen above 500 nm. Even at this low concentration the CT band is clearly visible as shown in the zoomed version (Figure 2.3.d).

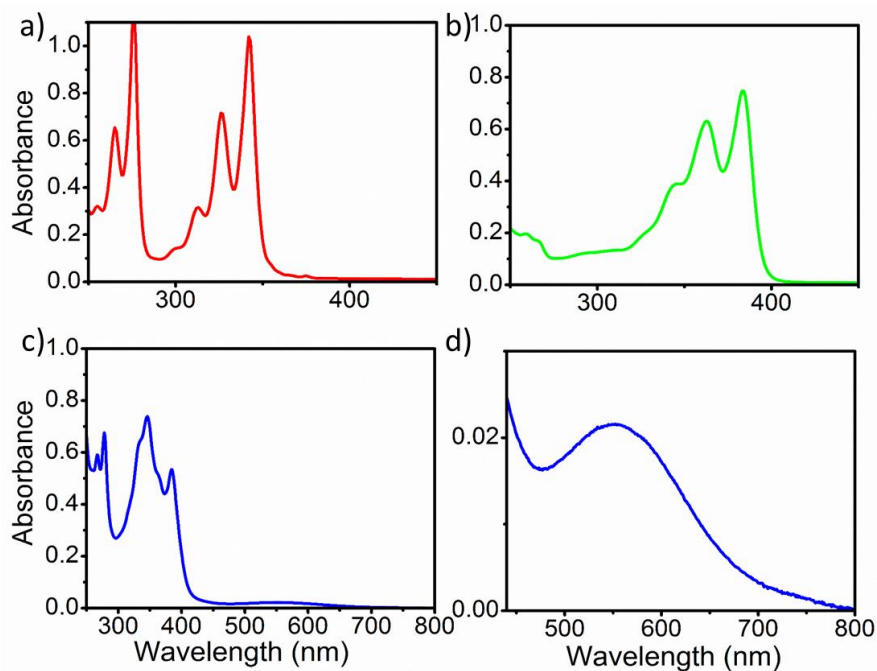


Figure 2.3. Absorption spectra of 2.5×10^{-5} M aq. solutions of a) PYCD, b) NDIAD, and c) NDIAD@PYCD. The CT absorption region in c is enlarged in d.

At concentrations higher than 10^{-4} M, NDIAD@PYCD exhibited dark violet colour.

Figure 2.4.a shows the CT band of NDIAD@PYCD (2.5×10^{-3} M) and its temperature dependence. For comparison, the CT band of NDIAD@PYP (2.5×10^{-3} M) and its temperature dependence is presented in Figure 2.4.b. Although the spectral profiles of the CT bands in NDIAD@PYCD and NDIAD@PYP are similar, several differences exist among these CT complexes.

The NDIAD@PYCD solution appears dark violet with the maximum absorbance of 1.05 at 568 nm. The NDIAD@PYP solution is pale red in color with the maximum absorbance of 0.58 at 495 nm. Upon increasing the temperature from 20 to 90 °C the CT absorption decreased only by 17% for NDIAD@PYCD whereas 60% decrease in the absorbance was observed for NDIAD@PYP. These results suggest that CT complex formed in the NDIAD@PYCD system is highly stable compared to that of the model system.

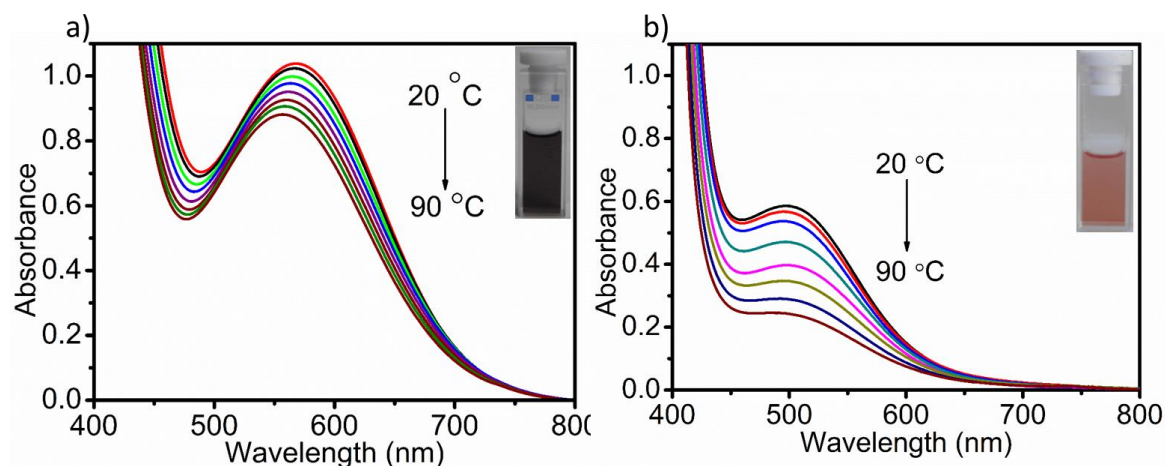


Figure 2.4. CT absorption bands of a) NDIAD@PYCD and b) NDIAD@PYP and their temperature dependence. Insets show the solution colors. Concentrations of the constituents were 2.5×10^{-3} M each, in both cases.

2.3.2.3. Isothermal titration calorimetric studies

ITC is the preferred technique to determine the thermodynamic aspects of binding interaction between molecules.²⁶ Binding interactions would involve heat changes and these changes can be directly observed in the ITC experiment. The instrument is equipped with sample and reference cells, maintained exactly at the same temperature. The host is taken in the sample cell and small aliquots of guest is added to it from a syringe with stirring. Every addition result in an increase or decrease of the temperature in the sample cell, depending on whether the host-guest interaction is exothermic or endothermic. A feedback system continuously monitors the temperatures of the sample and the reference cells and supplies small power to these cells to maintain the same temperature in the two cells. The amount of power ($\mu\text{cal}/\text{sec}$) required to maintain constant temperature in the sample and the reference cells during each addition is measured. The data obtained is then fitted using standard protocols to obtain binding parameters such as K_a , ΔH , ΔS , ΔG and the binding stoichiometry 'n'.

For the ITC experiment, NDIAD (2.0 mM in water) was taken in the syringe, and PYCD (0.2 mM in water) was taken in the cell. The ITC titration curve obtained is given in Figure 2.5. Aqueous NDIAD solution is highly viscous, and hence bubbles are formed during stirring. The small distortions in the titration curve are due to bubble formation, and fitting of the data gave $K_a = 3.64 \times 10^7 \text{ M}^{-1}$. Other parameters obtained from the ITC experiment are $\Delta H = -29.76 \text{ kJ mol}^{-1}$, $\Delta S = 44.76 \text{ J mol}^{-1} \text{ K}^{-1}$, and binding stoichiometry $n = 1.0$. Since NDIAD exists as aggregates in solution, de-aggregation must occur before CT complex formation. ΔS for complexation is positive most probably because of the de-aggregation process. The negative value of Gibbs energy change (ΔG°) confirms the favorable self- assembling process taking place between PYCD and NDIAD in water.

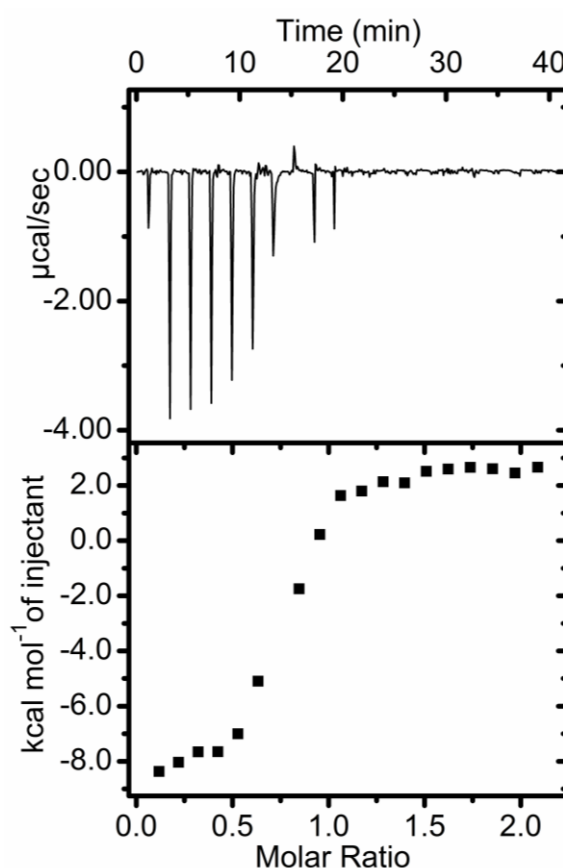


Figure 2.5. ITC titration curve for NDIAD@PYCD.

In the NDIAD@PYCD system studied here, the CT interaction is augmented by the inclusion binding interaction of adamantane moiety in β -CD cavity. If we take $K_{a(CT)} \sim 10^3 \text{ M}^{-1}$ for the CT interaction between PY and NDI chromophores and $K_{a(IN)} \sim 10^4 \text{ M}^{-1}$ for inclusion binding of adamantane in β -CD, the K_a value for NDIAD@PYCD = $K_{a(CT)} \times K_{a(IN)} \sim 10^7 \text{ M}^{-1}$, which is the value observed experimentally. This is the highest value reported for the PY-NDI donor-acceptor system so far.

For the NDIAD@PYP model system, ITC titration curve obtained was not satisfactory due to the low heat changes. Hence, we attempted to determine the association constant for this system using UV-Visible method. For this experiment we monitored the intensity of the CT band as a function of concentration. And the association constant of the NDIAD@PYP system was calculated using the equation 2.1.²⁷

$$\frac{d}{A_c} = \left(\frac{1}{K_a \epsilon_C l} \right)^{1/2} \frac{1}{(A_c)^{1/2}} + \frac{1}{\epsilon_C l} \quad (2.1)$$

Where d is the concentration, A_c is the absorbance maximum of CT band and K_a is the association constant. According to equation, plot of d/A_c vs. $1/(A_c)^{1/2}$ should be a straight line and K_a can be calculated from the slope and intercept of this plot. Figure 2.6a is the concentration dependence of the CT band and the corresponding linear plot of d/A_c versus $1/A_c^{1/2}$ is shown in Figure 2.6b. K_a thus obtained was $1.16 \times 10^3 \text{ M}^{-1}$ which agreed very well with literature reports.^{12, 13}

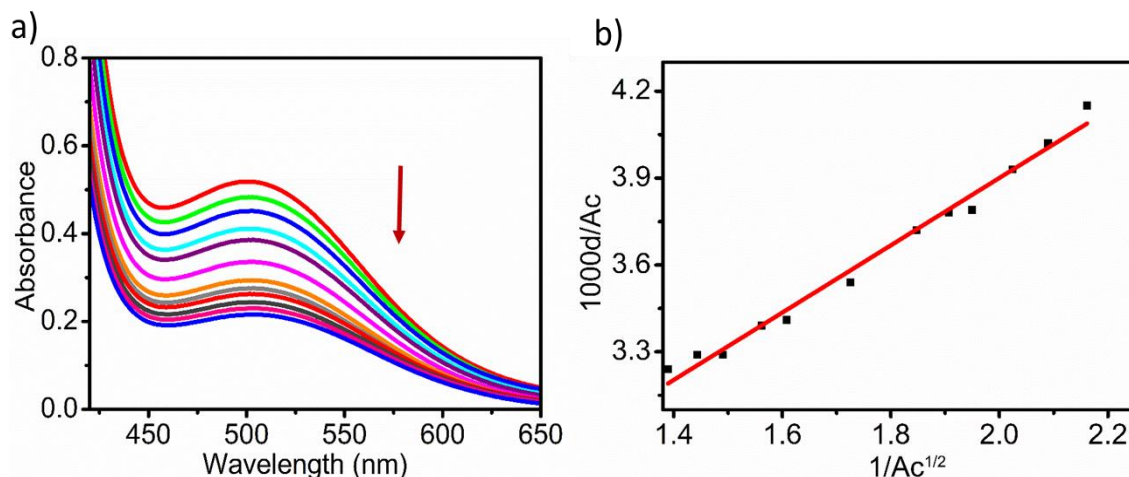


Figure 2.6. a) Concentration-dependent absorption spectra for NDIAD@PYP. The arrow represents the change in concentration from $1.5 \times 10^{-3} \text{ M}$ – $0.95 \times 10^{-3} \text{ M}$. b) Plot of d/A_c against $1/A_c^{1/2}$. ($K_a = 1.166 \times 10^3 \text{ M}^{-1}$).

2.3.2.4. ^1H NMR titration studies

NMR spectroscopy is a powerful techniques to probe the dynamic processes involved in host-guest interactions. D-A stacking usually leads to changes in the chemical shift values and also significant broadening for the ^1H NMR signals. Depending on the magnitude of the proton shift and broadening, the strength of the molecular interactions involved in the CT complex could be estimated. The binding constant can be estimated using observed chemical shift changes. In the case of the NDIAD@PYCD, binding constants in water cannot be estimated using ^1H NMR because NDIAD does not give a well-resolved ^1H NMR in water. This aspect is described in detail in the following sections.

NDIAD exhibited a well-resolve ^1H NMR spectrum with easily identifiable proton signals in DMSO-d_6 which is shown in the Figure 2.7. The aliphatic and aromatic regions are expanded and protons are also labeled in Figure 2.7. The signals, get broadened in the presence of D_2O as shown in Figure 2.8. Addition of small amounts of D_2O leads to loss of resolution and splitting pattern along with broadening of the signals (Figure 2.8).

In the aliphatic region, the splitting pattern of the AD protons exhibit some changes, but compared to the aromatic region the changes in the aliphatic region are less.

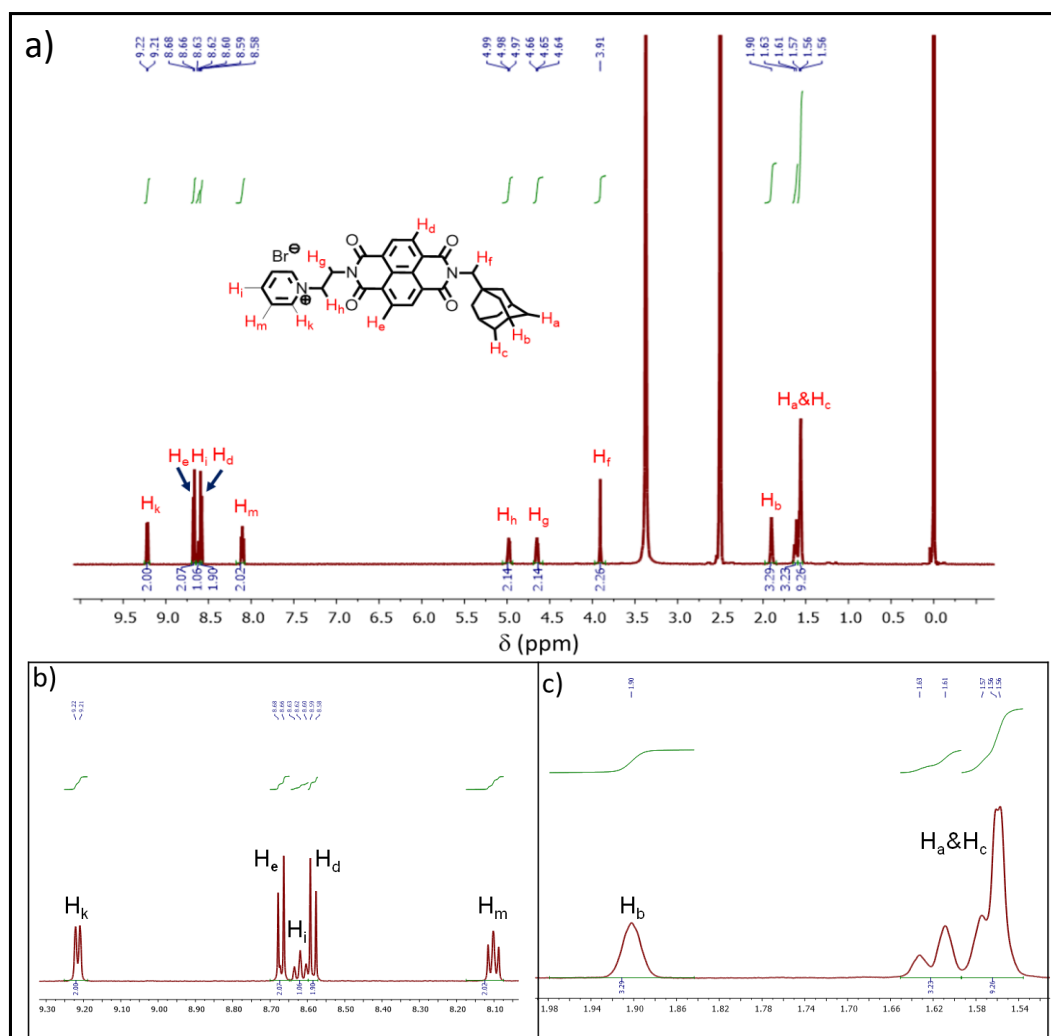


Figure 2.7. a) ^1H NMR spectrum of NDIAD in DMSO. The aromatic and aliphatic regions of the spectrum are enlarged in b and c, respectively.

The ^1H NMR spectrum of NDIAD in pure D_2O is shown in Figure 2.9a. The NDI and AD proton signals are highly broadened in the spectrum. The signal broadening is attributed to aggregation.²⁸⁻³⁰ The signals became relatively sharper upon increasing temperature (Figure 2.9b-f). The ^1H NMR signals are broad even at 80 $^\circ\text{C}$, indicating the presence of aggregates at this temperature as well.

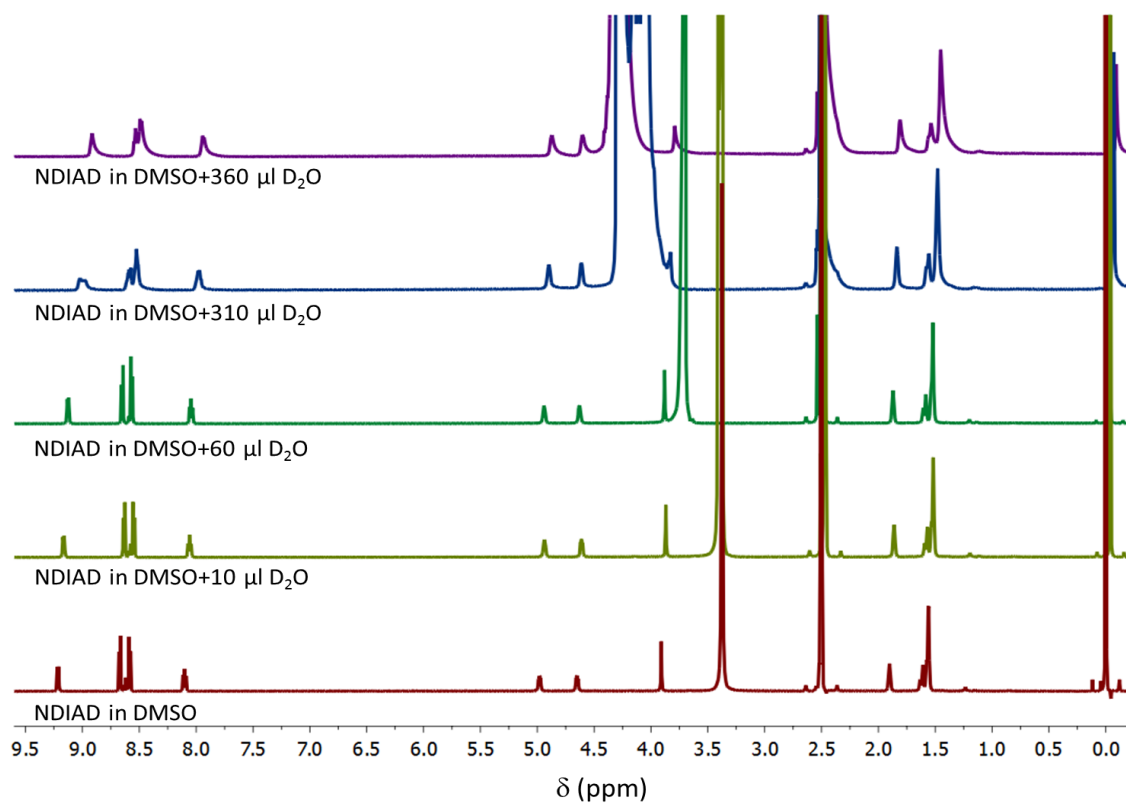


Figure 2.8. ^1H NMR titration of NDIAD in DMSO with the addition of D_2O .

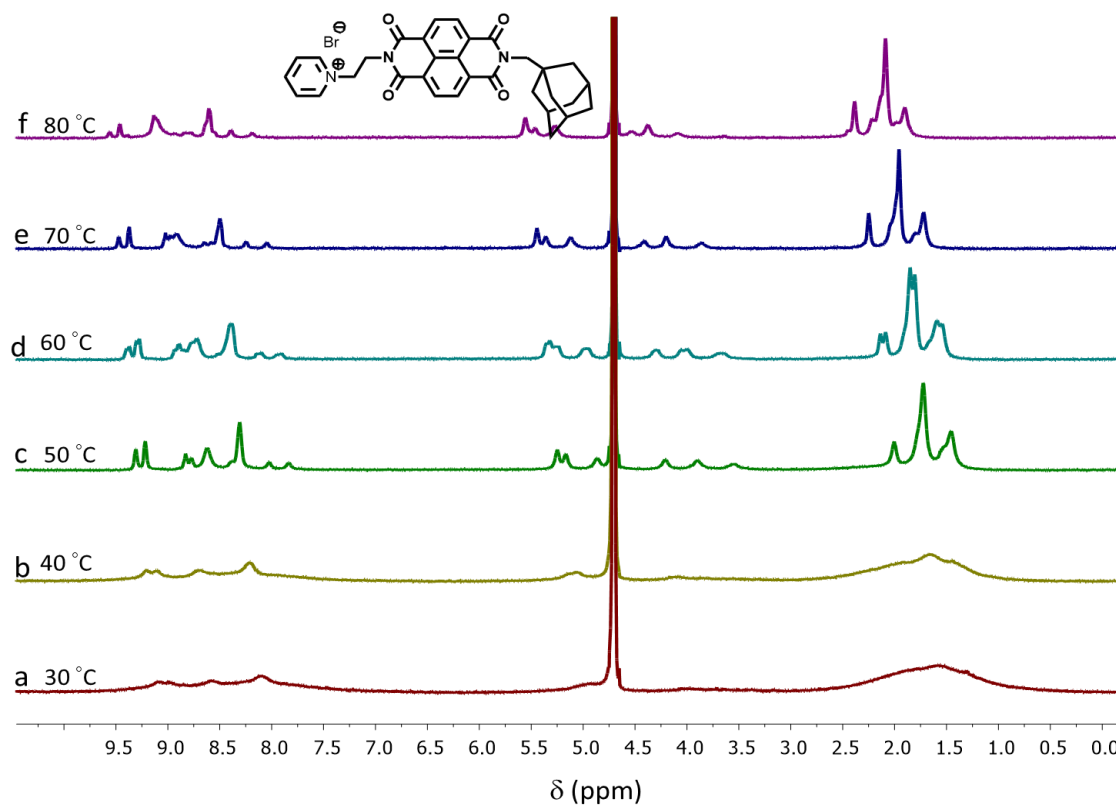


Figure 2.9. ^1H NMR spectrum of NDIAD in D_2O and its temperature dependence.

We observed that aggregation of NDIAD could be prevented by addition of β -CD. Figure 2.10 shows ^1H NMR of NDIAD in D_2O in the absence and presence of β -CD. For comparison, the NMR spectrum in D_2O at 80°C is also presented in the figure. As is evident from Figure 2.10c, the presence of β -CD, the NDI signals became sharper, but the AD protons exhibited broadening (relative to those in DMSO-d_6). In the presence of β -CD, the AD group gets encapsulated in the CD cavity and increases the solubility of the molecule. Increased solubility reduces the propensity for aggregation which is evident from the sharp signals in the aromatic region. Since the AD group is encapsulated, signals due to AD are broadened. In Figure 2.10c we can actually assign the signals due to NDI and AD protons without any difficulty. Since inclusion binding in β -CD is observed only in water, all studies reported herein were carried out in water.

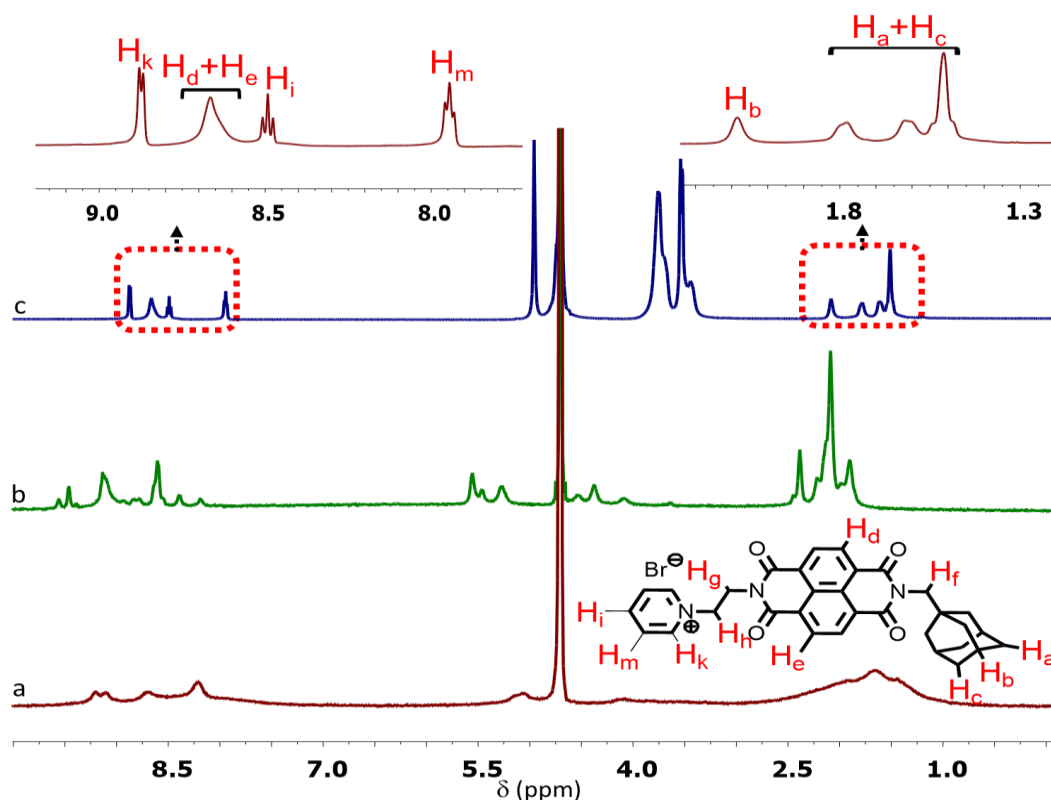


Figure 2.10. ^1H NMR spectra of a) NDIAD at 20°C , b) NDIAD at 80°C and c) NDIAD@ β -CD at 20°C in D_2O .

In order to understand the nature and conformation of the NDIAD@PYCD and NDIAD@PYP systems, a detailed NMR analysis was carried out. Figure 2.11 shows the ^1H NMR of NDIAD@PYCD in D_2O (panel b) along with those of the components PYCD (panel a) and NDIAD (panel d). For comparison purposes NMR of NDIAD@ β -CD is also shown in Figure 2.11 (panel c). ^1H NMR of 1-substituted adamantane derivatives generally show three signals: A singlet (3 protons) for H_b , singlet (6 protons) for H_c and a doublet of doublet (6 protons) for H_a . Sometimes the H_a and H_c proton signals get partially merged to give a complex pattern (as in Figure 2.11c).

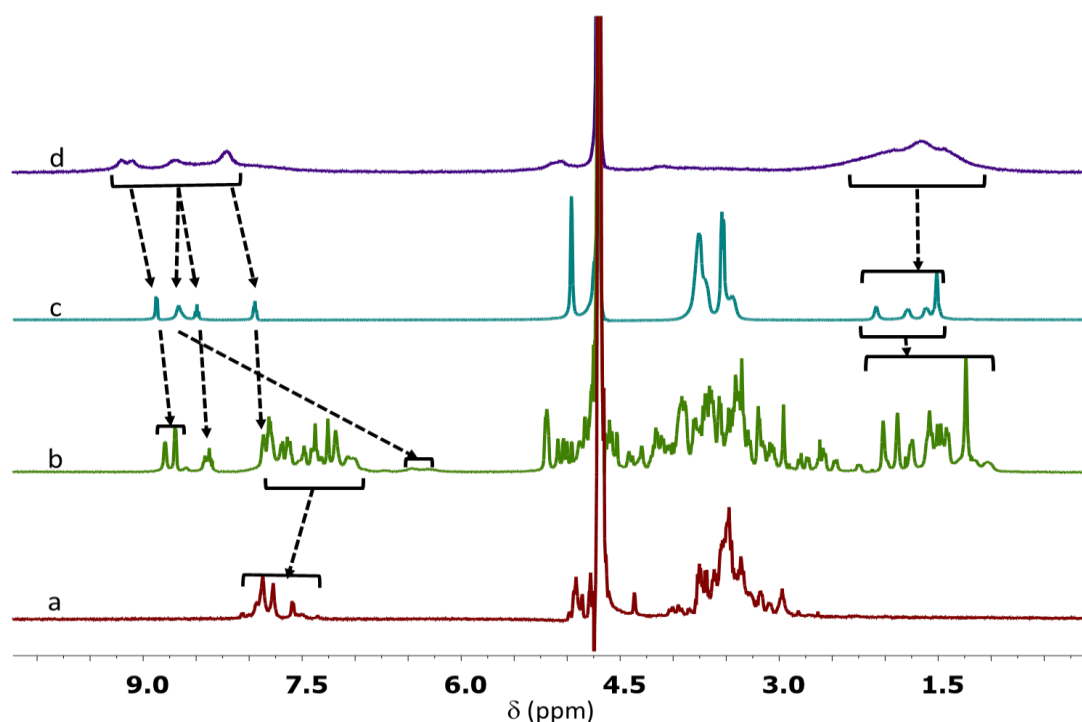


Figure 2.11. ^1H NMR spectra of a) PYCD, b) NDIAD@PYCD, c) NDIAD@ β -CD and d) NDIAD in D_2O . Major changes due to complexation are indicated by arrows.

When encapsulated in β -CD with the substituent remaining outside the wider rim, the H_a and H_b protons would be deep inside the cavity and NMR signals corresponding to these protons would be highly broadened and/or shifted. The H_c protons will be less affected. In most cases of $\text{AD@}\beta$ -CD, the three sets of protons can be easily identified in the NMR. In the case of NDIAD@PYCD (panel b, Figure 2.11), the

AD protons exhibited a very complex splitting pattern in the δ 0.95 – 2.05 ppm range. Such complex patterns were not observed previously for any AD@ β -CD systems, and this observation called for additional experiments to confirm the proton assignments.

The model compound PYP forms CT complex with NDIAD and Figure 2.12. (panel b) shows the ^1H NMR of NDIAD@PYP. For comparative purposes, NMR spectra of NDIAD and PYP are also given in Figure 2.12. In the NMR spectrum of the NDIAD@PYP complex, the signals corresponding to the AD protons appear as very sharp, clearly identifiable signals suggesting that CT complex formation proceeded with de-aggregation of NDIAD.

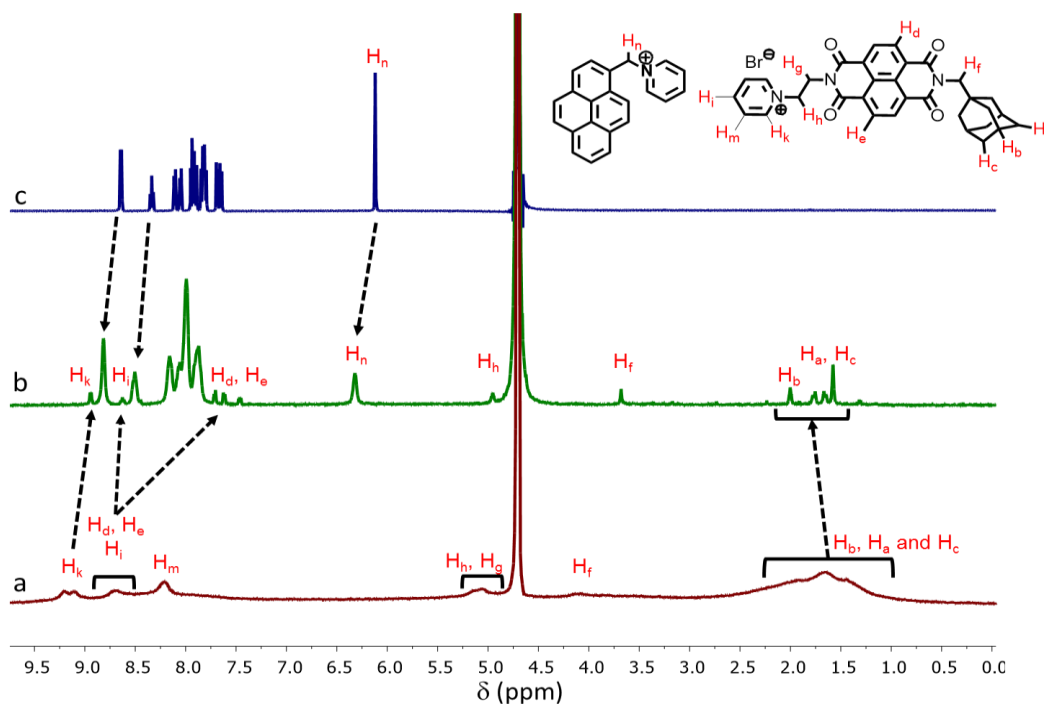


Figure 2.12. ^1H NMR spectra of a) NDIAD, b) NDIAD@PYP, c) PYP alone in D_2O .

In an attempt to understand the complex NMR pattern exhibited by NDIAD@PYCD, we have studied the temperature dependence of the NMR spectrum. Figure 2.4 showed that the intensity of the CT absorption decreased as temperature increases. We hoped that this will be reflected in the NMR spectrum as well, which in turn will give some idea about the observed NMR pattern. Temperature dependence of

the ^1H NMR spectrum of NDIAD@PYCD is shown in Figure 2.13. It can be seen that the complex pattern observed in the δ 0.95 – 2.05 ppm region at 25 $^\circ\text{C}$ got reduced into a less complex pattern at 80 $^\circ\text{C}$. Signals in the aromatic region are also considerably simplified at 80 $^\circ\text{C}$. For example, chemical shifts due to the pyridinium protons can be clearly identified at 80 $^\circ\text{C}$. If the peak at δ 9.25 ppm is identified as H_k (two protons), integration of the signals would show that the broad signals in the alkyl region (δ 1.72-2.55 ppm) correspond to fifteen protons due to the AD moiety. The small signal at δ 2.46 ppm corresponds to H_b (three protons), and the broad peak centered around δ 2.01 and 1.90 ppm corresponds to H_a and H_c (twelve protons). It may be noted that at 25 $^\circ\text{C}$ the H_k signal is split into two peaks. If these two peaks are integrated as two protons, then the complex pattern in the δ 0.95 – 2.05 ppm region would correspond to fifteen protons which can be sub divided into three groups of protons as shown in Figure 2.13 (lower panel). Since the H_c protons remain outside the cavity, we expect this proton to be less affected by complexation based on which we assign the single peak at δ 1.24 ppm to H_c and the multiplet pattern in the δ 1.36-1.65 ppm to H_a protons. This analysis has shown that the three H_b protons are not chemically equivalent. A similar situation applies to the six H_a protons. Thus, the temperature dependent NMR study has established the non-equivalency of the three H_b and six H_a protons. The non-equivalency of the protons could be due to the absence of free rotation for the AD group within the β -CD cavity and/or formation of secondary structures (vide infra).

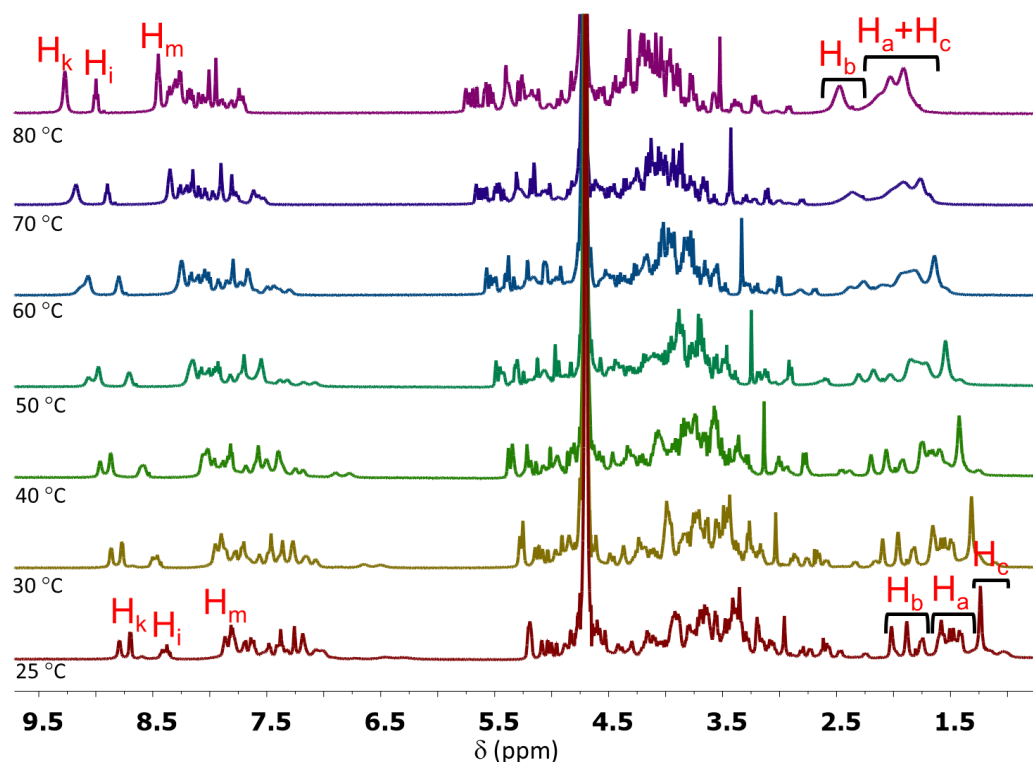


Figure 2.13. Temperature dependence of ^1H NMR of NDIAD@PYCD.

2.3.2.5. Circular dichroism studies

Achiral molecules do not exhibit any Cotton effect. If achiral molecules are associated with β -CD, they may show induced circular dichroism (ICD). Kodaka's rules can predict the orientation of the achiral molecule with respect to the β -CD axis using the sign and intensity of observed ICD signals.^{31,32} The rules predict the following: 1) For a chromophore placed inside the cavity, the sign of ICD signal will be positive for a transition polarized parallel to the axis of the β -CD, and negative for that polarized perpendicular to the axis, 2) the sign of ICD is reversed when the chromophore moves from the inside of the β -CD cavity to the outside, keeping the direction of the transition moment unchanged and 3) the absolute value of ICD is greater when a chromophore is placed on the outside of the narrower rim than when it is on the outside of the wider rim.

In order to have a detailed understanding of the complex splitting pattern in the NMR of NDIAD@PYCD complex, we have employed Circular Dichroism (CD) spectroscopy. PY and NDIAD are achiral chromophores and do not exhibit any Cotton effect, but they can exhibit induced circular dichroism (ICD) when associated with β -CD. We have reported previously that PYCD exhibits weak positive ICD signals which are similar to the $S_0 \rightarrow S_2$ transition of PY.³³ NDIAD@ β -CD exhibited a weak negative ICD signal which is shown in Figure 2.14 a . The lowest energy transition in the 300-400 nm in NDI is polarized along the N – N axis.³⁴ When the AD moiety of NDIAD is encapsulated in β -CD, the NDI chromophore is forced to stay outside the wider rim of β -CD. As can be seen in the inset in Figure 2.14b, the presence of the CH₂ group between the NDI and AD forces the NDI chromophore to adopt a conformation which is nearly parallel to the β -CD axis. The resulting ICD signal is expected to be very weak with a negative sign as per Kodaka's rule.

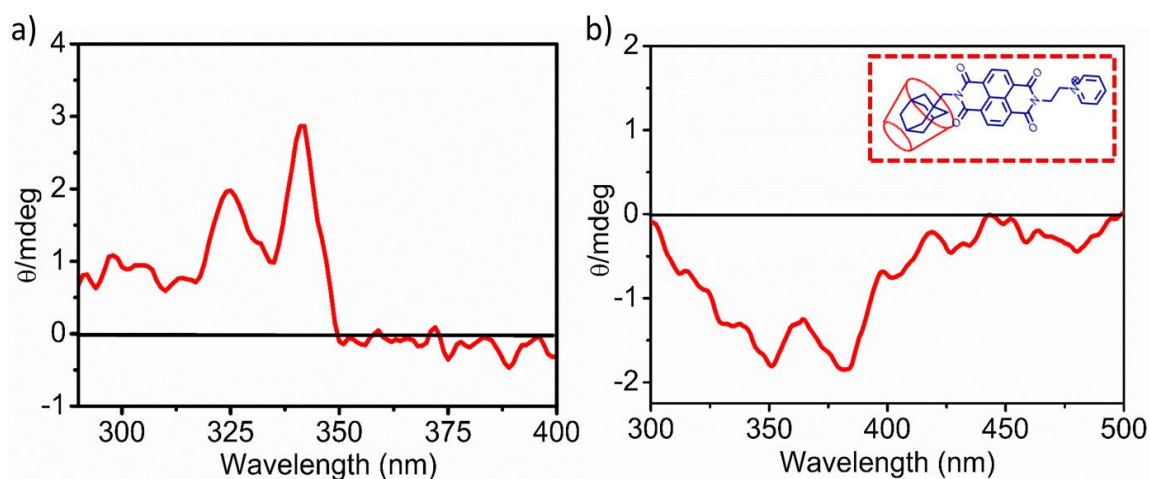


Figure 2.14. ICD spectrum of a) PYCD alone and b) NDIAD@ β -CD in water. Inset in b shows the probable orientation of NDIAD with respect to β -CD axis.

Figure 2.15a shows the ICD spectrum of NDIAD@PYCD (2.5×10^{-5} M). The spectrum exhibited a moderately strong signal in the 300-420 nm region and a weak

positive signal in the CT absorption region indicating that the CT complex is chiral. The intensity of CD signal in the CT region was low at the low concentration employed for this study. When the concentration of NDIAD@PYCD was increased to 2.5×10^{-3} M an intense CD signal was observed for CT band which is shown in Figure 2.15b (at this concentration the optical density in the region below 400 nm is significantly greater than 1.0, and hence CD spectrum of this region could not be recorded). Temperature dependence of the CD spectrum in the 20-80 °C is also shown in Figure 2.15b, which again supports the very high stability of the CT complex.

A comparison of Figure 2.15a with the absorption spectrum of the CT complex (Figure 2.3c) suggests that the observed signal (in the 300-420 nm region) is a bisignated CD signal with a first negative cotton effect. Bisignated signal arises due to exciton coupling when the chromophores involved are spatially very close and constitute a chiral system.^{20,35} In such a system the electronic transition moments would interact spatially so that the energy levels of the excited states split which will be reflected in the CD spectrum as the bisignated signal. Observation of the bisignated signal suggests that the NDIAD@PYCD complex constitute an exciton coupled bichromophoric system where the transition moments of the chromophores are rotated by a small angle.

The intense CD signal due to the CT band in Figure 2.15b cannot be attributed to induced chirality due to β -CD and we attribute this to supramolecular chirality resulting from twisted or helical structures formed by the hierarchical assembly of the CT complex as observed for PMDI@PYCD systems previously.³³

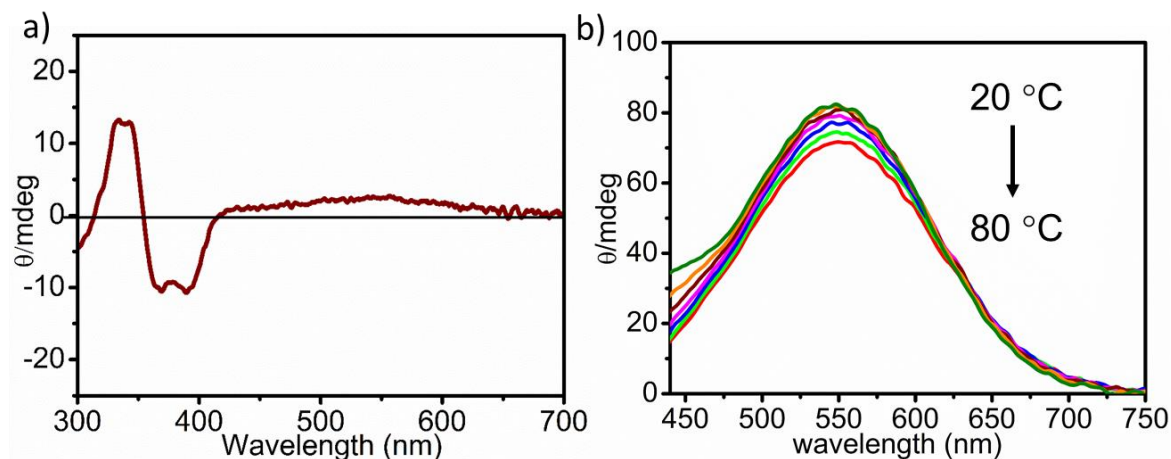


Figure 2.15. a) CD spectrum of NDIAD@PYCD (2.5×10^{-5} M) and b) CD spectrum of the CT band region (2.5×10^{-3} M) and its temperature dependence.

2.3.2.6. DLS and Tyndall effect studies

We observed the formation of nanoscopic objects in aqueous NDIAD@PYCD solutions. Presence of small particles in solution can be detected by Tyndall effect which involves the passing of a small laser beam through the sample solution. Small particles present in the path of the solution will scatter the light, making the light path visible to naked eye. The particle size distribution in the solution can be determined using dynamic light scattering (DLS) experiment.³⁶ We carried out DLS and Tyndall effect experiments to confirm the presence of supramolecular nanostructures in NDIAD@PYCD aqueous solution. The results are presented in Figure 2.16. The Tyndall effect experiment clearly showed the laser path and confirmed the presence of small particles in the NDIAD@PYCD solution (Figure 2.16a). The DLS experiment (Figure 2.16b) showed the presence of nanostructures with a narrow size distribution in the range of 60-100 nm, with average hydrodynamic size of ~ 80 nm even in dilute solutions (10^{-4} M) of 1:1 NDIAD@PYCD. In order to get a better understanding of these particles, AFM and TEM experiments were carried out.

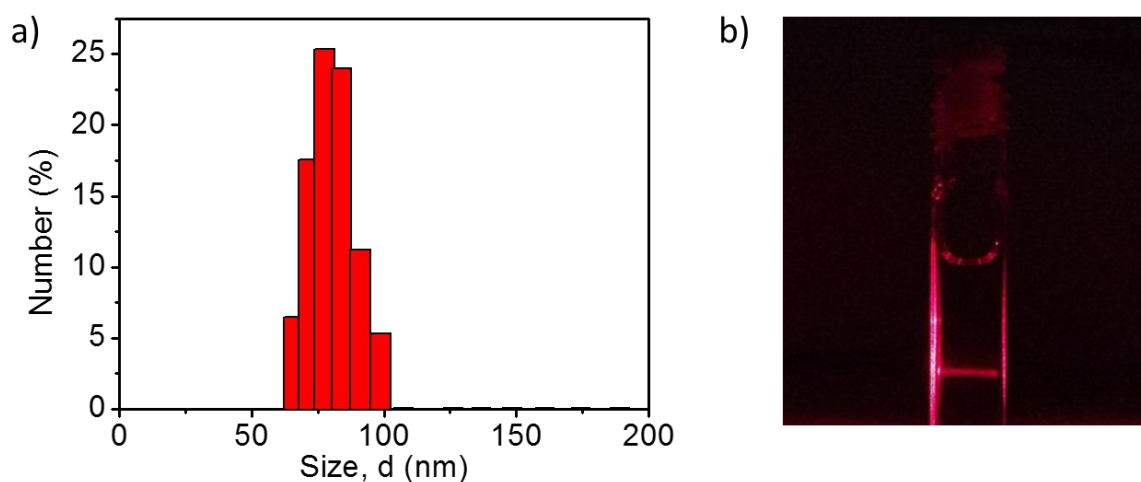


Figure 2.16. a) Size distribution profile of 10^{-4} M solution of 1:1 NDIAD@PYCD in water. b) Tyndall effect of 10^{-4} M solution of NDIAD@PYCD in water.

2.3.2.7. Morphological analysis

The presence of nanostructures in NDIAD@PYCD solution is further confirmed with the help of TEM and AFM analysis (Figure 2.17).

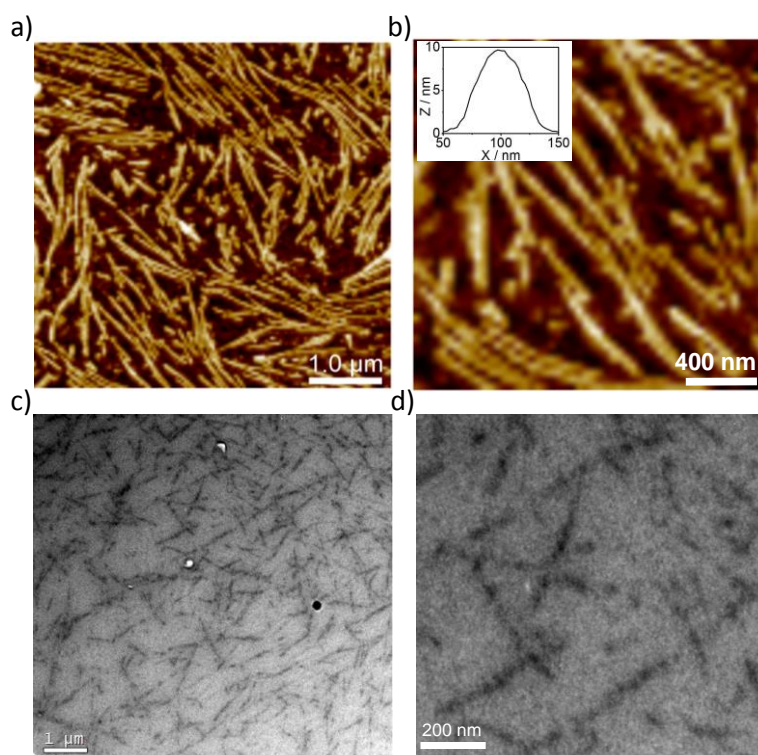
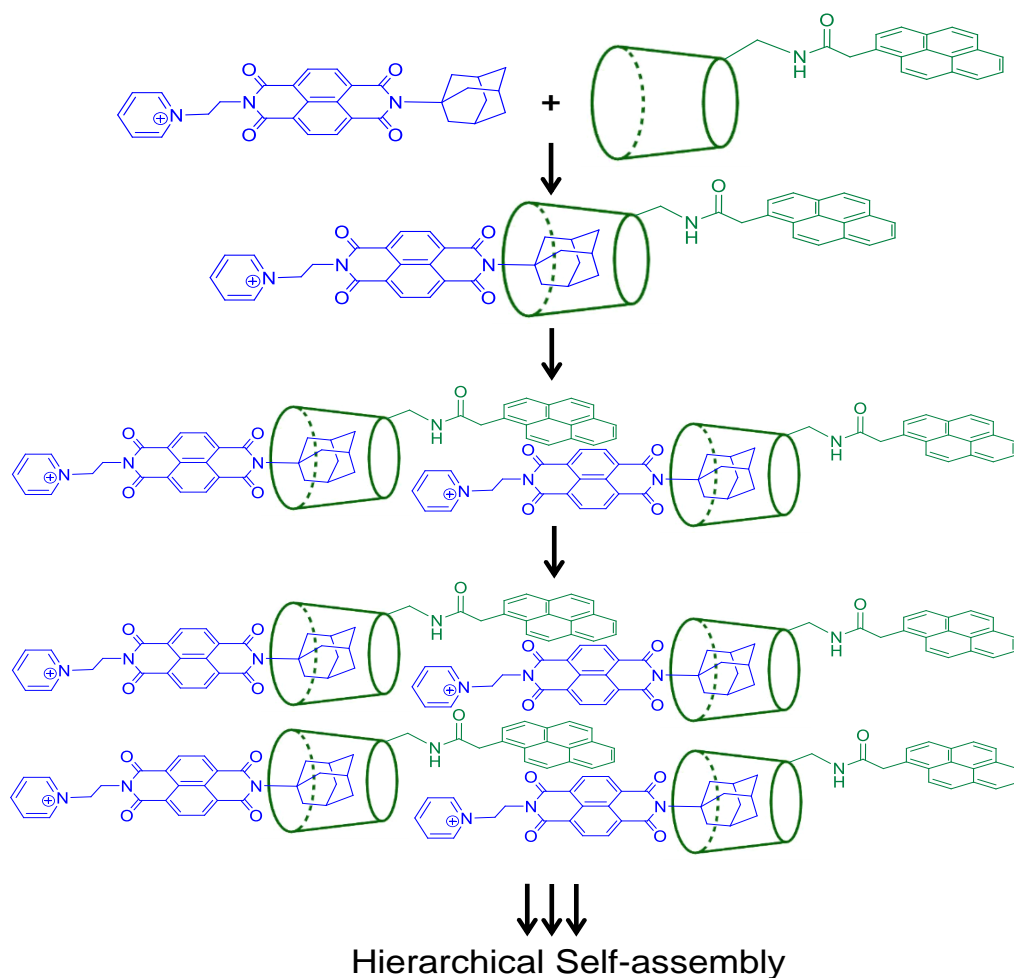


Figure 2.17. a, b) AFM and c, d) TEM images of nanofiber formation of NDIAD@PYCD in water. Inset in b shows the height profile of the nanofibers.

AFM and TEM images of NDIAD@PYCD (1×10^{-4} M, 1:1) showed the presence of twisted nanofibers of $\sim 1.0 \mu\text{m}$ length, 80-100 nm width and 7-10 nm height. The zoomed AFM and TEM images clearly show the twisted nature of the fibers. The CD signal due to the CT band can be attributed to the twisted supramolecular fibers seen in AFM. Using the AFM, the root mean square (rms) roughness of the film was measured and the value obtained was 2.6-3.6 nm, suggesting that film surface is very smooth or homogeneous.

2.3.2.8. Mechanism of self-assembly

As mentioned earlier, both CT and inclusion binding interactions are involved in the formation of NDIAD@PYCD. NMR, ICD and microscopic studies (vide infra) suggested that the inclusion/CT complex formed initially underwent hierarchical self-assembly. Since $K_{a(\text{IN})} > K_{a(\text{CT})}$, we propose Scheme 2.3 for the formation of NDIAD@PYCD and its further assembly into hierarchical structures. Further self-assembly occurs through cumulative CT interactions as shown in Scheme 2.3. The scheme, however, does not explain the complex pattern observed for the adamantyl and pyrene protons in the ^1H NMR spectrum of NDIAD@PYCD and the bisignated CD signal. In order to explain these aspects, we invoke a twisting between the pyrene and NDI moieties of the assembly.



Scheme 2.3. Formation of NDIAD@PYCD complex and its hierarchical self-assembly.

Several reports dealing with crystal structures of PY/NDI CT complexes are available in the literature.¹⁷ Gujrati *et al.* reported that in the CT complex, NDI and PY exist as alternating units in columnar stacks along the crystallographic *a* axis with an inter planar distance of 3.4 Å and a dihedral angle (θ) of $\sim 53^\circ$ between the long molecular axes of NDI and PY.³⁷ A computational study by Lin predicted θ values from 50 – 75° for the PY/NDI complexes.³⁸ Li *et al.* prepared PY/NDI complexes that exhibited reversible color changes in the solid state when treated with different organic solvents. The origin of the color changes was shown to be solvent inclusion which leads to changes in θ value. CT crystals which did not contain any solvent molecules appeared

orange in color ($\lambda_{\max} = 500 \text{ nm}$), and θ values for these were found to be $< 50^\circ$. CT crystals with purple or purple-red colors ($\lambda_{\max} \approx 530 \text{ nm}$) have two solvent molecules included in the crystal, and these have θ values $> 50^\circ$.¹⁷ The above reports provide valuable insights regarding the origin of the bisignated CD signal which is a consequence of the orientation of chromophores in the NDIAD@PYCD system.

The NDIAD@PYCD system exhibited deep violet color with $\lambda_{\max} = 568 \text{ nm}$. Applying the information from the crystal structures, we may predict that two water molecules are incorporated in the CT stack which increases the dihedral angle to nearly 70° . The CT system exhibited induced chirality because they are associated closely with β -CD, but since the chromophores exhibited a twist angle between their long molecular axes the resulting CD signal is bisignated. The signal intensity is small because the chirality is not intrinsic but induced. Thus, the π -stacking in NDIAD@PYCD could be as shown in Figure 2.18a or b. In the configuration shown in Figure 2.18a, the dihedral angle between PY and NDI is $> 50^\circ$, which is similar to the crystal structure reported by Gujrati *et al.*³⁷ In this configuration the orientation of PY and NDI chromophores are identical in successive stacks. This means that all PY residues have similar chemical environments throughout the assembly. The NDI moieties also have similar environments and hence all the AD units linked to NDI and included in PYCD cavities are also expected to have similar chemical and magnetic environments. Although Figure 2.18a explains the bisignated CD signal, it cannot explain the complex NMR pattern of NDIAD@PYCD reported in Figure 2.11b.

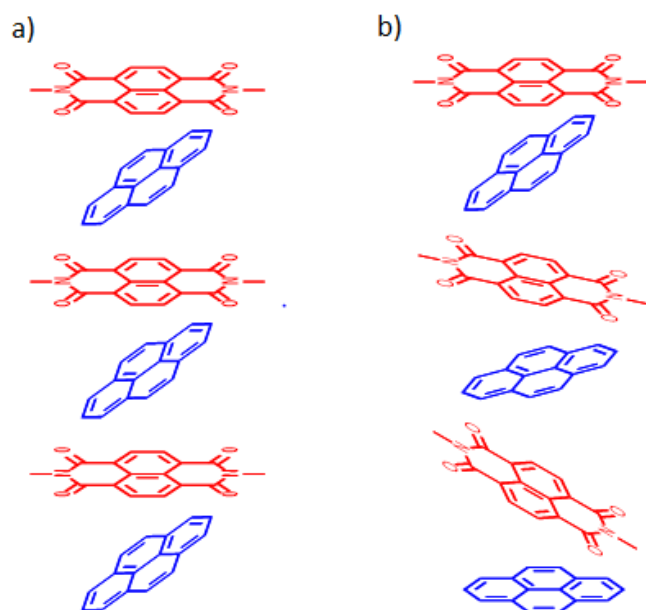
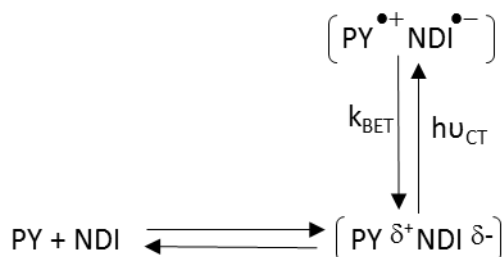


Figure 2.18. Possible π -stacking arrangements in NDIAD@PYCD.

In order to explain the complex NMR pattern in Figure 2.11b, we invoke the D-A stack configuration in Figure 2.18b where the dihedral angle between NDI and PY remains the same but each NDI-PY pair is rotated by some angle with respect to the preceding and succeeding NDI-PY pairs. Thus, each PY, NDI and AD groups have slightly different chemical and magnetic environments compared to their analogues in adjacent stacks. The origin of the complex NMR spectrum of NDIAD@PYCD and the bisignated CD signal can be explained using Figure 2.18b.

2.3.2.9. Femtosecond transient absorption studies

According to Mulliken's theory, CT complexes are formed by partial transfer of electron from the HOMO of the donor to the LUMO of the acceptor. The CT absorption band is due to this charge transfer. For the NDIAD@PYCD system the CT absorption occurs in the 400-700 nm region. Irradiation of the complex using 532 nm laser light is expected to produce the ion-pair state $[PY^{*+} NDI^{*-}]$ as shown in Scheme 2.4.



Scheme 2.4. Schematic representation of the formation of excited ion pair state.

$\text{PY}^{\bullet+}$ stands for the radical cation of the PY donor and $\text{NDI}^{\bullet-}$ stands for the radical anion of the NDI acceptor. k_{BET} is the rate constant of back electron transfer which regenerates of the CT ground state. We have employed nanosecond and femtosecond transient absorption spectroscopy to confirm the formation of radical ion species upon excitation of the CT complex. Nanosecond flash photolysis of NDIAD@PYCD employing 532 nm laser pulses did not yield any transient species indicating that excitation of the CT state did not furnish any long-lived species.

Femtosecond transient absorption studies, however, resulted in the formation of extremely short-lived species absorbing the 400-550 nm region. Since we have used 600 nm excitation, the region around the pump wavelength could not be probed. Transient absorption spectra obtained in the 4.5 ps – 24 ps time window are shown in Figure 2.19 a. The transient spectra showed maximum around 470 nm and shoulder at 425 nm. Using a peak fitting program, we could resolve the broad spectrum into two absorptions, as shown in Figure 2.19b, with λ_{max} at 440 nm and 474 nm. Based on previous reports by others^{39,40} and us,⁴¹ the 440 nm absorption was assigned to $\text{PY}^{\bullet+}$. $\text{NDI}^{\bullet-}$ is known to exhibit a broad absorption extending up to 800 nm with maximum around 470 nm.⁴²⁻⁴⁴ Hence we assign the 474 nm absorption to $\text{NDI}^{\bullet-}$. Thus, the femtosecond transient absorption studies confirmed the generation of the radical ion pair as per Scheme 2.4.

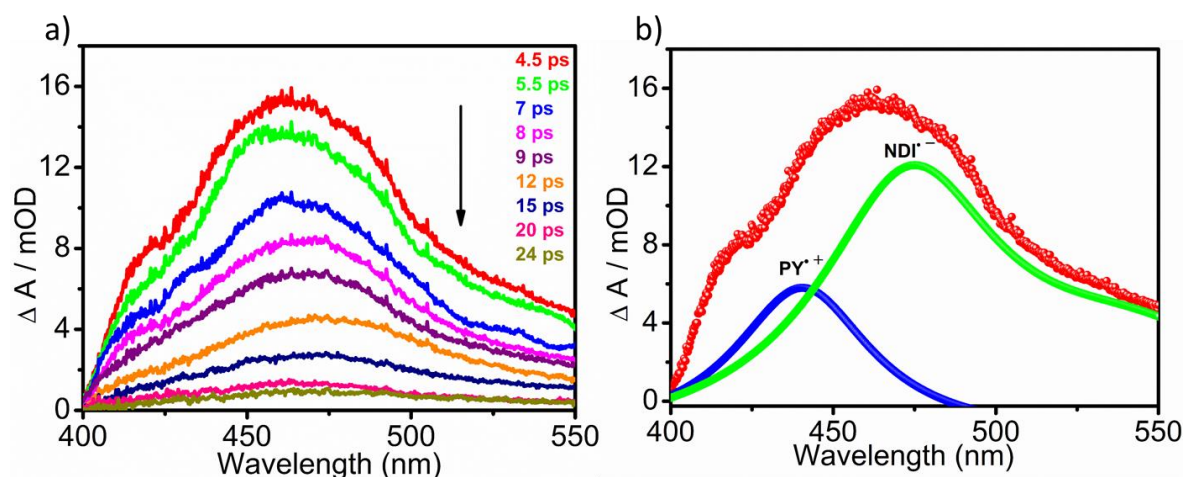


Figure 2.19. a) Femtosecond transient absorption spectra of NDIAD@PYCD recorded at different time delays (4.5 ps – 24 ps) upon excitation at 600 nm. b) Spectra of constituents generated by the peak fitting program.

The kinetic traces obtained at wavelengths 440 nm and 474 nm are shown in Figure 2.20. Examination of the kinetic profiles suggests that the transient species are formed within a very short time (<100 fs) and decay by first order kinetics. Fitting of the profiles gave lifetime of 6 ps for both absorptions, which correspond to decay rate of $1.66 \times 10^{11} \text{ s}^{-1}$. For several D-A complexes studied by Kochi and co-workers the k_{BET} values were in the range of $(1.6 - 2.0) \times 10^{10} \text{ s}^{-1}$ range.^{23, 24, 45-47} None of the systems studied by Kochi's group self-assembled into supramolecular systems. For a CT complex which formed supramolecular fibers, Aoki *et al.* reported k_{BET} value of $2.2 \times 10^{10} \text{ s}^{-1}$.²⁵ For the NDIAD@PYCD system studied here k_{BET} value obtained is one order of magnitude larger. The extremely fast formation and decay of the ion pairs suggest that PY and NDI chromophores are very tightly packed in the NDIAD@PYCD nano structures and the inter ionic separation in PY^{*+}/NDI^{*-} can be considered as very similar to that in contact ion pairs. Rapid formation and decay of this state confirms that the donor and acceptor precursors are residing in close proximity and both the forward and back electron transfers are static in nature.

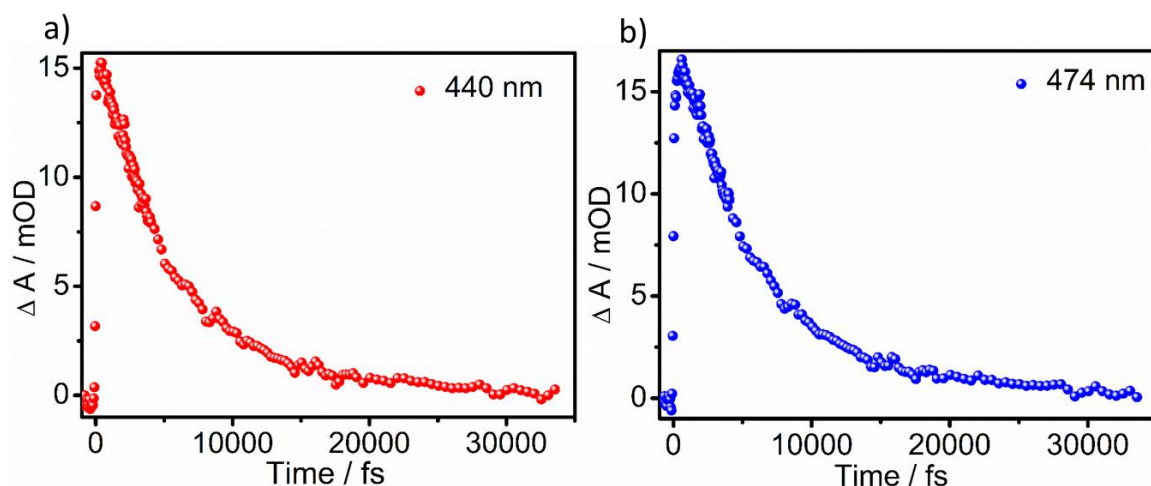


Figure 2.20. Kinetic decay obtained at the probe wavelengths a) 440 nm and b) 474 nm.

2.3.2.10. Conductivity measurements

Mixed stack CT complexes of aromatic molecules are well known for their inherent semiconducting properties. We carried out horizontal conductivity measurements of NDIAD@PYCD films. Initially we measured I-V measurement on the gold (red trace) and mica (blue trace) surfaces indicating the ohmic and insulator behaviour respectively as shown in Figure 2.21.

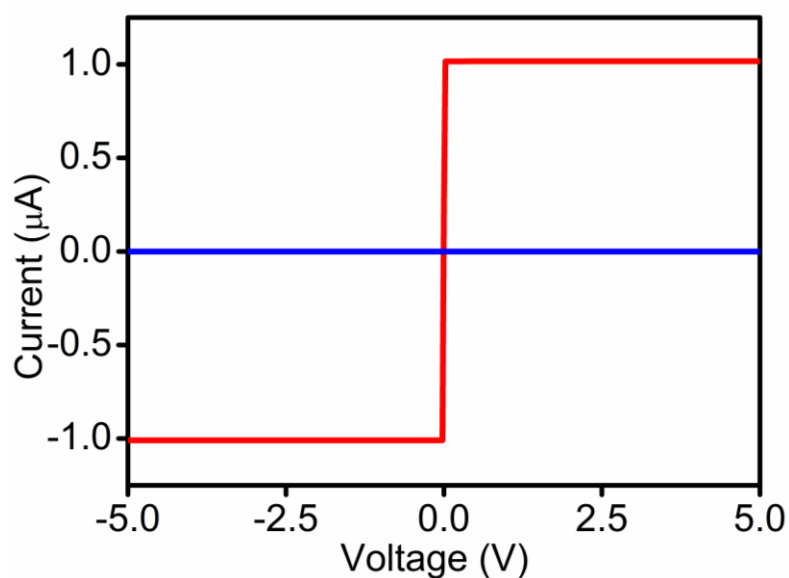


Figure 2.21. I-V measurements on gold (red trace) and mica (blue trace) surfaces.

For measuring the conductivity of NDIAD@PYCD films, gold metal was thermally evaporated on to a small unmasked area on a freshly cleaved mica surface. The mask was removed and a film of NDIAD@PYCD was deposited on to this region by drop casting 10^{-4} M solution. The NDIAD@PYCD fibers formed on the surface could be located by tapping mode AFM using a conductive tip (Figure 2.22).

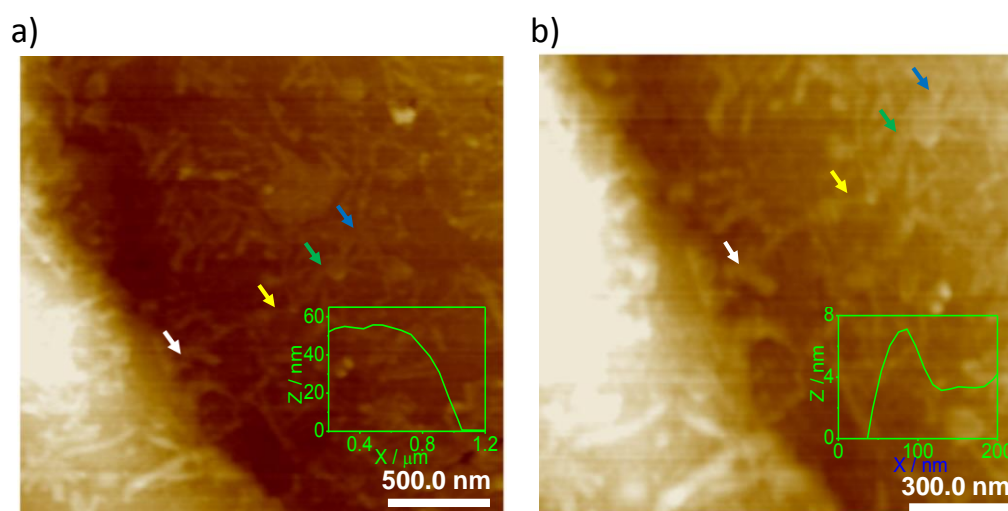


Figure 2.22. a) AFM image showing nanofibers of NDIAD@PYCD in contact with the gold metal electrode edge. b) Zoomed version of a. Insets in a and b show the thickness of the gold electrode and height of the nanofiber, respectively.

From the AFM image, we obtained the thickness of the gold electrode as 55 nm (inset in Figure 2.22a) and height of the nanofibers as 7 nm (inset in Figure 2.22b). The horizontal conductivity of nanofibers was calculated using the equation $\sigma = d/(A_t R)$ S/cm,⁴⁸ where d is the sample thickness (7 nm), R is the resistance of the sample and A_t is the area of the C-AFM probe in contact with the surface. ' A_t ' was calculated as πr_t^2 , assuming a contact radius of 35 nm between tip and sample. R is estimated from the inverse slope of the I-V curve. In Figure 2.22a the white arrow marks the junction between the gold electrode and nanofibers. The yellow, green and blue arrows represent locations at 500 nm, 800 nm, and 1.0 μm , respectively, from the junction. The

current along the nanofiber was measured by bringing the AFM tip in contact with the sample surface. I-V data of NDIAD@PYCD film was measured between -5V to 5V with the applied bias voltage of 1V. I-V curve obtained by keeping the tip at 500 nm from the junction is shown in Figure 2.23a. Nearly identical I-V curves were obtained at 800 nm (Figure 2.23b) and 1.0 μm (Figure 2.23c) distances also, which confirmed that there are no metal deposits on the nanofibers beyond the electrode edge. Nonlinear diode like nature of these I-V curves implies semiconducting nature of the nanofibers. The horizontal conductivity of the sample was calculated as $1.2 \times 10^{-3} \text{ S/cm}$ for nanofiber height of 7 nm and tip contact radius of 35 nm. The conductivity value obtained here is higher than that reported previously for a pyrene/NDI self-assembled CT complex.²⁰ This enhanced conductivity can be attributed to the high association constant for the NDIAD@PYCD CT complex formation.

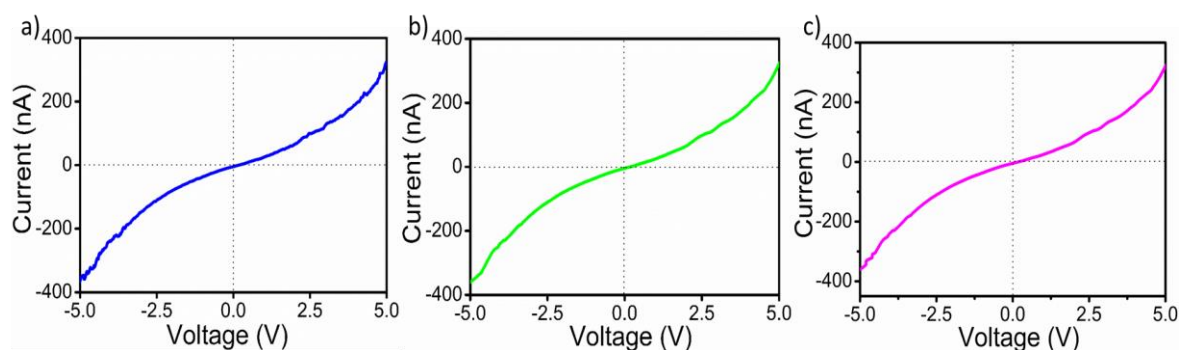


Figure 2.23. I-V measurement taken at a) 500 nm, b) 800 nm and c) 1 μm from the junction.

2.4. Conclusions

In conclusion, we have designed a highly stable PY-NDI CT complex by exploiting the high affinity of adamantane derivatives for inclusion binding in β -CD cavity to augment the CT interaction between PY and NDI chromophores. The association constant for complexation, as measured by ITC, was $3.64 \times 10^7 \text{ M}^{-1}$, which is the highest

value reported for any CT complex. π -stacking between PY and NDI, and inclusion binding of adamantane moiety in β -CD are probed using ^1H NMR. Adamantane protons within the CD cavity exhibited an extremely complex NMR pattern. Careful analysis with the aid of temperature-dependent NMR, supported by circular dichroism spectroscopy, suggested that protons of each PY, NDI, and adamantane groups have slightly different chemical and magnetic environments compared to their analogues in adjacent stacks. Based on these results we proposed that within the complex the PY and NDI exist as alternating units with a dihedral angle $> 50^\circ$ between them, but each PY-NDI pair is rotated slightly with respect to the preceding and succeeding pairs. The AFM and TEM analysis confirm that the CT complex undergo hierarchical self-assembly to give twisted fibers which showed horizontal conductivity of 1.2×10^{-3} S/cm and it may have potential applications in organic electronics. Excitation of the CT band in NDIAD@PYCD using femtosecond laser gave transients assignable to $\text{PY}^{\bullet+}$ and $\text{NDI}^{\bullet-}$ radical ion pairs. Ultrafast formation (<100 fs) and decay (~ 6 ps) confirms close packing of the PY and NDI moieties in the nano assembly.

2.5. Experimental Sections

2.5.1. Instrumentation and methods

All solvents and reagents were commercially available and used without further purification, unless otherwise specified. All experiments were performed in deionized water at 25 °C. Electronic absorption spectra were recorded on a Shimadzu UV-2600 UV-Vis spectrophotometer. ITC data was obtained using microcal iTC 200. The raw data obtained was fitted and analysed using origin 7.0 software provided along with the instrument. Circular dichroism experiments were performed on JASCO 810 spectrometer

using quartz cuvettes of 1 cm path length, equipped with peltier thermostatic cell holders for variable temperature studies. All NMR spectra were recorded in D₂O, and DMSO-d₆ purchased from Aldrich, using a 500 MHz Bruker Avance DPX spectrometer. ESI-HRMS mass spectra were recorded using orbitrap mass spectrometer (Thermo Exactive). TEM analyses were performed using a FEI-TECNAI T30 G2S-TWIN, 300 kV HRTEM microscope with an accelerating voltage of 100 kV and the samples were prepared by drop-casting the aqueous solution on a formvar coated copper grid (400 mesh) and evaporating excess water. AFM images were recorded on Multimode SPM (Bruker Nanoscope V) operating with a tapping mode regime. Antimony doped silicon cantilever with a resonant frequency of 300 kHz and spring constant of 40 Nm⁻¹ were used. The sample solution in water was drop casted directly on top of a mica substrate, and water was allowed to evaporate at ambient conditions and used for AFM analysis. For C-AFM measurement, the gold electrode deposition was carried out by the thermal evaporation in an ultra-high vacuum chamber, and platinum coated conductive probes (NTMDT-CSG series) were used in a humidity-controlled atmosphere (<40% relative humidity). Femtosecond transient absorption experiments were performed using a Ti: sapphire laser light centered around 800 nm (Mai Tai HP, Spectra Physics, USA) having pulse width <100 fs and 80 MHz repetition rate. The amplified laser beam was split into two in the ratio of 75:25%. The more intense beam was converted into the required wavelength (600 nm) for exciting the sample by using TOPAZ (Prime, Light Conversion). The white light continuum (340–1000 nm) was generated by focusing the less intense beam on to a 1-mm-thick CaF₂ plate and was split into two beams (sample and reference probe beams). The sample cell (0.4 mm path length) was refreshed by rotating at constant speed. Finally, the white light continuum was focused into a 100 μm optical

fiber coupled to imaging spectrometer after passing through the sample cell. The pump-probe spectrophotometer (ExciPro) setup was purchased from CDP Systems Corp, Russia. Transient absorption spectra were obtained by averaging about 2000 excitation pulses for each spectral delay. All the measurements were carried out at the magic angle (54.7°). The time resolution of the pump-probe spectrometer is found to be about 120 fs.

2.5.2. Materials

β -Cyclodextrin, 1,4,5,8-naphthalenetetracarboxylic dianhydride, 1-adamantyl methylamine and 1-pyreneacetic acid were purchased from Sigma Aldrich and used as received. All solvents and reagents were commercially available and used without further purification, unless otherwise specified. Procedures for the synthesis of PYCD and NDIAD are described below.

A) Synthesis of 2:

1, 4, 5, 8- naphthalenetetracarboxylic dianhydride 1 (6.0 g, 22.37 mmol) was dissolved in dry DMF (120 mL) and 1-adamantyl methylamine (3.69 g, 22.37 mmol) was added. After 1 h, 2-amino-1-ethanol (1.36 g, 22.37 mmol) was added and refluxed for 24 h at 130 °C. The reaction mixture after cooling was added to ice-cold water and the resulting precipitate was filtered and dried. This was purified by column chromatography over silica gel. Elution with methanol/chloroform (2:98) gave the product. Yield: 40%; mp > 300 °C; FT-IR (KBr): ν_{\max} = 3545, 3060, 2904, 2846, 1705, 1662, 1582, 1456 cm^{-1} ; ^1H NMR (500 MHz THF d_8) δ ppm: 8.71 (dd, 4H), 4.29 (t, 2H), 4 (s, 2H), 3.75 (t, 2H), 1.96 (s, 3H), 1.64 (m, 12H); ESI-MS: Calculated for $\text{C}_{27}\text{H}_{26}\text{N}_2\text{O}_5$ (M)⁺ =458.1842 and found m/z = 459.19.

B) Synthesis of 3:

Compound 2 (0.5 g, 1.09 mmol) was added to a mixture of aqueous HBr (4 mL) and conc. H₂SO₄ (1.5 mL). Conc. H₂SO₄ (1.5 mL) was again added and the solution was refluxed for 3h. The mixture was cooled and the product was extracted with dichloromethane and recrystallized from dichloromethane-methanol mixture to get the pure product. Yield: 50%; mp > 300 °C; FT-IR (KBr): ν_{\max} = 3079, 2900, 2846, 1701, 1666, 1576, 1450 cm⁻¹; ¹H NMR (500 MHz, CDCl₃) δ ppm: 8.78 (dd, 4H), 4.65 (t, 2 H), 4.04 (s, 2 H), 3.70 (t, 2H), 1.96 (s, 3H), 1.64 (m, 12H); ESI-MS: Calculated for C₂₇H₂₅BrN₂O₄ (M)⁺ = 520.099 and found 521.099.

C) Synthesis of 4 (NDIAD):

Compound 3 (0.1 g, 0.19 mmol) was refluxed in pyridine (10 mL) for 24 h and cooled. The solid separated was filtered and pyridine was removed by washing with hexane and chloroform. Yield: 75%; mp 294- 295 °C; FT-IR (KBr): ν_{\max} = 3057, 2908, 2850, 1703, 1665 cm⁻¹; ¹H NMR (500 MHz, DMSO d₆) δ ppm: 9.21 (d, 2H), 8.67 (d, 2H), 8.61 (t, 1H), 8.58 (d, 2H), 8.10 (t, 2H), 4.98 (t, 2H), 4.65 (t, 2H), 3.91 (s, 2H), 1.90(s, 3H), 1.58(m, 12H); ¹³C NMR (125 MHz, DMSO d₆) δ ppm: 163.65, 146.44, 146, 131.06, 128.39, 127.09, 126.43, 60.07, 50.64, 41.23, 36.75, 35.90, 28.24; ESI-MS: calculated for C₃₂H₃₀N₃O₄⁺ = 520.22 (M)⁺ Found m/z = 520.22.

D) Synthesis of 6 (PYCD):

5 was prepared by a reported procedure.⁴⁹ To a cooled solution (-10°C) of 1-pyreneacetic acid (0.21 g, 0.86 mmol) in DMF (4 mL), dicyclohexylcarbodiimide (DCC) (0.180 g, 0.80 mmol) and 1-hydroxybenzotriazole (1-HOBt) (0.109 g, 0.80 mmol) were added. The reaction mixture was stirred at -10 °C for 30 min. To the stirred solution 5

(0.45 g, 0.40 mmol) was added and stirring continued at $-10\text{ }^{\circ}\text{C}$ for 30 min. The mixture was then refluxed at $60\text{ }^{\circ}\text{C}$ for 24 h. The reaction mixture was cooled and DMF was removed under vacuum. The residue obtained was washed with excess acetone and dried. The solid obtained was dissolved in DMF and subjected to reverse phase column chromatography over silica gel. Elution with methanol/water mixture (1:1) gave 6. Yield: 52%; FT-IR (KBr): ν_{max} : 3334, 2933, 1651, 1537, 1153, 1029, 945, 848 cm^{-1} ; ^1H NMR (DMSO d_6) δ ppm: 8.01-8.39 (m, 10 H), 5.66-5.87 (m, 14 H), 4.83-4.97 (m, 7 H), 4.80 (t, 1 H), 4.24-4.50 (m, 7 H), 3.54- 3.62 (m, 14 H), 3.3-3.4 ppm (m, 32 H); ^{13}C NMR (DMSO d_6) δ ppm : 59.84, 72.01, 72.22, 72.40, 72.97, 73.16, 81.39, 81.63, 81.86, 99.49, 101.88, 101.97, 123.90, 124.04, 124.10, 124.68, 124.88, 125.02, 126.13, 126.76, 127.12, 127.37, 128.55, 128.99, 129.64, 130.34, 130.80, 131.06, 170.39; (ESI-MS): Calculated for $\text{C}_{60}\text{H}_{81}\text{NO}_{35}$ (M+H) $^{+}$ 1376.45 and found 1376.47.

2.6. References

- (1) Song, B.; Wei, H.; Wang, Z.; Zhang, X.; Smet, M.; Dehaen, W. Supramolecular nanofibers by self-organization of bola-amphiphiles through a combination of hydrogen bonding and π - π stacking interactions. *Adv. Mater.* **2007**, *19*, 416–420.
- (2) Das, A.; Molla, M. R.; Banerjee, A.; Paul, A.; Ghosh, S. Hydrogen-bonding directed assembly and gelation of donor-acceptor chromophores: Supramolecular reorganization from a charge-transfer state to a self-sorted state. *Chem. Eur. J.* **2011**, *17*, 6061–6066.
- (3) Mondal, T.; Basak, D.; Al Ouahabi, A.; Schmutz, M.; Mésini, P.; Ghosh, S. Extended supramolecular organization of π -systems using yet unexplored simultaneous intra- and inter-molecular H-bonding motifs of 1,3-dihydroxy derivatives. *Chem. Commun.* **2015**, *51*, 5040–5043.
- (4) Sun, Y.; Jiang, L.; Schuermann, K. C.; Adriaens, W.; Zhang, L.; Boey, F. Y. C.; De cola, L.; Brunsveld, L.; Chen, X. Semiconductive, one-dimensional, self-assembled

- nanostructures based on oligopeptides with π -conjugated segments. *Chem. Eur. J.* **2011**, *17*, 4746–4749.
- (5) Biedermann, F.; Scherman, O. A. Cucurbit[8]uril mediated donor–acceptor ternary complexes: A model system for studying charge-transfer interactions. *J. Phys. Chem. B* **2012**, *116*, 2842–2849.
- (6) Liu, H.; Brémond, É.; Prlj, A.; Gonthier, J. F.; Corminboeuf, C. Adjusting the local arrangement of π -stacked oligothiophenes through hydrogen bonds: A viable route to promote charge transfer. *J. Phys. Chem. Lett.* **2014**, *5*, 2320–2324.
- (7) Moughton, A. O.; O’Reilly, R. K. Noncovalently connected micelles, nanoparticles, and metal-functionalized nanocages using supramolecular self-assembly. *J. Am. Chem. Soc.* **2008**, *130*, 8714–8725.
- (8) Song, B.; Wu, G.; Wang, Z.; Zhang, X.; Smet, M.; Dehaen, W. Metal-ligand coordination-induced self-assembly of bolaamphiphiles bearing bipyrimidine. *Langmuir* **2009**, *25*, 13306–13310.
- (9) Wang, C.; Guo, Y.; Wang, Z.; Zhang, X. Superamphiphiles based on charge transfer complex: Controllable hierarchical self-assembly of nanoribbons. *Langmuir* **2010**, *26*, 14509–14511.
- (10) Kumar, N. S. S.; Gujrati, M. D.; Wilson, J. N. Evidence of preferential π -stacking: A study of intermolecular and intramolecular charge transfer complexes. *Chem. Commun.* **2010**, *46*, 5464–5466.
- (11) Das, A.; Ghosh, S. Stimuli-responsive self-assembly of a naphthalene diimide by orthogonal hydrogen bonding and its coassembly with a pyrene derivative by a pseudo-intramolecular charge-transfer interaction. *Angew. Chem. Int. Ed.* **2014**, *53*, 1092–1097.
- (12) Bhattacharjee, S.; Bhattacharya, S. Charge transfer induces formation of stimuli-responsive, chiral, cohesive vesicles-on-a-string that eventually turn into a hydrogel. *Chem. Asian J.* **2015**, *10*, 572–580.
- (13) Bhattacharjee, S.; Maiti, B.; Bhattacharya, S. First report of charge-transfer induced heat-set hydrogel. Structural insights and remarkable properties. *Nanoscale* **2016**, *8*, 11224–11233.
- (14) Avinash, M. B.; Sandeepa, K. V.; Govindaraju, T. Emergent behaviors in kinetically

- controlled dynamic self-assembly of synthetic molecular systems. *ACS Omega* **2016**, *1*, 378–387.
- (15) Bartocci, S.; Berrocal, J. A.; Guarracino, P.; Grillaud, M.; Franco, L.; Mba, M. Peptide-driven charge-transfer organogels built from synergetic hydrogen bonding and pyrene–naphthalenediimide donor–acceptor interactions. *Chem. Eur. J.* **2018**, *24*, 2920–2928.
- (16) Jalani, K.; Kumar, M.; George, S. J. Mixed donor-acceptor charge-transfer stacks formed via hierarchical self-assembly of a non-covalent amphiphilic foldamer. *Chem. Commun.* **2013**, *49*, 5174–5176.
- (17) Li, P.; Maier, J. M.; Hwang, J.; Smith, M. D.; Krause, J. A.; Mullis, B. T.; Strickland, S. M. S.; Shimizu, K. D. Solvent-induced reversible solid-state colour change of an intramolecular charge-transfer complex. *Chem. Commun.* **2015**, *51*, 14809–14812.
- (18) Staab, H. A.; Zhang, D.-Q.; Krieger, C. [3](N, N′)-1, 8;4, 5-Naphthalenetetracarboxydiimido-[3](2, 7)pyrenophane and its [4, 4] cyclophane homologue. *Liebigs Ann./Recueil* **1997**, *1997*, 1551–1556.
- (19) Vaiyapuri, R.; Greenland, B. W.; Colquhoun, H. M.; Elliott, J. M.; Hayes, W. Molecular recognition between functionalized gold nanoparticles and healable, supramolecular polymer blends—a route to property enhancement. *Polym. Chem.* **2013**, *4*, 4902–4909.
- (20) Khalily, M. A.; Bakan, G.; Kucukoz, B.; Topal, A. E.; Karatay, A.; Yaglioglu, H. G.; Dana, A.; Guler, M. O. Fabrication of supramolecular n/p-nanowires via coassembly of oppositely charged peptide-chromophore systems in aqueous media. *ACS Nano* **2017**, *11*, 6881–6892.
- (21) Mulliken, R. S.; Person, W. B. Donor-acceptor complexes. *Annu. Rev. Phys. Chem.* **1962**, *13*, 107–126.
- (22) Mulliken, R. S. Molecular compounds and their spectra. II. *J. Am. Chem. Soc.* **1952**, *74*, 811–824.
- (23) Rosokha, S. V.; Dibrov, S. M.; Rosokha, T. Y.; Kochi, J. K. Electronic structures of intermolecular charge-transfer states in fast electron transfers with tetrathiafulvalene donor. Thermal and photoactivation of [2 + 4] cycloaddition to o-chloranil acceptor. *Photochem. Photobiol. Sci.* **2006**, *5*, 914–924.

- (24) Hubig, S. M.; Kochi, J. K. Photoinduced electron transfer in charge-transfer crystals by diffuse-reflectance (picosecond) time-resolved spectroscopy. *J. Phys. Chem.* **1995**, *99*, 17578–17585.
- (25) Aoki, T.; Sakai, H.; Ohkubo, K.; Sakanoue, T.; Takenobu, T.; Fukuzumi, S.; Hasobe, T. Ultrafast photoinduced electron transfer in face-to-face charge-transfer π -complexes of planar porphyrins and hexaazatriphenylene derivatives. *Chem. Sci.* **2015**, *6*, 1498–1509.
- (26) Freyer, M. W.; Lewis, E. A. Isothermal titration calorimetry : Experimental design, data Analysis, and probing macromolecule/ ligand binding and kinetic interactions. *Methods cell Biol. Acad. Press* **2008**, *84*, 79–113.
- (27) Das, A.; Ghosh, S. Supramolecular assemblies by charge-transfer interactions between donor and acceptor chromophores. *Angew. Chem. Int. Ed.* **2014**, *53*, 2038–2054.
- (28) Molla, M. R.; Ghosh, S. Hydrogen-bonding-mediated vesicular assembly of functionalized naphthalene-diimide-based bolaamphiphile and guest-induced gelation in water. *Chem. Eur. J.* **2012**, *18*, 9860–9869.
- (29) Kumar, M.; George, S. J. Green fluorescent organic nanoparticles by self-assembly induced enhanced emission of a naphthalene diimide bolaamphiphile. *Nanoscale* **2011**, *3*, 2130–2133.
- (30) Shao, H.; Parquette, J. R. A π -conjugated hydrogel based on an Fmoc-dipeptide naphthalene diimide semiconductor. *Chem. Commun.* **2010**, *46*, 4285–4287.
- (31) Kodaka, M. Sign of circular dichroism induced by β -cyclodextrin. *J. Phys. Chem.* **1991**, *95*, 2110–2112.
- (32) Kodaka, M. A. General rule for circular dichroism induced by a chiral macrocycle. *J. Am. Chem. Soc.* **1993**, *115*, 3702–3705.
- (33) Krishnan, S. B.; Gopidas, K. R. Observation of supramolecular chirality in a hierarchically self-assembled mixed-stack charge-transfer complex. *Chem. Eur. J.* **2017**, *23*, 9600–9606.
- (34) Salerno, F.; Berrocal, J. A.; Haedler, A. T.; Zinna, F.; Meijer, E. W.; Di Bari, L. Highly circularly polarized broad-band emission from chiral naphthalene diimide-based supramolecular aggregates. *J. Mater. Chem. C* **2017**, *5*, 3609–3615.

- (35) You, L.; Pescitelli, G.; Anslyn, E. V.; Di Bari, L. An exciton-coupled circular dichroism protocol for the determination of identity, chirality, and enantiomeric excess of chiral secondary alcohols. *J. Am. Chem. Soc.* **2012**, *134*, 7117–7125.
- (36) Hallett, F. R. Particle size analysis by dynamic light scattering. *Food Res. Int.* **1994**, *27*, 195–198.
- (37) Gujrati, M. D.; Kumar, N. S. S.; Brown, A. S.; Captain, B.; Wilson, J. N. Luminescent charge-transfer complexes: Tuning emission in binary fluorophore mixtures. *Langmuir* **2011**, *27*, 6554–6558.
- (38) Yeh, M. Y.; Lin, H. C. Theoretical analysis of the intermolecular interactions in naphthalene diimide and pyrene complexes. *Phys. Chem. Chem. Phys.* **2014**, *16*, 24216–24222.
- (39) Hara, M.; Tojo, S.; Kawai, K.; Majima, T. Formation and decay of pyrene radical cation and pyrene dimer radical cation in the absence and presence of cyclodextrins during resonant two-photon ionization of pyrene and sodium 1-pyrene sulfonate. *Phys. Chem. Chem. Phys.* **2004**, *6*, 3215–3220.
- (40) Assel, M.; Höfer, T.; Laubereau, A.; Kaiser, W. Electron transfer complexes of the system pyrene/PMDA studied by transient absorption and degenerate four-wave mixing measurements. *J. Phys. Chem.* **1996**, *100*, 11836–11842.
- (41) Rakhi, A. M.; Gopidas, K. R. Generation of long-lived methylviologen radical cation in the triplet-state mediated electron transfer in a β -cyclodextrin based supramolecular triad. *Chem. Phys. Lett.* **2015**, *618*, 192–197.
- (42) Gosztola, D.; Niemczyk, M. P.; Svec, W.; Lukas, A. S.; Wasielewski, M. R. Excited doublet states of electrochemically generated aromatic imide and diimide radical anions. *J. Phys. Chem. A* **2000**, *104*, 6545–6551.
- (43) Martinez, J. F.; La Porte, N. T.; Wasielewski, M. R. Electron transfer from photoexcited naphthalene diimide radical anion to electrocatalytically active $\text{Re}(\text{Bpy})(\text{CO})_3\text{Cl}$ in a molecular triad. *J. Phys. Chem. C* **2018**, *122*, 2608–2617.
- (44) Ganesan, P.; Baggerman, J.; Zhang, H.; Sudholter, E. J. R.; Zuilhof, H. Femtosecond time-resolved photophysics of 1,4,5,8-naphthalene diimides. *J. Phys. Chem. A* **2007**, *111*, 6151–6156.
- (45) Kochi, J. K. Charge-transfer excitation of molecular complexes in organic and

- organometallic chemistry. *Pure Appl. Chem.* **1991**, *63*, 255–264.
- (46) Hilinski, E. F.; Masnovi, J. M.; Kochi, J. K.; Rentzepis, P. M. Role of ion pairs in the photochemistry of electron donor-acceptor complexes. Picosecond spectroscopic studies of arene-tetracyanoethylene systems. *J. Am. Chem. Soc.* **1984**, *106*, 8071–8077.
- (47) Kochi, J. K. Electron transfer and charge transfer: Twin themes in unifying the mechanisms of organic and organometallic reactions. *Angew. Chem. Int. Ed. Engl.* **1988**, *27*, 1227–1266.
- (48) Vittala, S. K.; Saraswathi, S. K.; Joseph, J. Fullerene cluster assisted self-assembly of short DNA strands into semiconducting nanowires. *Chem. Eur. J.* **2017**, *23* (62), 15759–15765.
- (49) Trotta, F.; Martina, K.; Robaldo, B.; Barge, A.; Cravotto, G. Recent advances in the synthesis of cyclodextrin derivatives under microwaves and power ultrasound. *J. Incl. Phenom. Macrocycl. Chem.* **2007**, *57*, 3–7.

Self-Assembly and Photoinduced Electron Transfer in a Bis(β -Cyclodextrin)-Linked Pyrene/ Bis(Adamantane)-Linked Methyl Viologen Donor- Acceptor System in Aqueous Solution

3.1. Abstract

Pyrene linked to two β -CD molecules (CD-PY-CD) and methylviologen linked to two adamantane groups (AD-MV²⁺-AD), self-assembled in water to give toroidal nanostructures. The toroids are formed by stacking of closed loop structures which in turn, are formed by self-assembly of inclusion complexes. Fluorescence of the pyrene chromophore was quenched in the toroid suggesting very efficient photoinduced electron transfer taking place in the toroid. The rate constant for electron transfer within the assembly was obtained from fluorescence lifetime studies. Evidence for photoinduced electron transfer from PY to MV²⁺ in the assembly was obtained from laser flash photolysis studies. Electron transfer leads to formation of radical ion products, PY^{•+} and MV^{•+}, immediately following laser irradiation. The radical ions react with chromophores or similar ions in adjacent stacks to give dimeric products. Since the dimeric species are not very stable, the reactions are reversed at longer time scales to generate the radical ions, which then undergo back electron transfer and regenerate the starting materials. Thus, irradiation of the toroidal system did not lead to formation of long-lived charge separated states.

3.2. Introduction

It was mentioned in Chapter 1 that generation of long-lived charge separated (CS) state is a very important goal in the study of photoinduced electron transfer (PET). Initial attempts to generate long-lived CS states were inspired by the architectural features of the photosynthetic bacteria which can be viewed as a protein scaffolding that hold light absorbers, electron donors (D) and acceptors (A) in appropriate positions for efficient sequential electron transfer. Sequential electron transfer increases the distance between the separated charges and slows down the rate of charge recombination (CR) reaction, leading to enhancement of CS state lifetime. Large numbers of molecular systems have been constructed in this way and CS state lifetimes of a few hundred microseconds have been achieved for some of these systems.¹⁻⁴ However, the CS state lifetimes and quantum yields of the synthetic systems were considerably lower than that in the bacterial reaction center. Several non-covalently bound D-A systems were also constructed and studied, but the CS state lifetimes in these systems were found to be very low as well.⁵⁻⁹ Confining D and A in restricted environments¹⁰⁻¹³ and/or periodically arranging them in supramolecular systems and mixed crystals^{5,6,14-16} are other approaches recently put forward to enhance CS state lifetimes. None of the above strategies are useful for generating long-lived CS states in aqueous media. For important applications such as solar water splitting, generation of CS states in aqueous solution is crucial and none of the above strategies are useful for this purpose.

Recently Huber *et al.* have suggested that molecular self-assembly can mimic the cascade type electron transfer observed in the bacterial reaction center and allow the spatial separation of photogenerated charges, leading to long-lived CS state.¹⁷ The donor

employed in their study is a conjugated polyelectrolyte, poly(fluorene-alt-thiophene) (PFT). PFT is a water-soluble, semiconducting polyelectrolyte having a bis-alkylated sp^3 -hybridized fluorenyl carbon. The molecule is wedge-shaped and forms rod-like micelles when dissolved in water. The acceptors employed in the study are regioisomers of fullerobis (pyrrolidinium) iodides ($C_{60}(PI)_2$). Structures of the pyrrolidinium bis-adducts, namely *trans*-1, *trans*-2, *trans*-3 and *trans*-4, are shown in Figure 3.1. Synthesis gave a mixed bis-adduct consisting of all four isomers which could be separated into two fractions designated as *trans*-1, 2 (mixture of *trans*-1 and *trans*-2) and *trans*-3, 4 (mixture of *trans*-3 and *trans*-4, predominantly). The authors studied the co-assembly of PFT with *trans*-1, 2, *trans*-3, 4 and mixed bis-adduct systems using small angle X-ray scattering (SAXS). Analysis of the SAXS data suggested that *trans*-3, 4 is assembled on the inside of the PFT polymer micelle whereas *trans*-1, 2 surrounds the outside of the micelle. The relative locations of the two isomeric sets in the PFT micelles were further confirmed by solvatochromic absorption measurements.

Fluorescence of the PFT/*trans*-1, 2 co-assembly was similar to that of PFT indicating the absence of PET in the system. In the PFT/*trans*-3, 4, on the other hand, the fluorescence was highly quenched suggesting efficient PET taking place from PFT to *trans*-3, 4. Fluorescence of the PFT/mixed bis-adduct also indicated facile PET in this system. Excitation of a dilute solution of the PFT/mixed bis-adduct using 470 nm laser showed ultrafast formation of C_{60} radical anion and PFT hole polaron (P^+). About 75% of the hole polarons decayed within 200 ps and the remaining fraction survived for several nanoseconds. In concentrated PFT/mixed bis-adduct solutions, exposure to light resulted

in a permanent colour change from yellow to deep green, which is attributed to formation of long-lived CS state.

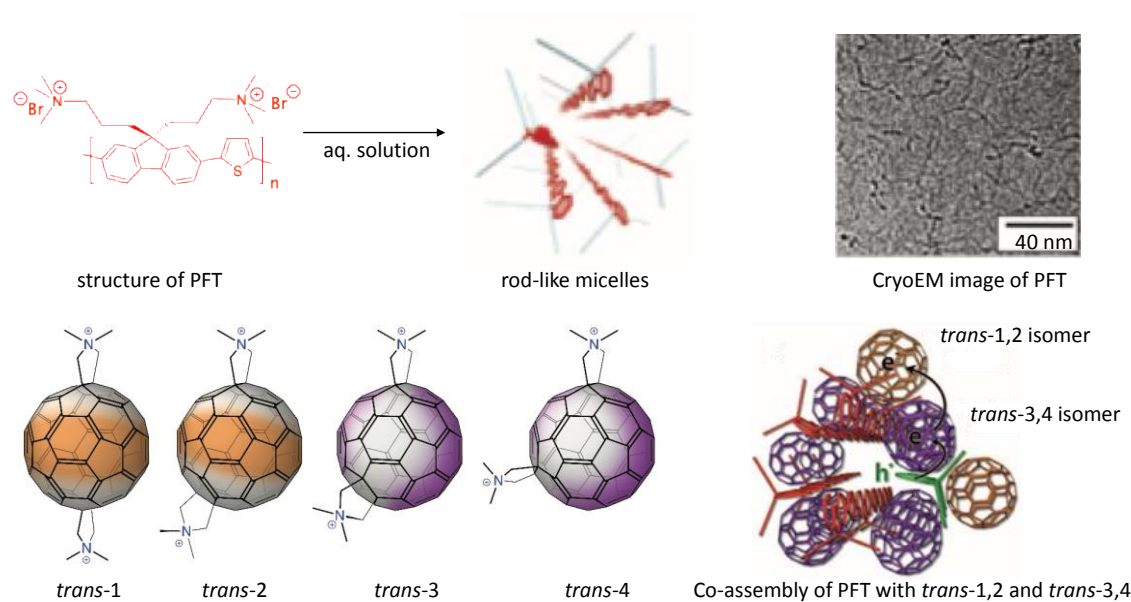


Figure 3.1. Structures of PFT and isomeric fullero-bis(pyrrrolidinium) adducts. Cartoon representation of PFT micelle and PFT-*trans*-1,2 and *trans*-3,4 co-assembly are also shown. “Reprinted with permission from (Huber, R. C. *et al.*, *Science*, **2015**, 348, 1340-1343). Copyright © 2015, American Association for the Advancement of Science.”

In the C₆₀-bis (pyrrrolidinium) adducts, the positively charged pyrrrolidinium groups are hydrophilic and C₆₀ is hydrophobic. In the *trans*-1, 2 adduct, the positive charges are on nearly opposite sides of C₆₀ and these molecules cannot easily insert into the hydrophobic interior of the PFT micelle. That is why *trans*-1, 2 assemble on the outside of the PFT micelle. In contrast, the angle between charges in *trans*-3 and *trans*-4 are 145 and 103°, respectively. These molecules have more amphiphilic character and hence can insert into the PFT micelle. In the PFT/mixed bis-adduct co-assembly, the PFT rod-like micelle has a layer of *trans*-3, 4 molecules tightly bound to it and an outer layer of loosely bound *trans*-1, 2 molecules as shown in Figure 3.1. Up on excitation, an electron is transferred from ¹PFT* to the tightly bound *trans*-3, 4 adduct. The loosely bound *trans*-1, 2 adduct then pulls away the transferred electron immediately, reducing the rate of CR

reaction. The PFT polaron remains inside the micelle and the transferred electron hops around within the outer C₆₀ layer, thereby enhancing the CS state lifetime. This report by Huber *et al.* is the only published work on D-A self-assembly that could sustain long-lived photoinduced charge separation in aqueous solution.

Unpublished work from our laboratory also support the contention that molecular self-assembly of D-A systems can prolong CS state lifetimes. In one of the studies, Nagaraj N. synthesised a bis-adamantane-linked anthracene (AD-AN-AD) as donor and a bis-pyromellitic diimide derivative (PI-PI) as acceptor.¹⁸ Structures of these molecules are shown in Figure 3.2. Earlier studies from our laboratory has shown that PI derivatives bind to the narrow rim of β -CD and we have designated this type of interaction as rim-binding.¹⁹ We also showed that a β -CD molecule can simultaneously encapsulate an AD moiety through inclusion binding and a PI moiety through rim-binding.^{20,21} Upon mixing equimolar amounts of β -CD, AD-AN-AD and PI-PI in aqueous solution, we observed formation of nanofiber assemblies as shown in Figure 3.2. We proposed that the propensity of AD to undergo inclusion binding and PI to undergo rim-binding with β -CD resulted in the formation of long fibers which can bundle together to give the observed nanofibers. Fluorescence of AN is thoroughly quenched in the assembly suggesting very facile PET from AN to PI. Nanosecond laser flash photolysis using 355 nm laser gave transient spectra which exhibited absorptions corresponding to AN^{•+} at 430 and 720 nm and PI^{•-} at 720 nm. A fraction of the charge separated state survived for nearly 60 μ s. The center to center distance between AN and PI in the linear fiber assembly is about 10 Å. In addition, hole-hopping through the adjacent AN moieties in the fiber bundles can increase

the $\text{AN}^{\bullet+}$ - $\text{PI}^{\bullet-}$ separation further. We believe that both these factors contribute in enhancing the CS state lifetime in this case.

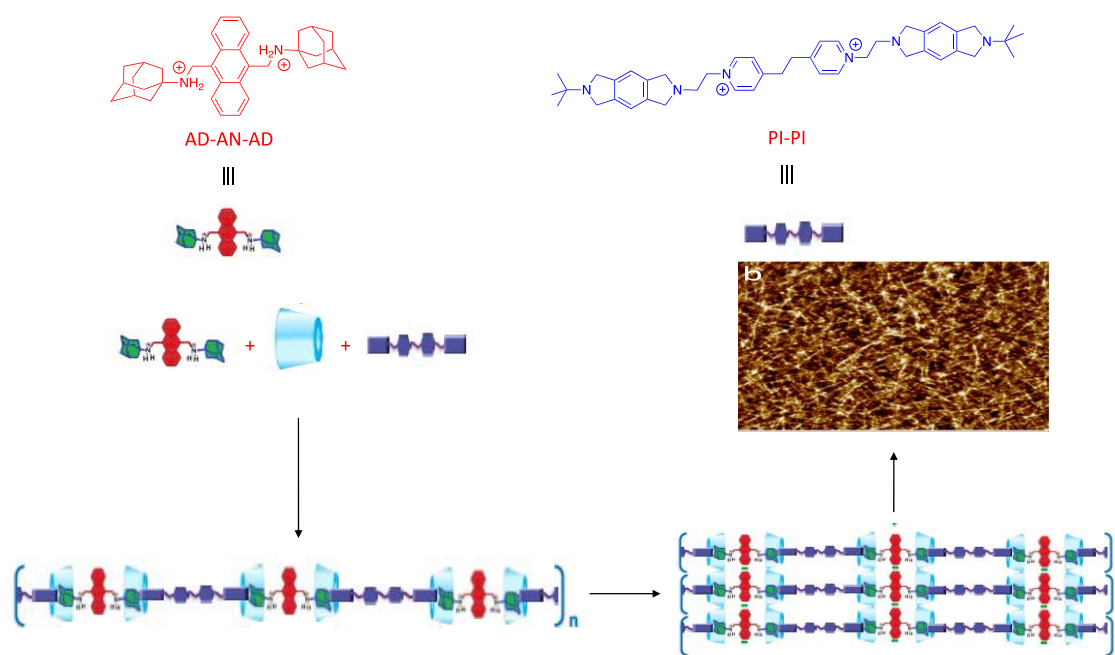


Figure 3.2. Structures of AD-AN-CD, PI-PI and various stages involved in the self-assembly of AD-AN-AD/ β -CD/PI-PI system into nanofibers.

In another study from our lab, Sumesh Babu K. synthesised AN linked to two β -CD molecules through their narrow rims (designated as CD-AN-CD) as donor and MV^{2+} linked to two AD moieties through alkyl chains (designated as AD- MV^{2+} -AD) as acceptor.²² Structures of these molecules are given in Figure 3.3. In aqueous solutions containing equimolar amounts of CD-AN-CD and AD- MV^{2+} -AD, self-assembly occurs through inclusion binding of AD in the β -CD cavity. The inclusion complex further undergoes hierarchical self-assembly to give toroidal nanostructures shown in Figure 3.3. Morphological analyses of these structures were performed using SEM, TEM and AFM. Formation of the nanostructure results in strong quenching of the fluorescence of AN suggesting that very facile PET occurs in the assembly. Nanosecond flash photolysis of dilute solutions showed formation of $\text{MV}^{\bullet+}$ which survived for more than 200 μs . Concentrated solutions of CD-

AN-CD/AD-MV²⁺-AD (1:1) when irradiated by a laser turned blue, indicating the formation of long-lived MV^{•+}.

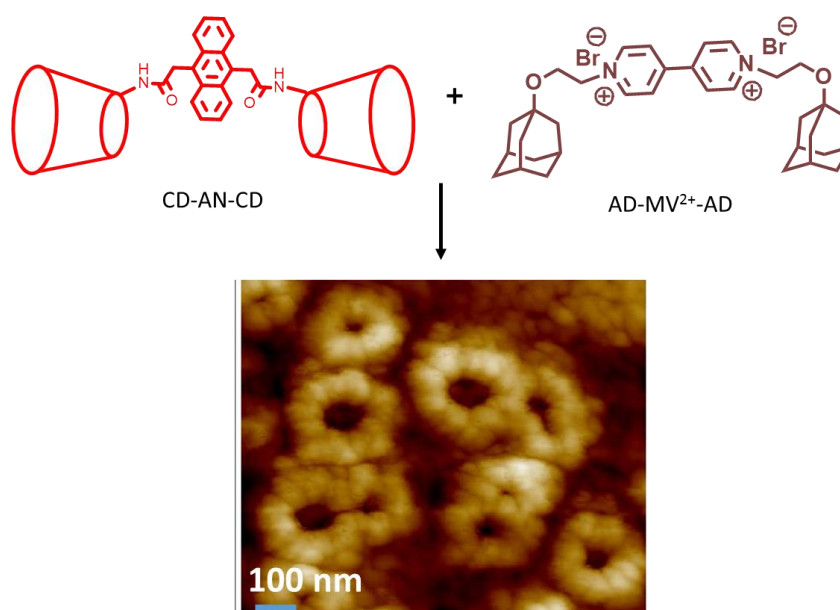


Figure 3.3. Structures of CD-AN-CD, AD-MV²⁺-AD and the AFM image of toroidal nanostructure formed in CD-AN-CD/AD-MV²⁺-AD (1:1) solution.

Work presented in this chapter is an extension of the above work. In this study we employed a pyrene linked to two β -CD molecules through their narrow rim as donor. This molecule is designated as CD-PY-CD. Structure of CD-PY-CD is shown in Figure 3.4. AD-MV²⁺-AD was used as the acceptor in this study also.

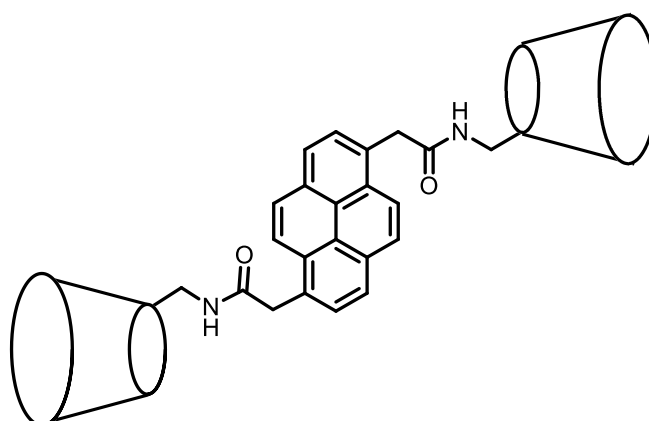


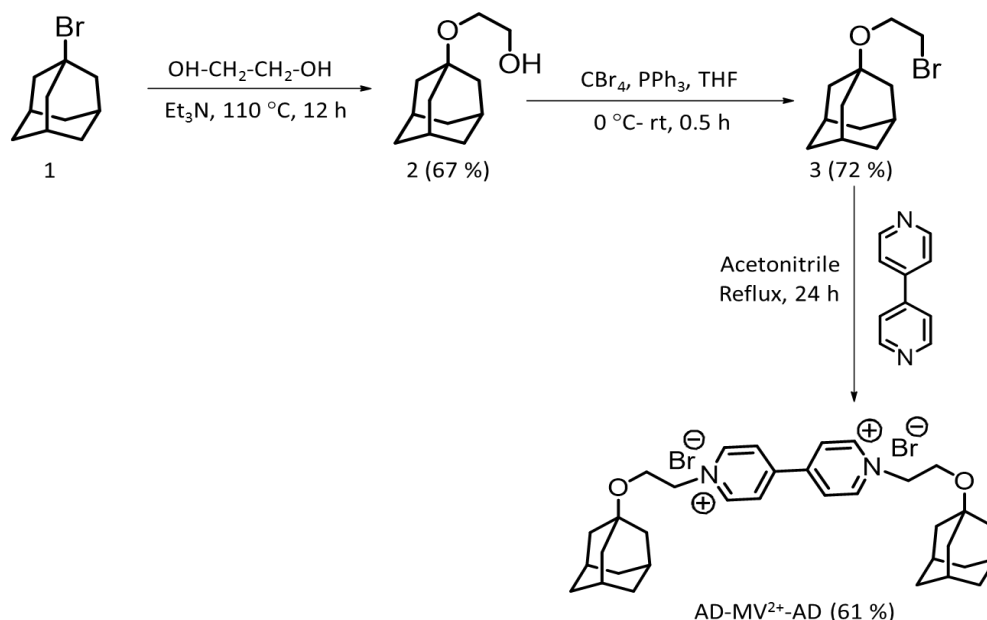
Figure 3.4. Structure of CD-PY-CD.

In aqueous solution containing equimolar amounts of CD-PY-CD and AD-MV²⁺-AD, self-assembly occurred through inclusion complexation and the inclusion complex underwent hierarchical self-assembly to give toroidal nanostructures. Fluorescence of PY is quenched in the assembly indicating very facile PET from PY to MV²⁺. Irradiation of CD-PY-CD/AD-MV²⁺-AD (1:1) aqueous solution using 355 nm laser resulted in ultrafast formation of PY*⁺ and MV*⁺. The MV*⁺ formed was found to undergo dimer formation. The results of these investigations are presented below.

3.3. Results and Discussions

3.3.1. Synthesis and characterization of molecules

The acceptor AD-MV²⁺-AD was reported previously from our laboratory.²² Synthesis of this molecule involved the steps shown in Scheme 3.1.

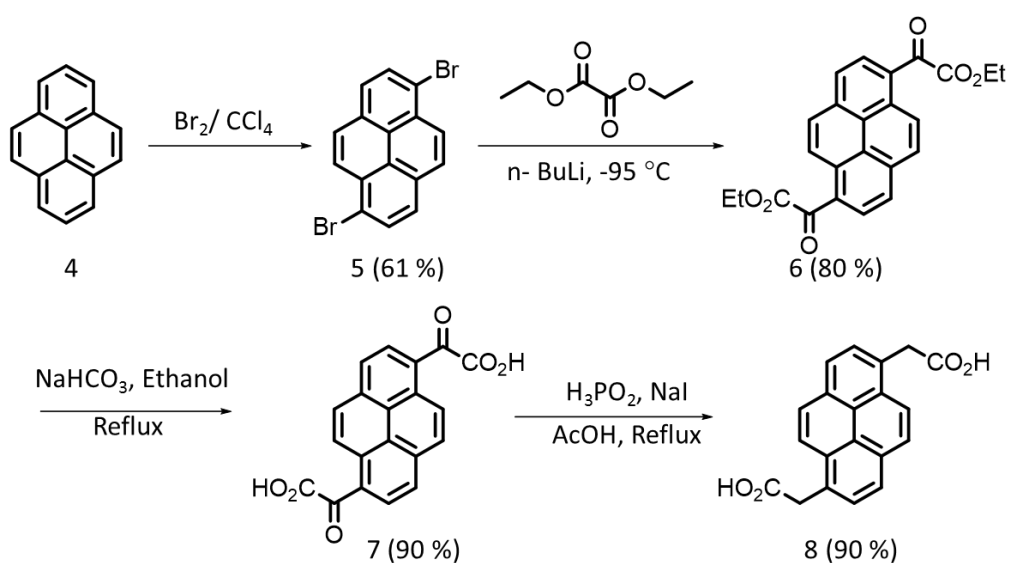


Scheme 3.1. Scheme for the synthesis of AD-MV²⁺-AD.

1-bromoadamantane 1 was converted to the hydroxyethyl ether derivative 2 by refluxing in ethylene glycol in the presence of triethylamine. 2 was subjected to Appel's

reaction to get the bromo derivative 3. The acceptor AD-MV²⁺-AD was obtained by refluxing 3 with the commercially available 4,4'-dipyridyl (0.5 equiv.) in dry acetonitrile (ACN) for 24 h.

The donor molecule CD-PY-CD was prepared by the coupling of pyrene-1,6-diacetic acid with β -CD monoamine. Pyrene-1,6-diacetic acid required for the synthesis was prepared by a recently reported procedure which employed the steps in Scheme 3.2.^{23,24}

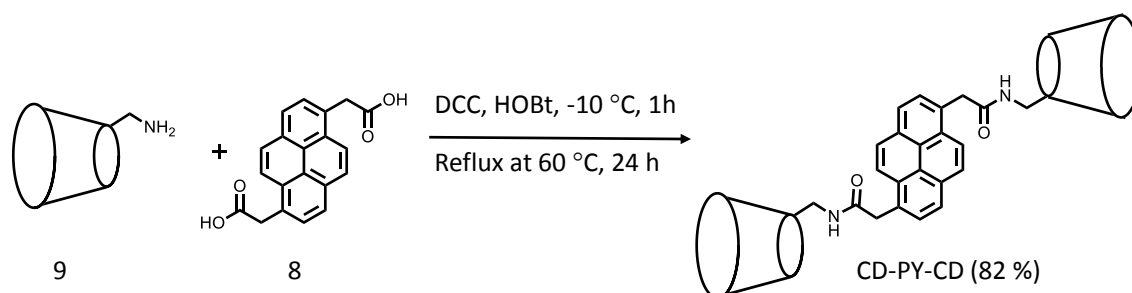


Scheme 3.2. Scheme for synthesis of pyrene-1,6-diacetic acid.

Pyrene was brominated using bromine in carbon tetrachloride to give a mixture of 1,6- and 1,8-dibromopyrenes. The 1,6- isomer 5 was separated and purified by recrystallization from toluene. This was then reacted with diethyl oxalate and *n*-butyllithium at -95 °C to give the pyrene-1,6-diketoester 6. 6 was hydrolysed and reduced to give the diacetic acid 8 as shown in Scheme 3.2.

The β -CD monoamine 9 was also prepared by a reported procedure.²⁵ The amine 9 was then treated with one equivalent of 8 in the presence of DCC and HOBT, first at -10 °C for 1 h and then refluxed at 60 °C for 24 h (Scheme 3.3). CD-PY-CD was purified by

repeated reverse phase column chromatography over silica gel and elution with methanol/ water mixture (2:8) gave product with 82 % yield.



Scheme 3.3. Synthesis of CD-PY-CD.

Structures of AD-MV²⁺-AD and CD-PY-CD were confirmed by spectroscopic techniques (see experimental section). ¹H NMR spectra of these molecules are presented below along with proton assignments.

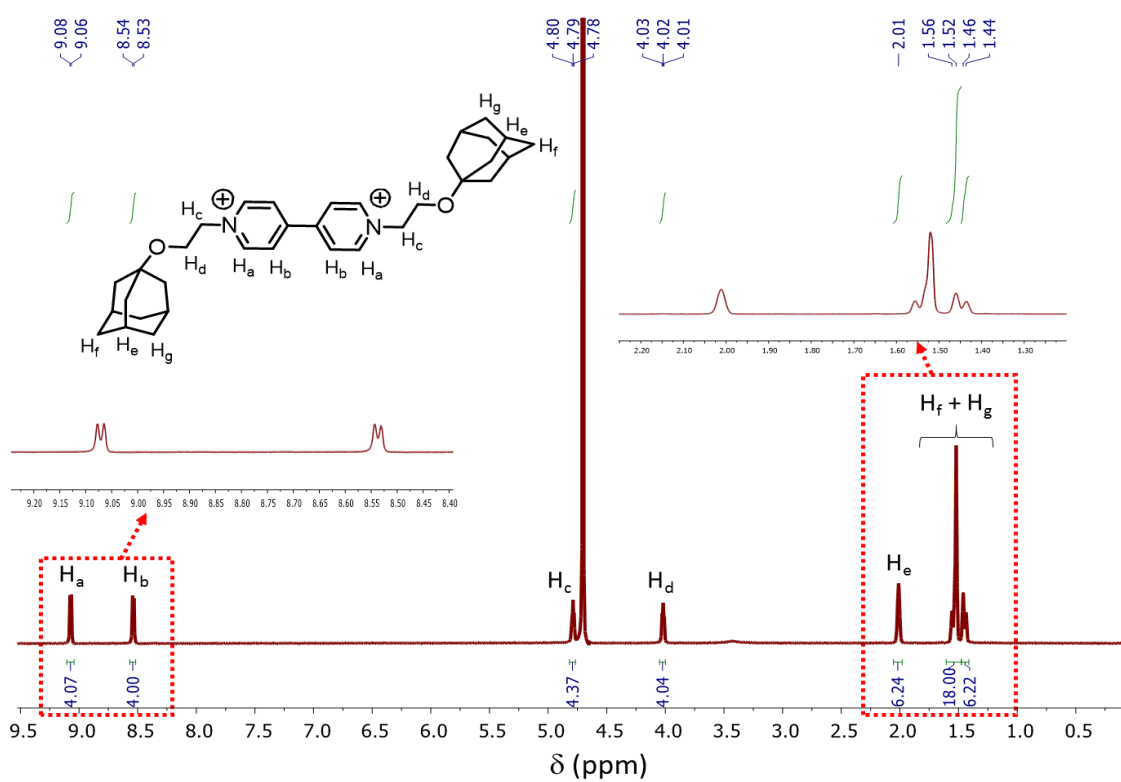


Figure 3.5. ¹H NMR spectrum of AD-MV²⁺-AD in D₂O.

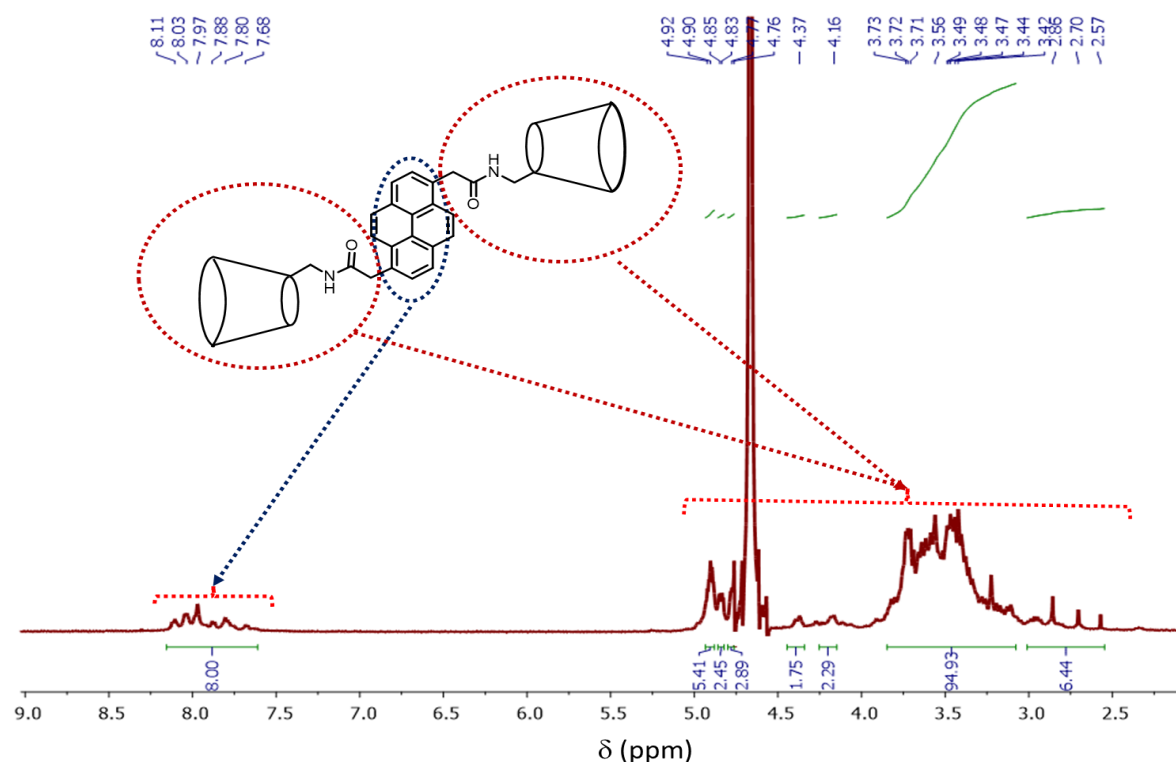


Figure 3.6. ^1H NMR spectrum of CD-PY-CD in D_2O .

3.3.2. ^1H NMR titration studies

^1H NMR spectroscopy is an excellent tool to probe the inclusion of guest molecules in CD cavities. We have carried out ^1H NMR titration of CD-PY-CD against AD-MV $^{2+}$ -AD in D_2O and the results are presented in Figure 3.7. Panel a shows the ^1H NMR spectrum of CD-PY-CD (5×10^{-3} M) and panels b, c and d shows the effect of adding varying amounts (0.3, 0.6 and 1.0 equiv.) of AD-MV $^{2+}$ -AD on the ^1H NMR of CD-PY-CD. Panel e on the top shows the ^1H NMR of AD-MV $^{2+}$ -AD. When AD group gets encapsulated in β -CD cavity, the AD proton signals undergo chemical shift changes and/or broadening. A comparison of d and e panels shows that the AD signals in the δ 1.25 – 2.0 region undergo signal broadening and change in splitting pattern, which can be taken as the signature for the encapsulation of the AD groups of AD-MV $^{2+}$ -AD in the CD cavities of CD-PY-CD.

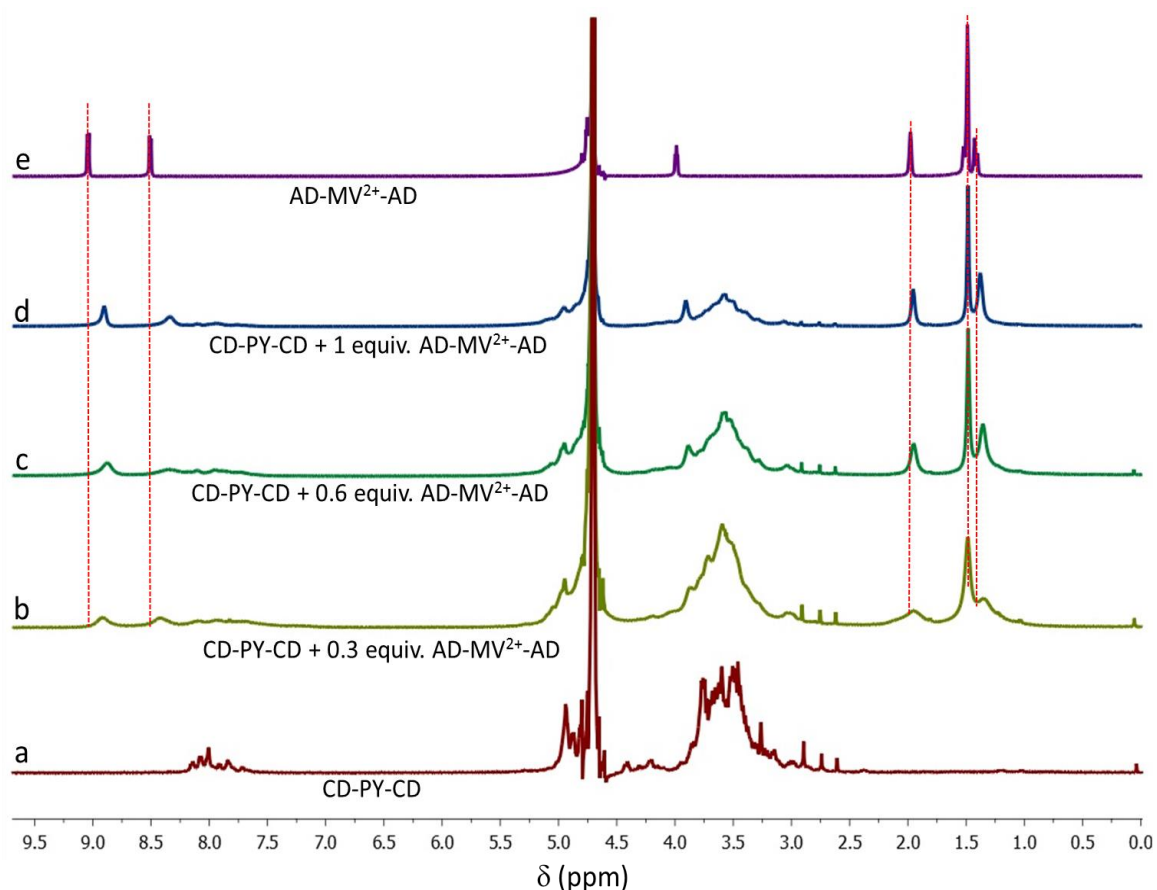


Figure 3.7. Panel a-d) ^1H NMR spectra of CD-PY-CD (5×10^{-3} M) with varying equivalents (0.3 – 1.0 equiv.) of AD-MV $^{2+}$ -AD. Panel e) ^1H NMR of pure AD-MV $^{2+}$ -AD (5×10^{-3} M). Changes in the AD and MV $^{2+}$ proton signals are indicated by red dotted lines.

Additional proof for the encapsulation of AD protons within the β -CD cavity was obtained from 2D ROESY NMR experiments. When AD gets encapsulated in the cavity, the H_a and H_b protons of AD will come near to the β -CD interior protons H-3 and H-5. When protons are within a distance of $\sim 4 \text{ \AA}$, through-space interactions will occur between them and this will be seen as cross-peaks in the 2D ROESY NMR spectrum. Figure 3.8 shows the 2D ROESY NMR spectrum of CD-PY-CD/AD-MV $^{2+}$ -AD (1:1) system in D₂O. Cross peaks observed in the δ 1.2 – 2.0 region are shown in the red dotted line boxes. These cross-peaks, which correspond to through-space interactions between AD protons and H-3 and H-5 protons of β -CD, undoubtedly confirm the encapsulation of AD groups of AD-MV $^{2+}$ -AD within the CD cavities of CD-PY-CD.

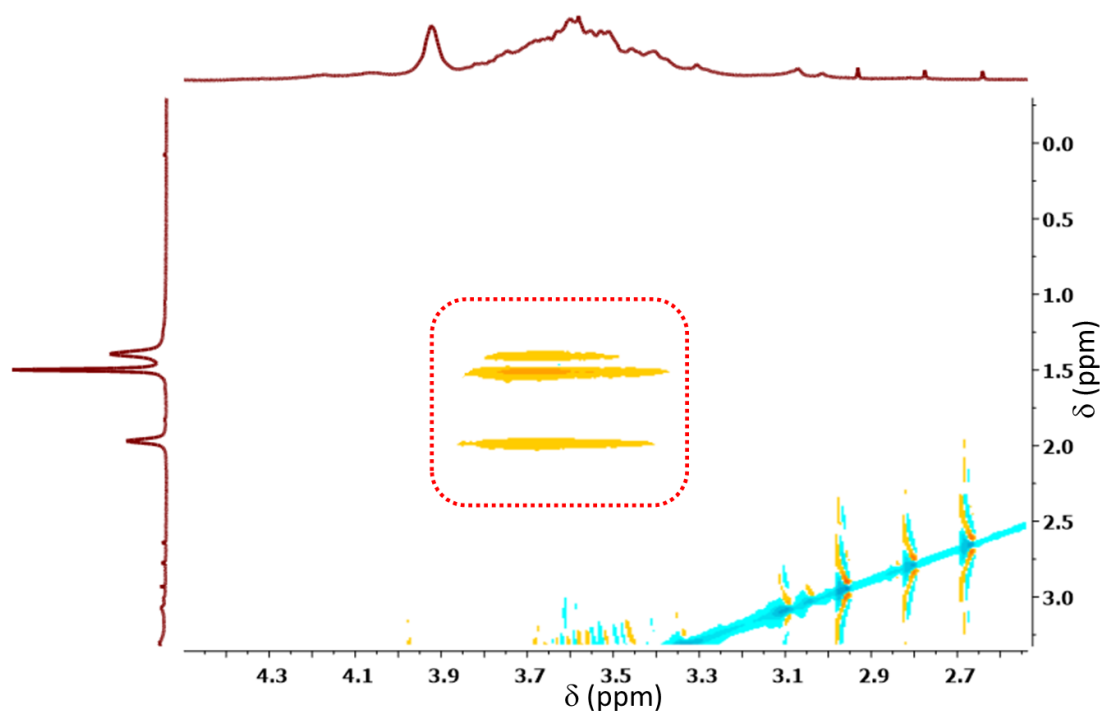


Figure 3.8. 2D ROESY NMR spectrum of CD-PY-CD/AD-MV²⁺-AD (5×10^{-3} M) in D₂O. The cross peaks referred to through space interactions among the protons are marked with boxes.

Apart from confirming inclusion of AD in β -CD cavities, the ¹H NMR titration in Figure 3.7 reveals few interesting aspects about the CD-PY-CD/AD-MV²⁺-AD interaction. The MV²⁺ protons which appeared as doublets at δ 8.5 and 9.0 ppm became broad singlets and shifted upfield in the presence of CD-PY-CD. These protons are away from the site of inclusion and are expected to be unaffected by AD/ β -CD interaction. Previously we observed that protons away from the site of inclusion also show broadening and chemical shift changes, and these were attributed to secondary interactions and/or hierarchical assembly of the inclusion complex into complex structures.^{26,27}

Another very important observation in Figure 3.7 is the severe damping of the ¹H NMR signals of PY and β -CD in the CD-PY-CD/AD-MV²⁺-AD (1:1) solution. This is clearly seen in Figure 3.9, which shows the PY and β -CD NMR signals expanded. Up on addition of AD-MV²⁺-AD, the ¹H NMR signals due to PY gets increasingly dampened and when one equiv. of AD-MV²⁺-AD was added, the PY signals are barely noticeable. The β -CD signals

also get dampened, but these could be seen in the 1:1 mixture. The reason for damping of NMR signals is not clearly understood at this time. We propose that the damping occurs due to stacking of PY over PY and β -CD over β -CD. Addition of AD-MV²⁺-AD to CD-PY-CD leads to inclusion complex formation as the first step. Since both CD-PY-CD and AD-MV²⁺-AD have two binding sites for each other, complexation can occur at both ends again and again, leading to formation of long supramolecular fibers. The ends of the fibers can join together to give ring-like structures as well. These secondary structures formed may undergo stacking which involve very compact PY-PY and CD- CD packing. The damping of NMR signals can be explained in this way.

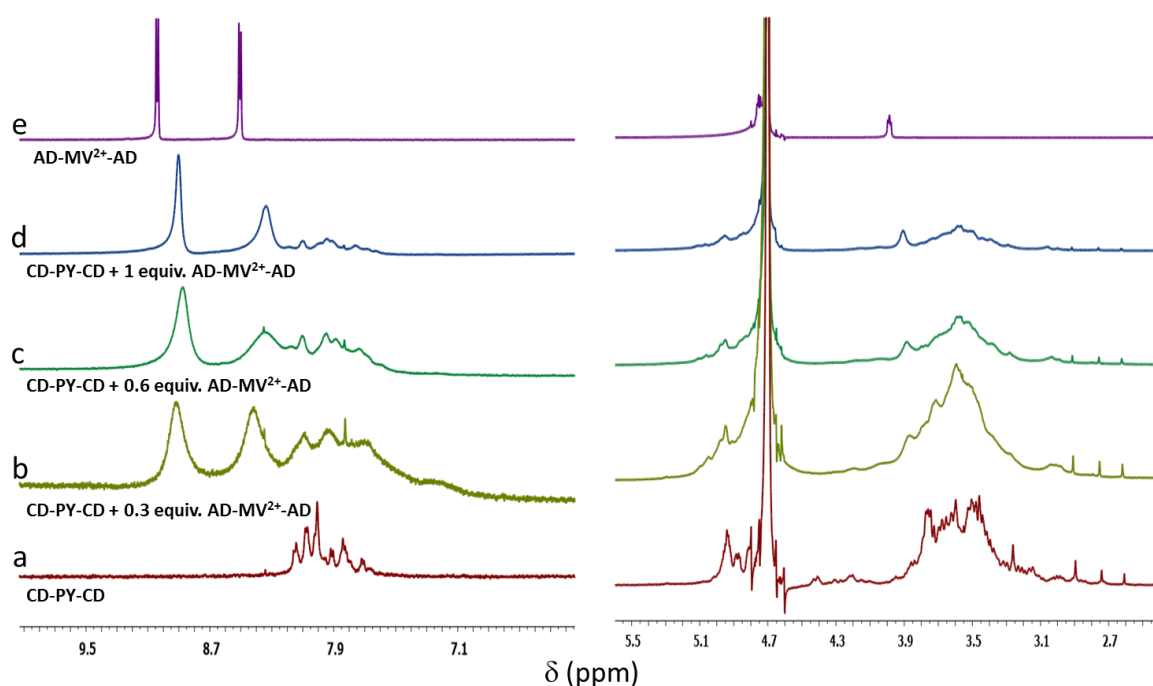


Figure 3.9. Expanded version of NMR titration, showing clearly the damping of signals due to PY and β -CD.

3.3.3. Photophysical properties of CD-PY-CD/AD-MV²⁺-AD

The absorption and fluorescence spectra of CD-PY-CD are identical to those of PY in aqueous solution, indicating that β -CD moiety has no effect on the photophysical properties of PY. In the presence of AD-MV²⁺-AD, the absorption spectrum of CD-PY-CD

exhibit a bathochromic shift of the absorption maximum along with dampening of signal intensity. This is shown in Figure 3.10. The changes observed are significant during addition of 0.2 – 0.4 equiv. of AD-MV²⁺-AD and thereafter only negligible changes were noted. Most probably, these changes can be attributed to aggregation of the PY chromophores. No bands assignable to CT complexation could be seen in the long wavelength region, suggesting that face to face stacking of PY and MV²⁺ did not occur in the self-assembled system.

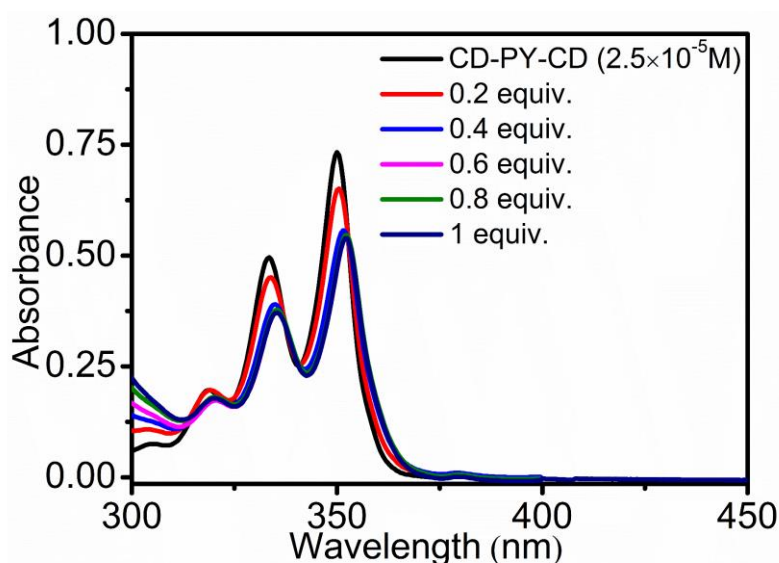


Figure 3.10. Absorption spectra of CD-PY-CD in the absence and presence (0.2-1 equiv.) of AD-MV²⁺-AD.

The emission spectrum of CD-PY-CD exhibited significant quenching in the presence of micromolar amounts of AD-MV²⁺-AD (Figure 3.11a). The fluorescence is almost completely quenched in the presence of one equiv. of AD-MV²⁺-AD. Figure 3.11b shows fluorescence spectrum of CD-PY-CD in the presence of one equiv. AD-MV²⁺-AD normalized with that of CD-PY-CD. The two spectra overlap completely, suggesting that emission from CT state is not observed in this case.

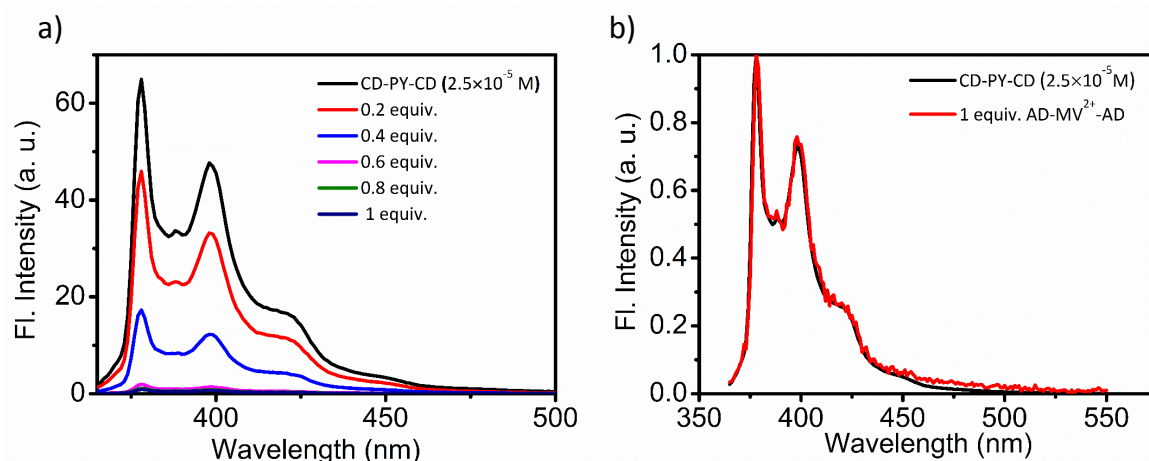


Figure 3.11. a) Emission spectra of CD-PY-CD in the presence of AD-MV²⁺-AD (0 – 1.0 equiv.) and b) Normalized fluorescence spectra of CD-PY-CD and CD-PY-CD/AD-MV²⁺-AD (1:1) aqueous solutions.

Achiral molecules complexed with β -CD often exhibit induced circular dichroism (ICD), the intensity and sign of which can be used to predict the orientation of the achiral molecule with respect to the β -CD, using Kodaka's rules.^{28,29} Both PY and MV²⁺ are achiral molecules and do not exhibit any Cotton effect. Since β -CD is chiral, these molecules may exhibit ICD if they are associated with β -CD. Figure 3.12a shows the ICD spectra of CD-PY-CD in the presence and absence of AD-MV²⁺-AD. The ICD signal due to PY in CD-PY-CD is negative in the 300 – 370 nm region and positive in the 250-300 nm region. For PY, the transition moment of the 300-370 nm absorption is polarized along the long axis and that of the 250-300 nm absorption is polarized along the short axis. In CD-PY-CD, the PY moiety is present outside the cavity as the molecular size is larger than the β -CD cavity. Hence the negative sign of ICD in the 300-370 nm and positive sign of ICD in the 250-300 nm region suggest that PY is present outside the narrow rim of β -CD with its long axis nearly parallel to the CD axis. When AD-MV²⁺-AD is added, the signal intensities increase suggesting that the orientation of PY became more parallel to the CD axis. Alternately, inclusion of AD (of AD-MV²⁺-AD) in the β -CD cavity of CD-PY-CD rigidifies the assembly,

leading to an enhancement of the ICD intensity. There is also a negative signal appears around 260 nm and this can be attributed to MV^{2+} , which is expected to remain outside the cavity with its transition moment parallel to the CD axis as shown in Figure 3.12b.

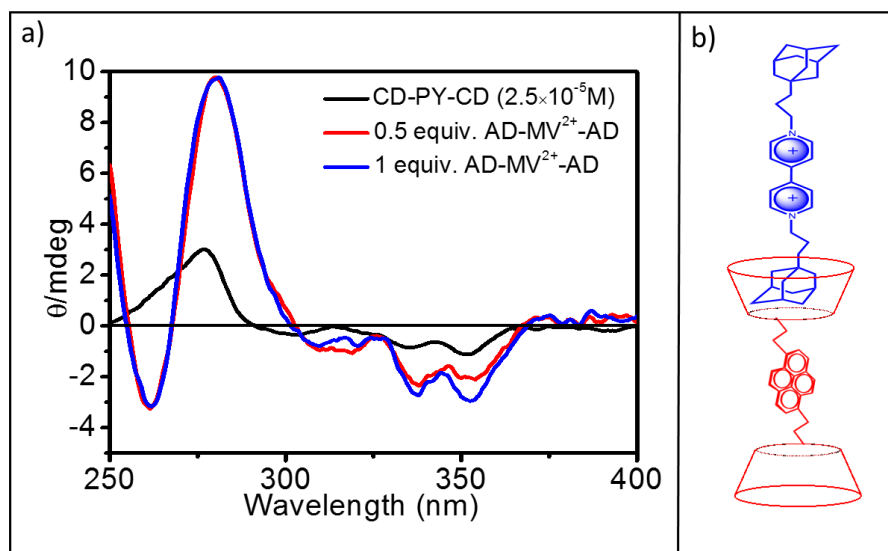


Figure 3.12. a) ICD spectra of CD-PY-CD in the presence of AD- MV^{2+} -AD (0 – 1.0 equiv.) and b) The orientation of PY and MV^{2+} in CD-PY-CD/AD- MV^{2+} -AD.

3.3.4. DLS and Tyndall effect studies

Recent studies from our laboratory have shown that AD/ β -CD bis-inclusion complexes undergo self-assembly to give various secondary structures such as nanofibers, vesicles, toroids etc.^{22,26,27} Formation of nano-assemblies in solution can be checked using tyndall effect and estimate of the size of the nano objects can be obtained using dynamic light scattering (DLS) experiments. For the CD-PY-CD/AD- MV^{2+} -AD system these experiments were carried out and the results are shown in Figure 3.13. In the Tyndall effect experiment the path of the laser beam through the solution can be clearly seen (Figure 3.13a), suggesting that particles capable of scattering the light are present in the solution. The DLS result is shown in Figure 3.13b, which confirmed the presence of

particles in solution with average hydrodynamic radius of 250 nm and particle size distribution in the 150-450 nm range.

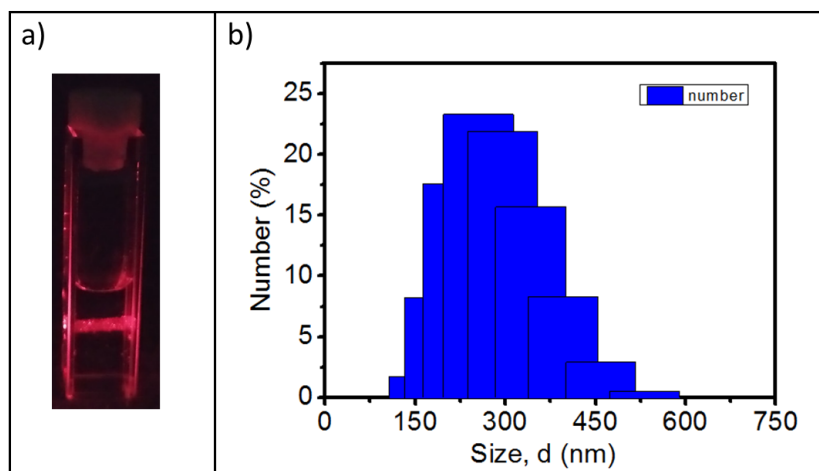


Figure 3.13. a) Tyndall effect showing the path of light through CD-PY-CD/AD-MV²⁺-AD (1:1, 1×10^{-4} M) in water and b) DLS spectrum of the same solution.

3.3.5. Morphological analysis

Results of the DLS and Tyndall effect studies suggested the presence of nanoscopic particles in aqueous 1:1 solution of CD-PY-CD/AD-MV²⁺-AD. In order to understand the morphological aspects of these nanomaterials we employed TEM, SEM and AFM imaging. Samples for AFM and SEM were prepared by drop-casting aqueous solution of 1:1 mixture of CD-PY-CD/AD-MV²⁺-AD (1×10^{-5} M and 1×10^{-4} M respectively) on silicon wafer. Same solution (10^{-5} M) was drop-casted on copper coated carbon grid for TEM analysis.

Figure 3.14 shows few TEM (a, b) and SEM (c, d) images of CD-PY-CD/AD-MV²⁺-AD (1:1) self-assembled system. These images show small spherical or oval shaped particles with a hollow central part. These images, however, does not give any insight into the constitution of these structures or how these structures are formed.

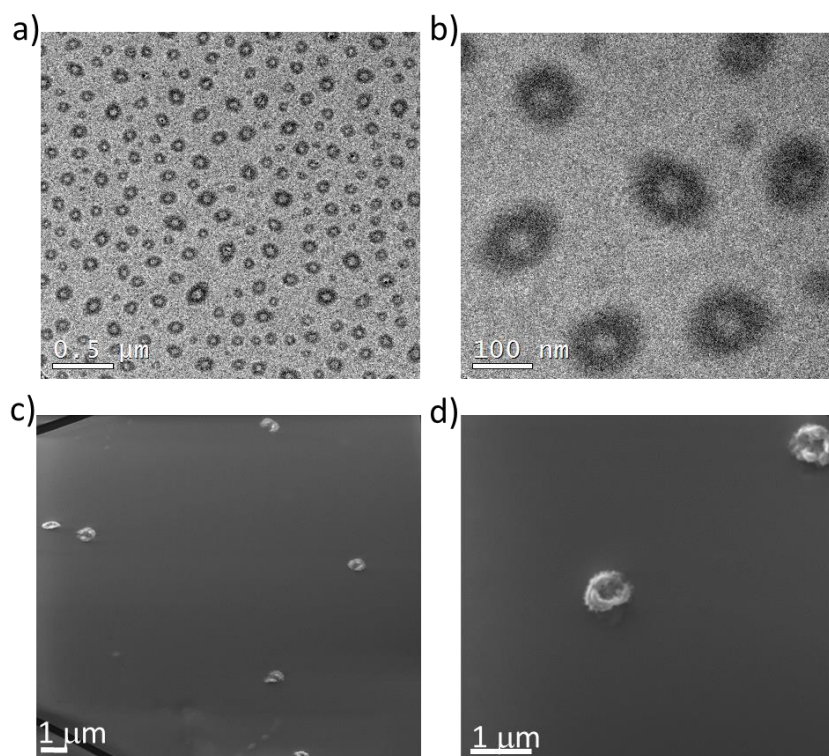


Figure 3.14. a, b) TEM images and c, d) SEM images of CD-PY-CD/AD-MV²⁺-AD (1:1) self-assembly on aluminium foil.

Figure 3.15 shows the AFM image of the CD-PY-CD/AD-MV²⁺-AD (1:1) self-assembled nanosystem. The AFM images in 3.15 a, c also shows toroidal objects with height and width of 10 and 500 nm, respectively. Figure 3.14 a gives us some insights regarding the formation of the toroidal nano-structures. The expanded regions of this figure show stacked ring-like structures. Most probably, the larger toroid structures are formed by the side by side stacking of ring-like structures to give hollow cylinders. The toroids are most probably the end-coalesced product of the cylindrical precursors. The smaller ring-like structures may be formed most probably from the bis-inclusion complexes.

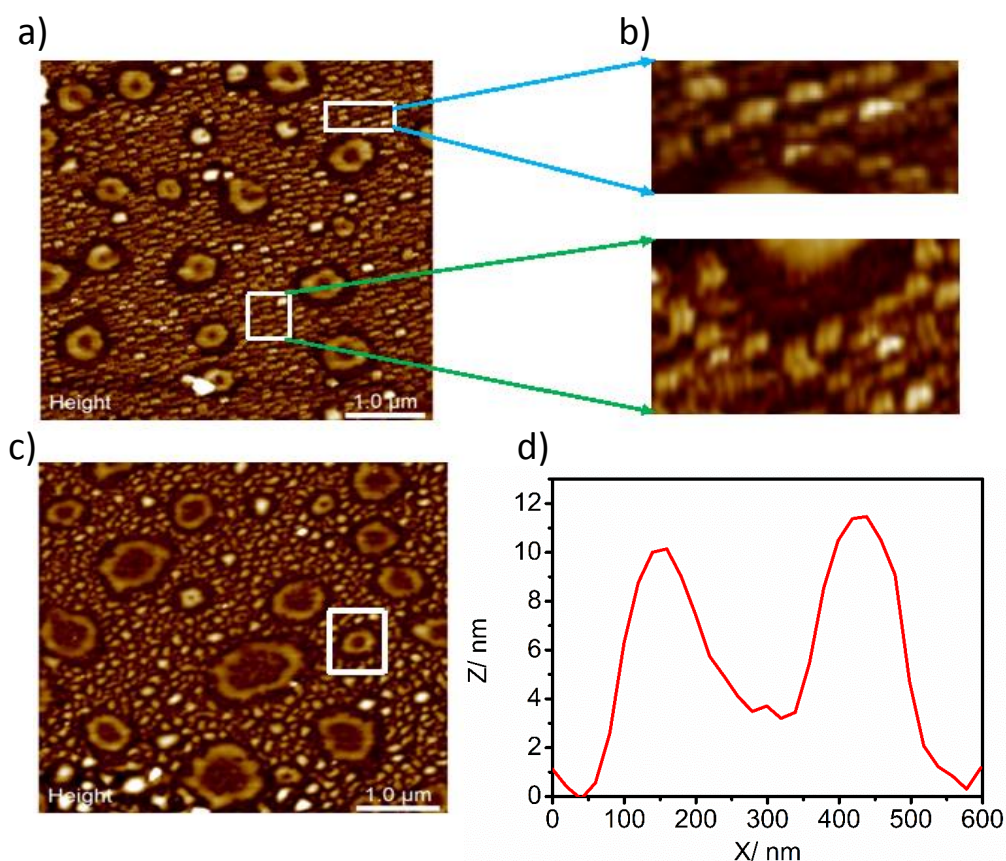


Figure 3.15. a) AFM images of nanostructures formed in the self-assembly of CD-PY-CD/AD-MV²⁺-AD (1:1) in aqueous solution. b) The expansion of the selected region in a. c) The height image and d) the height profile of marked nanostructure in c.

3.3.6. Mechanism for self-assembly in CD-PY-CD/AD-MV²⁺-AD (1:1)

Since both CD-PY-CD and AD-MV²⁺-AD have two binding sites for each other, binding can occur at both ends leading to formation of long supramolecular fibers as shown in Figure 3.16A. However, long fibrous structures were not observed. In the TEM, SEM and AFM images, only toroidal structures are observed. We propose that instead of forming long-fibers, closed-loop structures are formed by end-coalescence of the long fibers as shown in Figure 3.16B. The closed-loop structures then stack together to give the ring-like structures seen in Figure 3.15b. The ring-like structures continue to stack together to give hollow cylindrical structures as shown in Figure 3.16C. The hollow cylinders can undergo ring-coalescence to give the toroids as shown in Figure 3.16C.

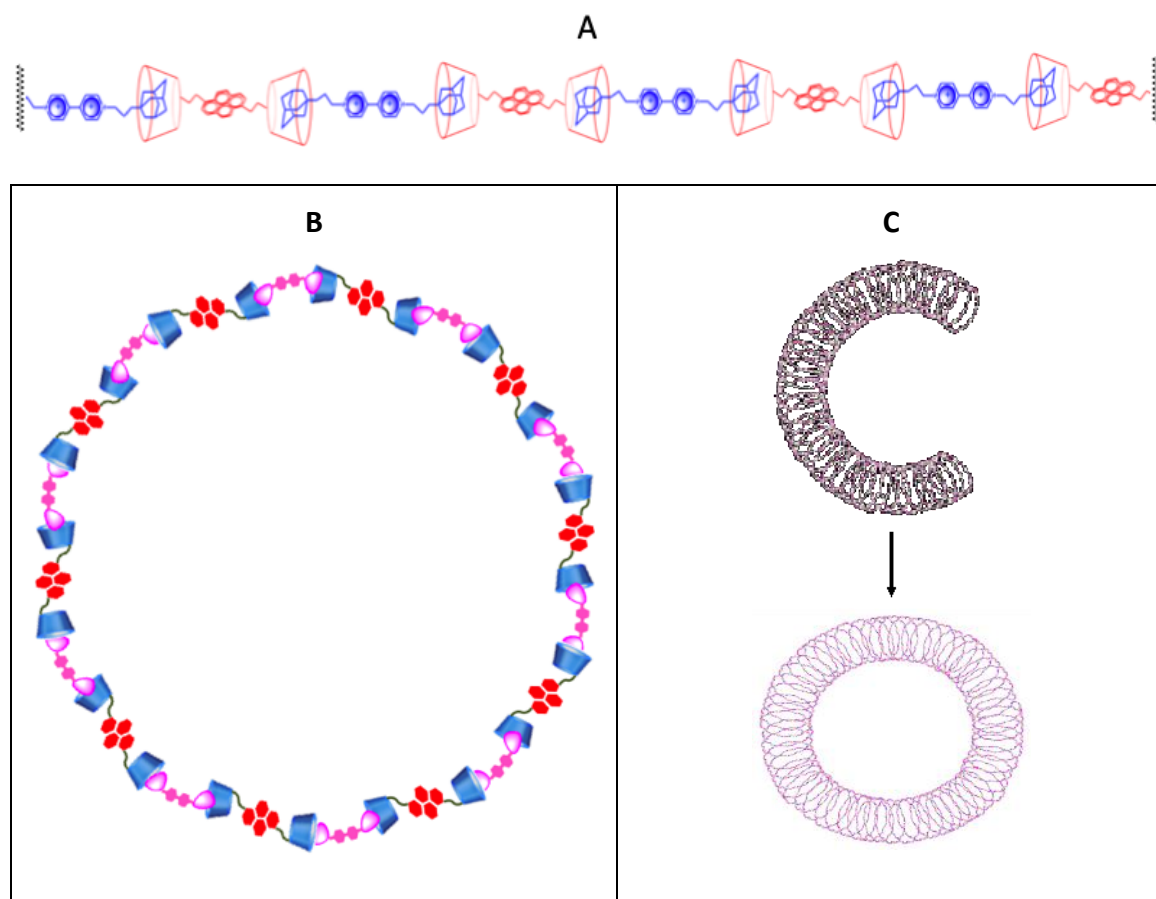


Figure 3.16. Formation of different hierarchical structures by self-assembly of CD-PY-CD/AD-MV²⁺-AD bis-inclusion complex: A) linear structures, B) closed-loop structure and C) hollow cylinder and ring-coalesced cylinders.

In the linear or ring-like structures shown in Figure 3.16A-B, the distance between two PY units would be > 3 nm and hence coupling between two PY units within a chain or ring is difficult to conceive. We observed significant damping of the NMR signals of PY and β -CD in the complex. We attribute this to the stacking of the ring loops shown in Figure 3.15c. When stacking of rings occurs, there will be regions of PY over PY and MV²⁺ over MV²⁺ stacks. Since no CT bands are observed in the absorption spectrum of CD-PY-CD/AD-MV²⁺-AD, we infer that there are no regions of PY stacked over MV²⁺. In such stacks we can have regular or slipped stacks, as shown in Figure 3.17.

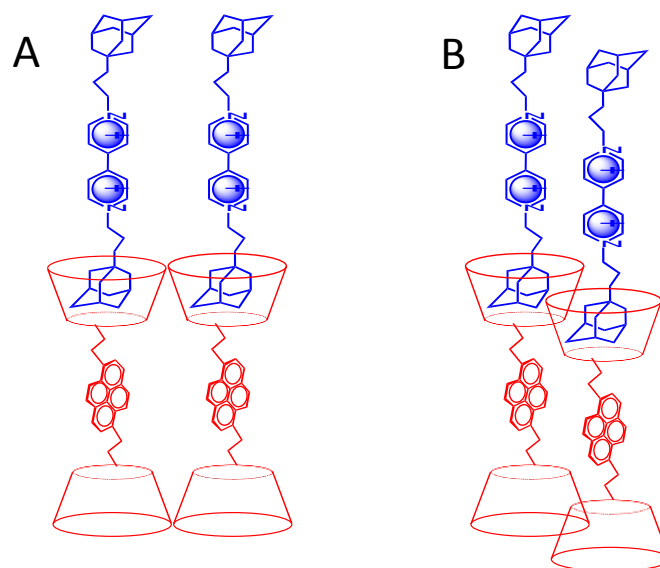


Figure 3.17. Schematic of A) regular and B) slipped stacks of the ring loops.

In the regular stacks, the center to center distance between the PY in two adjacent stacks will be the same as the outer diameter of the wider rim of β -CD, which is ~ 15.3 Å. At this distance the PY units of adjacent stacks can hardly interact and dampening of the NMR signals cannot occur. In the slipped stacks in Figure 3.17B, the distance between the PY units are much less and the PY moieties of adjacent stacks may interact with each other. Since dampening of NMR signals is very severe and the β -CD proton signals are also dampened, we believe that very strong π - π stacking occurs between PY moieties in adjacent stacks which led to partial deformation of the β -CD structure. When molecules stack one over another, free rotation of molecules is prevented and every proton in the molecules experience a different chemical and magnetic environment. This leads to different chemical shifts for every proton in the aggregate leading to significant broadening of the NMR signals.

-1.67 and -0.57 eV for PET from singlet and triplet excited states of PY to MV^{2+} , suggesting that these reactions are highly facile.

We observed that the fluorescence of CD-PY-CD was quenched by sub-millimolar amounts of AD- MV^{2+} -AD (Figure 3.11). The Stern-Völmer plot for the quenching is given in Figure 3.18, where Q refer to the quencher AD- MV^{2+} -AD, I_0 refer to the fluorescence intensity in the absence of quencher and I refer to the intensity in the presence of different quencher concentrations. The I_0/I curve exhibited three clear quenching regions, as shown by the lines in Figure 3.18. The quenching rate is very low in the initial and final stages of quenching. In fact, the slopes of the initial and final stages of quenching are nearly the same.

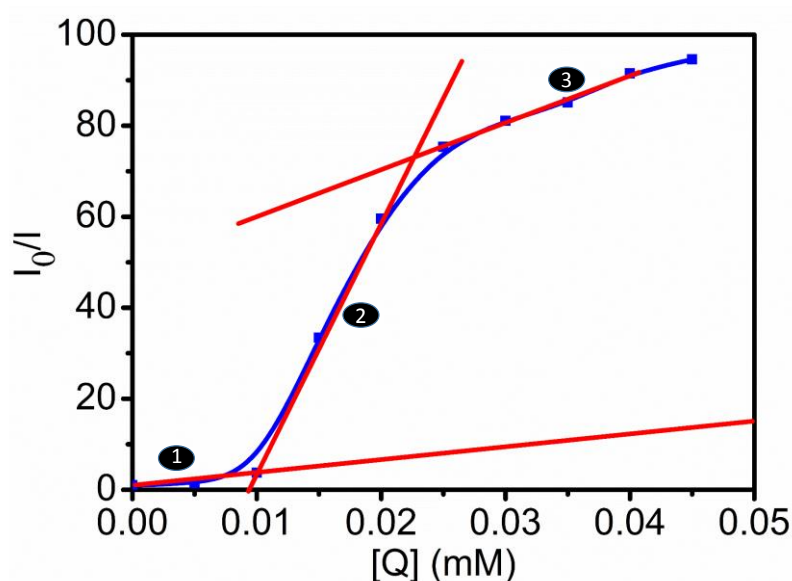


Figure 3.18. Stern-Völmer plot for the quenching of CD-PY-CD fluorescence quenching by AD- MV^{2+} -AD.

Concentration of CD-PY-CD employed for the quenching experiment is 10^{-5} M. The quenching is very slow until the quencher concentration reaches 1×10^{-5} M. Thereafter the quenching became extremely fast until the quencher concentration is 2.5×10^{-5} M. The quenching became slow with further increase in the concentration of the quencher.

The curve is similar to the micellization curve for amphiphilic molecules where the region of higher slope corresponds to micelle formation.³⁹ Using this analogy, we propose that the region where $[Q] = (1.0 - 2.5) \times 10^{-5}$ M corresponds to the formation of the nanostructures shown in Figures 3.14 and 3.15. In these structures, every PY molecules will have MV^{2+} moieties on either side of it with β -CD as spacer. Quenching will be very fast in this regime. When $[Q] < 1.0 \times 10^{-5}$ M, quenching will be mostly diffusion controlled. Since both CD-PY-CD and AD- MV^{2+} -AD are relatively large molecules, their diffusion coefficients in water will be very low and rate of diffusion mediated quenching rate will also be low. In the higher concentration range of $[Q] > 2.5 \times 10^{-5}$ M, most of the CD-PY-CD molecules will be engaged in the nanostructure formation and only a very small fraction of molecules will be free to undergo diffusion. In this regime also, quenching will be limited by diffusion rate and hence very slow. Behavior similar to this is also seen in the time-resolved fluorescence quenching experiments.

3.3.7.2. Time resolved fluorescence quenching studies

Fluorescence quenching in the CD-PY-CD/AD- MV^{2+} -AD system was also studied using fluorescence lifetime quenching method. We observed that the fluorescence of CD-PY-CD was mono-exponential with a lifetime $\tau_0 = 136$ ns (curve 'a' in Figure 3.19). This value is very similar to the fluorescence lifetime of pyrene in aqueous solution.^{34,35} In the presence of AD- MV^{2+} -AD, fluorescence decays became bi-exponential as shown in Figure 3.19 b-j as observed previously for several non-covalently bound donor-acceptor systems.^{34,40,41}

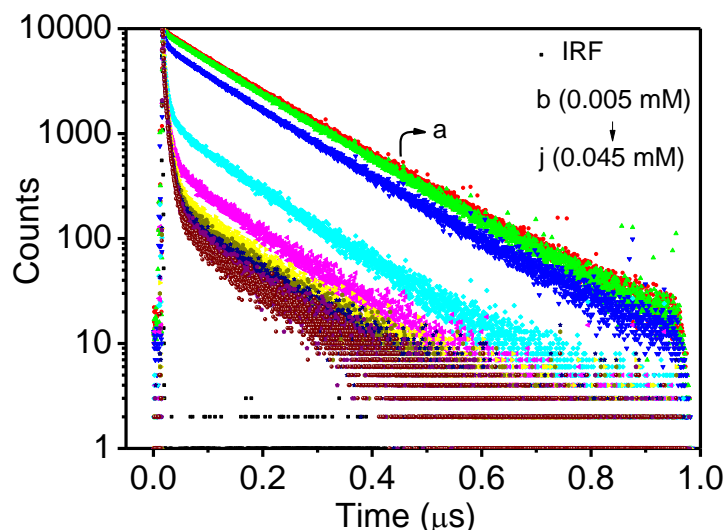
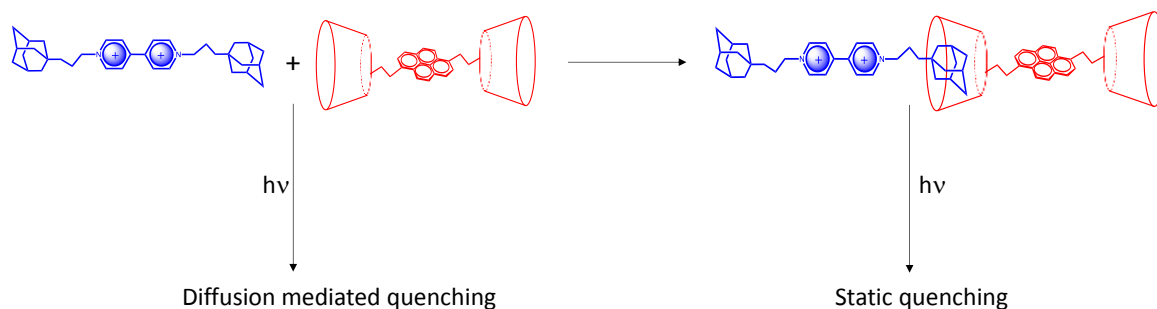


Figure 3.19. Fluorescence decay profiles of CD-PY-CD (2.5×10^{-5} M) a) in the absence and b-j) presence of various concentrations of AD-MV²⁺-AD (0 – 1.8 equiv.).

The bi-exponential fluorescence decay was attributed to diffusion mediated and unimolecular quenching processes as shown below in Scheme 3.5. In aqueous solution of CD-PY-CD/AD-MV²⁺-AD, a fraction of the molecules exist in the complexed form and the remaining fraction moves around as free molecules. When excited, the fluorescence quenching in the free fraction will be diffusion controlled and quenching in the complexed fraction will be static as shown in Scheme 3.5.



Scheme 3.5. Scheme showing diffusion mediated and intramolecular quenching.

In accordance with the previous reports, the observed fluorescence decays were fitted to the following bi-exponential function.⁴⁰

$$I_t = \chi_{(\text{complex})} \exp(-t/\tau_1) + \chi_{(\text{free})} \exp(-t/\tau_2) \quad (3.2)$$

where τ_1 and τ_2 are the two lifetime components and $\chi_{(\text{complex})}$ and $\chi_{(\text{free})}$ are their respective contributions. This observation supports Scheme 3.5 which shows that a D-A complex is formed within which electron transfer takes place and τ_1 corresponds to the fluorescence lifetime of the D-A complex and τ_2 corresponds to the fluorescence of the un-complexed CD-PY-CD. Compared to the fluorescence lifetime of CD-PY-CD ($\tau_0 = 136$ ns) value of τ_1 will be low because of the static quenching of fluorescence within the D-A complex by PET. It has been shown that^{40,41}

$$\tau_1 = (k_0 + k_{\text{et}})^{-1} \quad (3.3)$$

where k_{et} is the rate constant for the unimolecular electron transfer within the complex and $k_0 = 1/\tau_0$. The equation can be rearranged to

$$k_{\text{et}} = 1/\tau_1 - 1/\tau_0 \quad (3.4)$$

Lifetime τ_2 results from the intrinsic fluorescence decay of CD-PY-CD and its diffusion mediated quenching by AD-MV²⁺-AD. Under this condition, the lifetime τ_2 is defined by equation 3.5.^{40,41}

$$\tau_2 = (k_0 + k_q[\text{Q}])^{-1} \quad (3.5)$$

Equation 3.5 above can be rearranged to

$$\tau_0/\tau_2 = 1 + k_q \tau_0 [\text{Q}] \quad (3.6)$$

All decay profiles shown in Figure 3.19 were fitted with equation 3.2 and the fit parameters obtained including τ_1 and τ_2 are presented in Table 3.1. As per equations 3.3 and 3.5, τ_1 should be independent of AD-MV²⁺-AD concentration and plot of τ_0/τ_2 vs $[\text{Q}]$ should be linear. We can see from Table 3.1 that the value of τ_1 does not depend on quencher concentration as dictated by equation 3.3. The average value of $\tau_1 = 6.85$ ns.

Substituting the average value of τ_1 in equation 3.4 we get $k_{et} = 1.39 \times 10^8 \text{ s}^{-1}$, suggesting that the rate of PET within the nanostructure is very high.

Table 3.1. Table showing the fluorescence lifetime values (τ_1 and τ_2), fractional contributions ($\chi_{(\text{complex})}$ and $\chi_{(\text{free})}$) and χ^2 values obtained for fluorescence lifetime quenching of CD-PY-CD with AD-MV²⁺-AD.

Conc. of AD-MV ²⁺ -AD, mM	τ_1 , ns	$\chi_{(\text{complex})}$	τ_2 , ns	$\chi_{(\text{free})}$	χ^2
0			136	100	1.2
0.005 mM	6.27	0.58	134.03	99.42	1.07
0.015 mM	6.82	19.25	115.66	80.75	1.16
0.02 mM	6.94	37.08	116.21	62.92	1.13
0.025 mM	6.92	54.03	111.34	45.97	1.12
0.03 mM	6.99	61.58	108.5	38.42	1.15
0.035 mM	7.00	66.94	107.37	33.06	1.12
0.04 mM	6.95	72.36	103.5	27.64	1.06
0.045 mM	6.93	73.46	102.61	26.54	1.04

An inspection of Figure 3.18 and Table 3.1 show that the contribution due to intra-ensemble quenching (χ_{complex}) increases drastically as the quencher concentration goes from 0.015 to 0.030 mM. This corresponds to the high quenching domain in Figure 3.18 and as suggested earlier, may mark the formation of nanostructures in the solution.

3.3.7.3. Nanosecond laser flash photolysis studies

The CD-PY-CD/AD-MV²⁺-AD system was subjected to nanosecond laser flash photolysis using the third harmonic of a Nd-YAG laser. The transient absorption spectra obtained at different times following the laser flash are shown in Figure 3.20a. The transient absorption spectrum obtained at short times exhibited sharp peaks at 400 and 460 nm and a broad peak around 610 nm. Based on literature,^{36,42} the 400 and 610 nm absorptions can be assigned to MV^{•+} and the 460 nm peak can be assigned to PY^{•+}, both formed following PET from PY to MV²⁺ as per Scheme 3.4.

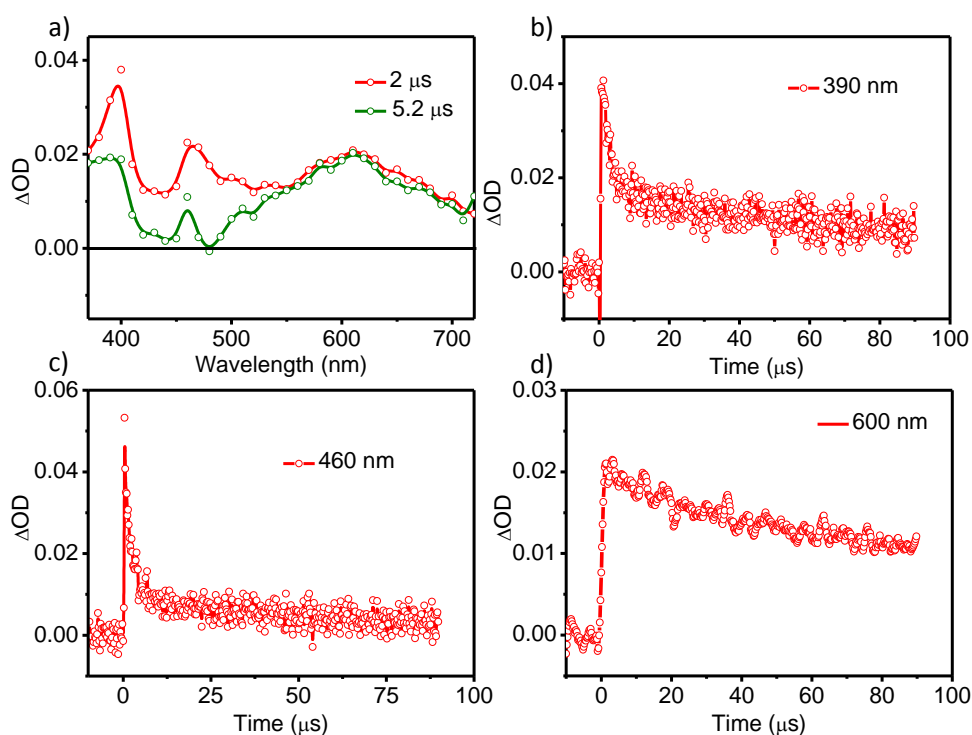


Figure 3.20. a) The transient absorption spectra obtained at 2 and 5.2 μs in the flash photolysis of CD-PY-CD/AD-MV²⁺-AD (5×10^{-5} M). b-d) Kinetic traces at the various peak maxima.

Kinetic profiles of the various transients are shown in Figure 3.20 b-d. The 390 nm transient shows an initial fast decay followed by a slow decay at longer times. The 460 nm

transient assigned to $PY^{\bullet+}$ undergo very fast decay within few μs . The 610 nm transient showed about 50% decay within the 100 μs time window.

At very long times the peak intensity at 390 nm decreases and the maximum shifts to < 380 nm. The changes that occur to the $MV^{\bullet+}$ absorption at 390 nm is consistent with the dimerization of the radical cation into a di-cation as shown in equation 3.7.



The dimer exhibits absorption at 360 and 560 nm.^{36,43,44} In Figure 3.20a, we can see that the peak at 390 nm decreases in intensity and leads to formation of a new peak with maximum < 380 nm. The 610 nm peak, however, differs somewhat from the reported absorption spectrum of the dimer, as it does not show maximum at 560 nm.

The $MV^{\bullet+}$ dimer was studied in great detail.⁴³⁻⁵⁰ The spatial orientation postulated for $MV^{\bullet+}$ dimer is one in which the two radical cations lie face to face in a sandwich type structure linked by the two π -clouds overlapping to form a π - π bond as shown in Figure 3.21a.³⁶ Such a dimer would be unstable with respect to coulombic repulsion due to the close proximity of the two positive charges. It has been reported that the radical cation is in equilibrium with its dimer and the fraction of dimer increases as temperature decreases. This suggests that the spin-pairing energy of dimer formation is greater than the instability caused by coulombic repulsion.

In the present case, however, a face to face dimer as shown in Figure 3.21a cannot be formed. In Figure 3.17 we proposed a slipped-stack arrangement for the ring loops, which suggest that the $MV^{\bullet+}$ in adjacent stacks will also be arranged in a slipped-stack manner. The dimer formed in this case will have slightly different structure and we

propose that the absorption spectrum obtained at 5.2 μs in Figure 3.20 correspond to the slipped-stack dimer (Figure 3.21b). We propose that the <380 nm and 610 nm absorptions are due to the species shown in Figure 3.21b. This is supported by the kinetic profile at 370 nm (Figure 3.21c), which is very similar to the decay of the 610 nm species in Figure 3.20d. A fit of the slow decay at 370 nm and 610 nm gave lifetime of 45 μs .

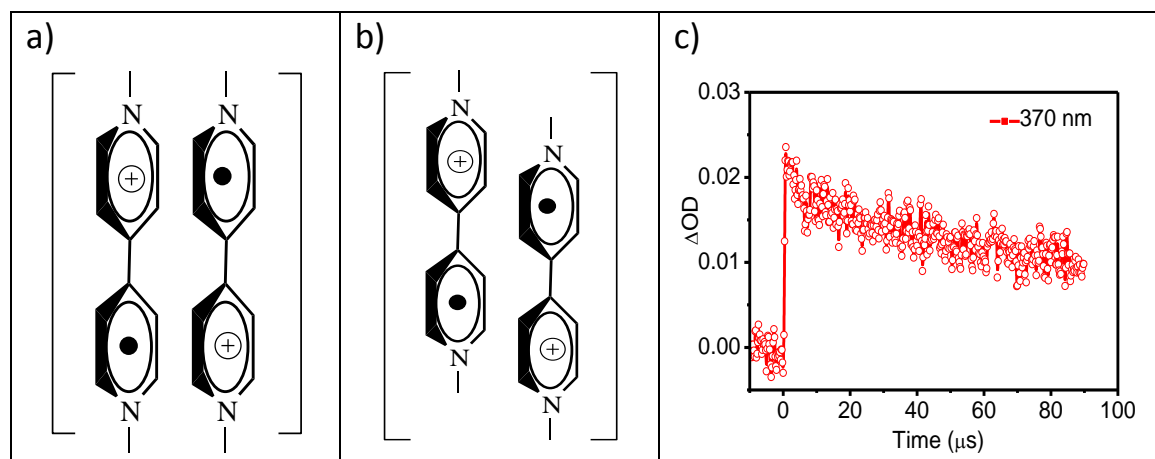


Figure 3.21. a, b) Probable π -dimers of $\text{MV}^{\bullet+}$ and c) decay profile of the 370 nm species.

Figure 3.20c shows that the $\text{PY}^{\bullet+}$ absorption at 460 nm showed a very fast decay. We attribute this to the reaction of $\text{PY}^{\bullet+}$ with PY in adjacent stack as shown in equation 3.8.



Reaction of $\text{PY}^{\bullet+}$ with PY to give $(\text{PY-PY})^{\bullet+}$ is well investigated in the literature.⁵¹⁻⁵³ The dimer radical ion absorption is around 800 nm and > 1300 nm, and hence is not seen in the transient spectra. This species is unstable and decomposes to PY and $\text{PY}^{\bullet+}$ at longer timescales. In the discussion above we have not considered formation of $(\text{MV}^{\bullet+} \dots \text{MV}^{2+})$ and dimerization of $\text{PY}^{\bullet+}$, as both these species are not reported, to the best of our knowledge.

PET as shown in Scheme 3.4 generates $\text{PY}^{\bullet+}$ and $\text{MV}^{\bullet+}$ in equimolar amounts. Equation 3.7 needs two $\text{MV}^{\bullet+}$ which requires absorption of two photons. Equation 3.8 has only one radical species and require only one photon for its generation. The reactions most probably occur in a step-wise manner. Absorption of the first photon leads to generation of $\text{PY}^{\bullet+}$ and $\text{MV}^{\bullet+}$ as shown in Scheme 3.4. The $\text{PY}^{\bullet+}$ formed immediately reacts with a PY moiety in adjacent stack. A second photon is then absorbed from the pulse, which produces the two radicals and the $\text{PY}^{\bullet+}$ formed will react again leaving the $\text{MV}^{\bullet+}$ aside. This process leaves two $\text{MV}^{\bullet+}$ in the stacks, which will not be able to undergo BET as $\text{PY}^{\bullet+}$ is not available. The $\text{MV}^{\bullet+}$ will most probably undergo charge hopping or hole-transfer with MV^{2+} in adjacent stacks until two $\text{MV}^{\bullet+}$ moieties come closer and lead to dimer formation.

We have recorded the absorption spectrum of CD-PY-CD/AD- MV^{2+} -AD after flash photolysis. The spectrum was identical to the absorption spectrum before irradiation. This suggest that complete back electron transfer occurs and both PY and MV^{2+} are regenerated fully after the irradiation. The $(\text{PY}\cdots\text{PY})^{\bullet+}$ and $(\text{MV}\cdots\text{MV})^{2+}$ formed decay to the constituents in the long time scale. The radical ions then undergo BET and regenerate the starting donor-acceptor system. Contrary to the CD-AN-CD/AD- MV^{2+} -AD system reported earlier,²² the CD-PY-CD/AD- MV^{2+} -AD system did not give long-lived charge separation upon steady-state irradiation.

3.4. Conclusions

In this chapter we report assembly of a supramolecular dyad, which undergo hierarchical assembly to form higher order structures. We observed that pyrene linked to two β -CD molecules (CD-PY-CD) and methylviologen linked to two adamantane groups

(AD-MV²⁺-AD), when dissolved in water, form an inclusion complex. Since both the molecules have two binding sites for each other, repeated binding occurs to give closed loop structures, which then stack together to give toroids. Fluorescence of the pyrene chromophore was quenched in the toroid suggesting very efficient photoinduced electron transfer taking place in the toroid. The rate constant for electron transfer within the assembly was obtained from fluorescence lifetime studies. Evidence for photoinduced electron transfer from PY to MV²⁺ in the assembly was obtained from laser flash photolysis studies. Electron transfer leads to formation of radical ion products, PY^{•+} and MV^{•+}, immediately following laser irradiation. The PY^{•+} formed undergo a fast reaction with PY in adjacent stacks. The MV^{•+} formed also reacts with MV^{•+} in adjacent stacks to give a dimeric species. Since products of radical ion reactions are not very stable, the reactions are reversed at longer time scales to regenerate the radical ions, which then undergo back electron transfer and regenerate the starting materials. Thus, irradiation of the toroidal system did not lead to formation of long-lived charge separated states.

3.5. Experimental Sections

3.5.1. Instrumentation and methods

All solvents and reagents were commercially available and used without further purification, unless otherwise specified. All experiments were performed in deionized water at 25 °C. Electronic absorption spectra were recorded on a Shimadzu UV-2600 UV-Vis spectrophotometer and the emission spectra were recorded on a SPEX Fluorolog 3 Spectrofluorimeter. Circular dichroism experiments were performed on JASCO 810 spectrometer using quartz cuvettes of 1 cm path length, equipped with peltier thermostatic cell holders for variable temperature studies. All NMR spectra were recorded

in D₂O and DMSO-d₆ purchased from Aldrich, using a 500 MHz Bruker Avance DPX spectrometer. ESI-HRMS mass spectra were recorded using orbitrap mass spectrometer (Thermo Exactive). TEM analyses were performed using a FEI-TECNAI T30 G2S-TWIN, 300 kV HRTEM microscope with an accelerating voltage of 100 kV and the samples were prepared by drop-casting the aqueous solution on a formvar coated copper grid (400 mesh) and evaporating excess water. Atomic Force Microscopy (AFM) images were recorded on Multimode SPM (Bruker Nanoscope V) operating with a tapping mode regime. Antimony doped silicon cantilever with a resonant frequency of 300 kHz and spring constant of 40 Nm⁻¹ were used. The SEM images were recorded by using JEOL JSM-5600 LV scanning electron microscope. The operating range was between 5-30 kV at 50-60 Hz single phase. The sample solution in water was drop-casted directly on the top of the silicon wafer and water was allowed to evaporate at ambient conditions and analysed for SEM and AFM. Nanosecond laser flash photolysis experiments were performed by using an Applied Photophysics Model LKS-20 laser kinetic spectrometer by using the third harmonic (355 nm) from a GCR-12 series Quanta Ray Nd: YAG laser. The analysing and laser beams were fixed at right angles to each other. Solutions for laser flash photolysis studies were de-aerated by purging with argon for 20 min before experiments.

3.5.2. Materials

β- Cyclodextrin, pyrene, 4, 4'-bipyridine and 1-bromoadamantane were purchased from Sigma Aldrich and used as received. All solvents and reagents were commercially available and used without further purification, unless otherwise specified. The procedure for the synthesis of AD- MV²⁺-AD and CD-PY-CD are described below.

A) Synthesis of 2:

A solution of 1-bromoadamantane (**1**) (1.5 g, 6.972 mmol) and triethylamine (2.17 mL, 1.52 g), 15.54 mmol) in ethylene glycol (30 mL) was heated at 110 °C for 12 h. The mixture was allowed to cool to room temperature, CH₂Cl₂ (50 mL) was added, and the solution was washed with dil. HCl (1 M, 3 × 20 mL) and water (2 × 20 mL). The organic layer was dried over Na₂SO₄, and the solvent was evaporated under reduced pressure. **2** was obtained as a pale-yellow liquid. Yield: 67%; ¹H NMR (500 MHz, CDCl₃) δ ppm: 3.68 (t, 2 H), 3.52 (t, 2 H), 2.15 (br.s, 1 H), 1.96 (br.s, 3 H), 1.72 (br.s, 6 H), 1.57 (m, 6 H); ¹³C NMR (125 MHz, CDCl₃) δ ppm: 74.59, 63.41, 61.95, 41.37, 36.23, 30.48.

B) Synthesis of 3:

Compound **2** (0.81 g, 4.15 mmol) and tetrabromomethane (1.72 g, 5.18 mmol) were dissolved in dry THF under an inert atmosphere. Triphenylphosphine (1.35 g, 5.18 mmol) was added to this at 0 °C and stirred at room temperature for 0.5 h. The reaction was quenched with a few drops of water, and was partitioned between CH₂Cl₂ (150 mL) and H₂O (100 mL). The organic layer was washed with water (3 × 50 mL) and brine (50 mL). The organic layer was dried over Na₂SO₄, and the solvent was evaporated under reduced pressure. The compound was purified by column chromatography over silica gel. Elution with chloroform gave compound **3** as a light brown liquid. Yield: 72%; ¹H NMR (500 MHz, CDCl₃) δ ppm: 3.71 (t, 2 H), 3.40 (t, 2 H), 1.94 (br.s, 3 H), 1.67 (br.s, 6 H), 1.57 ppm (m, 6 H); ¹³C NMR (125 MHz, CDCl₃) δ ppm: 72.51, 60.14, 41.33, 36.27, 33.54, and 31.42.

C) Synthesis of AD- MV²⁺-AD:

Compound 3 (0.5 g, 1.93 mmol) and 4,4'-bipyridine 4 (0.15 g, 0.96 mmol) were dissolved in acetonitrile in a sealed tube and refluxed for 24 h. The light-yellow precipitate formed was filtered and washed repeatedly with dry acetonitrile to yield the product in 61% yield. mp = >300 °C; ¹H NMR (500 MHz, D₂O) δ ppm: 9.02 (d, 4 H), 8.50 (t, 4 H), 4.74 (t, 4 H), 3.97 (t, 4 H), 1.96 (br.s, 6 H), 1.48 (br.s, 18 H), 1.41 (m, 6 H); ¹³C NMR (125 MHz, CDCl₃) δ ppm: 156.86, 144.42, 123.40, 74.89, 67.52, 56.50, 35.72, 33.08, 30.26; (ESI-MS): Calculated for C₃₄H₄₆Br₂N₂O₂ 514.3548 (= M-2Br)⁺ and found 514.3618.

D) Synthesis of 5:

Twenty grams of pyrene and 500 mL of carbon tetrachloride were placed into a 2 L two necked flask. A solution of 10 mL of bromine in 500 mL of carbon tetrachloride was added dropwise with vigorous stirring at ambient temperature for 5 h. The mixture was stirred under the same conditions for 12 h. The precipitate was separated by filtration and recrystallized from toluene. Yield: 61%; mp = 220–222 °C (lit.: 221–222 °C).

E) Synthesis of 6:

A 2.5 M solution of butyllithium in hexane (35 mL, 87.5 mmol) was added dropwise to a stirred suspension of 1,6-dibromopyrene (5) (8.0 g, 22.2 mmol) in dry THF (250 mL) under argon, at -75 °C, and the mixture was stirred for 1 h at -75 °C. The cooling bath was removed and stirring was continued for 2 h at room temperature. The mixture was cooled again to -75 °C, and diethyl oxalate (30 mL, 220 mmol) was quickly added, and the mixture was stirred for 1 h. Then, the cooling bath was removed and stirring was continued for 1 h at room temperature. The mixture was poured into 2 M aqueous hydrochloric acid (200 mL), extracted with CH₂Cl₂ (3 x 100 mL), and the combined organic phases were dried over

sodium sulfate and concentrated. The product was purified by recrystallization in ethanol. Yield: 80%; mp = 162–165 °C; ^1H NMR (500 MHz, CDCl_3) δ ppm: 9.34 (d, 9 Hz, 2H), 8.40 (d, 8 Hz, 2H), 8.30 (d, 8 Hz, 2H), 8.26 (d, 9 Hz, 2H), 4.55 (q, 7 Hz, 4H), 1.49 ppm (t, 7 Hz, 6H); ^{13}C NMR (125 MHz, CDCl_3) δ ppm: 189.0, 164.7, 134.2, 131.0, 130.6, 130.3, 127.4, 126.3, 125.8, 123.8, 62.9, 14.4.

F) Synthesis of 7:

A solution of sodium bicarbonate (17 g, 0.2 mol) in water (200 mL) was added to a stirred solution of 6 (3.0 g, 7.5 mmol) in ethanol (80 mL) heated to reflux, and the mixture was stirred at reflux for 16 h. The homogenous solution was cooled to room temperature and poured cautiously into 2 M aqueous hydrochloric acid (200 mL), the precipitate was filtered off and washed with water on a glass frit. The crude product was dissolved in acetone, the acetone-insoluble salts were filtered off and discarded, and the acetone was evaporated. The solid obtained was used without further purification. Yield: 90%; ^1H NMR (500 MHz, $\text{DMSO } d_6$) δ ppm: 9.22 (d, 9 Hz, 2H), 8.57 (d, 8 Hz, 2H), 8.53 (d, 8 Hz, 2H), 8.50 ppm (d, 9 Hz, 2H); ^{13}C NMR (125 MHz, $\text{DMSO } d_6$) δ ppm: 191.2, 166.3, 133.6, 130.53, 130.46, 130.0, 126.6, 126.3, 123.3.

G) Synthesis of 8:

Hypophosphorous acid (1.7 mL, 16 mmol), was added to a mixture of 7 (2.0 g, 5.8 mmol) and sodium iodide (0.8 g, 5 mmol) in acetic acid (20 mL) under argon. The mixture was heated at reflux for 16 h. The yellow solution was cooled to room temperature, THF (100 mL) was added, and the mixture was filtered. The solid obtained was washed with THF and used without further purification. Yield: 90%; ^1H NMR (500 MHz, $\text{DMSO } d_6$) δ ppm: 12.50 (br s, 2H), 8.25 (d, 8 Hz, 2H), 8.24 (d, 9 Hz, 2H), 8.21 (d, 9 Hz, 2H), 8.00 (d, 8 Hz, 2H),

4.35 (s, 4H); ^{13}C NMR (125MHz, DMSO d_6) δ ppm: 172.8, 129.8, 129.6, 129.2, 128.9, 127.5, 124.8, 124.2, 123.3; mp: 295-296 °C; ESI-MS: m/z calcd for $\text{C}_{20}\text{H}_{14}\text{O}_4$: 318.0892 [M^+]; found: 318.0880.

H) Synthesis of CD-PY-CD:

To a cooled (-10 °C) solution of **8** (0.056 g, 0.176 mmol) in DMF (6 mL), dicyclohexylcarbodiimide (DCC) (0.145 g, 0.704 mmol) and 1-hydroxybenzotriazole (1-HOBt) (0.095 g, 0.704 mmol) were added. The reaction mixture was stirred at -10 °C for 30 min. **9** (0.4 g, 0.3524 mmol) was then added and stirring continued at -10 °C for 30 min. The mixture was then refluxed at 60 °C for 24 h. The reaction mixture was cooled and DMF was removed under vacuum. The residue obtained was washed with excess acetone and dried. The solid obtained was dissolved in DMF and subjected to reverse phase column chromatography over silica gel. Elution with methanol/water mixture (2:8) gave CD-PY-CD. Yield: 82%; mp = >300 °C; ^1H NMR (500 MHz, D_2O) δ ppm: 8.11-7.68 (m, 8H), 4.92-4.76 (m, 11H), 4.37(m, 2H), 4.16 (m, 2H), 3.73-2.57 (m, 101 H); (ESI-MS): Calculated for $\text{C}_{104}\text{H}_{152}\text{N}_2\text{O}_{70}$ is 2548.8396 ($\text{M}+\text{H}$) $^+$ and found 2549.8518.

3.6. References

- (1) Kashiwagi, Y.; Ohkubo, K.; McDonald, J. A.; Blake, I. M.; Crossley, M. J.; Araki, Y.; Ito, O.; Imahori, H.; Fukuzumi, S. Long-lived charge-separated state produced by photoinduced electron transfer in a zinc imidazoporphyrin- C_{60} dyad. *Org. Lett.* **2003**, *5*, 2719–2721.
- (2) Gust, D.; Moore, T. A.; Moore, A. L.; Lee, S. J.; Bittersmann, E.; Luttrull, D. K.; Rehms, A. A.; Degraziano, J. M.; Ma, X. C.; Gao, F.; Belford, R. E.; Trier, T. T. Efficient multistep photoinitiated electron transfer in a molecular pentad. *Science* **1990**, *248*, 199–201.
- (3) Wijesinghe, C. A.; El-Khouly, M. E.; Zandler, M. E.; Fukuzumi, S.; D'Souza, F. A charge-stabilizing, multimodular, ferrocene-bis(triphenylamine)-zinc-porphyrin-fullerene

- polyad. *Chem. Eur. J.* **2013**, *19*, 9629–9638.
- (4) Flamigni, L.; Baranoff, E.; Collin, J. P.; Sauvage, J. P. A triad based on an iridium(III) bisterpyridine complex leading to a charge-separated state with a 120 ms lifetime at room temperature. *Chem. Eur. J.* **2006**, *12*, 6592–6606.
- (5) Mallia, A. R.; Salini, P. S.; Hariharan, M. Nonparallel stacks of donor and acceptor chromophores evade geminate charge recombination. *J. Am. Chem. Soc.* **2015**, *137*, 15604–15607.
- (6) Mallia, A. R.; Hariharan, M. Self-assembled donor-acceptor trefoils: Long-lived charge separated state through aggregation. *J. Phys. Chem. C* **2017**, *121*, 4778–4788.
- (7) Harriman, A.; Kubo, Y.; Sessler, J. L. Molecular recognition via base pairing: Photoinduced electron transfer in hydrogen-bonded zinc porphyrin-benzoquinone conjugates. *J. Am. Chem. Soc.* **1992**, *114*, 388–390.
- (8) El-khouly, M. E.; El-mohsnawy, E.; Fukuzumi, S. Solar energy conversion : From natural to artificial photosynthesis. *J. Photochem. Photobiol. C* **2017**, *31*, 36–83.
- (9) KC, C. B.; D'Souza, F. Design and photochemical study of supramolecular donor – acceptor systems assembled via metal – ligand axial coordination. *Coord. Chem. Rev.* **2016**, *322*, 104–141.
- (10) Yonemoto, E. H.; Kim, Y.; Schmechl, R. H.; Wallin, J. O.; Shoulders, B. A.; Richardson, B. R.; Haw, J. F.; Mallouk, T. E. Photoinduced electron transfer reactions in zeolite-based donor-acceptor and donor-donor-acceptor diads and triads. *J. Am. Chem. Soc.* **1994**, *116*, 10557–10563.
- (11) Kimoto, K.; Satoh, T.; Iwamura, M.; Nozaki, K.; Horikoshi, T.; Suzuki, S.; Kozaki, M.; Okada, K. Very long-lived photoinduced charge-separated states of triphenylamine – naphthalenediimide dyads in polymer matrices. *J. Phys. Chem. A* **2016**, *120*, 8093–8103.
- (12) Cai, N.; Takano, Y.; Numata, T.; Inoue, R.; Mori, Y.; Murakami, T.; Imahori, H. Strategy to attain remarkably high photoinduced charge- separation yield of donor – acceptor linked molecules in biological environment via modulating their cationic moieties. *J. Phys. Chem. C* **2017**, *121*, 17457–17465.
- (13) Fukuzumi, S.; Itoh, A.; Suenobu, T.; Ohkubo, K. Formation of the long-lived charge-separated state of the 9-mesityl-10-methylacridinium cation incorporated into

- mesoporous aluminosilicate at high temperatures. *J. Phys. Chem. C* **2014**, *118*, 24188–24196.
- (14) Mallia, A. R.; Philip, A. M.; Bhat, V.; Hariharan, M. Persistent charge-separated states in self-assembled twisted nonsymmetric donor-acceptor triads. *J. Phys. Chem. C* **2017**, *121*, 4765–4777.
- (15) Jin, S.; Supur, M.; Addicoat, M.; Furukawa, K.; Chen, L.; Nakamura, T.; Fukuzumi, S.; Irle, S.; Jiang, D. Creation of superheterojunction polymers via direct polycondensation: Segregated and bicontinuous donor-acceptor π -columnar arrays in covalent organic frameworks for long-lived charge separation. *J. Am. Chem. Soc.* **2015**, *137*, 7817–7827.
- (16) Fiala, T.; Ludvikova, L.; Heger, D.; Svec, J.; Slanina, T.; Vetrakova, L.; Babiak, M.; Necas, M.; Kulhanek, P.; Klan, P.; Sindelar, V. Bambusuril as a one-electron donor for photoinduced electron transfer to methyl viologen in mixed crystals. *J. Am. Chem. Soc.* **2017**, *139*, 2597–2603.
- (17) Huber, R. C.; Ferreira, A. S.; Thompson, R.; Kilbride, D.; Knutson, N. S.; Devi, L. S.; Toso, D. B.; Challa, J. R.; Zhou, Z. H.; Rubin, Y.; Schwartz, B. J.; Tolbert, S. H. Long-lived photoinduced polaron formation in conjugated polyelectrolyte-fullerene assemblies. *Science* **2015**, *348*, 1340–1343.
- (18) Nayak, N. Ph.D Thesis, AcSIR, 2017.
- (19) Krishnan, R.; Rakhi, A. M.; Gopidas, K. R. Study of β - cyclodextrin – pyromellitic diimide complexation. Conformational analysis of binary and ternary complex structures by induced circular dichroism and 2D NMR spectroscopies. *J. Phys. Chem. C* **2012**, *116*, 25004–25014.
- (20) Krishnan, R.; Gopidas, K. R. β -cyclodextrin as an end-to-end connector. *J. Phys. Chem. Lett.* **2011**, *2*, 2094–2098.
- (21) Nayak, N.; Gopidas, K. R. Integrative self-sorting in a three component system leading to formation of long fibrous structures. *Chemistryselect* **2016**, *5*, 1028–1032.
- (22) Krishnan, S. B. Ph. D. Thesis, AcSIR, 2017.
- (23) Giroto, E.; Ferreira, M.; Sarkar, P.; Bentaleb, A.; Hillard, E. A.; Gallardo, H.; Durola, F.; Bock, H. Plank-shaped column-forming mesogens with substituents on one side only. *Chem. Eur. J.* **2015**, *21*, 7603–7610.

- (24) Robert, A.; Dechambenoit, P.; Bock, H.; Duroola, F. A Carboxyfunctionalized (2₄)-1,6-pyrenophane-tetraene by glyoxylic perkin condensation. *Can. J. Chem.* **2017**, *95*, 450–453.
- (25) Trotta, F.; Martina, K.; Robaldo, B.; Barge, A.; Cravotto, G. Recent advances in the synthesis of cyclodextrin derivatives under microwaves and power ultrasound. *J. Incl. Phenom. Macrocycl.Chem.* **2007**, *57*, 3–7.
- (26) Nayak, N.; Gopidas, K. R. Unusual self-assembly of a hydrophilic β -cyclodextrin inclusion complex into vesicles capable of drug encapsulation and release. *J. Mater. Chem. B* **2015**, *3*, 3425-3428.
- (27) Nayak, N.; Gopidas, K. R. Self-assembly of β -cyclodextrin bis-inclusion complex into a highly crystalline fiber network. An effective strategy for null aggregate design. *J. Phys. Chem. B* **2019**, *123*, 8131-8139.
- (28) Kodaka, M. Sign of circular dichroism induced by β -Cyclodextrin. *J. Phys. Chem.* **1991**, *95*, 2110-2112.
- (29) Kodaka, M. A. General rule for circular dichroism induced by a chiral macrocycle. *J. Am. Chem. Soc.* **1993**, *115*, 3702-3705.
- (30) Nakashima, K.; Miyamoto, T.; Hashimoto, S. Photoinduced electron transfer from pyrene to methylviologen in polystyrene latex dispersions as studied by diffuse reflectance laser flash photolysis. *Chem. Commun.* **1999**, 213-214.
- (31) Gong, Y.-K.; Miyamoto, T.; Nakashima, K.; Hashimoto, S. Photoinduced electron transfer from 3-(9-Anthracene)propyltrimethyl ammonium bromide and pyrene to methyl viologen on the surface of polystyrene latex particles. *J. Phys. Chem. B* **2000**, *104*, 5772-5778.
- (32) Nakashima, K.; Kido, N. Fluorescence quenching of 1-pyrenemethanol by methylviologen in polystyrene latex dispersions. *Photochem. Photobiol.* **1996**, *64*, 296-302.
- (33) Slama-Schwok, A.; Ottollegghi, M.; Avnir, D. Long-lived photoinduced charge separation in a redox system trapped in a sol-gel glass. *Nature* **1992**, *355*, 240-242.
- (34) Balan, B.; Gopidas, K. R. Photoinduced electron transfer in α -cyclodextrin-based supramolecular dyads: A free-energy-dependence study. *Chem. Eur. J.* **2006**, *12*, 6701-6710.

- (35) Krishnan, R.; Krishnan, S. B.; Balan, B.; Gopidas, K. R. Self-assembly and photoinduced electron transfer in a donor- β -cyclodextrin-acceptor supramolecular system. *J. Chem. Sci.* **2018**, 130:134.
- (36) Monk, P. M. S. The Viologens: Physicochemical properties, synthesis and applications of the salts of 4, 4'-bipyridine, John Wiley and Sons, Chichester, **1988**, p. 59.
- (37) Murov, S. L.; Carmichael, I.; Hug, G. L. Handbook of photochemistry, Second Edition, Revised and Expanded, Marcel Dekker, New York, **1993**, p 45.
- (38) Rehm, D.; Weller, A. Kinetics of fluorescence quenching by electron and H-atom transfer. *Isr. J. Chem.* **1970**, 8, 259-271.
- (39) Tanford, C. The hydrophobic effect: Formation of micelles and biological membranes, 2nd Edition, John Wiley and sons, Somerset, NJ, 1980.
- (40) De Rege, J. F.; Williams, S. A.; Therien, M. J. Direct evaluation of electronic coupling mediated by hydrogen bonds: implications for biological electron transfer. *Science* **1995**, 269, 1409-1413.
- (41) Prasad, E.; Gopidas, K. R. Photoinduced electron transfer in hydrogen bonded donor-acceptor systems. Study of the dependence of rate on free energy and simultaneous observation of the marcus and rehm-weller behaviors. *J. Am. Chem. Soc.* **2000**, 122, 3191-3196.
- (42) Shida, T. Electronic absorption spectra of radical ions, *Elsevier Science Publishers B. V. Amsterdam*, **1988**, p 71.
- (43) Lee, C.; Lee, Y. M.; Moon, M. S.; Park, S. H.; Park, J. W.; Kim, K. G.; Jeon, S.-J. UV-vis-NIR and Raman spectroelectrochemical studies on viologen cation radicals: evidence for the presence of various types of aggregate species. *J. Electroanal. Chem.* **1996**, 416, 139-144.
- (44) Lee, C.; Sung, Y. W.; Park, J. W. Dependence of dimerization of electrogenerated methylalkylviologen radical cations on the length of alkyl chain in the presence of γ -cyclodextrin. *J. Electroanal. Chem.* **1997**, 431, 133-139.
- (45) Evans, A. G.; Evans, J. C.; Baker, M. W. Study of bipyridyl radical cations. Part 5. Effect of structure on the dimerisation equilibrium. *J. Chem. Soc. Perkin Trans 2*, **1977**, 1787-1789.

- (46) Iordache, A.; Oltean, M.; Milet, A.; Thomas, F.; Baptiste, B.; Saint-Aman, E.; Bucher, C. Redox control of rotary motions in ferrocene-based elemental ball bearings. *J. Am. Chem. Soc.* **2012**, *134*, 2653-2671.
- (47) Moon, K.; Grindstaff, J.; Sobransingh, D.; Kaifer, A. E. Cucurbit[8]uril-mediated redox-controlled self-assembly of viologen-containing dendrimers. *Angew. Chem. Int. Ed.* **2004**, *43*, 5496-5499.
- (48) Lipke, M. C.; Cheng, T.; Wu, Y.; Arslan, H.; Xiao, H.; Wasielewski, M. R.; Goddard, W. A. III; Stoddart, J. F. Size-matched radical multivalency. *J. Am. Chem. Soc.* **2017**, *139*, 3986-3998.
- (49) Porter, W. W. III; Vaid, T. P. Isolation and characterization of phenyl viologen as a radical cation and neutral molecule. *J. Org. Chem.* **2005**, *70*, 5028-5035.
- (50) Park, J. W.; Choi, N. H.; Kim, J. H. Facile dimerization of viologen radical cations covalently bonded to β -cyclodextrin and suppression of the dimerization by β -cyclodextrin and amphiphiles. *J. Phys. Chem.* **1996**, *100*, 769-774.
- (51) Naqvi, K. R.; Melø, T. B. Reduction of tetranitromethane by electronically excited aromatics in acetonitrile: Spectra and molar absorption coefficients of radical cations of anthracene, phenanthrene and pyrene. *Chem. Phys. Lett.* **2006**, *428*, 83-87.
- (52) Rodgers, M. A. J. Nanosecond pulse radiolysis of acetone. Kinetic and thermodynamic properties of some aromatic radical cations. *J. Chem. Soc. Faraday Trans. 1* **1972**, *68*, 1278-1286.
- (53) Mori, Y.; Shinoda, H.; Nakano, T.; Kitagawa, T. Formation and decay behaviors of laser-induced transient species from pyrene derivatives 1. Spectral discrimination and decay mechanisms in aqueous solution. *J. Phys. Chem. A* **2002**, *106*, 11743-11749.

Generation of Long-Lived Charge Separated State in a Supramolecular Donor-Acceptor System Self-Assembled into Vesicles and Fibers

4.1. Abstract

In this chapter, we employed the donor CD-PY-CD (same as that employed in chapter 3) and used the acceptor Ms-(AD-MV²⁺)₃, that has AD-linked MV²⁺ moieties on all three arms of a mesitylene core. In aqueous solution the donor-acceptor system initially self-assembled into vesicles which later coalesced to give long fibers. The Self-assembly was studied using ¹H NMR, 2D NMR, ICD, TEM, SEM and AFM analysis. Fluorescence of the pyrene chromophore was quenched within the self-assembled system due to efficient photoinduced electron transfer from PY to MV²⁺. PET is confirmed through identification of product radical ions in flash photolysis experiments. The transients observed in the flash photolysis were long-lived. Steady-state irradiation of the self-assembled system in an optical bench led to the formation of methyl viologen radical cation (MV^{•+}), which was stable for a few hours. Longevity of the radical cation was attributed to the fast reaction of PY^{•+} with adjacent PY to give an unstable adduct, which slows down the BET process.

4.2. Introduction

Tolbert and co-workers have reported that molecular self-assembly can mimic the cascade type electron transfer observed in the bacterial reaction center and allow the spatial separation of photogenerated charges, leading to long-lived charge separated (CS) state.¹ They reported that micelle-forming cationic poly(fluorine-alt-thiophene) co-assembled in water with cationic fullerene derivatives to produce single micellar aggregates that could sustain photoinduced charge separation for days in aqueous solution (see introduction section of Chapter 3). Although the generation of long-lived CS state in aqueous solution through irradiation of self-assembled donor-acceptor system appears very attractive, this strategy has not been exploited further. Recently, long-lived charge separation in a self-assembled donor-acceptor system was reported from our laboratory.² Anthracene (AN) linked to two β -cyclodextrin (β -CD) molecules (CD-AN-CD) and methyl viologen (MV^{2+}) linked to two adamantane (AD) units (AD- MV^{2+} -AD) formed an inclusion complex in water, which further self-assembled into well-defined toroidal nanostructures. Irradiation of the aqueous toroidal solution led to formation of a CS state which was stable for few hours. In Chapter 3 of the thesis, this work was followed up by employing pyrene (PY) in place of anthracene. The donor CD-PY-CD and acceptor AD- MV^{2+} -AD self-assembled in water to generate ring-like structures which then stacked together to give toroidal nanostructures. Irradiation of the solution containing the nanostructure led to generation of $PY^{\bullet+}$ and $MV^{\bullet+}$ radical ions. The $PY^{\bullet+}$ formed undergo a fast reaction with PY in adjacent stacks. The $MV^{\bullet+}$ formed also reacts with $MV^{\bullet+}$ in adjacent stacks to give a dimeric species. Since products of the radical ion reactions are not very stable, the reactions are reversed at longer time scales to

generate the radical ions, which then undergo back electron transfer to regenerate the starting materials. Thus, irradiation of the toroidal system did not lead to formation of long-lived CS states. Absence of long-lived CS state in this case can be attributed to the extremely close packing of PY on PY and MV^{2+} on MV^{2+} within the toroidal assembly.

This chapter also deals with self-assembly of a donor- acceptor system capable of undergoing photoinduced electron transfer (PET). We have selected the same donor CD-PY-CD, studied in Chapter 3. The structure of the acceptor used in this study, $Ms-(AD-MV^{2+})_3$ is shown in Figure 4.1. $Ms-(AD-MV^{2+})_3$ has three AD-linked MV^{2+} moieties attached to a central mesitylene unit as shown in Figure 4.1. Because of the branched structure, the inclusion complex formed will not be able to stack tightly to form toroidal structures. Self-assembly may lead to formation of different types of structures and we hoped that PET in this system may lead to long-lived CS states.

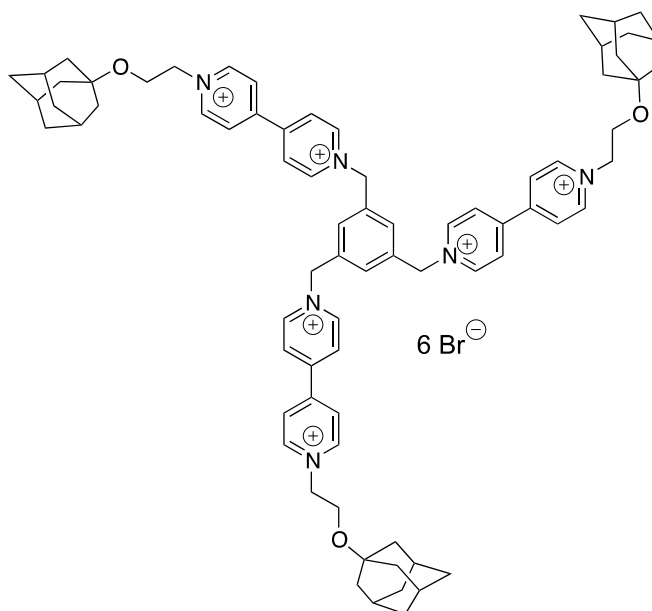
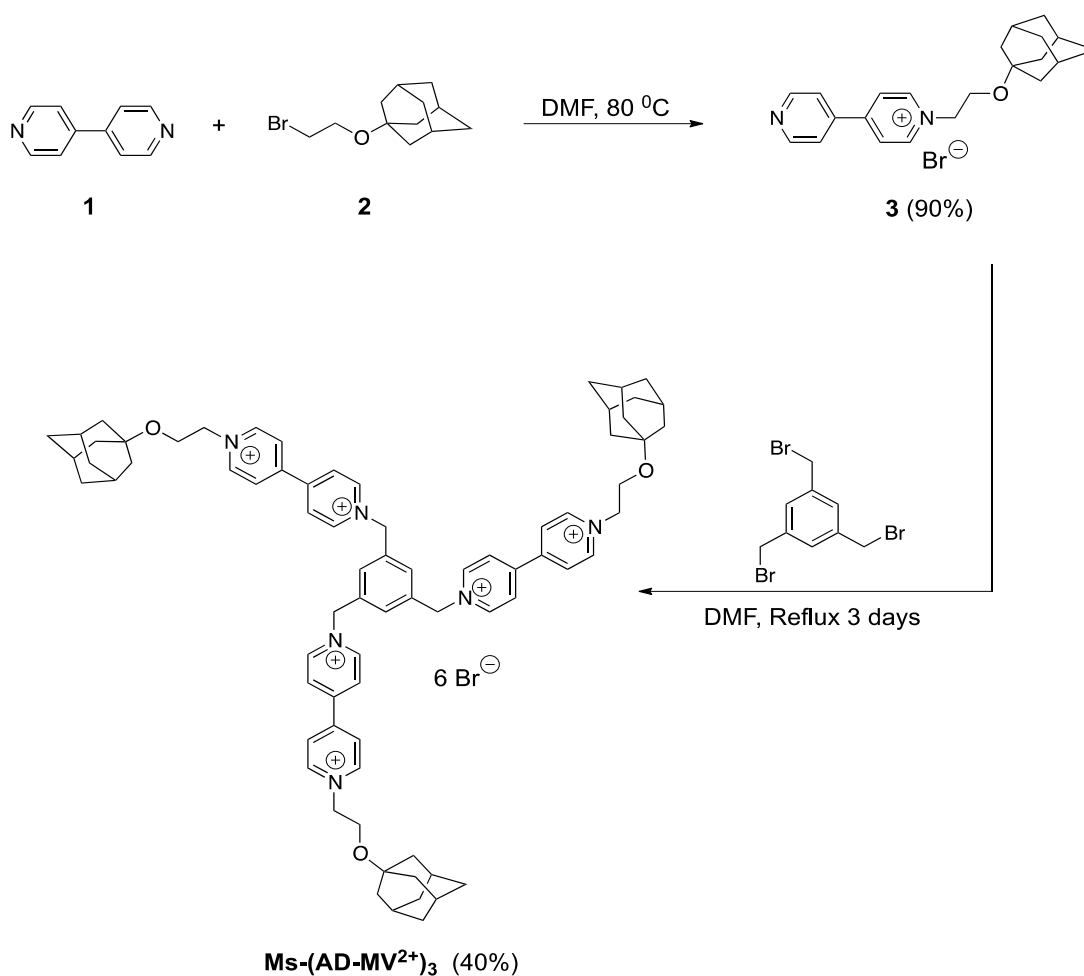


Figure 4.1. Structure of $Ms-(AD-MV^{2+})_3$.

4.3. Results and Discussions

4.3.1. Synthesis and characterization of molecules

Synthesis and ^1H NMR spectrum of CD-PY-CD was discussed in chapter 3. The acceptor $\text{Ms}-(\text{AD-MV}^{2+})_3$ was synthesized by adaptation of a reported procedure.³ The synthetic route is shown in Scheme 4.1.



Scheme 4.1. Scheme for the synthesis of $\text{Ms}-(\text{AD-MV}^{2+})_3$.

Preparation of the bromo derivative 2 was discussed in Chapter 3. Compound 2 was converted to 3 by stirring with 4,4'-bipyridine in DMF at 80 °C under argon atmosphere. The acceptor $\text{Ms}-(\text{AD-MV}^{2+})_3$ was obtained by refluxing 3 with commercially available 1,3,5-tris(bromomethyl)benzene in DMF under argon for 3 days. Structure of

Ms-(AD-MV²⁺)₃ was confirmed by spectroscopic techniques (see experimental section).

¹H NMR spectrum of Ms-(AD-MV²⁺)₃ in DMSO is presented in Figure 4.2.

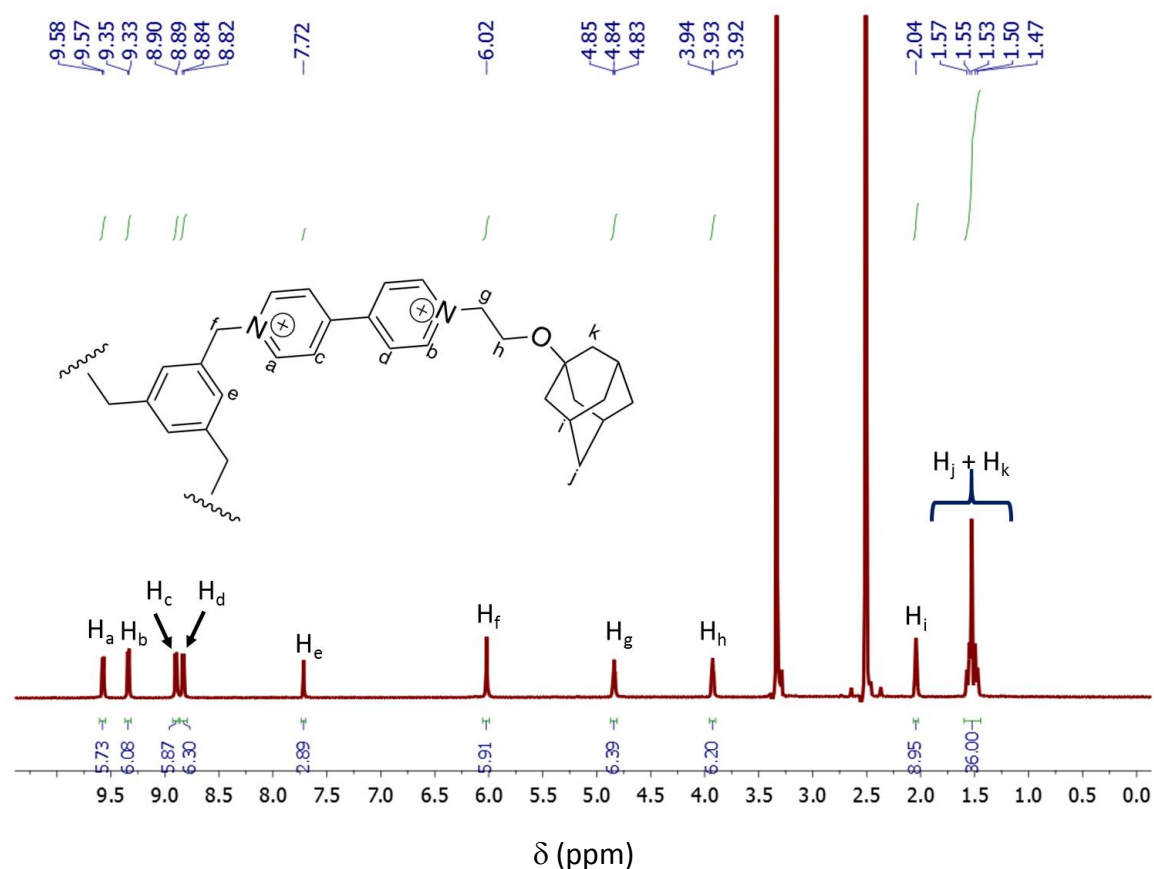


Figure 4.2. ¹H NMR spectrum of Ms-(AD-MV²⁺)₃ in DMSO.

4.3.2. ¹H NMR titration studies

Inclusion complex formation between the acceptor Ms-(AD-MV²⁺)₃ and CD-PY-CD was studied by ¹H NMR titration. The NMR titration experiments were performed in D₂O and the results are presented in Figure 4.3. Panel a shows the ¹H NMR spectrum of CD-PY-CD (5 × 10⁻³ M) and panel e shows that of Ms-(AD-MV²⁺)₃ in D₂O. The ¹H NMR of Ms-(AD-MV²⁺)₃ in D₂O is slightly different from that in DMSO shown in Figure 4.2. The major differences are the coalescence of the two peaks around δ 8.8 ppm into one peak and merger of the peak at δ 3.9 ppm with the HOD peak. Panels b, c and d shows the effect of adding 0.5, 1.0 and 1.5 equiv., respectively, of Ms-(AD-MV²⁺)₃ on the ¹H NMR of CD-

PY-CD. Encapsulation of the AD in β -CD cavity will lead to chemical shift changes and broadening of the AD proton signals.⁴⁻⁷ A comparison of d and e panels shows that the AD protons in the δ 1.36 – 2.0 ppm has undergone signal broadening and change in splitting pattern, which can be taken as the signature for the encapsulation of the AD groups of $\text{Ms}-(\text{AD-MV}^{2+})_3$ in the CD cavities of CD-PY-CD.

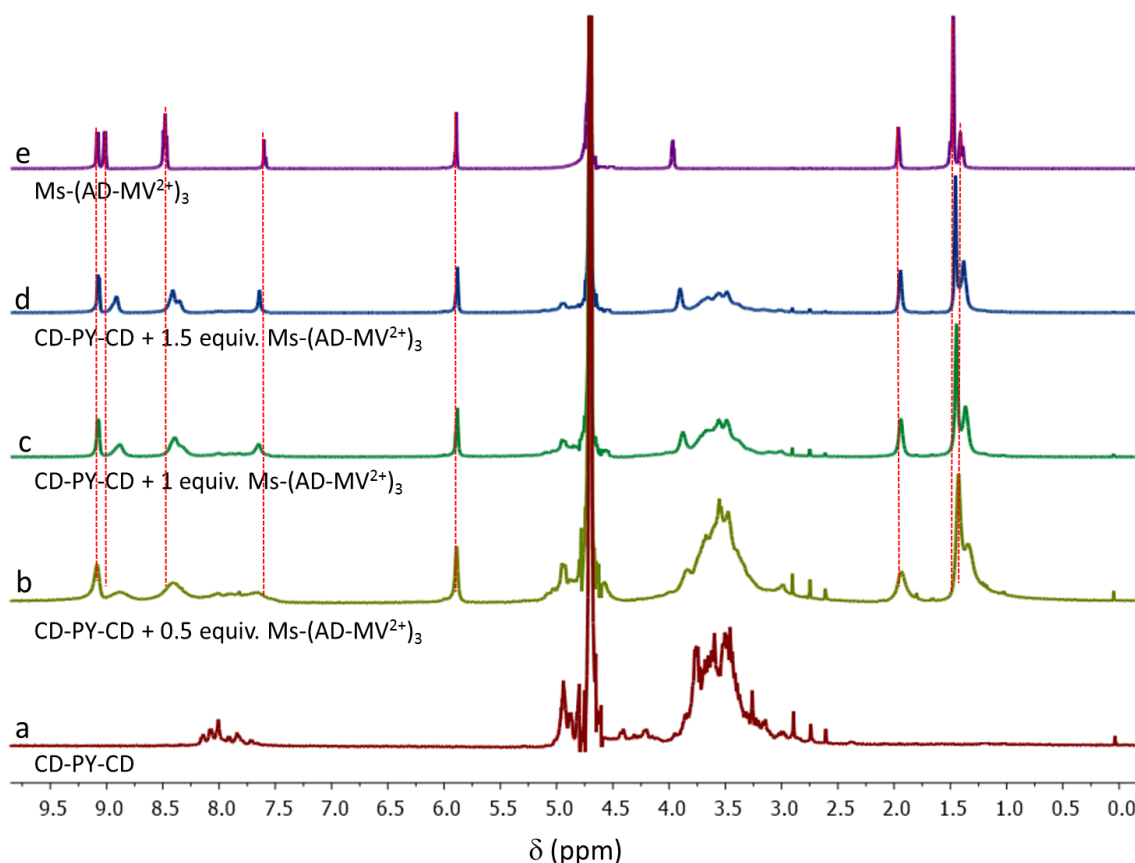


Figure 4.3. Panel a-d) ^1H NMR spectra of CD-PY-CD (5×10^{-3} M) with varying equivalents (0.5 – 1.5 equiv.) of $\text{Ms}-(\text{AD-MV}^{2+})_3$. Panel e) ^1H NMR of pure $\text{Ms}-(\text{AD-MV}^{2+})_3$. Changes in the AD and MV^{2+} proton signals are indicated by red dotted lines.

The encapsulation of AD protons within the β -CD cavity was further confirmed from 2D ROESY NMR experiments. When AD gets encapsulated in the cavity, the AD protons and β -CD interior protons H-3 and H-5 will interact spatially and this will be observed as cross-peaks in the 2D ROESY NMR spectrum. Figure 4.4 shows the 2D ROESY NMR spectrum of CD-PY-CD/ $\text{Ms}-(\text{AD-MV}^{2+})_3$ (1:1.5) system in D_2O . Cross peaks observed

in the δ 1.36 – 2.0 ppm region are shown in the red dotted line box. These cross-peaks, which correspond to through-space interactions between AD protons and H-3 and H-5 protons of β -CD, confirm the encapsulation of AD groups of $\text{Ms}-(\text{AD-MV}^{2+})_3$ within the CD cavities of CD-PY-CD.

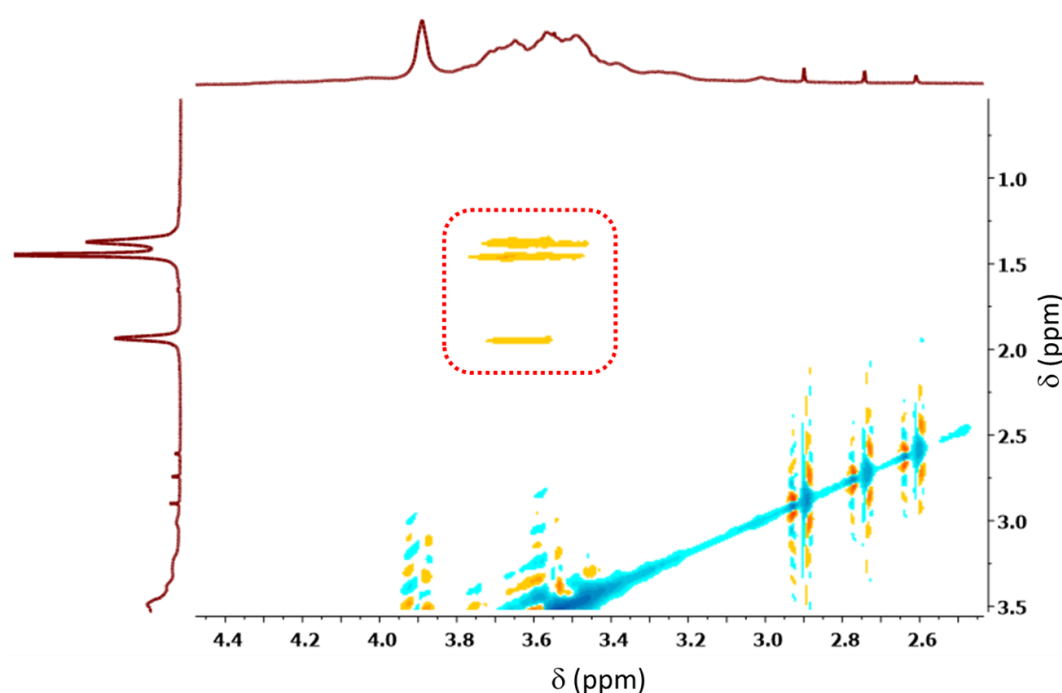


Figure 4.4. 2D ROESY NMR spectrum of CD-PY-CD/ $\text{Ms}-(\text{AD-MV}^{2+})_3$ (1:1.5) in D_2O . The cross peaks referred to through space interactions among the protons are marked with boxes.

^1H NMR titration of CD-PY-CD/ $\text{Ms}-(\text{AD-MV}^{2+})_3$ shown in Figure 4.3 is similar to the ^1H NMR titration of CD-PY-CD/ AD-MV^{2+} -AD system reported in chapter 3. Signals due to the viologen protons which are away from the site of inclusion also undergo changes. For example, the doublets at δ 9 ppm and multiplet at δ 8.5 ppm became broad singlets and shifted upfield in the presence of CD-PY-CD. We attribute these to secondary interactions and/or hierarchical assembly of the inclusion complex into complex structures based on previous observations⁴ and results of chapter 3.

The ^1H NMR titration in Figure 4.3 also shows that the signals due to PY and β -CD are highly dampened and this is clearly seen in the expanded spectra in Figure 4.5.

We observed a similar phenomenon for the CD-PY-CD/AD-MV²⁺-AD system described in Chapter 3, where we have attributed the signal dampening to the stacking of PY over PY and β -CD over β -CD, leading to formation of toroidal nanostructures. For the present system also, we attribute the signal dampening to formation of nanostructures which may involve stacking of PY over PY and β -CD over β -CD.

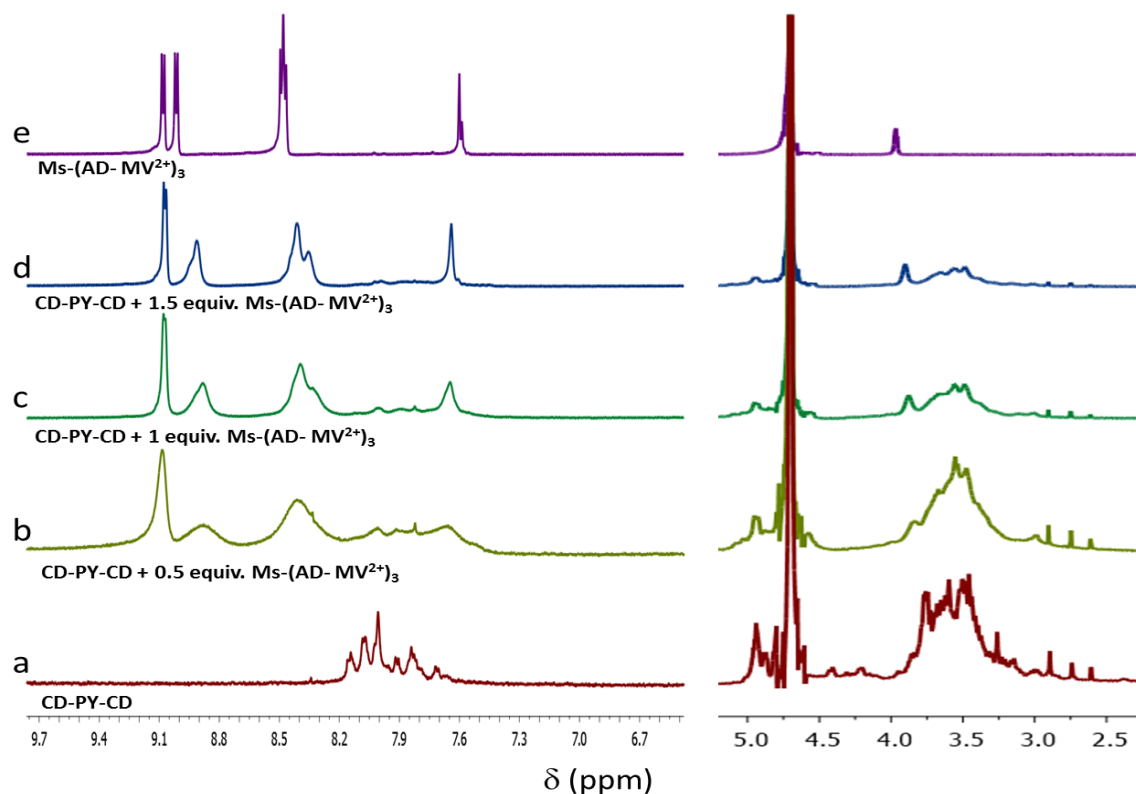


Figure 4.5. Expanded version of NMR titration, showing clearly the damping of signals due to PY and β -CD.

4.3.3. Photophysical properties of CD-PY-CD/Ms-(AD-MV²⁺)₃

In the presence of Ms-(AD-MV²⁺)₃, the absorption spectrum of CD-PY-CD exhibited dampening of signal intensity and shift of the absorption onset to longer wavelengths as shown in Figure 4.6 a, b. The changes observed are significant during addition of 0.25 – 0.5 equiv. of Ms-(AD-MV²⁺)₃ and thereafter only negligible changes were noted. Upon addition of 0.25 equiv. of Ms-(AD-MV²⁺)₃, the absorbance of CD-PY-CD at 350 nm got reduced by 25%. No bands assignable to CT formation could be seen in

the long wavelength region, suggesting that face to face stacking of PY and MV^{2+} did not occur in the self-assembled system.

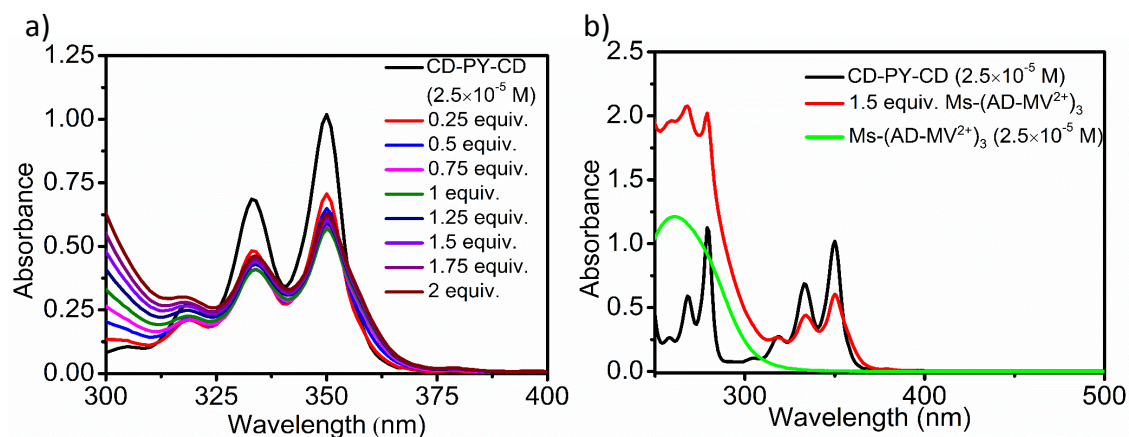


Figure 4.6. a) Absorption spectra of CD-PY-CD in the absence and presence (0.25-2.0 equiv.) of $Ms-(AD-MV^{2+})_3$ and b) Absorption spectra of CD-PY-CD with 1.5 equiv. $Ms-(AD-MV^{2+})_3$, CD-PY-CD and $Ms-(AD-MV^{2+})_3$

The emission spectrum of CD-PY-CD exhibited significant quenching in the presence of micromolar amounts of $Ms-(AD-MV^{2+})_3$ (Figure 4.7a). The fluorescence is almost completely quenched in the presence of one equiv. of $Ms-(AD-MV^{2+})_3$. Figure 4.7b shows fluorescence spectrum of CD-PY-CD in the presence of one equiv. $Ms-(AD-MV^{2+})_3$ normalized with that of CD-PY-CD. The two spectra overlap completely, suggesting that emission from CT state is not observed in this case.

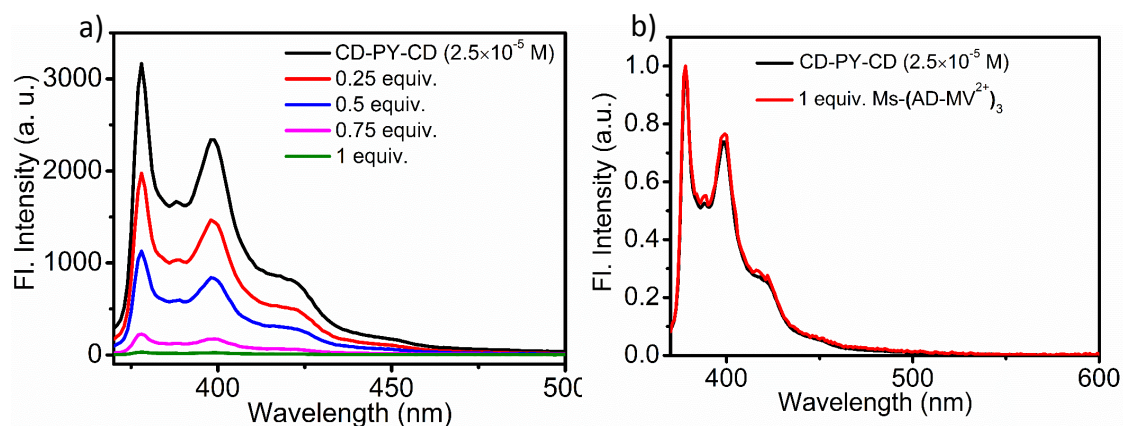


Figure 4.7. a) Emission spectra of CD-PY-CD in the presence of $Ms-(AD-MV^{2+})_3$ (0 – 1.0 equiv.) and b) Normalized fluorescence spectra of CD-PY-CD and CD-PY-CD/ $Ms-(AD-MV^{2+})_3$ (1:1) aqueous solutions.

As described in detail in chapter 3, the intensity and sign of ICD signals can be used to predict the orientation of achiral molecules associated with β -CD. Figure 4.8 shows the ICD spectra of CD-PY-CD in the presence and absence of $\text{Ms}-(\text{AD-MV}^{2+})_3$. The ICD signal due to PY in CD-PY-CD is described in Chapter 3. When $\text{Ms}-(\text{AD-MV}^{2+})_3$ is added, intensities of signals in the 300-370 nm and 250-300 nm regions increase suggesting that the orientation of PY became more parallel to the CD axis. In the case of the CD-PY-CD/AD-MV²⁺-AD system studied in Chapter 3, a negative signal due to MV²⁺ was observed at higher concentrations of AD-MV²⁺-AD (Figure 3.12a), suggesting that MV²⁺ is also placed outside the CD cavity and aligned parallel to the CD axis. In the case of CD-PY-CD/ $\text{Ms}-(\text{AD-MV}^{2+})_3$ system studied here, the negative peak due to MV²⁺ is absent. In this case also, MV²⁺ most probably is aligned parallel to the β -CD axis outside the wider rim of the CD, but since the MV²⁺ residues are part of a branched system, tight packing of the D-A system may not be possible which explains absence of the negative signal due to MV²⁺.

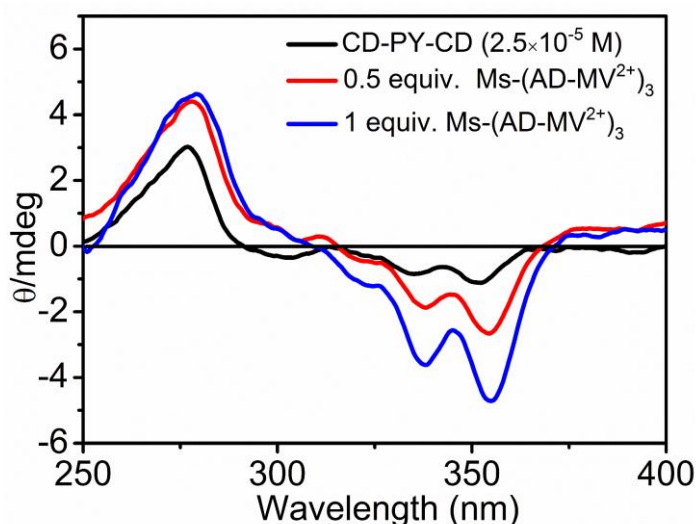


Figure 4.8. ICD spectra of CD-PY-CD in the absence and presence of (0.5 and 1.0 equiv.) $\text{Ms}-(\text{AD-MV}^{2+})_3$.

4.3.4. DLS and Tyndall effect studies

In the case of CD-PY-CD/Ms-(AD-MV²⁺)₃ system also we observed formation of nanostructures through Tyndall effect and DLS studies (Figure 4.9). The laser path inside the solution become clearly visible due to light scattering by the nanoscopic particles in the solution (Figure 4.9a). The DLS result is shown in Figure 4.9 b, which confirmed the presence of particles in solution with average hydrodynamic radius of 400 nm and particle size distribution in the 150-800 nm range.

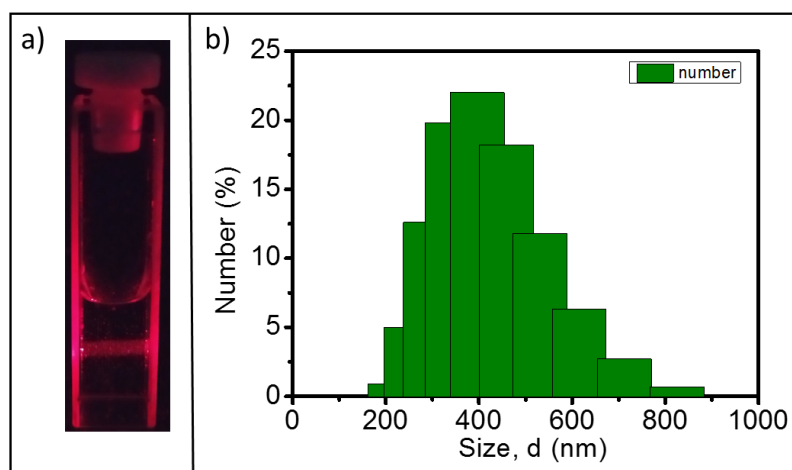


Figure 4.9. a) Tyndall effect showing the path of light through CD-PY-CD/Ms-(AD-MV²⁺)₃ (1:1.5) in water and b) DLS spectrum of the same solution.

4.3.5. Morphological analysis

We confirmed the presence of nanostructures in aqueous CD-PY-CD/Ms-(AD-MV²⁺)₃ solution by dynamic light scattering (DLS) and Tyndall effect studies. In order to understand the morphological aspects of these nanomaterials, we employed TEM, SEM and AFM imaging. Samples for AFM and SEM were prepared by drop-casting aqueous solutions of CD-PY-CD/Ms-(AD-MV²⁺)₃ (1:1.5) on silicon wafer. For TEM analysis a solution was drop-casted on copper coated carbon grids and air dried.

Figure 4.10 shows TEM and SEM images of CD-PY-CD/Ms-(AD-MV²⁺)₃ (1:1.5) self-assembled system. The TEM images show ultra-long fibers formed from self-assembly of the inclusion complex. The SEM images also shows clusters of fibrous structures. These images, however, do not give any insight as to how these structures are formed.

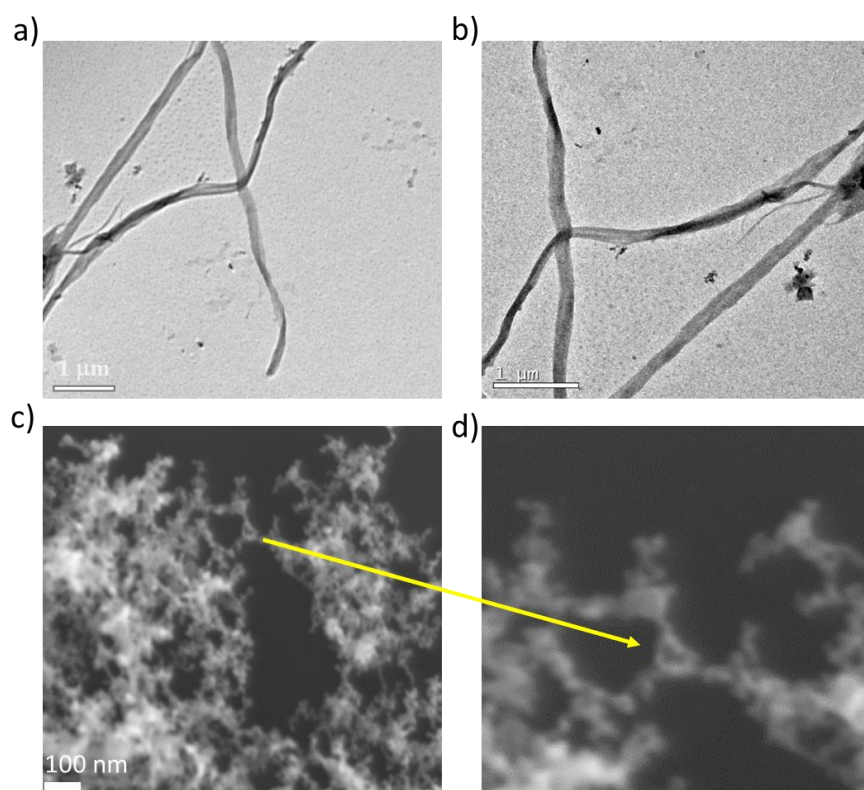


Figure 4.10. a, b) TEM and c, d) SEM images of CD-PY-CD/Ms-(AD-MV²⁺)₃ (1:1.5) self-assembled nanostructures.

Figure 4.11a-e show the AFM images of the CD-PY-CD/Ms-(AD-MV²⁺)₃ (1:1.5) self-assembled nanostructures. Figure 4.11 clearly shows the various stages involved in the self-assembly of CD-PY-CD/Ms-(AD-MV²⁺)₃ into fibrous structures. Self-assembly occurs initially to form vesicle-type structures (Figure 4.11a). The hole at the center of the spherical objects suggests that these are actually vesicles. Figures 4.11b, c shows joining together of vesicles to give larger nanostructures. Joining of vesicles is a function of concentration of components and time. Figure 4.11d,e shows fusion of the nanostructures to give long fibers. Figure 4.11f shows the height profile of the nano

structures. The nanostructures and fibers have a height of ~ 10 nm and width of ~ 200 nm. The width of the fiber is nearly the same in the TEM images.

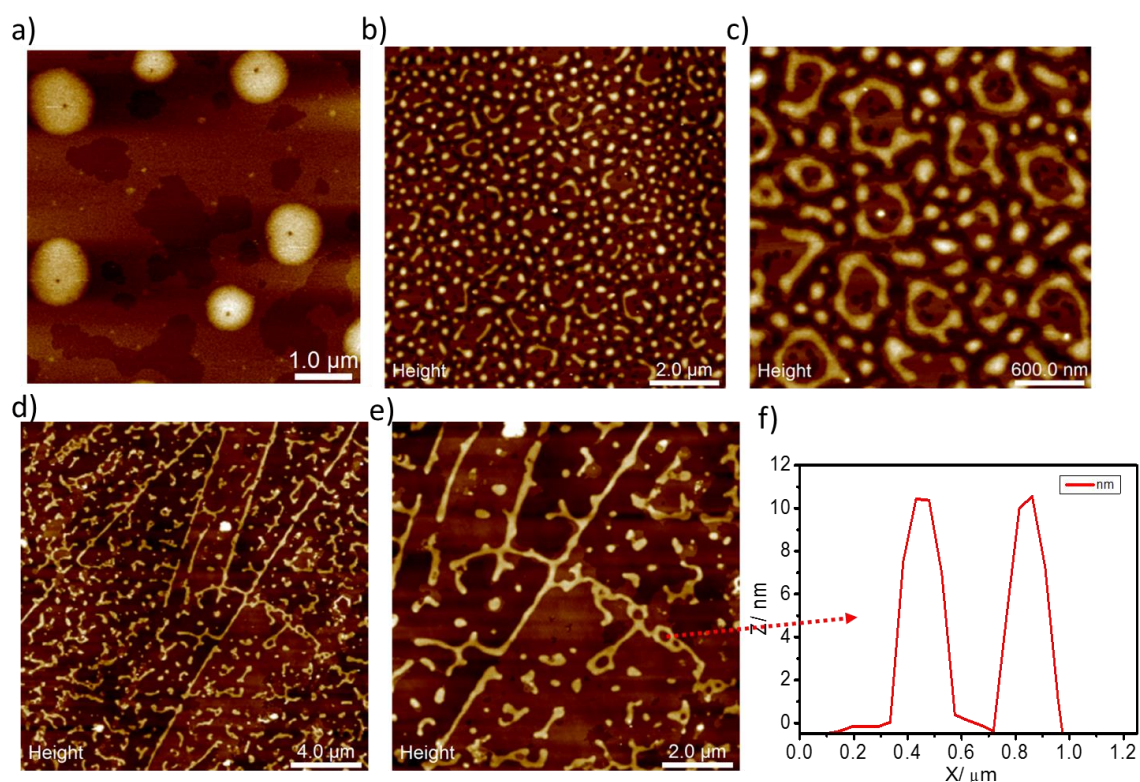


Figure 4.11. a-e) AFM images showing the various stages in the self-assembly of CD-PY-CD/Ms-(AD-MV²⁺)₃ (1:1.5) into fibers in aqueous solution. f) The height profile of nanostructure indicated by the arrow.

4.3.6. Mechanism of self-assembly in CD-PY-CD/Ms-(AD-MV²⁺)₃

CD-PY-CD has two β -CD groups and hence has two binding sites for AD. The acceptor Ms-(AD-MV²⁺)₃, on the other hand, has three binding sites for β -CD. Inclusion of the three AD units in β -CD cavities of CD-PY-CD will result in a branched system which cannot self-assemble into ring-like loops as observed in the case of CD-PY-CD/AD-MV²⁺-AD (Figure 3.16) studied in Chapter 3. Figure 4.12 shows the formation of inclusion complex from CD-PY-CD and Ms-(AD-MV²⁺)₃. Further inclusion binding can occur at all the three termini of the complex. A branched system, resembling a supramolecular

dendrimer, can form by repeated inclusion binding. Ultimately the dendritic system can self-assemble into a vesicle, which grows into fibers through vesicle fusion and growth.

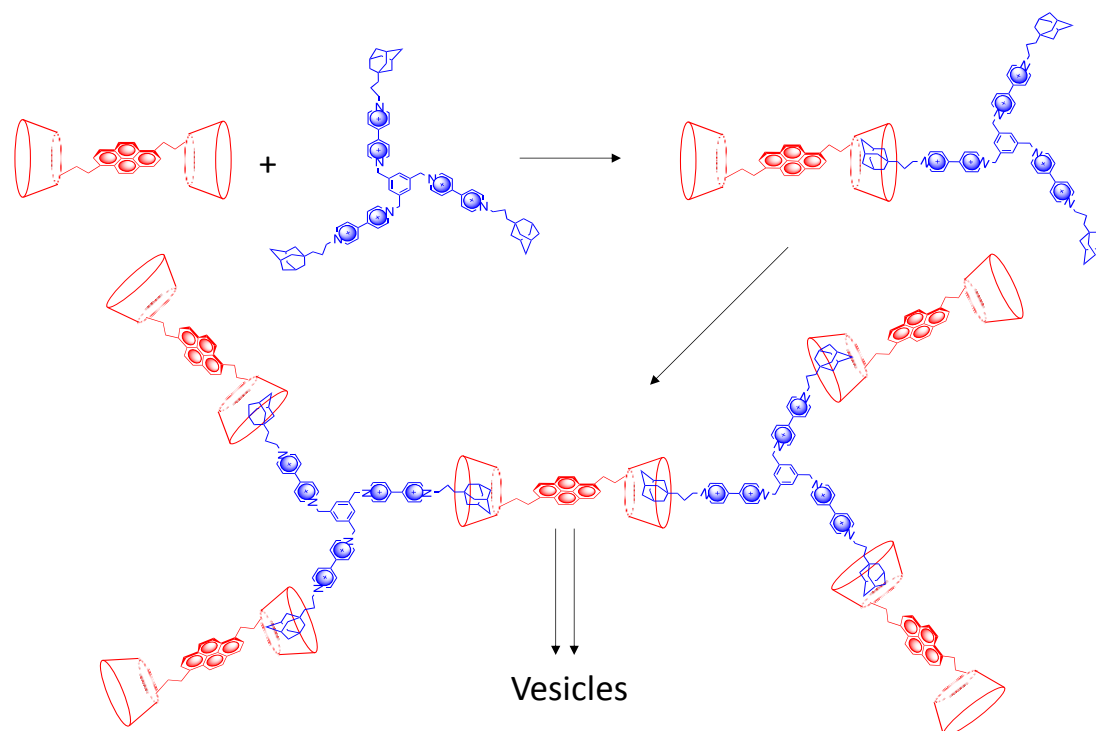


Figure 4.12. Schematic of the formation of inclusion complex in the CD-PY-CD/Ms-(AD-MV²⁺)₃ system and its self-assembly into vesicles.

Self-assembly of branched and dendritic systems into vesicles is reported in several studies.⁸⁻¹⁵ For example, Tao *et al.* reported formation of a linear-hyperbranched supramolecular amphiphile by the noncovalent coupling of adamantane-functionalized long alkyl chain compounds and hyperbranched polyglycerol grafted from β -cyclodextrin by the specific AD/CD host-guest interactions. The obtained supramolecular inclusion system self-assembled into unilamellar vesicles.¹⁰ Mao *et al.* reported self-assembly of doxorubicin prodrug-cucurbit[n]uril host-guest complex into vesicles.¹¹ Joining together of vesicles to give fibers are reported by others and by us also.^{8,15,16} Formation of vesicles and fibers from the dendritic inclusion complex can be thus be explained. However, close packing of PY over PY and β -CD over β -CD may not occur in such a vesicle

formation and the severe dampening observed for the ^1H NMR cannot be explained this way. Most probably there may be regions of PY stacked over PY and $\beta\text{-CD}$ stacked over $\beta\text{-CD}$ as shown in Figure 4.13 within the vesicle and fibers formed by fusion of the vesicles. The hydrophobicity and π -stacking ability may bring the PY moieties very close as observed in the case of CD-PY-CD/AD-MV $^{2+}$ -AD system reported in Chapter 3 and this will result in the dampening of NMR signals observed in this case also. It may be noted that stacking of PY over MV $^{2+}$ is not occurring during vesicle formation as is evident from the absence of CT bands in the absorption spectrum of CD-PY-CD/Ms-(AD-MV $^{2+}$) $_3$ shown in Figure 4.6.

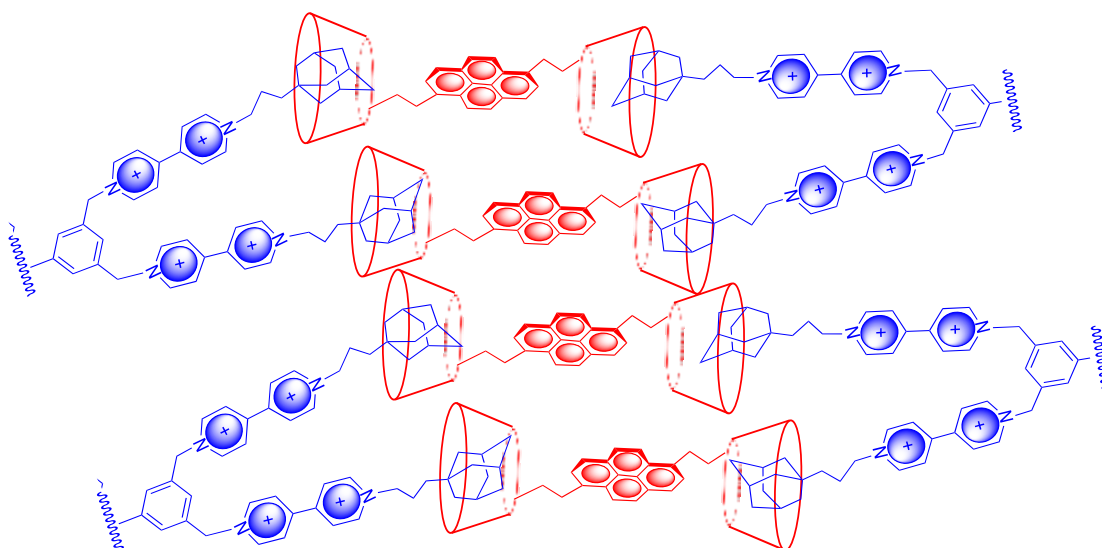


Figure 4.13. Probable arrangement of PY over PY and $\beta\text{-CD}$ over $\beta\text{-CD}$ within the vesicle.

4.3.7. Photoinduced electron transfer in CD-PY-CD/Ms-(AD-MV $^{2+}$) $_3$

4.3.7.1. Steady-state fluorescence quenching

We observed that the fluorescence of CD-PY-CD was quenched by sub-millimolar amounts of Ms-(AD-MV $^{2+}$) $_3$ (Figure 4.7). The Stern-Völmer plot for the quenching is given in Figure 4.14, where Q refer to the quencher Ms-(AD-MV $^{2+}$) $_3$, I_0 refer to the

fluorescence intensity in the absence of quencher and I refer to the intensity in the presence of different quencher concentrations. The I_0/I curve is very similar to that observed for the CD-PY-CD/AD-MV²⁺-AD system shown in Figure 3.18 in Chapter 3. Three regions, as indicated by the lines in Figure 4.14, can be identified for the quenching. The line with the highest slope represents formation of the vesicles and quenching within it. The regions of lower slope most probably will correspond to diffusion mediated quenching.

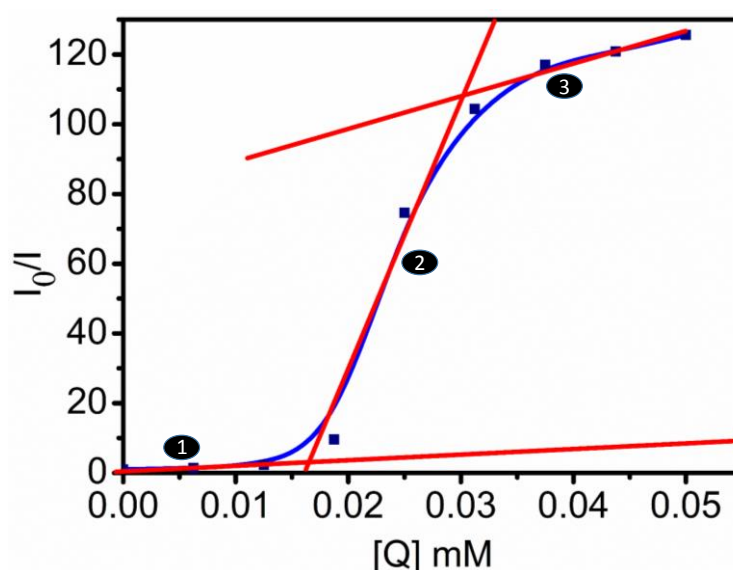


Figure 4.14. Stern-Völmer plot for the quenching of CD-PY-CD fluorescence by Ms-(AD-MV²⁺)₃.

4.3.7.2 Time resolved fluorescence quenching studies

Fluorescence quenching in the CD-PY-CD/Ms-(AD-MV²⁺)₃ system was also studied using fluorescence lifetime quenching method and the lifetime profiles in the absence and presence of different concentrations of Ms-(AD-MV²⁺)₃ are shown in Figure 4.15. As mentioned in Chapter 3, fluorescence decay of CD-PY-CD was mono-exponential with lifetime $\tau_0 = 136$ ns (curve 'a' in Figure 4.15). In the presence of Ms-(AD-MV²⁺)₃, fluorescence profiles became bi-exponential as shown in Figure 4.15b-j. The bi-exponential fluorescence decay was attributed to diffusion mediated and unimolecular

quenching processes as explained in Chapter 3, Scheme 3.5.^{17,18} The decay profiles were fitted using equation 3.2 (Chapter 3) and the values of the fit parameters τ_1 , τ_2 , $\chi_{(\text{complex})}$, $\chi_{(\text{free})}$ and χ^2 values are presented in Table 4.1. It may be noted from Table 4.1 that the τ_1 values obtained at different concentrations of $\text{Ms}-(\text{AD-MV}^{2+})_3$ are nearly the same and satisfy the requirements of Scheme 3.5. Substituting the average value of τ_1 in equation 3.4 gave the rate constant for quenching within the complex, $k_{\text{et}} = 7.85 \times 10^7 \text{ s}^{-1}$.

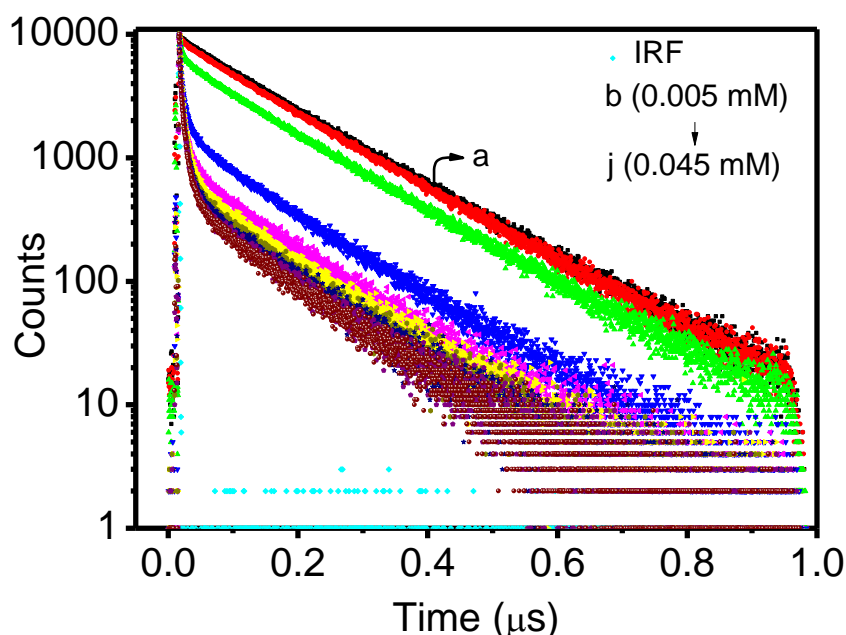


Figure 4.15. Fluorescence decay profiles of CD-PY-CD ($2.5 \times 10^{-5} \text{ M}$) a) in the absence and b-j) presence of various concentrations of $\text{Ms}-(\text{AD-MV}^{2+})_3$ (0 – 1.8 equiv.).

An inspection of Table 4.1 shows that the contribution due to intra-ensemble quenching (χ_{complex}) exhibits a sudden increase when the concentration of $\text{Ms}-(\text{AD-MV}^{2+})_3$ increases from 0.010 to 0.025 mM. This corresponds to the rising part of the rapid quenching region in the Stern-Völmer plot (Figure 4.14). However, the upper part of the Stern-Völmer curve, where the rate slows down, is not obvious in Table 4.1.

Table 4.1. Table showing the fluorescence lifetime values (τ_1 and τ_2), fractional contributions ($\chi_{(\text{complex})}$ and $\chi_{(\text{free})}$) and χ^2 values obtained for fluorescence lifetime quenching of CD-PY-CD with Ms-(AD-MV²⁺)₃.

Conc. of Ms-(AD-MV ²⁺) ₃ mM	τ_1 , ns	$\chi_{(\text{complex})}$	τ_2 , ns	$\chi_{(\text{free})}$	χ^2
0			136.74	100.00	1.17
0.005 mM	11.85	0.78	135.18	99.22	1.13
0.010 mM	11.37	2.74	132.55	97.26	1.08
0.015 mM	11.86	12.47	117.77	87.53	1.05
0.020 mM	11.74	18.88	117.56	81.12	1.09
0.025 mM	11.24	23.52	116.71	76.48	1.12
0.030 mM	11.87	24.69	116.26	75.31	1.18
0.035 mM	11.81	27.81	116.80	72.19	1.18
0.040 mM	11.49	28.45	115.57	71.55	1.14
0.045 mM	11.62	31.21	114.93	68.79	1.11

A comparison of Tables 3.1 and 4.1 reveals several differences between the PET processes within the nanostructures formed in the CD-PY-CD/AD-MV²⁺-AD and CD-PY-CD/Ms-(AD-MV²⁺)₃ systems. In the case of the CD-PY-CD/AD-MV²⁺-AD system studied in Chapter 3, the fraction of associated CD-PY-CD molecules at the highest quencher concentration is 73.46%, whereas the corresponding value in the case of CD-PY-CD/Ms-(AD-MV²⁺)₃ is only 31.21%. The k_{et} value obtained for the CD-PY-CD/Ms-(AD-MV²⁺)₃ system is $7.85 \times 10^7 \text{ s}^{-1}$, which is much less compared to $k_{\text{et}} = 1.39 \times 10^8 \text{ s}^{-1}$ obtained for the CD-PY-CD/AD-MV²⁺-AD system. Since the fluorophore is PY and quencher is MV²⁺ in both cases, the low PET rate in the case of CD-PY-CD/Ms-(AD-MV²⁺)₃ most probably will be due to higher average distance between PY and MV²⁺ in vesicular and/or fibrous

assemblies. The mechanisms for vesicle formation shown in Figures 4.12 and 4.13 may not allow tight binding of AD moieties within the CD cavities and this may result in higher average distance between the PY and MV²⁺ residues within the assembly.

4.3.7.3. Nanosecond laser flash photolysis studies

Aqueous CD-PY-CD/Ms-(AD-MV²⁺)₃ (1:1.5, 5.0 × 10⁻⁵ M) solution was subjected to nanosecond laser flash photolysis using the third harmonic of a Nd-YAG laser. The transient absorption spectra obtained at different times following the laser flash are shown in Figure 4.16a.

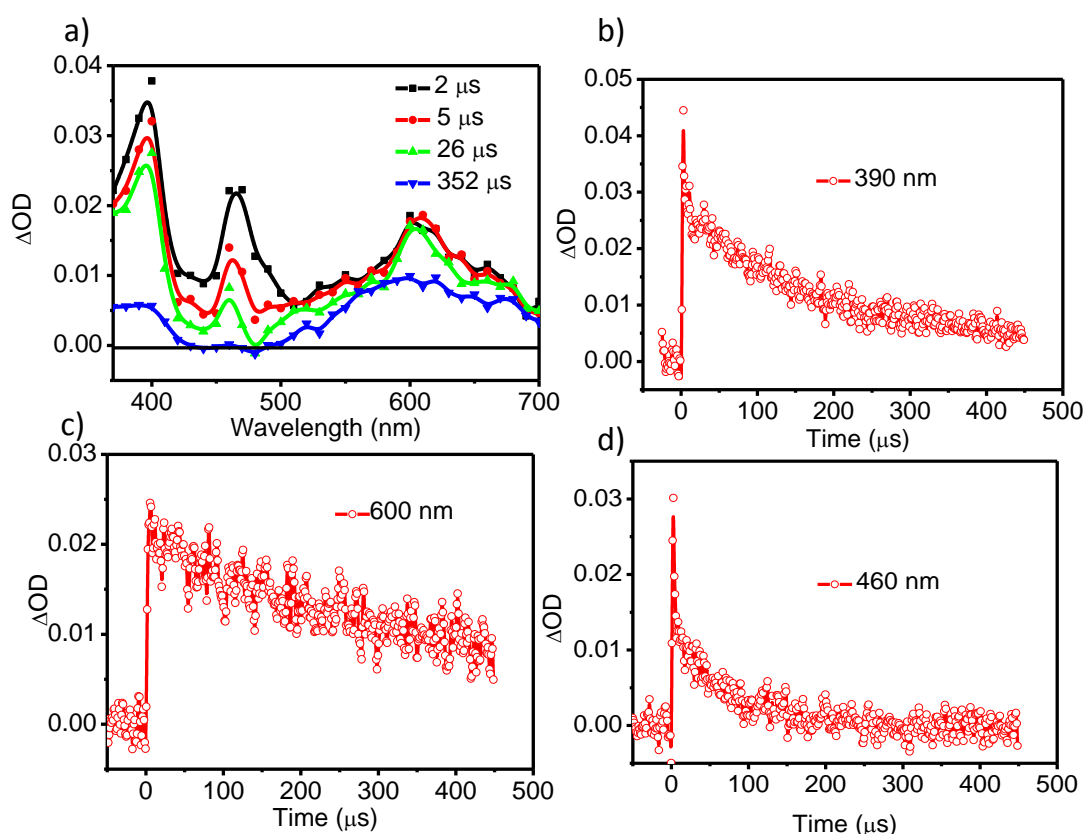


Figure 4.16. a) The transient absorption spectra obtained at 2, 5, 26 and 352 μs in the flash photolysis of CD-PY-CD/Ms-(AD-MV²⁺)₃ (5 × 10⁻⁵ M). b-d) Kinetic traces at the various peak maxima.

The transient absorption spectra obtained at short times exhibited sharp peaks at 390 and 460 nm and a broad peak around 600 nm. Based on literature,^{19,20} the 390

and 600 nm absorptions can be assigned to $MV^{•+}$ and the 460 nm peak can be assigned to $PY^{•+}$, both formed following PET from PY to MV^{2+} . The decay profiles of the various absorptions given in Figures 4.16b-d are very different and hence cannot be attributed to one single process.

The 460 nm peak assigned to $PY^{•+}$ exhibited initial fast decay (nearly 50%), followed by a slow decay (Figure 4.16d). The fast decay most probably is due to reaction of $PY^{•+}$ with PY to give $(PY^{•+}-PY)$, as described in Chapter 3.²¹⁻²³ The data suggests that nearly 40% of $PY^{•+}$ decays at a much slower rate. Most probably this decay corresponds to $PY^{•+}$ having no PY neighbors and this fraction must decay through the BET channel. A fit of the slow decay gave lifetime of 50 μ s ($k_{BET} = 2.0 \times 10^4 \text{ s}^{-1}$). As mentioned earlier, the average distance between the PET partners are large in this system and hence BET is expected to be slow.

The decay of $MV^{•+}$ at 390 nm (Figure 4.16b) shows an initial fast decay ($\sim 20\%$), which can be attributed to the dimerization of $MV^{•+}$. As mentioned earlier, this requires absorption of two photons. The second part of the decay is similar to the decay of $PY^{•+}$ at longer times and this may be attributed to BET process. The spectrum obtained at very long-time scales (352 μ s, Figure 4.16a) can be assigned to the dimer as the 390 nm peak is absent and the 600 nm absorption has become very broad. The last part of the decay can be assigned to the formation of $MV^{•+}$ from the dimer followed by BET with $(PY^{•+}-PY)$ to regenerate the starting donor-acceptor system.

Decay of the 600 nm absorption is complex and it involves dimerization of $MV^{•+}$, direct BET with $PY^{•+}$, decay of the dimer to $MV^{•+}$ and BET with $(PY^{•+}-PY)$. It may be noted

that nearly 40% of the absorption still persists even at 500 μs after the laser flash. Since the absorption due to $\text{MV}^{\bullet+}$ and its dimer are similar in the 550-700 nm region, the absorbing species may be $\text{MV}^{\bullet+}$ or its dimer.

During the laser flash photolysis experiments we observed that the solution acquires slight blue color after a few laser shots. Within a few hours the color faded and absorption spectrum taken afterwards suggested that no change has occurred during irradiation. We also observed that upon irradiation using an Oriel lamp (150 W, 20 min., no filter) the colorless CD-PY-CD/MS-(AD- MV^{2+})₃ (1:1.5, 2.5×10^{-4} M) aqueous solution turns blue and retained the color for few hours. The absorption spectrum of the blue solution taken immediately and 4 h after irradiation are shown in Figure 4.17a. The spectrum taken immediately after irradiation shows the absorption spectrum of $\text{MV}^{\bullet+}$ superimposed with absorption due to PY. The 400 and 600 nm absorptions are identical with the absorption spectrum of $\text{MV}^{\bullet+}$ reported previously. The fine structure in the 400 nm band suggest that the $\text{MV}^{\bullet+}$ dimer is not formed in the irradiation. Presence of absorption bands due to PY in the irradiated solution suggested that not all the PY present are utilized in the PET reaction that led to formation of long-lived MV^{2+} . The time dependence of the 400 nm absorption of the irradiated solution is shown in Figure 4.17b. The absorption decays completely in ~ 200 min. The spectrum taken after 4 h (Figure 4.17a) shows that $\text{MV}^{\bullet+}$ has decayed completely and the donor-acceptor system is regenerated fully.

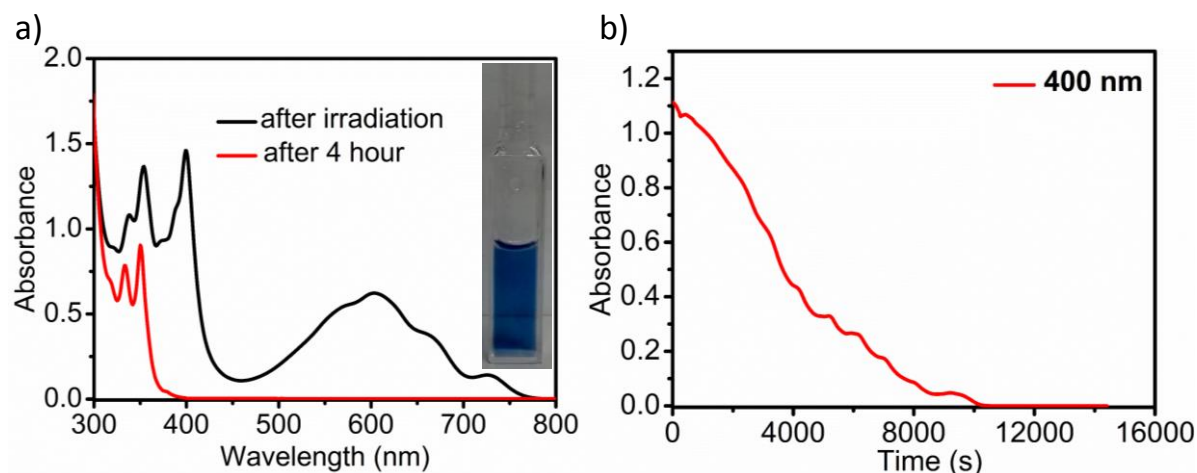


Figure 4.17. a) Absorption spectrum of CD-PY-CD/Ms-(AD-MV²⁺)₃ (1:1.5, 2.5 × 10⁻⁴ M) immediately and 4 h after irradiation with oriel lamp. Inset shows the blue color of the solution. b) The time dependence of the absorption at 400 nm.

The reported value of the extinction coefficient for MV^{•+} at 605 nm is 13,700 M⁻¹ cm⁻¹.²⁰ Using this value we calculated the concentration of MV^{•+} formed in the irradiation = 4.6 × 10⁻⁵ M, which is 18% of the donor concentration employed. Thus, the quantum yield for formation of long-lived MV^{•+} is 0.18. Since no sacrificial donor or acceptor was employed, the quantum yield of 0.18 obtained is very good.

We have obtained the ¹H NMR spectra of CD-PY-CD/Ms-(AD-MV²⁺)₃ solution in D₂O (1:1.5, 2.5 × 10⁻⁴ M) before irradiation, immediately after irradiation and one day after the irradiation (when the blue colour was completely discharged). The spectra are shown in Figure 4.18. It can be seen that in the spectrum of the irradiated solution, signals due to PY and MV²⁺ moieties are highly broadened or absent. This suggest that both PY and MV²⁺ are present as radical species in solution. Radical species are paramagnetic in nature and these act as local magnets which spoil the magnetic homogeneity throughout the sample. As a result, lines get broadened and nuclei near the paramagnetic electron are generally not observed. The spectrum obtained after complete discharge of the colour is identical with that of unirradiated solution,

suggesting that no permanent changes have occurred in the irradiation and the starting D-A system is completely regenerated. Since both PY and MV²⁺ moieties are present as radical species in the irradiated solution, it can be considered as a long-lived CS state.

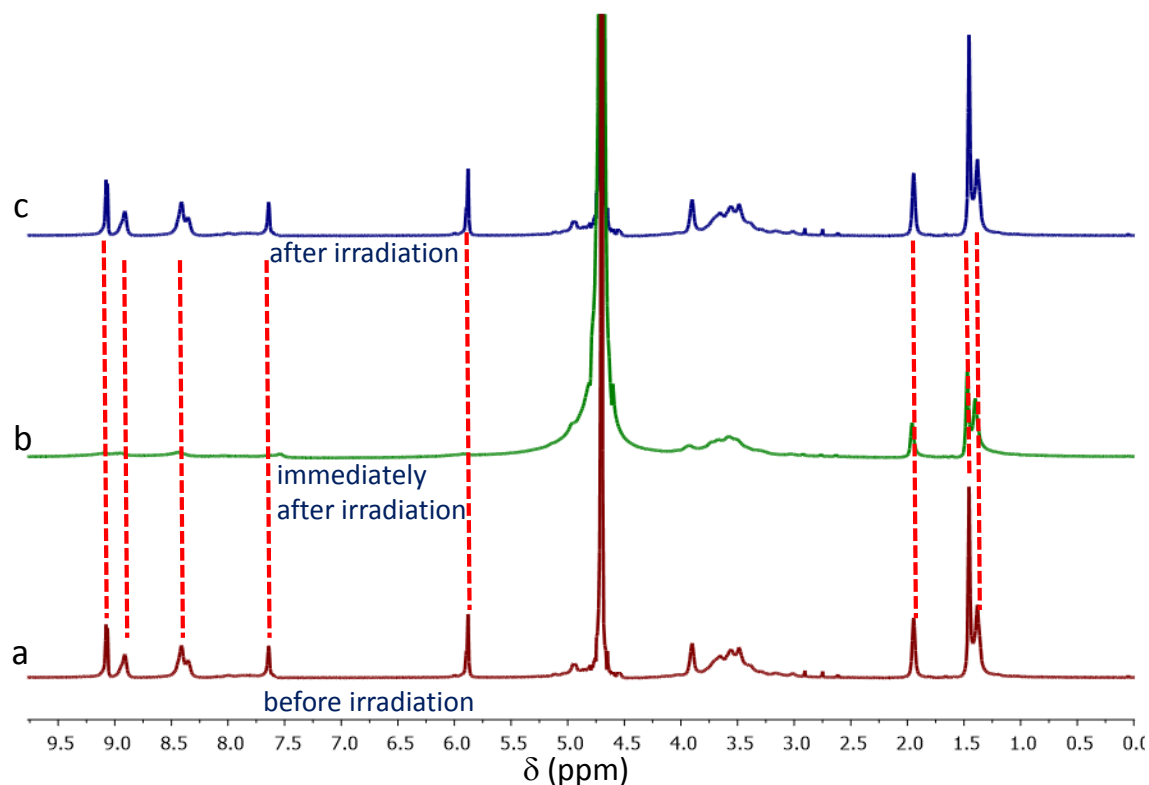


Figure 4.18. ¹H NMR spectra of CD-PY-CD/Ms-(AD-MV²⁺)₃ (1:1.5) solution in D₂O (2.5 × 10⁻⁴ M) a) before irradiation, b) immediately after irradiation and c) one day after irradiation.

4.4. Conclusions

In this chapter we report assembly of a supramolecular donor-acceptor system using the inclusion binding of adamantane residues in β -CD. The donor CD-PY-CD has two binding sites for the donor and acceptor Ms-(AD-MV²⁺)₃ has three binding sites. Self-assembly resulted in the formation of branched entities which further assembled into vesicles and long fibers. Fluorescence of the PY moiety within the assembly was highly quenched due to PET. Rate constant for the PET process within the assembly was obtained using fluorescence lifetime studies. Using laser flash photolysis, we confirmed

formation of the radical ion pairs $\text{PY}^{\bullet+}$ and $\text{MV}^{\bullet+}$ in the PET reaction. A fraction of $\text{PY}^{\bullet+}$ undergo a fast reaction with adjacent PY moieties in the assembly and the remaining fraction underwent slow BET. A small fraction of $\text{MV}^{\bullet+}$ undergo reversible dimerization and the remaining fraction undergo BET with $\text{PY}^{\bullet+}$ and/or $(\text{PY}^{\bullet+}\text{-PY})$. Nearly 40% of the $\text{MV}^{\bullet+}$ formed did not decay even at 500 μs after the laser flash. Steady-state irradiation of the donor-acceptor system led to formation of $\text{MV}^{\bullet+}$, which was stable for a few hours. This study, thus confirmed earlier reports from our laboratory that self-assembly of donor-acceptor system into hierarchical assemblies can lead to long-lived photoinduced charge separation.

4.5. Experimental Sections

4.5.1. Instrumentation and methods

All solvents and reagents were commercially available and used without further purification, unless otherwise specified. All experiments were performed in deionized water at 25 °C. Electronic absorption spectra were recorded on a Shimadzu UV-2600 UV-Vis spectrophotometer and the emission spectra were recorded on a SPEX Fluorolog 3 Spectrofluorimeter. Circular dichroism experiments were performed on JASCO 810 spectrometer using quartz cuvettes of 1 cm path length, equipped with peltier thermostatic cell holders for variable temperature studies. All NMR spectra were recorded in D_2O and DMSO-d_6 purchased from Aldrich, using a 500 MHz Bruker Avance DPX spectrometer. ESI-HRMS mass spectra were recorded using orbitrap mass spectrometer (Thermo Exactive). TEM analyses were performed using a FEI-TECNAI T30 G2S-TWIN, 300 kV HRTEM microscope with an accelerating voltage of 100 kV and the samples were prepared by drop-casting the aqueous solution on a formvar coated

copper grid (400 mesh) and evaporating excess water. Atomic Force Microscopy (AFM) images were recorded on Multimode SPM (Bruker Nanoscope V) operating with a tapping mode regime. Antimony doped silicon cantilever with a resonant frequency of 300 kHz and spring constant of 40 Nm^{-1} were used. The SEM images were recorded by using JEOL JSM-5600 LV scanning electron microscope. The operating range was between 5-30 kV at 50-60 Hz single phase. The sample solution in water was drop-casted directly on the top of the silicon wafer and water was allowed to evaporate at ambient conditions and analysed for SEM and AFM. Nanosecond laser flash photolysis experiments were performed by using an Applied Photophysics Model LKS-20 laser kinetic spectrometer by using the third harmonic (355 nm) from a GCR-12 series Quanta Ray Nd:YAG laser. The analysing and laser beams were fixed at right angles to each other. Solutions for laser flash photolysis studies were de-aerated by purging with argon for 20 min before experiments.

4.5.2. Materials

β -Cyclodextrin, pyrene, 4,4'-bipyridine, 1-bromoadamantane and 1,3,5-tris(bromomethyl)benzene were purchased from Sigma Aldrich and used as received. All solvents and reagents were commercially available and used without further purification, unless otherwise specified. The synthesis of CD-PY-CD was described in Chapter 3 and the procedure for the synthesis of $\text{Ms}-(\text{AD}-\text{MV}^{2+})_3$ is described below.

A) Synthesis of 3:

Compound 1 (9.0 g, 57.85 mmol) and 2 (3.0 g, 11.57 mmol) were dissolved in DMF (80 mL) and stirred at 80°C under argon for 12 h and cooled to room temperature. The solution was then poured into ethyl acetate (200 mL). The precipitate formed was

collected by filtration and washed with ethyl acetate and dried to provide compound 3. Yield: 90%; ^1H NMR (500 MHz, DMSO d_6) δ ppm: 9.08 (d, 2H), 8.81 (d, 2H), 8.58 (d, 2H), 7.99 (d, 2H), 4.69 (t, 2H), 3.82 (t, 2H), 1.96 (s, 3H), 1.45 (m, 12H); ^{13}C NMR (125 MHz, CDCl_3) δ ppm: 152.52, 151.11, 150.88, 145.77, 140.71, 124.88, 124.69, 121.95, 121.78, 72.35, 60.88, 58.60, 40.68, 39.51, 35.63, 29.69.

B) Synthesis of $\text{Ms}-(\text{AD-MV}^{2+})_3$:

Compound 3 (1.78 g, 4.3 mmol) and 1,3,5-tris(bromomethyl)benzene (0.47 g, 1.3 mmol) were dissolved in DMF (60 mL) and the solution was stirred at 80 $^\circ\text{C}$ under argon for 3 days. After cooling the reaction mixture to room temperature, precipitate formed was collected by filtration and washed with minimum amount of DMF and dried to provide $\text{Ms}-(\text{AD-MV}^{2+})_3$. The product was purified by recrystallization from EtOH/ H_2O to get the pale-yellow powder. Yield: 40%; mp = >300 $^\circ\text{C}$; ^1H NMR (500 MHz, DMSO d_6) δ ppm: 9.58 (d, 6H), 9.34 (d, 6H), 8.90 (d, 6H), 8.83 (d, 6H), 7.72 (s, 3H), 6.02 (s, 6H), 4.84 (t, 6H), 3.93 (t, 6H), 2.04 (s, 9H), 1.52 (m, 36H); ^{13}C NMR (125 MHz, D_2O) δ ppm: 150.57, 150.28, 146.03, 145.69, 143.71, 133.94, 129.35, 127.32, 127.23, 126.76, 126.68, 75.17, 64.13, 62.83, 62.52, 58.83, 40.51, 35.44, 30.25; ESI-MS: calculated for $\text{C}_{75}\text{H}_{90}\text{N}_6\text{O}_3^{6+}$ = 1122.7052 (M) $^+$ and found = 1122.72.

4.6. References

- (1) Huber, R. C.; Ferreira, A. S.; Thompson, R.; Kilbride, D.; Knutson, N. S.; Devi, L. S.; Toso, D. B.; Challa, J. R.; Zhou, Z. H.; Rubin, Y.; Schwartz, B. J.; Tolbert, S. H. Long-lived photoinduced polaron formation in conjugated polyelectrolyte-fullerene assemblies. *Science* **2015**, *348*, 1340–1343.
- (2) Krishnan, S. B. Ph. D. Thesis, AcSIR, 2017.
- (3) Zhang, Q.; Qu, D.-H.; Ma, X.; Tian, H. Sol–gel conversion based on photoswitching between noncovalently and covalently linked netlike supramolecular polymers.

- Chem. Commun.* **2013**, *49*, 9800–9802.
- (4) Nayak, N.; Gopidas, K. R. Self-assembly of a β -cyclodextrin bis-inclusion complex into a highly crystalline fiber network . An effective strategy for null aggregate design. *J. Phys. Chem. B* **2019**, *123*, 8131–8139.
- (5) Krishnan, R.; Krishnan, S. B.; Balan, B.; Gopidas, K. R. Self-assembly and photoinduced electron transfer in a donor- β -cyclodextrin-acceptor supramolecular system. *J. Chem. Sci.* **2018**, *130*:134.
- (6) Krishnan, S. B.; Krishnan, R.; Gopidas, K. R. Effect of N-alkyl substituents on the hierarchical self-assembly of β -cyclodextrin-linked pyrene-pyromellitic diimide charge- transfer complex. *Chem. Eur. J.* **2018**, *24*, 11451–11460.
- (7) Krishnan, S. B.; Gopidas, K. R. Observation of supramolecular chirality in a hierarchically self-assembled mixed-stack charge-transfer complex. *Chem. Eur. J.* **2017**, *23*, 9600–9606.
- (8) Zhang, J.; Liu, Q.; Wu, W.; Peng, J.; Zhang, H.; Song, F.; He, B.; Wang, X.; Sung, H. H.-Y.; Chen, M.; Li, B. S.; Liu, S. H.; Lam, J. W. Y.; Tang, B. Z. Real-time monitoring of hierarchical self-assembly and induction of circularly polarized luminescence from achiral luminogens. *ACS Nano* **2019**, *13*, 3618–3628.
- (9) Zhao, G.-Z.; Chen, L.-J.; Wang, W.; Zhang, J.; Yang, G.; Wang, D.-X.; Yu, Y.; Yang, H.-B. Stimuli-responsive supramolecular gels through hierarchical self-assembly of discrete rhomboidal metallacycles. *Chem. Eur. J.* **2013**, *19*, 10094–10100.
- (10) Tao, W.; Liu, Y.; Jiang, B.; Yu, S.; Huang, W.; Zhou, Y.; Yan, D. A linear-hyperbranched supramolecular amphiphile and its self-assembly into vesicles with great ductility. *J. Am. Chem. Soc.* **2012**, *134*, 762–764.
- (11) Mao, W.; Mao, D.; Yang, F.; Ma, D. Transformative supramolecular vesicles based on acid-degradable acyclic cucurbit[n]uril and a prodrug for promoted tumoral-cell uptake. *Chem. Eur. J.* **2019**, *25*, 2272–2280.
- (12) Wang, Q.; Tian, L.; Xu, J.; Xia, B.; Li, J.; Lu, F.; Lu, X.; Wang, W.; Huang, W.; Fan, Q. Multifunctional supramolecular vesicles for combined photothermal/photodynamic/hypoxia-activated chemotherapy. *Chem. Commun.* **2018**, *54*, 10328–10331.
- (13) Gao, L.; Wang, T.; Jia, K.; Wu, X.; Yao, C.; Shao, W.; Zhang, D.; Hu, X.-Y.; Wang, L.

- Glucose-responsive supramolecular vesicles based on water-soluble pillar[5]arene and pyridylboronic acid derivatives for controlled insulin delivery. *Chem. Eur. J.* **2017**, *23*, 6605–6614.
- (14) Rothenbühler, S.; Bösch, C. D.; Langenegger, S. M.; Liu, S.-X.; Häner, R. Self-assembly of a redox-active bolaamphiphile into supramolecular vesicles. *Org. Biomol. Chem.* **2018**, *16*, 6886–6889.
- (15) Hu, X.-Y.; Gao, L.; Mosel, S.; Ehlers, M.; Zellermann, E.; Jiang, H.; Knauer, S. K.; Wang, L.; Schmuck, C. From supramolecular vesicles to micelles: Controllable construction of tumor-targeting nanocarriers based on host–guest interaction between a pillar[5]arene-based prodrug and a RGD-sulfonate guest. *Small* **2018**, *14*, 1803952.
- (16) Nayak, N.; Gopidas, K. R. Integrative self-sorting in a three component system leading to formation of long fibrous structures. *Chemistryselect* **2016**, *5*, 1028–1032.
- (17) De Rege, P. J. F.; Williams, S. A.; Therien, M. J. Direct evaluation of electronic coupling mediated by hydrogen bonds: Implications for biological electron transfer. *Science* **1995**, *269*, 1409-1413.
- (18) Prasad, E.; Gopidas, K. R. Photoinduced electron transfer in hydrogen bonded donor-acceptor systems. Study of the dependence of rate on free energy and simultaneous observation of the marcus and rehm-weller behaviors. *J. Am. Chem. Soc.* **2000**, *122*, 3191-3196.
- (19) Shida, T. Electronic absorption spectra of radical ions, Elsevier Science Publishers B. V. Amsterdam, 1988, p 71.
- (20) Monk, P. M. S. The viologens: Physicochemical properties, synthesis and applications of the salts of 4,4'-bipyridine, John Wiley and Sons, Chichester, 1988, p. 59.
- (21) Naqvi, K. R.; Melø, T. B. Reduction of tetranitromethane by electronically excited aromatics in acetonitrile: Spectra and molar absorption coefficients of radical cations of anthracene, phenanthrene and pyrene. *Chem. Phys. Lett.* **2006**, *428*, 83–87.
- (22) Rodgers, M. A. J. Nanosecond pulse radiolysis of acetone. Kinetic and

thermodynamic properties of some aromatic radical cations. *J. Chem. Soc., Faraday Trans. 1* **1972**, *68*, 1278-1286.

- (23) Mori, Y.; Shinoda, H.; Nakano, T.; Kitagawa, T. Formation and decay behaviors of laser-induced transient species from pyrene derivatives 1. Spectral discrimination and decay mechanisms in aqueous solution. *J. Phys. Chem. A* **2002**, *106*, 11743–11749.

List of publications

- 1) **Jeevan, A. K.;** Gopidas, K. R. Hierarchical self-assembly of pyrene-linked cyclodextrin and adamantane-linked naphthalene diimide system: A case of inclusion-binding-assisted charge-transfer interaction. *Chemistryselect* **2019**, *4*, 506-514.
- 2) **Jeevan, A. K.;** Krishnan, S. B.; Gopidas, K. R. Structural deformation to β -cyclodextrin due to strong π -stacking in the self-assembly of inclusion complex. *Chemistryselect* **2020**, *5*, 14966-14970.
- 3) **Jeevan, A. K.;** Gopidas, K. R. Photoinduced electron transfer in a self-assembled bis(β -cyclodextrin)-linked pyrene/ bis(adamantane)-linked methyl viologen donor-acceptor system in aqueous solution. (Manuscript under revision).
- 4) **Jeevan, A. K.;** Gopidas, K. R. Generation of long-lived charge separated state in a supramolecular donor-acceptor system self-assembled into vesicles and fibers. (Manuscript to be submitted)

List of Posters Presented at Conferences

- 1) Hierarchically Self-Assembled Mixed-Stack Charge Transfer Complex Exhibiting Supramolecular Chirality
Athira Kanakkattusery Jeevan, Sumesh Babu Krishnan, Karical Raman Gopidas*
8th East Asia Symposium on Functional Dyes and Advanced Materials, 20-22 September 2017, CSIR-NIIST, Thiruvanthapuram. (Poster Presentation)
- 2) Hierarchically Self-Assembled Nanofiber Networks of Mixed-Stack Charge Transfer Complex with Potential for Organic Electronic Applications
Athira Kanakkattusery Jeevan, Karical Raman Gopidas*
First Indian Materials Conclave and 30th Annual General Meeting of MRSI, 12-15th February 2019, IISc, Bangalore (Poster Presentation)
- 3) Hierarchically Self-Assembled Mixed-Stack Charge Transfer Complex with Potential for Organic Electronic Applications
K. J. Athira, V. R. Rajeev, K. N. Narayanan Unni, K. R. Gopidas*
International Conference on Materials for the Millennium, 14-16th March 2019, CUSAT, Ernakulam

Organic & Supramolecular Chemistry

Hierarchical Self-Assembly of Pyrene-Linked Cyclodextrin and Adamantane-Linked Naphthalene Diimide System: A Case of Inclusion-Binding-Assisted Charge-Transfer Interaction

Athira Kanakkattusery Jeevan^[a, b] and Karical Raman Gopidas^{*[a, b]}

Mixed stack charge transfer complexation between pyrene donor linked to β -cyclodextrin and naphthalene diimide acceptor linked to adamantane, where the charge transfer interaction is augmented by inclusion binding of the adamantane moiety in β -cyclodextrin, is studied. The association constant for the charge transfer complexation was $3.64 \times 10^7 \text{ M}^{-1}$, which is the highest value reported so far for any charge transfer complex. Complex formation was probed using $^1\text{H NMR}$, isothermal titration calorimetry, and circular dichroism studies. The results suggested that within the charge transfer

complex the donor and acceptor exist as alternating units at an inter-planar distance of 3.7 \AA with a dihedral angle $> 50^\circ$ between them with each donor-acceptor pair rotated slightly with respect to the preceding and succeeding pairs. The charge transfer complex undergo hierarchical self-assembly to give twisted nanofibers as confirmed by Atomic force microscopic and Transmission electron microscopic studies. The excited state relaxation process in the charge transfer complex was investigated by femtosecond time-resolved pump-probe spectroscopy.

Introduction

Intermolecular CT interactions between aromatic D and A molecules generally occur with low or moderate association constants which in turn hinders the formation of organized assemblies with long-range order. The association constant can be enhanced several fold if the CT interaction is augmented by other non-covalent forces such as hydrogen bonding,^[1] π -stacking,^[2] metal-ligand coordination,^[3] or hydrophobic interactions.^[4] In the recent past large numbers of supramolecular architectures such as micelles,^[5] vesicles,^[6] gels,^[7] foldamers,^[8] nanotubes,^[9] liquid crystal assemblies,^[10] rotaxanes,^[11] molecular necklaces,^[12] rotaxane dendrimers^[13] etc. have been realized by employing CT interactions reinforced with other non-covalent interactions. Even after invoking support from additional non-covalent interactions the currently available 'high' K_a values for CT complexation is only in the 10^3 – 10^4 M^{-1} range. Among the common D–A systems the pyrene (PY)-naphthalene diimide (NDI) complexes are the most well-known.^[14] Wilson and co-workers have performed a systematic study on co-assembly of homopolymers containing different pendent D and A groups and identified the PY-NDI system as the best D–A system for

CT complexation.^[14e] Several groups have determined the association constants for the PY-NDI CT complex and the reported values include $6.0 \times 10^3 \text{ M}^{-1}$ in methylcyclohexane,^[14a] $9.0 \times 10^2 \text{ M}^{-1}$ in 2:1 water : methanol,^[14b] and $8.9 \times 10^2 \text{ M}^{-1}$ in 99:1 water : DMF.^[14d] Various research groups have attempted to reinforce the CT interactions in the PY-NDI system with other non-covalent forces.^[15] For example, Khalily *et al.* reported the construction of supramolecular 1D nanowires of PY-NDI system with a high K_a value of $5.18 \times 10^5 \text{ M}^{-1}$ employing a combination of H-bonding, CT, and electrostatic interactions,^[16] which was the highest K_a value reported for the PY-NDI system so far.

Recently our group has shown that CT complexation between PY and pyromellitic diimide (PI) in aqueous solution proceeds with very high association constant if the PY is linked to β -cyclodextrin (β -CD) and the PI is linked to adamantane (AD).^[17] For PY-PI intermolecular systems, CT complexation was observed only at high concentrations for which the association constant K_{CT} was estimated as $< 10^2 \text{ M}^{-1}$.^[14e] For several AD derivatives association constants for inclusion binding (K_{IN}) in β -CD are $\sim 10^4 \text{ M}^{-1}$.^[18] For the PIAD/PYCD system we reported, the association constant (K_a) determined using isothermal titration calorimetry (ITC) was $1.82 \times 10^6 \text{ M}^{-1}$, which is the highest value reported so far for CT complexes.^[17] The major contribution to the high association constant came from the inclusion binding interaction. This synergistic interaction led to the formation of 2D sheets which underwent twisting to give helical fibers. We also observed that when the AD substituent in PIAD is replaced by alkyl groups such as *t*-butyl or methyl the binding mode with β -CD changed from inclusion binding to rim-binding with the associated decrease in the value of K_a .^[19] The PYCD/PI-*t*-Bu system also exhibited high association

[a] A. K. Jeevan, Dr. K. R. Gopidas
Photosciences and Photonics Section, Chemical Sciences and Technology Division, CSIR-National Institute for Interdisciplinary Science and Technology, Trivandrum 695 019, India
E-mail: gopidaskr@gmail.com

[b] A. K. Jeevan, Dr. K. R. Gopidas
Academy of Scientific and Innovative Research (AcSIR), New Delhi 110001, India

Supporting information for this article is available on the WWW under <https://doi.org/10.1002/slct.201803166>

constant ($K_a = 2.91 \times 10^4 \text{ M}^{-1}$) and formed twisted fibers through hierarchical self-assembly.

Herein we report the construction of a highly stable PY-NDI CT complex where the CT interaction is augmented by AD/ β -CD inclusion binding. The β -CD moiety is linked to PY to give the donor system designated here as PYCD. One of the N atoms of NDI is connected to AD group through a methylene linker, and the other N atom is linked to a pyridinium moiety to increase water solubility. The AD-linked acceptor is designated as NDIAD in this study. Structures of PYCD and NDIAD are given in Figure 1. We also used a water-soluble pyrene

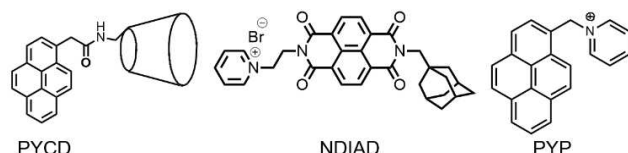


Figure 1. Structures of molecules employed in this study.

derivative PYP (Figure 1) for few control experiments. We observed that PYCD/NDIAD system exhibited $K_a > 10^7 \text{ M}^{-1}$ and underwent hierarchical self-assembly to give long fibers.

According to Mulliken theory, excitation of the CT band should result in the direct formation of radical ion pair ($D^{\cdot+}/A^{\cdot-}$) states.^[20] Kochi and co-workers have studied the ultrafast formation and decay of radical ion pairs by exciting the CT band in D/A systems.^[21] However, to the best of our knowledge only one study is available which reported formation of ion pairs in self-assembled nanostructures of CT complexes.^[22] Herein we report the femtosecond pump-probe spectroscopic study of the PYCD/NDIAD CT complex. We observed direct formation of the radical ion pair when the CT band is excited. The charge separated state was extremely short lived (~ 6 ps), thereby confirming the close proximity of the donor and acceptor in the hierarchically self-assembled system.

Results and Discussion

Synthesis and characterization of PYCD and PYP were reported by us previously.^[17] NDIAD was synthesized as shown in Scheme S1. All intermediates and final product were thoroughly characterized by state of the art spectroscopic methods (see SI, pages S4- S11 for the details of synthesis and characterization).

NDIAD gave a good ^1H NMR spectrum in DMSO- d_6 wherein all proton signals are easily identifiable (Figure S1, S2). In D_2O , however, the NMR spectrum is highly broadened as shown in Figure 2a, which was attributed to aggregation, based on results of NMR titration of NDIAD in DMSO- d_6 with D_2O (Figure S3), AFM studies (Figure S4) and previous reports.^[23] Upon increasing the temperature, the signals became relatively sharper as seen in Figure 2b, which shows the NMR taken at 80 $^\circ\text{C}$ (see Figure S5 for the temperature dependence study). Signals due to NDI and AD moieties are broad even at 80 $^\circ\text{C}$,

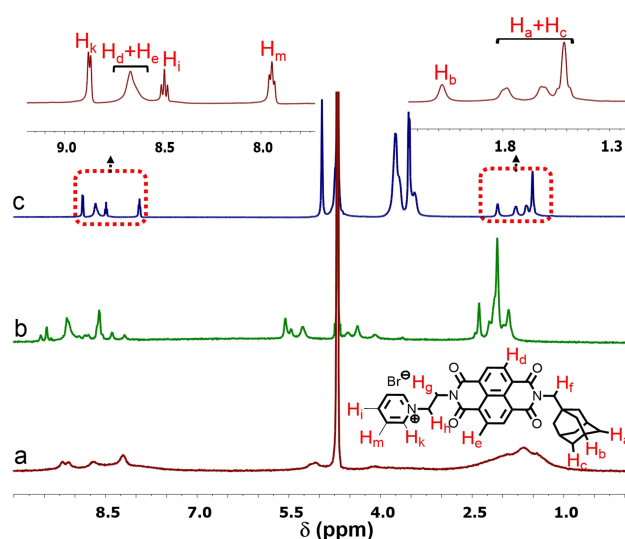


Figure 2. ^1H NMR spectra of (a) NDIAD at 20 $^\circ\text{C}$, (b) NDIAD at 80 $^\circ\text{C}$ and (c) NDIAD@ β -CD at 20 $^\circ\text{C}$. All spectra were taken in D_2O .

indicating the presence of aggregates even at this temperature.

We observed that aggregation could be prevented by addition of β -CD as is evident from the NMR spectrum in Figure 2c. In the presence of β -CD, the AD protons exhibit broadening (relative to those in DMSO- d_6) due to inclusion in the cavity which also increases the solubility of the molecule. Increased solubility reduces the propensity for aggregation which is evident from the sharp signals in the aromatic region. In Figure 2c we can actually assign the signals due to NDI and AD protons without any difficulty. CT interaction between PY and NDI is well reported in the literature. Since inclusion binding in β -CD is observed only in water, all studies reported herein were carried out in water. Aqueous 1:1 NDIAD and PYCD solution is designated in this study as NDIAD@PYCD.

Figure 3a-c shows the absorption spectra of PYCD, NDIAD, and NDIAD@PYCD ($2.5 \times 10^{-5} \text{ M}$). Even at this low concentration the CT band is clearly visible in the absorption spectrum of NDIAD@PYCD, as shown in the zoomed version (Figure 3d).

At concentrations higher than 10^{-4} M NDIAD@PYCD exhibited dark violet color. Figure 4a shows the absorption spectrum of the CT band of NDIAD@PYCD ($2.5 \times 10^{-3} \text{ M}$) and its temperature dependence. In order to make a comparison we prepared the CT complex using NDIAD and PYP ($2.5 \times 10^{-3} \text{ M}$ each (this complex is designated as NDIAD@PYP)). The CT absorption spectrum of NDIAD@PYP and its temperature dependence are presented in Figure 4b. Although the spectral profiles of the CT bands in NDIAD@PYCD and NDIAD@PYP are similar, several differences exist among these CT complexes. The NDIAD@PYCD solution appears dark violet with the maximum absorbance of 1.05 at 568 nm. The NDIAD@PYP solution is pale red in color with the maximum absorbance of 0.58 at 495 nm. Up on increasing the temperature from 20 to 90 $^\circ\text{C}$ the CT absorption decreased only by 17% for NDIAD@PYCD whereas 60% decrease in the absorbance was observed

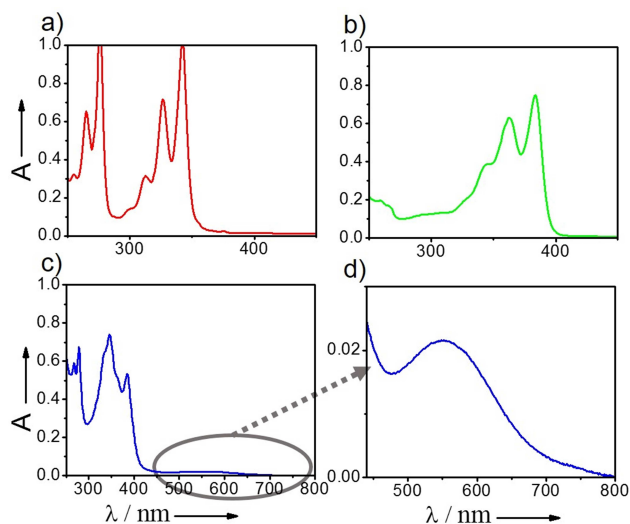


Figure 3. a-d Absorption spectra of 2.5×10^{-5} M aq. solutions of (a) PYCD, (b) NDIAD, and (c) NDIAD@PYCD. The CT absorption region is enlarged in (d).

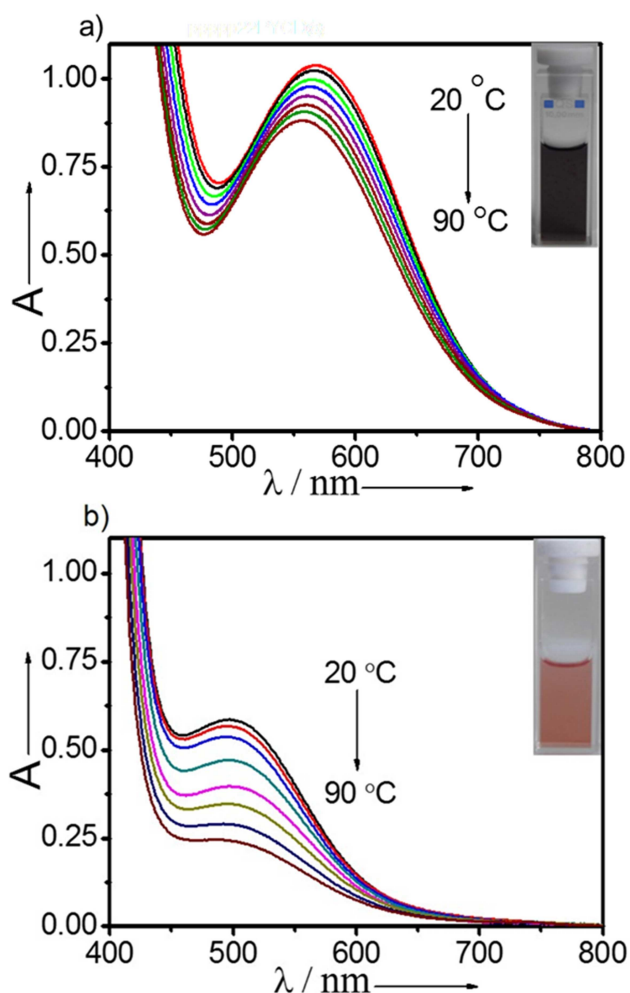


Figure 4. CT absorption bands of (a) NDIAD@PYCD and (b) NDIAD@PYP and their temperature dependence. Insets show the solution colors. Concentrations of the constituents were 2.5×10^{-3} M each, in both cases.

for NDIAD@PYP. These results suggest that CT complex formed in the NDIAD@PYCD system is highly stable compared to that of the model system.

In order to have a clear understanding of the complexation processes in these systems, we have attempted to determine the association constants for the two systems. For the NDIAD@PYCD system, K_a was determined using isothermal titration calorimetry (ITC). For the experiment, NDIAD (2.0 mM in water) was taken in the syringe, and PYCD (0.2 mM in water) was taken in the cell. The ITC titration curve obtained is given in Figure 5. Aqueous NDIAD solution is highly viscous, and

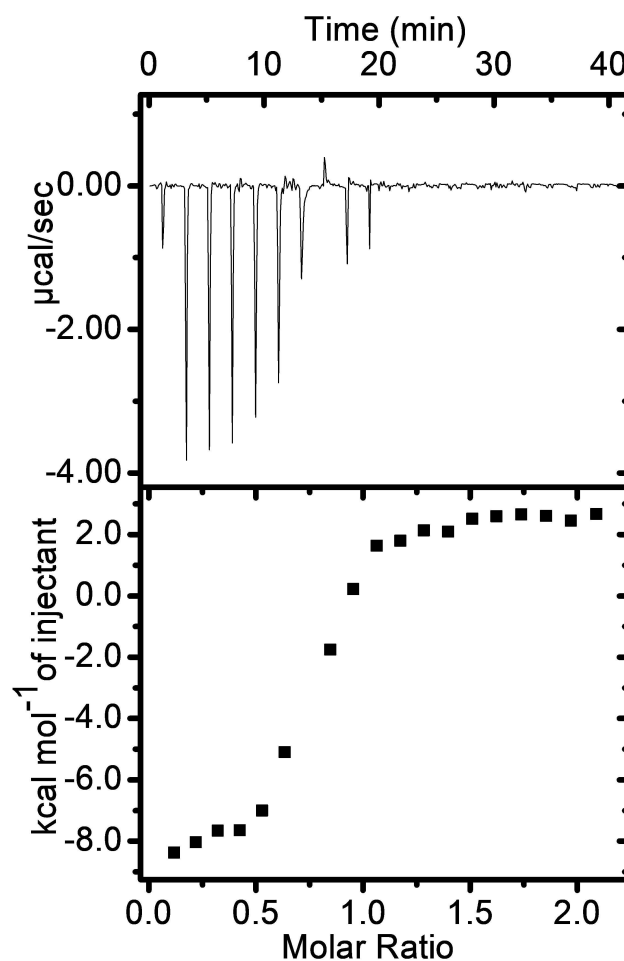


Figure 5. ITC titration curve for NDIAD@PYCD.

hence bubbles are formed during stirring. The small distortions in the titration curve are due to bubble formation, and fitting of the data gave $K_a = 3.64 \times 10^7 \text{ M}^{-1}$. Other parameters obtained from the ITC experiment are $\Delta H = -29.76 \text{ kJ mol}^{-1}$, $\Delta S = 44.76 \text{ J mol}^{-1} \text{ K}^{-1}$, and binding stoichiometry $n = 0.8$ (which for practical purposes can be taken as 1:1 binding). Since NDIAD exists as aggregates in solution, de-aggregation must occur before CT complex formation. ΔS for complexation is positive most probably because of the de-aggregation process. The negative value of Gibbs energy change (ΔG°)

confirms the favorable self- assembling process taking place between PYCD and NDIAD in water.

In the NDIAD@PYCD system studied here, the CT interaction is augmented by the inclusion binding interaction of adamantane moiety in β -CD cavity. If we take $K_{a(CT)} \sim 10^3 \text{ M}^{-1}$ for the CT interaction between PY and NDI chromophores and $K_{a(IN)} \sim 10^4 \text{ M}^{-1}$ for inclusion binding of adamantane in β -CD, the K_a value for NDIAD@PYCD = $K_{a(CT)} \times K_{a(IN)} \sim 10^7 \text{ M}^{-1}$, which is the value observed experimentally. This is the highest value reported for the PY-NDI donor-acceptor system so far.

For the NDIAD@PYP system, ITC titration curves obtained were not satisfactory, and hence we resorted to UV-Vis dilution experiment (Figure S12). K_a thus obtained was $1.16 \times 10^3 \text{ M}^{-1}$, which agreed very well with literature reports.^[14b,d]

ESI-HRMS analysis further confirmed the complexation between PYCD and NDIAD in 1:1 ratio (Figure S13). The calculated molecular weight of 1:1 NDIAD@PYCD complex is 1895.67. The observed m/z value is at 1895.66 (the Br^- counter ion is not included) (Figure S13a). The expansion of 1895.66 peak region shows peak at 1896.66 which corresponds to $[\text{M} + \text{H}]^+$ (Figure S13b).

In order to further confirm the supramolecular association between NDIAD and PYCD, we have employed diffusion ordered NMR spectroscopy (DOSY). Molecules in solution undergo both rotational and translational motion constantly. Translational motion of molecules in solution is commonly known as self-diffusion, which is characterized by a self-diffusion coefficient D ($\text{m}^2 \text{ s}^{-1}$). The value of D is inversely related to the hydrodynamic radius of the molecule through the Stoke-Einstein equation. Strictly speaking, the equation is valid only for spherical molecules, but it is generally used to estimate the sizes of all types of molecules in solution. DOSY-NMR experiments can give information about the D values of molecules, which in turn can be used to obtain information about intermolecular interactions in supramolecular chemistry.^[24]

We have performed DOSY experiments with D_2O solutions of PYCD and NDIAD@PYCD complex (see SI for details). The 2D-DOSY spectra obtained are given in Figure S14 (SI). From the DOSY experiments we obtained $D = 2.634 \times 10^{-10} \text{ m}^2 \text{ s}^{-1}$ for PYCD and $D = 1.798 \times 10^{-10} \text{ m}^2 \text{ s}^{-1}$ for NDIAD@PYCD. It can be noted that D value obtained for NDIAD@PYCD is much lower compared to that obtained for PYCD, suggesting that complexation occurs between NDIAD and PYCD to give a complex, whose size is much larger than PYCD.

Wide-angle XRD analysis of 1:1 NDIAD@PYCD complex showed a peak of $2\theta = 24^\circ$ which corresponds to a 'd' value of 3.7 \AA (Figure S15). This can be assigned to the π - π stacking distance between PYCD and NDIAD. Wide angle XRD of PY-NDI system previously reported was very similar to Figure S15.^[14c]

In order to understand the nature and conformation of the NDIAD@PYCD and NDIAD@PYP systems, a detailed NMR analysis was carried out. Figure 6 shows the ^1H NMR of NDIAD@PYCD in D_2O (panel b) along with those of the components PYCD (panel a) and NDIAD (panel d). For comparison purposes NMR of NDIAD@ β -CD is also shown in Figure 6 (panel c). ^1H NMR of 1-substituted adamantane deriva-

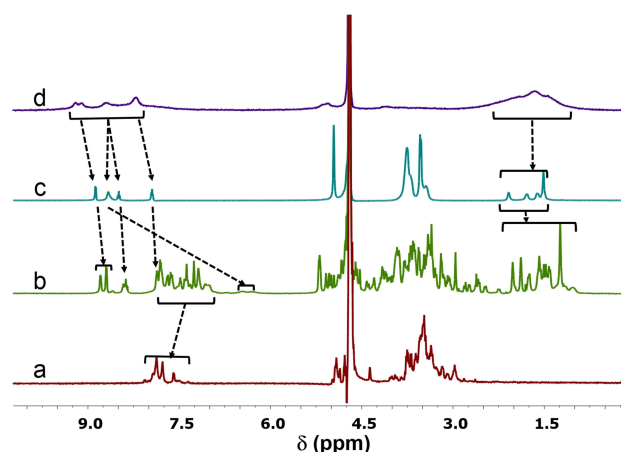


Figure 6. ^1H NMR spectra of PYCD (panel a), NDIAD@PYCD (panel b), NDIAD@ β -CD (panel c) and NDIAD (panel d). Major changes due to complexation are indicated by arrows.

tives generally show three signals: A singlet (3 protons) for H_b , singlet (6 protons) for H_c and a doublet of doublet (6 protons) for H_a . Sometimes the H_a and H_c proton signals get partially merged to give a complex pattern (as in Figure 6c and Figure S1). When encapsulated in β -CD with the substituent remaining outside the wider rim, the H_a and H_b protons would be deep inside the cavity and NMR signals corresponding to these protons would be highly broadened and/or shifted. The H_c protons will be less affected. In most cases of AD@ β -CD the three sets of protons can be easily identified in the NMR. In the case of NDIAD@PYCD (panel b, Figure 6) the AD protons exhibited a very complex splitting pattern in the δ 0.95 – 2.05 ppm range. Such complex patterns were not observed previously for any AD@ β -CD systems which called for additional experiments to confirm the proton assignments.

The model compound PYP forms CT complex with NDIAD and Figure S16 (panel b) shows the ^1H NMR of NDIAD@PYP. For comparative purposes, NMR spectra of NDIAD and PYP are also given in Figure S16. In the NMR spectrum of the NDIAD@PYP complex, the signals corresponding to the AD protons appear as very sharp, clearly identifiable signals suggesting that CT complex formation proceeds with de-aggregation of NDIAD.

Temperature dependence of the ^1H NMR spectrum of NDIAD@PYCD is shown in Figure 7. It can be seen that the complex pattern observed in the δ 0.95 – 2.05 ppm region at 25°C got reduced into a less complex pattern at 80°C . Signals due to the pyridinium protons can be clearly identified at 80°C . If the peak at δ 9.25 ppm is identified as H_k (two protons), integration of the signals shows that the broad signals in the alkyl region (δ 1.72–2.55 ppm) correspond to fifteen protons due to the AD moiety. The small signal at δ 2.46 ppm corresponds to H_b (three protons), and the broad peak centered around δ 2.01 and 1.90 ppm corresponds to H_a and H_c (twelve protons). It may be noted that at 25°C the H_k signal is split into two peaks. If these two peaks are integrated as two protons, then the complex pattern in the δ 0.95 – 2.05 ppm region would correspond to fifteen protons which can be sub divided

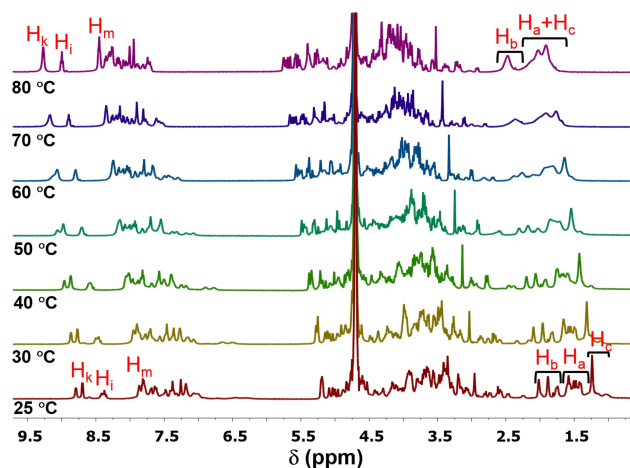


Figure 7. Temperature dependence of ^1H NMR of NDIAD@PYCD.

into three groups of protons as shown in Figure 7 (lower panel). Since the H_c protons remain outside the cavity, we expect this proton to be less affected by complexation based on which we assign the single peak at δ 1.24 ppm to H_c and the multiplet pattern in the δ 1.36–1.65 ppm to H_a protons. This analysis has shown that the three H_b protons are not chemically equivalent. A similar situation applies to the six H_a protons. The non-equivalency of the protons can be due to the absence of free rotation for the AD group within the β -CD cavity and/or formation of secondary structures (vide infra).

In order to have a detailed understanding of the complex splitting pattern in the NMR of NDIAD@PYCD we have employed Circular Dichroism (CD) spectroscopy. PY and NDIAD are achiral chromophores and do not exhibit any cotton effect, but they can exhibit induced circular dichroism (ICD) when associated with β -CD. We have reported previously that PYCD exhibits weak positive ICD signals which are similar to the $\text{S}_0 \rightarrow \text{S}_2$ transition of PY (Figure S17a).^[19] NDIAD@ β -CD exhibited a weak negative ICD signal which is shown in Figure S17b. The lowest energy transition in the 300–400 nm in NDI is polarized along the N – N axis.^[25] When the AD moiety of NDIAD is encapsulated in β -CD, the NDI chromophore is forced to stay outside the wider rim of β -CD. As can be seen in the inset in Figure S17b, the presence of the CH_2 group between the NDI and AD forces the NDI chromophore to adopt a conformation which is nearly parallel to the β -CD axis. The resulting ICD signal is expected to be very weak with a negative sign as per Kodaka's rule.^[26]

Figure 8a shows the CD spectrum of NDIAD@PYCD (2.5×10^{-5} M). The CD spectrum exhibited a moderately strong signal in the 300–420 nm region and a weak positive signal in the CT absorption region indicating that the CT complex is chiral. The intensity of CD signal in the CT region was low at the low concentration employed for this study. When the concentration of NDIAD@PYCD was increased to 2.5×10^{-3} M an intense CD signal was observed for CT band which is shown in Figure 8b (at this concentration the optical density in the region below 400 nm is significantly greater than 1.0, and hence CD

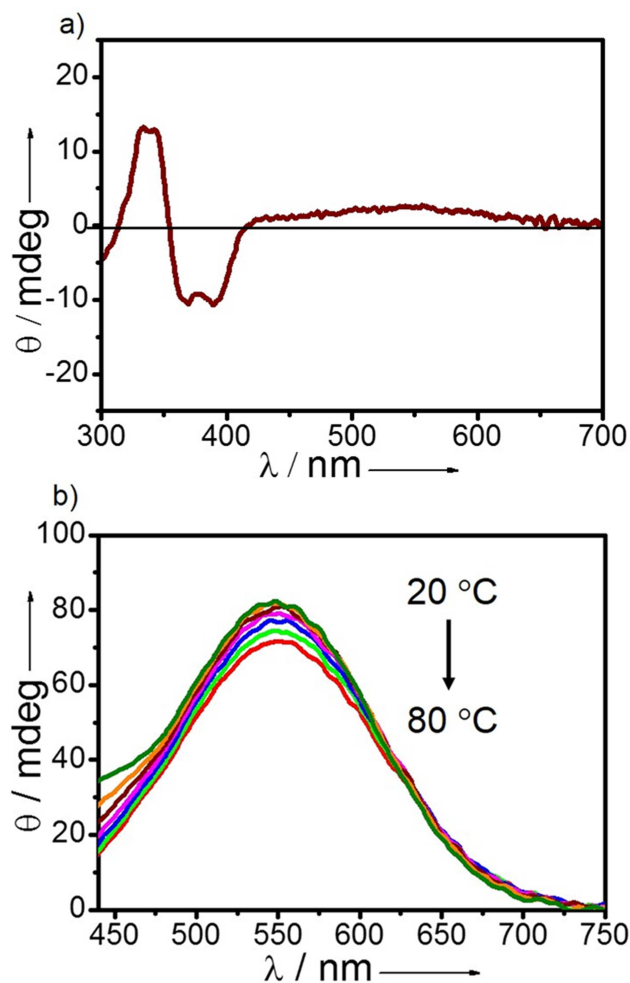


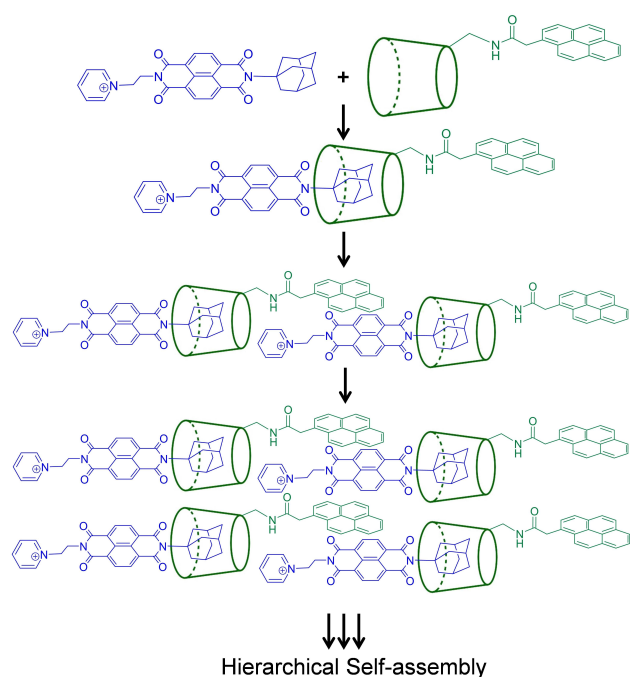
Figure 8. (a) CD spectrum of NDIAD@PYCD (2.5×10^{-5} M) and (b) CD spectrum of the CT band region (2.5×10^{-3} M) and its temperature dependence.

spectrum of this region could not be recorded). Temperature dependence of the CD spectrum in the 20–80 °C is also shown in Figure 8b, which again supports the very high stability of CT complex.

A comparison of Figure 8a with the absorption spectrum of the CT complex (Figure 3c) suggests that the observed signal (in the 300–420 nm region) is a bisignated CD signal with a first negative cotton effect. Bisignated signal arises due to exciton coupling when the chromophores involved are spatially very close and constitute a chiral system.^[16,27] In such a system the electronic transition moments would interact spatially so that the energy levels of the excited states split which will be reflected in the CD spectrum as the bisignated signal. Observation of the bisignated signal suggests that the NDIAD@PYCD complex constitute a exciton coupled bichromophoric system where the transition moments of the chromophores are rotated by a small angle.

As mentioned earlier, both CT and inclusion binding interactions are involved in the formation of NDIAD@PYCD. NMR, ICD and microscopic studies (vide infra) suggested that

the inclusion/CT complex formed initially underwent hierarchical self-assembly. Since $K_{a(IN)} > K_{a(CT)}$, we propose Scheme 1 for



Scheme 1. Scheme for the formation of NDIAD@PYCD and its hierarchical assembly

the formation of NDIAD@PYCD and its further assembly into hierarchical structures. Further self-assembly occurs through cumulative CT interactions as shown in Scheme 1. Previously we have invoked similar schemes for the self-assembly of PIAD/PYCD complexes.^[17,19] Scheme 1, however, does not explain the complex pattern observed for the adamantyl and pyrene protons in the NMR spectrum of NDIAD@PYCD and the bisignated CD signal. In order to explain these aspects we invoke a twisting between the pyrene and NDI moieties of the assembly, as described below.

Several reports dealing with crystal structures of PY/NDI CT complexes are available in the literature.^[15d] Gujrati *et al.* reported that in the CT complex NDI and PY exist as alternating units in columnar stacks along the crystallographic *a* axis with an inter planar distance of 3.4 Å and a dihedral angle (θ) of $\sim 53^\circ$ between the long molecular axes of NDI and PY.^[28] A computational study by Lin predicted θ values from $50\text{--}75^\circ$ for the PY/NDI complexes.^[29] Li *et al.* prepared PY/NDI complexes that exhibited reversible color changes in the solid state when treated with different organic solvents. The origin of the color changes was shown to be solvent inclusion which leads to changes in θ value. CT crystals which did not contain any solvent molecules appeared orange in color ($\lambda_{\text{max}} = 500$ nm), and θ values for these were found to be $< 50^\circ$. CT crystals with purple or purple-red colors ($\lambda_{\text{max}} \approx 530$ nm) have two solvent molecules included in the crystal, and these have θ values $> 50^\circ$.^[15d] The above reports provide valuable insights regarding

the origin of the bisignated CD signal which is a consequence of the orientation of chromophores in the NDIAD@PYCD system.

The NDIAD@PYCD system exhibited deep violet color with $\lambda_{\text{max}} = 568$ nm. Applying the information from the crystal structures, we may predict that two water molecules are incorporated in the CT stack which increases the dihedral angle to nearly 70° . The CT system exhibited induced chirality because they are associated closely with β -CD, but since the chromophores exhibited a twist angle between their long molecular axes the resulting CD signal is bisignated. The signal intensity is small because the chirality is not intrinsic but induced. Thus the π -stacking in NDIAD@PYCD could be as shown in Figure 9a or b. In the configuration shown in

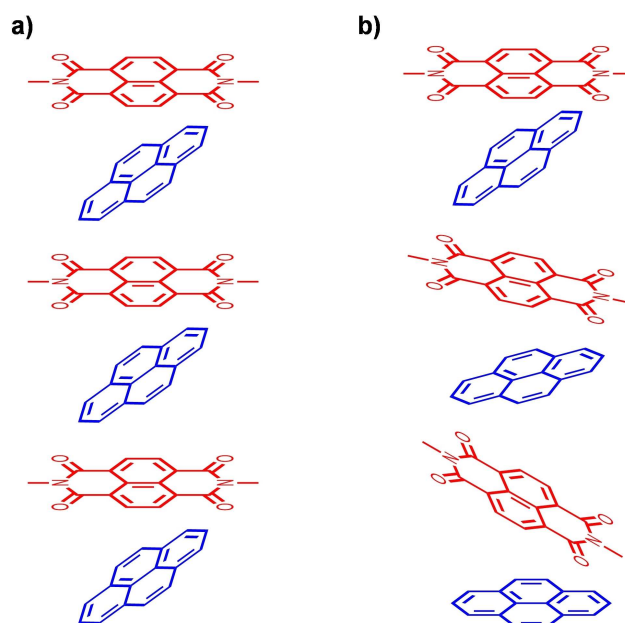


Figure 9. Possible π -stacking arrangements in NDIAD@PYCD.

Figure 9a, the dihedral angle between PY and NDI is $> 50^\circ$, which is similar to the crystal structure reported by Gujrati *et al.*^[28] In this configuration the orientation of PY and NDI chromophores are identical in successive stacks. This means that all PY residues have similar chemical environments throughout the assembly. The NDI moieties also have similar environments and hence all the AD units linked to NDI and included in PYCD cavities are also expected to have similar chemical and magnetic environments. Although Figure 9a explains the bisignated CD signal, it cannot explain the complex NMR pattern of NDIAD@PYCD reported in Figure 6b.

In order to explain the complex NMR pattern in Figure 6b, we invoke the D–A stack configuration in Figure 9b where the dihedral angle between NDI and PY remains the same but each NDI–PY pair is rotated by some angle with respect to the preceding and succeeding NDI–PY pairs. Thus each PY, NDI and AD groups have slightly different chemical and magnetic environments compared to their analogues in adjacent stacks.

The origin of the complex NMR spectrum of NDIAD@PYCD and the bisignated CD signal can be explained using Figure 9b.

The intense CD signal due to the CT band in Figure 8b cannot be attributed to induced chirality due to β -CD and we attribute this to supramolecular chirality resulting from twisted or helical structures formed by the hierarchical assembly of the CT complex as observed for PMDI@PYCD systems previously.^[17] We have confirmed the presence of nanostructures even in dilute solutions of NDIAD@PYCD through the observation of dynamic light scattering and tyndall effect experiments (Figure S18). This is further confirmed with the help of TEM and AFM analysis (Figure 10 and Figure S19). AFM and TEM images

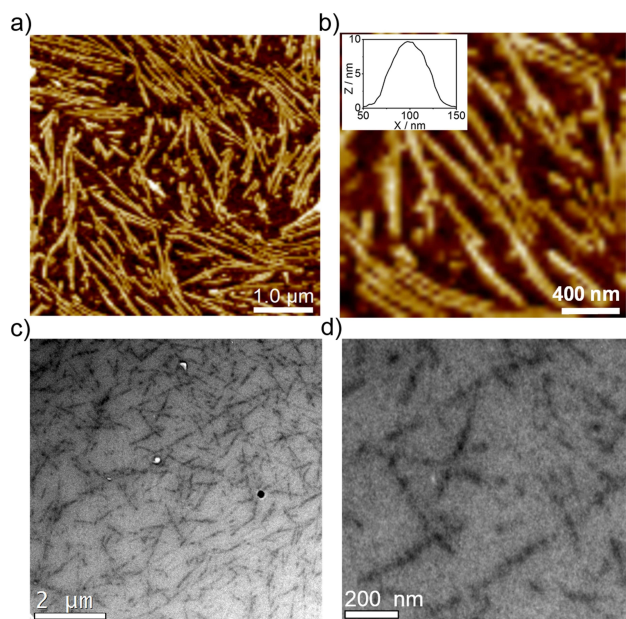
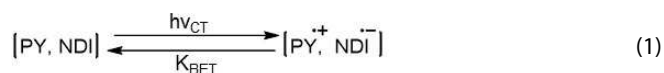


Figure 10. AFM (a, b) and TEM (c, d) images of nanofibers formation of NDIAD@PYCD in water. Inset in b shows the height profile of the nanofibers. NDIAD@PYCD (10^{-4} M) was used for the experiments.

showed the presence of twisted nanofibers of ~ 1.0 μm length, 80–100 nm width and 7–10 nm height. The zoomed AFM and TEM images clearly show the twisted nature of the fibers. The rms roughness measured was 2.6–3.6 nm from AFM which indicate smoothness of the film.

For the NDIAD@PYCD system the CT absorption occurs in the 400–700 nm region. According to Mulliken theory, excitation of the CT band should lead to formation of the radical ion pair system as shown by equation (1),



where $\text{PY}^{\bullet+}$ stands for the radical cation of the PY donor and $\text{NDI}^{\bullet-}$ stands for the radical anion of the NDI acceptor and k_{BET} is the rate of back electron transfer for regeneration of the ground CT state. We have employed nanosecond and femtosecond transient absorption spectroscopy to detect the transient species formed in the photoexcitation of NDIAD@PYCD.

Nanosecond flash photolysis of NDIAD@PYCD employing 532 nm laser pulses did not yield any transient species indicating that the CT excited state do not furnish any long lived charge separated states. Femtosecond transient absorption studies, however, resulted in the formation of extremely short-lived species absorbing the 400–550 nm region. Since we have used 600 nm excitation the region around the pump wavelength was not probed. Transient absorption spectra obtained in the 4.5 ps – 24 ps time window are shown in Figure 11a. The transient absorption spectra showed maximum

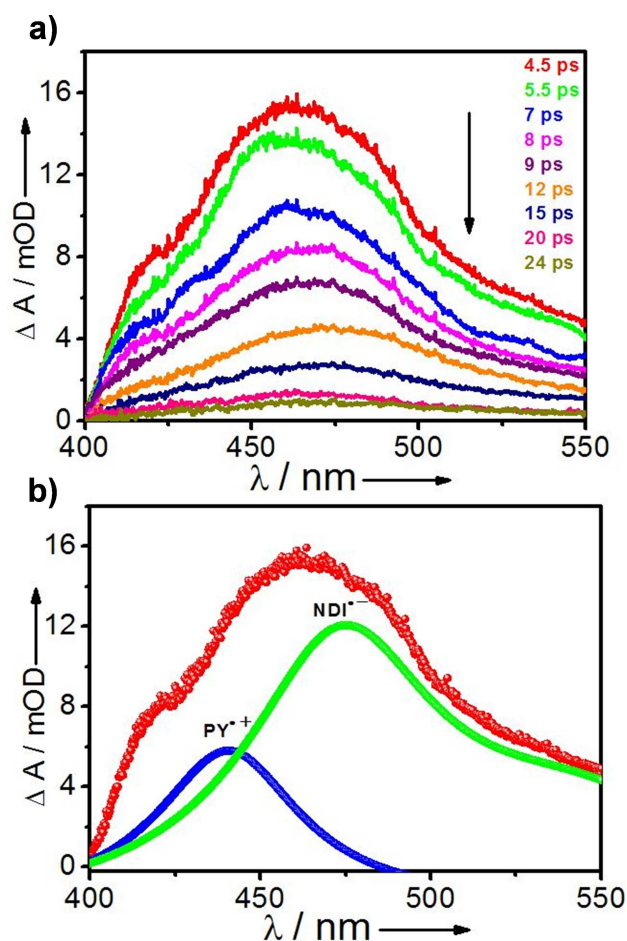


Figure 11. a) Femtosecond time-resolved transient absorption spectra of NDIAD@PYCD in aqueous media recorded at different time delays (4.5 ps–24 ps) upon excitation at 600 nm. b) assigning peaks corresponds to $\text{PY}^{\bullet+}$ and $\text{NDI}^{\bullet-}$.

around 470 nm and shoulder at 425 nm. Using a peak fitting program we could resolve the broad spectrum into two spectra as shown in Figure 11b with λ_{max} at 440 nm and 474 nm. Based on previous reports by others^[30a,b] and us,^[30c] the 440 nm absorption was assigned to $\text{PY}^{\bullet+}$. $\text{NDI}^{\bullet-}$ is known to exhibit a broad absorption extending up to 800 nm with maximum around 470 nm.^[31] Hence we assign the 474 nm absorptions to $\text{NDI}^{\bullet-}$. Thus the femtosecond transient absorption studies confirmed the generation of the radical ion pair as per the above equation.

The kinetic traces obtained at wavelengths 440 nm and 474 nm are shown in Figure 12a,b. Examination of the kinetic

and both the forward and back electron transfers are static in nature.

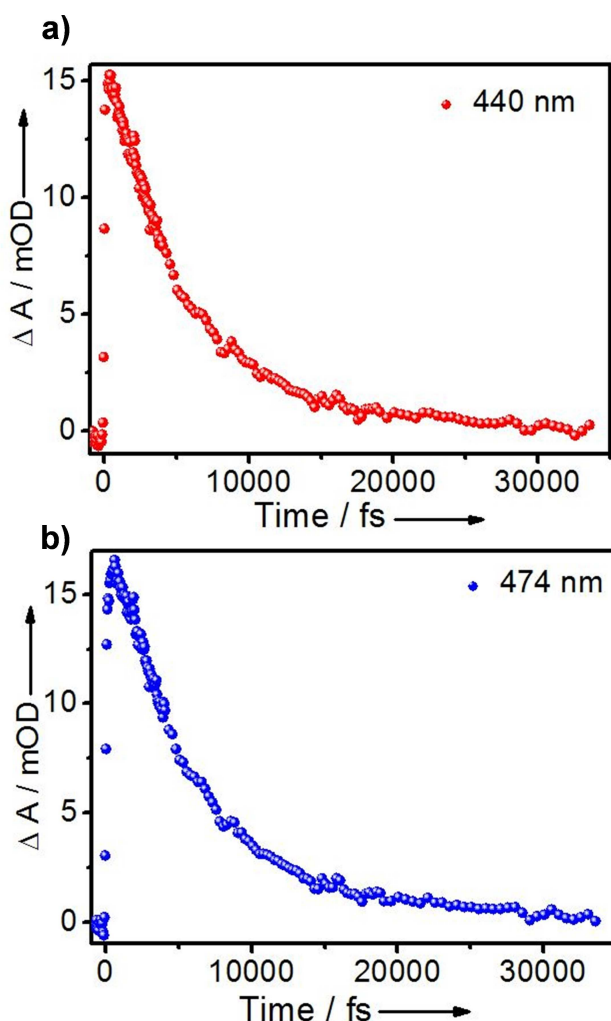


Figure 12. Kinetic decay obtained at the probe wavelengths a) 440 nm and b) 474 nm.

profiles suggests that the transient species are formed within a very short time (< 100 fs) and decay by first order kinetics. Fitting of the profiles gave 6 ps lifetime for both absorptions, which correspond to a decay rate of $1.66 \times 10^{11} \text{ s}^{-1}$. For several D–A complexes studied by Kochi and co-workers the k_{BET} values were in the range of $(1.6 - 2.0) \times 10^{10} \text{ s}^{-1}$ range.^[21] None of the systems studied by Kochi's group self-assembled into supramolecular systems. For the CT complex which formed supramolecular fibers, Aoki et al. reported k_{BET} value of $2.2 \times 10^{10} \text{ s}^{-1}$.^[22] For the NDIAD@PYCD system studied here k_{BET} value is one order of magnitude larger. The extremely fast formation and decay of the ion pairs suggest that PY and NDI chromophores are very tightly packed in the NDIAD@PYCD nano structures and the inter ionic separation in $\text{PY}^{*+}/\text{NDI}^{*-}$ can be considered as very similar to that in contact ion pairs.

Rapid formation and decay of this state confirms that the donor and acceptor precursors are residing in close proximity

Conclusions

In conclusion, we have designed a highly stable PY-NDI CT complex by exploiting the high affinity of adamantane derivatives for inclusion binding in β -CD cavity to augment the CT interaction between PY and NDI chromophores. The association constant for complexation, as measured by ITC, was $3.64 \times 10^7 \text{ M}^{-1}$, which is the highest value reported for any CT complex. π -stacking between PY and NDI, and inclusion binding of adamantane moiety in β -CD are probed using ^1H NMR. Adamantane protons within the CD cavity exhibited an extremely complex NMR pattern. Careful analysis with the aid of temperature-dependent NMR supported by circular dichroism spectroscopy suggested that protons of each PY, NDI, and adamantane groups have slightly different chemical and magnetic environments compared to their analogues in adjacent stacks. Based on these results we proposed that within the complex the PY and NDI exist as alternating units with a dihedral angle $> 50^\circ$ between them, but each PY-NDI pair is rotated slightly with respect to the preceding and succeeding pairs. The AFM and TEM analysis confirms formation of twisted fibers from hierarchical self-assembly of charge transfer complex. Excitation of the CT band in NDIAD@PYCD using femtosecond laser gave transients assignable to PY^{*+} and NDI^{*-} radical ion pairs. Ultrafast formation (< 100 fs) and decay (~ 6 ps) confirms close packing of the PY and NDI moieties in the nano assembly.

Supporting Information Summary

Details about the synthesis of NDIAD, characterisation of PYCD and NDIAD with ^1H NMR, ^{13}C NMR, HRMS analysis and physical data of charge transfer complexes NDIAD@PYCD and NDIAD@-PYP can be found in supporting information.

Acknowledgements

We thank CSIR, Government of India (project no. HCP0012) for financial support. We are thankful to Mr. Kiran Mohan and Mr. Robert Philip for TEM analysis, Mr. Vibhu Dharsan, Mr. Aswin Maheswar, Mr. M. Vishnu for AFM analysis. Ms. Chinju Govind for Femtosecond time-resolved transient absorption studies. AKJ gratefully thanks Mr. Sumesh babu krishnan for discussions during work.

Conflict of Interest

The authors declare no conflict of interest.

Keywords: β -Cyclodextrin · Charge-transfer complex · Chiralnano fibers · Inclusion binding · Supramolecular self-assembly

- [1] a) B. Song, H. Wei, Z. Wang, X. Zhang, M. Smet, W. Dehaen, *Adv. Mater.* **2007**, *19*, 416–420; b) A. Das, M. R. Molla, A. Banerjee, A. Paul, S. Ghosh, *Chem. Eur. J.* **2011**, *17*, 6061–6066; c) T. Mondal, D. Basak, A. A. Ouahabi, M. Schmutz, P. Mesini, S. Ghosh, *Chem. Commun.* **2015**, *51*, 5040–5043.
- [2] a) Y. Sun, L. Jiang, K. C. Schuermann, W. Andriaens, L. Zhang, F. Y. C. Boey, L. De Cola, L. Brunsveld, X. Chen, *Chem. Eur. J.* **2011**, *17*, 4746–4749; b) F. Biedermann, O. A. Scherman, *J. Phys. Chem. B* **2012**, *116*, 2842–2849; c) H. Liu, É. Brémond, A. Prlj, J. F. Gonthier, C. Corminboeuf, *J. Phys. Chem. Lett.* **2014**, *5*, 2320–2324.
- [3] a) A. O. Moughton, R. K. O'Reilly, *J. Am. Chem. Soc.* **2008**, *130*, 8714–8725; b) B. Song, G. Wu, Z. Wang, X. Zhang, M. Smet, W. Dehaen, *Langmuir* **2009**, *25*, 13306–13310.
- [4] C. Wang, Y. Guo, Y. Wang, H. Xu, R. Wang, X. Zhang, *Angew. Chem. Int. Ed.* **2009**, *48*, 8962–8965; *Angew. Chem.* **2009**, *121*, 9124–9127.
- [5] a) K. Wang, Y. Liu, C. Li, S.-X. Cheng, R.-X. Zhuo, X.-Z. Zhang, *ACS Macro Lett.* **2013**, *2*, 201–205; b) Y.-C. Wu, B. P. Bastakoti, M. Pramanik, Y. Yamauchi, S.-W. Kuo, *Polym. Chem.* **2015**, *6*, 5110–5124; c) C. Shan, X. Huang, H. Wei, W. Wei, H. Sun, X. Tang, *RSC Adv.* **2014**, *4*, 11216–11218.
- [6] a) C. Wang, S. Yin, S. Chen, H. Xu, Z. Wang, X. Zhang, *Angew. Chem. Int. Ed.* **2008**, *47*, 9049–9052; *Angew. Chem.* **2008**, *120*, 9189–9192; b) Q. Yan, J. Yuan, Z. Cai, Y. Xin, Y. Kang, Y. Yin, *J. Am. Chem. Soc.* **2010**, *132*, 9268–9270; c) P. Xing, T. Sun, A. Hao, *RSC Adv.* **2013**, *3*, 24776–24793.
- [7] a) X. Du, J. Zhou, J. Shi, B. Xu, *Chem. Rev.* **2015**, *115*, 13165–13307; b) Y. Liu, N. Zheng, T. Chen, L. Jin, B. Yin, *Org. Biomol. Chem.* **2014**, *12*, 6927–6936; c) L. Wang, X. Shi, Y. Wu, J. Zhang, Y. Zhu, J. Wang, *Soft Matter* **2018**, *14*, 566–573.
- [8] a) D.-W. Zhang, W.-K. Wang, Z.-T. Li, *Chem. Rec.* **2015**, *15*, 233–251; b) D. J. Hill, M. J. Mio, R. B. Prince, T. S. Hughes, J. S. Moore, *Chem. Rev.* **2001**, *101*, 3893–4012; c) Z. Merican, K. D. Johnstone, M. J. Gunter, *Org. Biomol. Chem.* **2008**, *6*, 2534–2543.
- [9] a) W. Jin, Y. Yamamoto, T. Fukushima, N. Ishii, J. Kim, K. Kato, M. Takata, T. Aida, *J. Am. Chem. Soc.* **2008**, *130*, 9434–9440; b) D. M. Eisele, J. Knoester, S. Kirstein, J. P. Rabe, D. A. V. Bout, *Nat. Nanotechnol.* **2009**, *4*, 658–663; c) J. P. Hill, W. Jin, A. Kosaka, T. Fukushima, H. Ichihara, T. Shimomura, K. Ito, T. Hashizume, N. Ishii, T. Aida, *Science* **2004**, *304*, 1481–1483.
- [10] a) J. Uchida, M. Yoshio, S. Sato, H. Yokoyama, M. Fujita, T. Kato, *Angew. Chem. Int. Ed.* **2017**, *56*, 14085–14089; *Angew. Chem.* **2017**, *129*, 14273–14277; b) M. Manickam, M. Belloni, S. Kumar, S. K. Varshney, D. S. S. Rao, P. R. Ashton, J. A. Preece, N. Spencer, *J. Mater. Chem.* **2001**, *11*, 2790–2800; c) L. Schmidt-Mende, A. Fechtenkötter, K. Müllen, E. Moons, R. H. Friend, J. D. MacKenzie, *Science* **2001**, *293*, 1119–1122.
- [11] a) A. Harada, A. Hashizume, H. Yamaguchi, Y. Takashima, *Chem. Rev.* **2009**, *109*, 5974–6023; b) G. Wenz, B. H. Han, A. Müller, *Chem. Rev.* **2006**, *106*, 782–817; c) M. A. Soto, J. Tiburcio, *Chem. Commun.* **2016**, *52*, 14149–14152.
- [12] Y. H. Ko, K. Kim, J.-K. Kang, H. Chun, J. W. Lee, S. Sakamoto, K. Yamaguchi, J. C. Fettinger, K. Kim, *J. Am. Chem. Soc.* **2004**, *126*, 1932–1933.
- [13] J. W. Lee, S. C. Han, J. H. Kim, Y. H. Ko, K. Kim, *Bull. Korean Chem. Soc.* **2007**, *28*, 1837–1840.
- [14] a) A. Das, S. Ghosh, *Angew. Chem. Int. Ed.* **2014**, *53*, 1092–1097; *Angew. Chem.* **2014**, *126*, 1110–1115; b) S. Bhattacharjee, S. Bhattacharya, *Chem. Asian J.* **2015**, *10*, 572–580; c) A. Sikder, B. Ghosh, S. Chakraborty, A. Paul, S. Ghosh, *Chem. Eur. J.* **2016**, *22*, 1908–1913; d) S. Bhattacharjee, B. Maiti, S. Bhattacharya, *Nanoscale* **2016**, *8*, 11224–11233; e) N. S. S. Kumar, M. D. Gujrati, J. N. Wilson, *Chem. Commun.* **2010**, *46*, 5464–5466.
- [15] a) M. B. Avinash, K. V. Sandeepa, T. Govindaraju, *ACS Omega* **2016**, *1*, 378–387; b) S. Bartocci, J. A. Berrocal, P. Guarracino, M. Grillaud, L. Franco, M. Mba, *Chem. Eur. J.* **2018**, *24*, 2920–2928; c) K. Jalani, M. Kumar, S. J. George, *Chem. Commun.* **2013**, *49*, 5174–5176; d) P. Li, J. M. Maier, J. Hwang, M. D. Smith, J. A. Krause, B. T. Mullis, S. M. S. Strickland, K. D. Shimizu, *Chem. Commun.* **2015**, *51*, 14809–14812; e) H. A. Staab, D.-Q. Zhang, C. Krieger, *Liebigs Ann. Recueil* **1997**, 1551–1556; f) R. Vaiyapuri, B. W. Greenland, H. M. Colquhoun, J. M. Elliott, W. Hayes, *Polym. Chem.* **2013**, *4*, 4902–4909.
- [16] M. A. Khalily, G. Bakan, B. Kucukoz, A. E. Topal, A. Karatay, H. G. Yaglioglu, A. Dana, M. O. Guler, *ACS Nano* **2017**, *11*, 6881–6892.
- [17] S. B. Krishnan, K. R. Gopidas, *Chem. Eur. J.* **2017**, *23*, 9600–9606.
- [18] a) M. V. Rekharsky, Y. Inoue, *Chem. Rev.* **1998**, *98*, 1875–1918; b) N. Nayak, K. R. Gopidas, *J. Mater. Chem. B* **2015**, *3*, 3425–3428; c) W. C. Cromwell, K. Bystrom, M. R. Eftink, *J. Phys. Chem.* **1985**, *89*, 326–332; d) R. Krishnan, K. R. Gopidas, *J. Phys. Chem. Lett.* **2011**, *2*, 2094–2098.
- [19] S. B. Krishnan, R. Krishnan, K. R. Gopidas, *Chem. Eur. J.* **2018**, *24*, 11451–11460.
- [20] a) R. S. Mulliken, W. B. Person, *Annu. Rev. Phys. Chem.* **1962**, *13*, 107–126; b) R. S. Mulliken, *J. Am. Chem. Soc.* **1952**, *74*, 811–824.
- [21] a) J. K. Kochi, *Pure & Appl. Chem.* **1991**, *63*, 255–264; b) E. F. Hilinski, J. M. Masnovi, J. K. Kochi, P. M. Rentzepis, *J. Am. Chem. Soc.* **1984**, *106*, 8071–8077; c) J. K. Kochi, *Angew. Chem. Int. Ed. Engl.* **1988**, *27*, 1227–1266; *Angew. Chem.* **1988**, *100*, 1331–1372; d) S. V. Rosokha, S. M. Dibrov, T. Y. Rosokha, J. K. Kochi, *Photochem. Photobiol. Sci.* **2006**, *5*, 914–924; e) S. M. Hubig, J. K. Kochi, *J. Phys. Chem.* **1995**, *99*, 17578–17585.
- [22] T. Aoki, H. Sakai, K. Ohkubo, T. Sakanoue, T. Takenobu, S. Fukuzumi, T. Hasobe, *Chem. Sci.* **2015**, *6*, 1498–1509.
- [23] a) M. R. Molla, S. Ghosh, *Chem. Eur. J.* **2012**, *18*, 9860–9869; b) H. Shao, J. R. Parquette, *Chem. Commun.* **2010**, *46*, 4285–4287; c) M. Kumar S. J. George, *Nanoscale* **2011**, *3*, 2130–2133.
- [24] a) A. Kasprzak, M. Poplawska, H. Krawczyk, S. Molchanov, M. Kozlowski and M. Bystrzejewski, *J. Inclusion Phenom. Macrocyclic Chem.* **2017**, *87*, 53–65; b) Y. Cohen, L. Avram, L. Frish, *Angew. Chem., Int. Ed.* **2005**, *44*, 520–554; *Angew. Chem.* **2005**, *117*, 524–560; c) C. S. Johnson Jr., *Prog. Nucl. Magn. Reson. Spectrosc.* **1999**, *34*, 203–256; d) Nonappa, David Saman, Erkki Kolehmainen *Magn. Reson. Chem.* **2015**, *53*, 256–260.
- [25] F. Salerno, J. A. Berrocal, A. T. Haedler, F. Zinna, E. W. Meijer, L. D. Bari, *J. Mater. Chem. C* **2017**, *5*, 3609–3615.
- [26] a) M. Kodaka, *J. Am. Chem. Soc.* **1993**, *115*, 3702–3705; b) M. Kodaka, *J. Phys. Chem.* **1991**, *95*, 2110–2112.
- [27] L. You, G. Pescitelli, E. V. Anslyn, L. D. Bari, *J. Am. Chem. Soc.* **2012**, *134*, 7117–7125.
- [28] M. D. Gujrati, N. S. S. Kumar, A. S. Brown, B. Captain, J. N. Wilson, *Langmuir* **2011**, *27*, 6554–6558.
- [29] M.-Y. Yeh, H.-C. Lin, *Phys. Chem. Chem. Phys.* **2014**, *16*, 24216–24222.
- [30] a) M. Hara, S. Tojo, K. Kawai, T. Majima, *Phys. Chem. Chem. Phys.* **2004**, *6*, 3215–3220; b) M. Assel, T. Hofer, A. Laubereau, W. Kaiser, *J. Phys. Chem.* **1996**, *100*, 11836–11842; c) A. M. Rakhi, K. R. Gopidas, *Chem. Phys. Lett.* **2015**, *618*, 192–197.
- [31] a) D. Gosztola, M. P. Niemczyk, W. Svec, A. S. Lukas, M. R. Wasielewski, *J. Phys. Chem. A* **2000**, *104*, 6545–6551; b) J. F. Martinez, N. T. L. Porte, M. R. Wasielewski, *J. Phys. Chem. C* **2018**, *122*, 2608–2617; c) P. Ganesan, J. Baggerman, H. Zhang, E. J. R. Sudholter, H. Zuilhof, *J. Phys. Chem. A* **2007**, *111*, 6151–6156; d) A. L. Jones, M. K. Gish, C. J. Zeman, J. M. Papanikolas, K. S. Schanze, *J. Phys. Chem. A* **2017**, *121*, 9579–9588.

Submitted: October 9, 2018

Accepted: December 27, 2018

Materials Science inc. Nanomaterials & Polymers

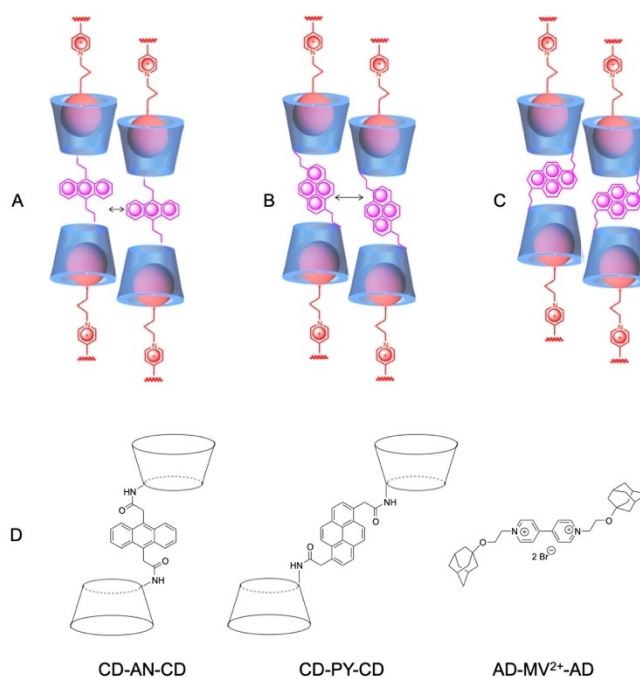
Structural Deformation to β -Cyclodextrin Due to Strong π -Stacking in the Self-Assembly of Inclusion ComplexAthira K. Jeevan,^[a, b] Sumesh B. Krishnan,^[a, b] and Karical R. Gopidas^{*[a, b]}

We report severe distortion to the structure of β -cyclodextrin and partial de-encapsulation of included guest prompted by strong π -stacking of appended pyrene moieties in the self-assembly of inclusion complex into toroidal nanostructures. The inclusion complex formed from bis(β -cyclodextrin)-substituted pyrene and bis(adamantane)-substituted methyl viologen assembled into ring-like structures. The rings undergo further self-assembly which involve strong face-to-face π -stacking of pyrene chromophores. Close approach of the pyrenes for π -stacking demands severe distortion of the cyclodextrin truncated cone structure and partial de-encapsulation of the guest from the cavity. The understanding that β -CD can be distorted severely during self-assembly may be helpful in the design of molecular architectures.

For many years cyclodextrins (CDs) were considered as rigid truncated cones of high symmetry with specific diameters and height.^[1–4] The truncated cone structure has a wider rim of C-2 and C-3 hydroxyl groups and a narrow rim composed of the C-6 primary hydroxyl groups of the glucose monomers. At the wider rim, flip-flop hydrogen bonds are formed between the C-2 hydroxyl of one glucose unit with C-3 hydroxyl of adjacent glucose. The secondary hydrogen bond belt, which is complete in β -CD, is regarded as the reason for the better rigidity and lower water solubility of β -CD compared to α - and γ -CDs. Experimental^[5–8] and theoretical^[9–15] studies now show that CD structures are flexible due to local fluctuations in the individual glucose rings and distortions of the macrocyclic structures. These disorders, however, are considered dynamic and reorientation to the symmetric structures occur rapidly. In this paper we describe strong deformation of β -CD structure due to strong π - π stacking, which is found to be stable even at 80 °C.

Self-assembly of bis(β -CD)-linked anthracene (CD-AN-CD) and bis(adamantane)-linked methyl viologen (AD-MV²⁺-AD) into toroidal nanostructures is reported by us recently.^[16] The mechanism involved formation of a ring structure from the

inclusion complex and stacking of the rings via edge-to-edge overlap of AN π -clouds. Since β -CD has a truncated cone structure with outer diameter of 15.3 Å, we proposed the skewed or slipped stack arrangement shown in Scheme 1A, where the edge-to-edge distance between ANs in successive rings is < 4 Å. In order to confirm the two important aspects of our proposal, namely, formation of closed loop structures and stacking of the ring loops, we have substituted pyrene (PY) in place of AN and designed the molecule CD-PY-CD (Scheme 1). Similar to the CD-AN-CD/AD-MV²⁺-AD system, we expected the CD-PY-CD/AD-MV²⁺-AD inclusion complex to form closed loop structures in which the PY chromophores can arrange with their long axis parallel (Scheme 1B) or perpendicular (Scheme 1C) to the β -CD axis. If the β -CD has a rigid structure, then the PY chromophores in Scheme 1B cannot undergo edge-to-edge stacking because of the > 5 Å separation. For Scheme 1C, edge-to-edge distance will be < 4 Å and stacking is possible which, however, will be weak because of the 1,6-substituents on PY. Thus, we expected to see only ring structures and no toroids in the self-assembly of CD-PY-CD/AD-MV²⁺-AD (desig-



Scheme 1. Probable arrangement of AN and PY chromophores in (A) CD-AN-CD@AD-MV²⁺-AD and (B,C) CD-PY-CD@AD-MV²⁺-AD ring stacks. Panel D shows structures of molecules. The cone-like structure represents β -CD.

[a] A. K. Jeevan, Dr. S. B. Krishnan, Dr. K. R. Gopidas
Chemical Sciences and Technology Division, CSIR-National Institute for Interdisciplinary Science and Technology, Thiruvananthapuram 695 019, India
E-mail: gopidaskr@gmail.com

[b] A. K. Jeevan, Dr. S. B. Krishnan, Dr. K. R. Gopidas
Academy of Scientific and Innovative Research (AcSIR), Ghaziabad - 200 002, India

Supporting information for this article is available on the WWW under <https://doi.org/10.1002/slct.202004488>

nated here as CD-PY-CD@AD-MV²⁺-AD). Contrary to our expectation, we observed toroidal nanostructures in self-assembled CD-PY-CD@AD-MV²⁺-AD, where the PY chromophores are present as in Scheme 1B. Instead of the edge-to-edge π -interaction expected, the PY chromophores undergo face-to-face stacking at ~ 3.6 Å separation, which is possible only if the β -CD undergoes considerable structural deformation. Since the CD cavity is occupied by very rigid AD group, partial de-encapsulation of AD from the CD cavity must occur prior to deformation. Details are presented here.

Equimolar amounts (1×10^{-5} M each) of CD-PY-CD and AD-MV²⁺-AD when dissolved in water self-assembled to give nanoscopic particles, the presence of which are confirmed by Tyndall effect and dynamic light scattering (DLS) (Figure S5, SI). DLS confirmed the presence of particles with average hydrodynamic diameter of 250 nm and 150–450 nm size distribution. TEM, SEM and AFM (Figure 1A–C, see Figure S6 also) show small spherical or oval shaped particles with a hollow central part (toroids). The size of the particles in all the figures are similar and agree very well with DLS. In addition, the AFM gives good insights regarding the mechanism of toroid formation. Two sections of the AFM are expanded in Figure 1D, where we can clearly identify large numbers of stacked ring-like (or golden bangle-like) structures. Most probably the larger toroids are formed by side-stacking of rings structures (vide infra) to give hollow cylinders, which undergo end-coalescing. End-coalescing of cylindrical precursors is an important mechanism for toroid formation.^[17–20]

Spectroscopic experiments confirm that the inclusion complex formed in CD-PY-CD@AD-MV²⁺-AD self-assembled into toroidal nanostructures. Figures S8 and S9 show the changes observed for the NMR signals of AD-MV²⁺-AD when encapsulated in native β -CD. The MV²⁺ and AD signals undergo slight downfield shifts, but the splitting patterns remain

unaffected. In contrast, interaction of AD-MV²⁺-AD with CD-PY-CD results in small upfield shifts and significant changes in the splitting patterns of MV²⁺ and AD protons (Figure 2, and Figures S10,S11). The doublets due to H_f and H_g protons of MV²⁺ become broad singlets of unequal intensity and AD signals have become broader with the H_a protons losing its 'dd' splitting pattern. The most important observation in Figure 2B, however, is the severe dampening of PY (8 protons) and β -CD (98 protons without counting OH) signals. The anomeric protons of β -CD (proton attached to the C-1 of glucose units) appeared as a relatively strong peak around δ 5 ppm in CD-PY-CD (Figure 2A). In the ¹H NMR of CD-PY-CD@AD-MV²⁺-AD, this peak is highly broadened. The spread of this signal in the downfield region can be clearly seen in Figure 2B, but the spread in the upfield region is masked by the strong D₂O peak. Progressive dampening of this signal can be clearly seen in Figures S10 and S11 (marked by the red arrows). The 2D ROESY NMR spectrum of CD-PY-CD@AD-MV²⁺-AD (Figure S12) exhibits cross peaks between AD and β -CD protons which confirm the close spatial association between the moieties. Temperature dependence of NMR (Figures S13–S16) show that the signals due to PY and β -CD remain severely dampened even at 80 °C. The H_f and H_g signals of MV²⁺ shifts downfield and exhibits nearly equal intensity and the former became doublet at 80 °C. All AD protons also showed downfield shift but the splitting pattern remains unchanged.

Severe dampening of PY and β -CD signals in Figure 2B is attributed to aggregation of these molecular segments which restricts mobility of the whole aggregate and/or molecular segments in comparison to free molecules.^[21–26] Aromatic ring current effect also contribute to severe dampening of PY signals.^[27–29] Disc-like molecules such as PY undergo π - π stacking which results in shielding of protons lying directly above or below the ring system and de-shielding of outside protons (Figure S17). Since most of the protons are in the shielding region, it suggests a skewed π - π stacking of PY groups as shown in Figure S17. Loss of splitting pattern and

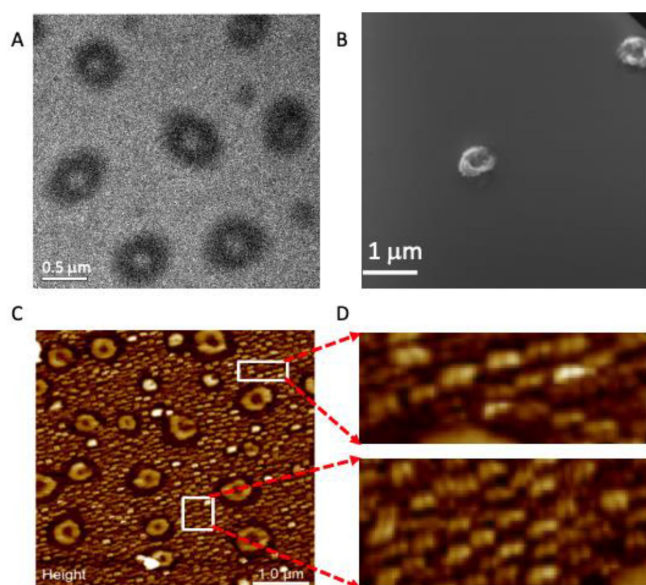


Figure 1. Images of nanostructures formed in CD-PY-CD@AD-MV²⁺-AD: (A) TEM, (B) SEM and (C) AFM. (D) shows expanded regions of image in (C).

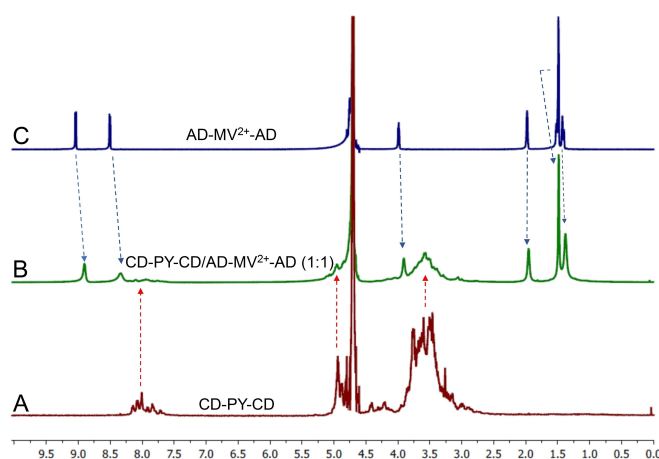


Figure 2. ¹H NMR spectra in D₂O of (A) CD-PY-CD, (B) CD-PY-CD/AD-MV²⁺-AD (1:1) and (C) AD-MV²⁺-AD. Chemical shift changes due to complexation are marked by arrows.

broadening of AD and MV^{2+} signals are also due to restricted rotation of the corresponding molecular segments. The different signal intensities of the H_f and H_g protons of MV^{2+} suggest that the two pyridinium rings are not coplanar. Loss of coplanarity will have little effect on the H_f protons but the H_g protons, which are placed in the region between the two rings, will experience different environments. As a result, these four protons will have slightly different chemical shifts and the resulting signal will be highly broadened with reduced intensity.

The face-to-face stacking of PY in CD-PY-CD@AD- MV^{2+} -AD, is corroborated by absorption spectroscopy. Figure 3A shows the absorption spectra of CD-PY-CD in the absence and presence of different concentrations of AD- MV^{2+} -AD. The absorption spectra exhibit three features, very typical of face-to-face π -stacking of PY in PY-tagged polymers in water.^[26,30–35] (i) The vibrational bands in the 300–360 nm region, which corresponds to the $S_0 \rightarrow S_2$ transition in PY, are broadened and red-shifted by 3 nm; (ii) a decrease of the peak to valley ratio (which is the ratio of absorbance at the maximum of the most intense peak to that of the adjacent minimum at shorter

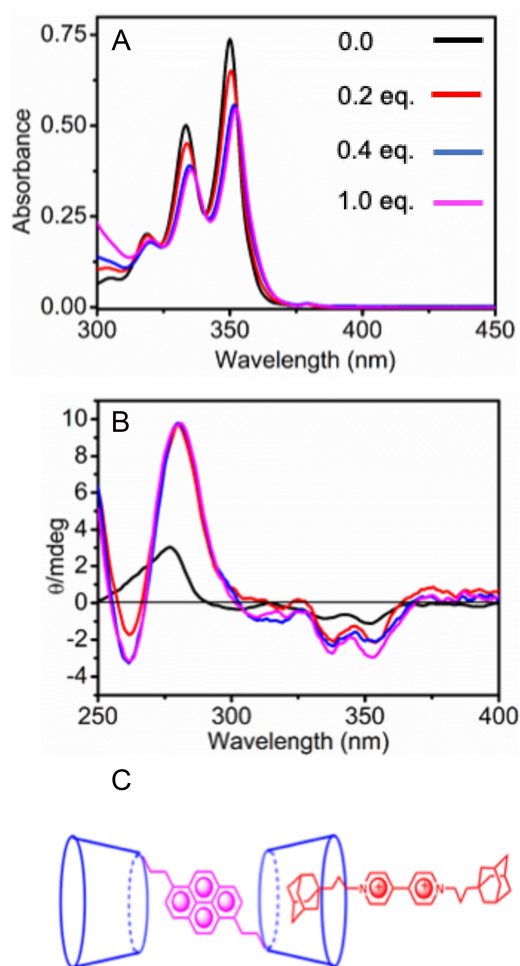


Figure 3. (A) Absorption and (B) ICD spectra of CD-PY-CD (2×10^{-5} M) in the absence and presence of AD- MV^{2+} -AD. (C) shows the orientation of PY and MV^{2+} with respect to β -CD as inferred from ICD data.

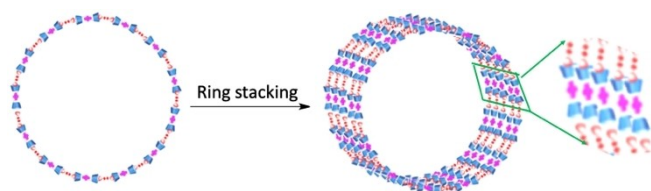
wavelength side) from 2.96 (typical of free PY) to 2.3 (typical value for face-to-face stacked PY), and (iii) hypochromism, which is the decrease in the extinction coefficient of the absorption band. The extinction coefficient decreased from $37,000 \text{ M}^{-1} \text{ cm}^{-1}$ in the free molecule to $27,000 \text{ M}^{-1} \text{ cm}^{-1}$ in CD-PY-CD@AD- MV^{2+} -AD.

All these features are indicative of electronic interactions among PY chromophores in the ground state to form PY aggregates.^[26,30–35] The PY-PY distance in these aggregates is considered to be similar to that in crystals. Theoretical calculations of the pyrene crystal excimer by Warshel and Huler^[36] showed that the PY...PY distance is $\sim 3.44 \text{ \AA}$. More recently, Haedler et al. performed DFT calculations (B3LYP/6-31G) on four pyrene hexamer aggregates.^[35] Their results suggested that the PY...PY distances in these aggregates are in the 3.38–3.52 \AA range. Since CD-PY-CD@AD- MV^{2+} -AD is not a regular molecular system, we assumed a value of 3.6 \AA (which is generally considered as the stacking distance in aromatic π -systems) for the PY...PY separation. Thus, we propose that the PY moieties in CD-PY-CD@AD- MV^{2+} -AD are π -stacked with their planes parallel and a PY...PY distance of $\sim 3.6 \text{ \AA}$.

Addition of AD- MV^{2+} -AD to CD-PY-CD did not result in the formation of charge transfer (CT) complex. Formation of CT complexes can be easily identified by the presence of long wavelength bands in the absorption spectrum. Figure S18 shows the absorption spectrum of CD-PY-CD in the absence and presence of different concentrations of AD- MV^{2+} -AD in the 250–600 nm region. Figure S18 shows that new absorptions attributable to CT complex is not present in the spectrum of CD-PY-CD@AD- MV^{2+} -AD.

Circular dichroism experiments were carried out to elucidate the orientation of PY with respect to β -CD in CD-PY-CD@AD- MV^{2+} -AD. Achiral molecules complexed with β -CD exhibit induced circular dichroism (ICD), the intensity and sign of which are used to predict the orientation of the achiral molecule, using Kodaka's rules (section S14 and Figure S19).^[37,38] Figure 3B shows the ICD spectra of CD-PY-CD in the absence and presence of AD- MV^{2+} -AD. CD-PY-CD exhibits negative ICD in the 300–370 nm region and positive signal in the 250–300 nm region, which according to Kodaka's rules is indicative of PY remaining outside with its long axis parallel to β -CD axis, as shown in Figure 3C. When AD- MV^{2+} -AD is added, the signal intensities increase suggesting that the PY became more parallel to the CD axis. Alternately, inclusion of AD (of AD- MV^{2+} -AD) in the β -CD cavity of CD-PY-CD rigidifies the assembly, leading to an enhancement of the ICD intensity. The negative signal around 260 nm in CD-PY-CD@AD- MV^{2+} -AD is in the region of MV^{2+} absorption. The negative signal suggests that MV^{2+} is positioned outside the CD cavity with its long axis parallel to the CD axis as shown in Figure 3C.

We propose that the toroids are formed as shown in Figure S20. The inclusion complex assembled into ring-like structures. Face-to-face π -stacking of PY in the rings leads to ring stacking as shown in Scheme 2. The golden bangle-type structures seen in Figure 1D are stacks of few rings. Ring stacking continues to give hollow cylindrical structures which undergo end-coalescence^[17–20] to give the observed toroids.



Scheme 2. Formation of toroids by self-assembly of CD-PY-CD@AD-MV²⁺-AD inclusion complex through ring formation (A) and stacking of rings (B). (β -CD distortion is not shown).

¹H NMR spectrum and its temperature dependence confirm aggregation of PY and β -CD in CD-PY-CD@AD-MV²⁺-AD. To the best of our knowledge, dampening of β -CD NMR signals due to aggregation of inclusion complex is not reported. π -stacking of PY in PY tagged water-soluble polymers is reported in large number of papers.^[30–35] In CD-PY-CD@AD-MV²⁺-AD, π -stacking of PY moieties leads to formation of nearly uniform sized ring stacks in Figure 1D. If the CD maintains a rigid structure with AD included within its cavity, PY groups in the rings will not be able to approach each other to within the 3.6 Å required for face-to-face π -stacking. The situation is shown in Figure S21A. Within the ring structures, the β -CD (with encapsulated AD) is present in-between PY and MV²⁺. If the PY and MV²⁺ moieties have to come closer within 3.6 Å for stacking, two conditions must be satisfied: (i) the AD included in the CD cavity must come out, at least partially and (ii) the structure of β -CD must get distorted severely, which are the main contentions of this paper. Most probably, the β -CD structure is deformed to give flattened cylinders, with outer diameter < 4 Å at the narrow side, which makes PY...PY...PY stacking possible as shown in Figure S21B. The severe dampening of the anomeric protons also supports deformation of the CD. The flip-flop hydrogen bonds on the wider rim of the CD breaks and the individual glucose rings reorient to a distorted structure that will accommodate PY...PY...PY stacking. When the PY rings stack the MV²⁺ groups of adjacent rings also will come closer, which will be unfavorable due to charge repulsion. Face-to-face stacking of the MV²⁺ moieties is avoided by rotation of one of the rings with respect to the other and lead to observed changes in the ¹H NMR signals of MV²⁺ (vide supra).

In conclusion, this study shows that the stabilization and rigidity of β -CD, attributed to the flip-flop hydrogen bonds at the wider rim, can be easily upset when strong secondary interactions are at work. The distortions are not transitory in nature and lead to formation of assemblies which are stable even at high temperatures. The structure and properties of cyclodextrins continue to inspire chemists.^[39–46] In this context the understanding that CD structures are not inflexible may lead to design of novel molecular architectures in the future. Structural deformation of cyclodextrin is subject to several theoretical studies, but none of the studies have considered large deformations to its structure. We hope that this study may pave the way for rigorous theoretical studies in this direction also.

Supporting Information Summary

Experimental procedures for synthesis of CD-PY-CD, and its characterization data, Tyndall effect and DLS experiment, additional TEM, SEM and AFM images, ¹H NMR titration of AD-MV²⁺-AD with native β -CD and CD-PY-CD, 2D ROESY NMR, temperature dependence of NMR spectrum, application of Kodaka's rules and scheme for toroid formation.

Acknowledgements

We thank the Department of Science and Technology (DST), Government of India (CRG/2019/001047) for financial support. KRG thanks CSIR for the Emeritus Scientist Scheme (1093, Letter No. 21(1048)/18/EMR-II), AKJ and SBK thanks CSIR for research fellowships.

Conflict of Interest

The authors declare no conflict of interest.

Keywords: host-guest systems · inclusion complexes · nanostructures · pi-stacking · self-assembly

- [1] G. Crini, *Chem. Rev.* **2014**, *114*, 10940–10975.
- [2] K. Linder, W. Saenger, *Carbohydr. Res.* **1982**, *99*, 103–115.
- [3] C. Betzel, W. Saenger, B. E. Hingerty, G. M. Brown, *J. Am. Chem. Soc.* **1984**, *106*, 7545–7557.
- [4] J.-Y. Li, D.-F. Sun, A.-Y. Hao, H.-Y. Sun, J. Shen, *Carbohydr. Res.* **2010**, *345*, 685–688.
- [5] H. Dodziuk, *J. Mol. Struct.* **2002**, *614*, 33–45.
- [6] V. Zabel, W. Saenger, S. A. Mason, *J. Am. Chem. Soc.* **1986**, *108*, 3664–3673.
- [7] M. G. Usha, R. J. Wittebort, *J. Am. Chem. Soc.* **1992**, *114*, 1541–1548.
- [8] T. Steiner, A. M. M. da Silva, J. J. C. Teixeira-Dias, J. Müller, W. Saenger, *Angew. Chem. Int. Ed.* **1995**, *34*, 1452–1453; *Angew. Chem.* **1995**, *107*, 1573–1575.
- [9] K. B. Lipkowitz, *J. Org. Chem.* **1991**, *56*, 6357–6367.
- [10] K. J. Naidoo, J. Y.-J. Chen, J. L. M. Jansson, G. Widmalm, A. Maliniak, *J. Phys. Chem. B* **2004**, *108*, 4236–4238.
- [11] Á. Piñeiro, X. Banquy, S. Pérez-Casas, E. Tovar, A. García, A. Villa, A. Amigo, A. E. Mark, M. Costas, *J. Phys. Chem. B* **2007**, *111*, 4383–4392.
- [12] W. Cai, T. Sun, X. Shao, C. Chipot, *Phys. Chem. Chem. Phys.* **2008**, *10*, 3236–3243.
- [13] M. Jana, S. Bandyopadhyay, *J. Phys. Chem. B* **2011**, *115*, 6347–6357.
- [14] H. Zhang, C. Ge, D. van der Spoel, W. Feng, T. Tan, *J. Phys. Chem. B* **2012**, *116*, 3880–3889.
- [15] W. Khuntawee, M. Karttunen, J. Wong-ekkabut, *Phys. Chem. Chem. Phys.* **2017**, *19*, 24219–24229.
- [16] S. B. Krishnan, K. R. Gopidas, *J. Phys. Chem. B* **2020**, *124*, 9546–9555.
- [17] Y. Kim, W. Li, S. Shin, M. Lee, *Acc. Chem. Res.* **2013**, *46*, 2888–2897.
- [18] S. Yagai, M. Yamauchi, A. Kobayashi, T. Karatsu, A. Kitamura, T. Ohba, Y. Kikkawa, *J. Am. Chem. Soc.* **2012**, *134*, 18205–18208.
- [19] D. J. Pochan, Z. Chen, H. Cui, K. Hales, K. Qi, K. L. Wooley, *Science* **2004**, *306*, 94–97.
- [20] Z. Chen, H. Cui, K. Hales, Z. Li, K. Qi, D. J. Pochan, K. L. Wooley, *J. Am. Chem. Soc.* **2005**, *127*, 8592–8593.
- [21] H. Yoshioka, K. Nonaka, K. Fukuda, S. Kazama, *Biosci. Biotechnol. Biochem.* **1995**, *59*, 1901–1904.
- [22] W. J. Harrison, D. L. Mateer, G. J. Tiddy, *J. Phys. Chem.* **1996**, *100*, 2310–2321.
- [23] C. Schnorpfel, H. Meier, M. Irie, *Helv. Chim. Acta* **2001**, *84*, 2467–2475.
- [24] J. Xiang, X. Yang, C. Chen, Y. Tang, W. Yan, G. Xu, *J. Colloid Interface Sci.* **2003**, *258*, 198–205.

- [25] H. Hong, Y. Mai, Y. Zhou, D. Yan, Y. Chen, *J. Polym. Sci. Part A* **2008**, *46*, 668–681.
- [26] G. Singh, P. K. Singh, *Langmuir* **2019**, *35*, 14628–14638.
- [27] T. Nakano, *Polym. J.* **2010**, *42*, 103–123.
- [28] F. Parenti, F. Tassinari, E. Libertini, M. Lanzi, A. Mucci, *ACS Omega* **2017**, *2*, 5775–5784.
- [29] R. D. Majumdar, T. Montina, O. C. Mullins, M. Gerken, P. Hazendonk, *Fuel*, **2017**, *193*, 359–368.
- [30] F. M. Winnik, *Chem. Rev.* **1993**, *93*, 587–614.
- [31] I. Yamazaki, F. M. Winnik, M. A. Winnik, S. Tazuke, *J. Phys. Chem.* **1987**, *91*, 4213–4216.
- [32] F. M. Winnik, M. A. Winnik, S. Tazuke, C. K. Ober, *Macromolecules* **1987**, *20*, 38–44.
- [33] F. M. Winnik, *Macromolecules* **1990**, *23*, 233–242.
- [34] H. Siu, J. Duhamel, *J. Phys. Chem. B* **2008**, *112*, 15301–15312.
- [35] A. T. Haedler, H. Misslitz, C. Buehlmeier, R. Q. Albuquerque, A. Köhler, H.-W. Schmidt, *ChemPhysChem* **2013**, *14*, 1818–1829.
- [36] A. Warshel, E. Huler, *Chem. Phys.* **1974**, *6*, 463–488.
- [37] M. Kodaka, *J. Phys. Chem.* **1991**, *95*, 2110–2112.
- [38] M. Kodaka, *J. Am. Chem. Soc.* **1993**, *115*, 3702–3705.
- [39] M. J. Klemes, L. P. Skala, M. Ateia, B. Trang, D. E. Helbling, W. R. Dichtel, *Acc. Chem. Res.* **2020**, *53*, 2314–2324.
- [40] I. M. Mavridis, K. Yannakopoulou, *J. Med. Chem.* **2020**, *63*, 3391–3424.
- [41] S. Pan, R. Guo, N. Bertleff-Zieschang, S. Li, Q. A. Besford, Q.-Z. Zhong, G. Yun, Y. Zhang, F. Cavalieri, Y. Ju, E. Goudeli, J. J. Richardson, F. Caruso, *Angew. Chem. Int. Ed.* **2020**, *59*, 275–280.
- [42] S. Loescher, A. Walther, *Angew. Chem. Int. Ed.* **2020**, *59*, 5515–5520.
- [43] S. Sinn, J. Krämer, F. Biedermann, *Chem. Commun.* **2020**, *56*, 6620–6623.
- [44] J. C. K. Kung, N. Vurgun, J. C. Chen, M. Nitz, R. A. Jockusch, *Chem. Eur. J.* **2020**, *26*, 3479–3483.
- [45] Y. Yu, F. Peng, J. M. Heuvelmans, S. Li, R. J. M. Nolte, D. A. Wilson, *Angew. Chem. Int. Ed.* **2019**, *58*, 8687–8691.
- [46] S. Zhang, C. Zhang, H. Chen, S. J. Kieffer, F. Neubrech, H. Giessen, A. G. Alleyne, P. V. Braun, *Angew. Chem. Int. Ed.* **2019**, *58*, 18165–18170.

Submitted: November 30, 2020

Accepted: December 7, 2020